Electrical Intensification of CO2 Reduction Electrolysis

Sassenburg, M.

DOI
10.4233/uuid:aaf923ba-18c2-4262-ba20-4e62a1a60598

Publication date
2023

Document Version
Final published version

Citation (APA)
Sassenburg, M. (2023). *Electrical Intensification of CO2 Reduction Electrolysis*. [Dissertation (TU Delft), Delft University of Technology]. https://doi.org/10.4233/uuid:aaf923ba-18c2-4262-ba20-4e62a1a60598

Electrical Intensification of CO_2 Reduction Electrolysis

by

Mark Sassenburg

Electrical Intensification of CO_2 Reduction Electrolysis

Dissertation

for the purpose of obtaining the degree of doctor
at Delft University of Technology
by the authority of the Rector Magnificus
prof. dr. ir. T.H.J.J. van der Hagen
chair of the Board for Doctorates,

to be defended publicly on

Wednesday 11 October 2023 at 10:00 o'clock

by
Mark SASSENBURG
Master of Science in Sustainable Energy Technologies
Delft University of Technology, the Netherlands
born in Rotterdam, the Netherlands

This dissertation has been approved by the promotors.

Prof. dr. W.A. Smith	Delft University of Technology, promotor
Prof. dr. ir. J.T. Padding	Delft University of Technology, promotor
Dr. T.E. Burdyny	Delft University of Technology, promotor

Composition of the doctoral committee:

Rector Magnificus	chairperson
Prof. dr. W.A. Smith	Delft University of Technology, promotor
Prof. dr. ir. J.T. Padding	Delft University of Technology, promotor
Dr. T.E. Burdyny	Delft University of Technology, promotor

Independent members:

Prof. dr. ir. A. Urakawa	Delft University of Technology
Prof. dr. B. Dam	Delft University of Technology
Prof. dr. M. Escudero Escribano	Catalan Institute of Nanoscience and Nanotechnology
Dr. A. Anastasopol	TNO

The work described in this thesis has been carried out in the Materials for Energy Conversion and Storage (MECS) group, Department of Chemical Engineering, Faculty of Applied Sciences, Delft University of Technology.

This work has received financial support from the European Research Commission (ERC), and from the Electrons to Chemical Bonds programme (E2CB) on behalf of the Dutch Research Council (NWO).

Cover design by Mark Sassenburg
Printed by Proefschrift Specialist
An electronic version of this thesis is freely available at: https://repository.tudelft.nl

Contents:

Chapter 1.

Climate Change and CO_2 electrolysis

"This that I have brought you is called 'fire,'" Prometheus said. It is an ill-natured spirit, a little brother of the sun, but if you handle it carefully, it can change your whole life. It is very greedy; you must feed it twigs, but only until it becomes a proper size. Then you must stop, or it will eat everything in sight—and you too.

– 'Prometheus Retold' by Bernard Evslin.

1.1 Troubling trends - Emissions and global warming

Since the dawn of time, mankind has been marked by its ability to analyze its surroundings and adapt to it in order to make life easier. We used fire to provide heat and scare off predators. Rivers were expanded into irrigation networks to grow crops and settle down. The wind was utilized through sails, allowing ships to traverse vast oceans and interconnect the world and the earth was mined for its resources to create tools and build houses. Each of these elements provided a benefit to society and transformed the way we lived. Though it was clear these transformations improved the quality of life, the natural elements were not to be underestimated, as they contained a destructive power that needed to be respected. Flashfloods, wildfires, hurricanes and landslides were disasters that damaged the built infrastructure and endangered human life, but versatility and resilience caused man to bounce right back and continue the march of progress.

Fast forward to the Industrial Revolution (circa 1760-1840), where humanity learned to replace a large fraction of heavy manual labor with various automated machines. This critical stage of technological development enabled a myriad of inventions to come forth. Key developments made were the steam and combustion engines that provided mechanical power, and the fundamental understanding of electricity generation that would lead to coal-fired power plants in the 1880s. These inventions were rapidly implemented throughout the world and enabled society to leap

forward technologically into the 20th century by utilizing the untapped energy stored underneath the earth for millions of years, fossil fuels.

At the start of the 20th century a physicist/chemist named Svante Arrhenius [1] was weary of the drastic effects of burning coal and how excessive use might impact the longevity of the human race. Despite the scientists' early warning, the possibilities of not only coal, but other fossil fuels like oil and gas to produce efficient energy caused numerous industrial sectors to boom, and along with that came emissions of greenhouse gases such as CO_2. It was not until the late 1960s that scientific evidence of local and global effects of pollution were raised to the public. [2] Though little action was taken directly after, as large oil companies put the scientific findings in question, concerns for national and global security led to the founding of governmental and global entities such as the National Oceanic and Atmospheric Administration (NOAA) and the Intergovernmental Panel on Climate Change (IPCC). These monitoring agencies have been quantifying emissions and climate developments up until this day.

In particular, NOAA has recorded (and backtracked) the development of the atmospheric CO_2 concentrations since the Industrial Revolution as is shown in Fig. 1.1. The initial skepticism of whether the increase in atmospheric CO_2 was due to anthropogenic activities or due to a natural phenomenon was reasonable then, since it was unclear if the concentration difference between pre-industrial data (270-280 ppm) and 1960s (~320 ppm) was part of a natural cycle or induced by human activity.

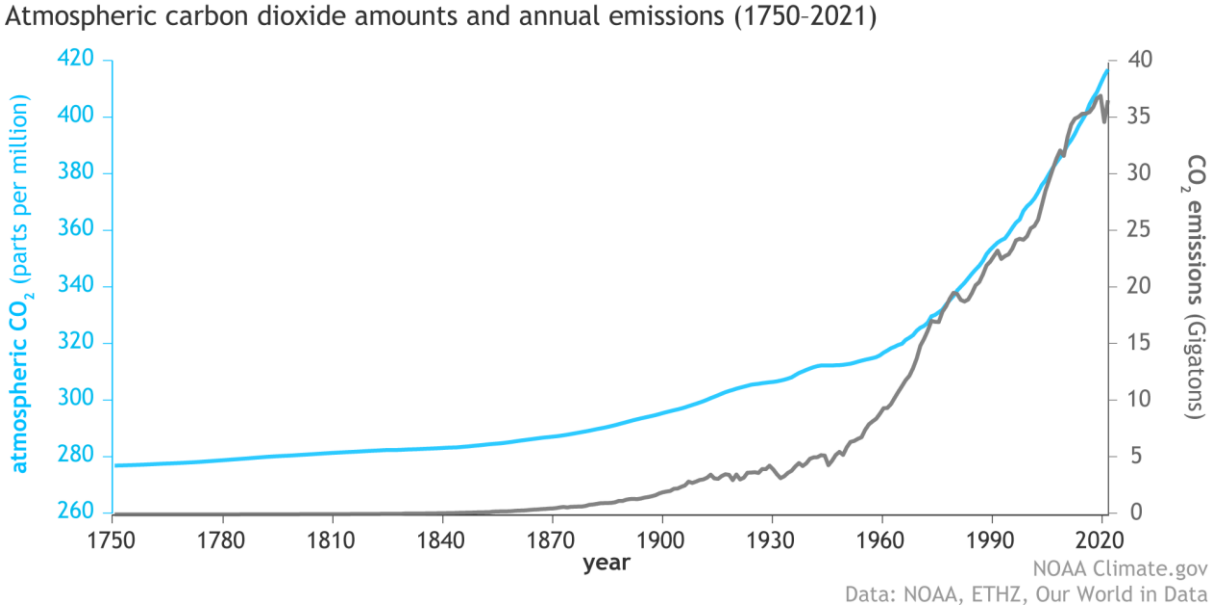

Figure 1.1 Atmospheric carbon dioxide amounts and annual emissions between 1750-2021. [3]

However, the economic growth the world has seen in the past 60 years has been accompanied by an explosive growth of over 700 % in CO_2 emissions. At the present time over 35 Gt of CO_2 is emitted annually, resulting in atmospheric CO_2 concentrations that surpassed 420 ppm in 2022, an increase of 50 % since pre-industrial times.

Being a greenhouse gas, CO_2 contributes to global warming by trapping radiative heat from the sun in the atmosphere and reflecting it back to Earth, acting as a blanket. The cumulative amount of emitted CO_2 accounts for 75% of all greenhouse gasses and has led to a natural imbalance that continues to have consequences for both natural and inhabited parts of the world. The rise in atmospheric CO_2 and temperature has caused a cascade of negative reactions that endanger biodiversity and human life. A range of environmental feedback loops arose, leading to ecological changes and an increased frequency of extreme weather events [4]. Oceans take up about one third of atmospheric CO_2 through dissolution, causing an acidification unsustainable to the ecosystem and leading to a limited diversity of marine life. In the past decade however, the increase in oceanic temperatures has limited the solubility of CO_2 as well as the stability of icy methane clusters stored in the ocean floor, and thus led to further release of GHGs into the atmosphere. Permafrost in polar regions have begun to melt, which both reduces the amount of sunlight reflected back into space and opens up previously encapsulated methane gas deposits. Increased wildfires and droughts also release sequestrated carbon from plant life while severe flashfloods, tsunamis and hurricanes have damaged infrastructure causing upheaval and requiring costly reconstruction, leading to further pollution.

To aid in understanding the consequences of unregulated emissions, the IPCC has been presenting extensive reports since the 1990's in order to objectively address climate change to promote public awareness and inform policymakers about the cause and effect of (in)action. In its recently published Sixth Assessment Report (AR6) is a 1991 page document [5] that covers a variety of topics including global emission trends, mitigation strategies, projected scenarios and consequences on different timescales and distinguished impacts in the energy, agriculture, transport, construction and industry sector. As a continuation of previous international agreements like the Kyoto Protocol in 1997 [6] and the Paris Agreements in 2015 [7], AR6 highlights the importance of national policies and international collaboration in order to achieve

these borderless climate goals. One of the most convincing *(and looming)* charts from the 'Summary for Policymakers' is the projected shift in global average temperature for the 21st century on the basis of emission policy decisions made in the present. Fig. 1.2 highlights two of the projections made for the current decade. The first projection (orange) shows a rise in temperature of 3.5 to 4.5 °C as compared to the pre-industrial

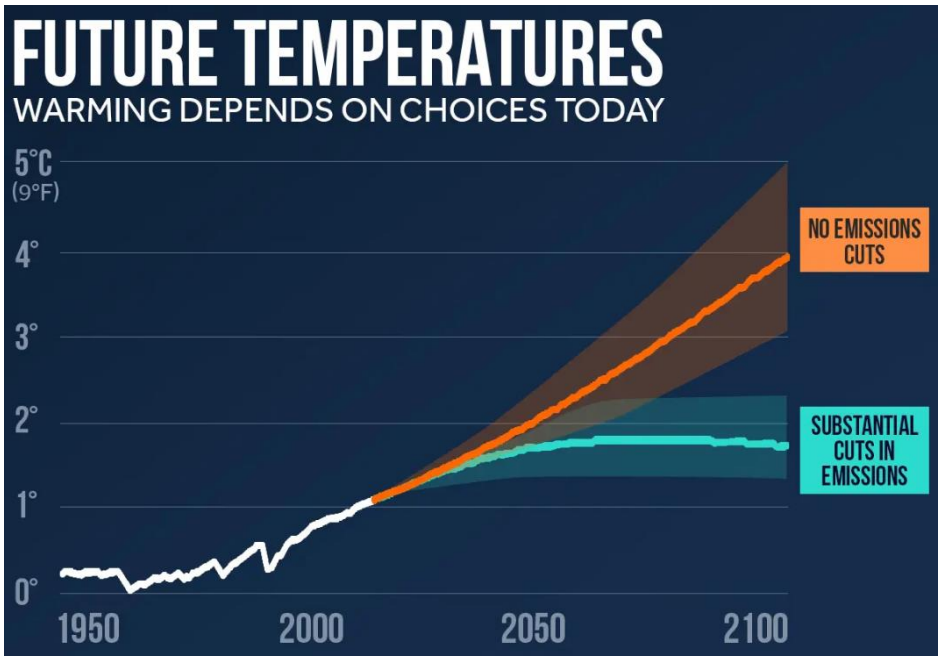

Figure 1.2 Two extreme scenarios coined by the IPCC on the global average temperature that is to be expected in the 21st century. The 'No Emission Cuts' scenario in orange indicates how inaction will lead to a rise of temperature of +3.5 to +4.5 °C as compared to the pre-industrial average. The 'Substantial Cuts in Emissions' scenario in green assumes carbon neutrality will be achieved by 2050, leveling out global warming at +2 °C. After stabilizing, the regeneration of the natural balance will then gradually decrease temperatures as CO_2 is sequestered from the atmosphere. [5]

average will happen if the policies and agreements currently in place are not adjusted. Alternatively, the second projection (green) shows the ambitious goal to limit the temperature change to 1.5-2 °C by becoming CO_2 neutral, which will require electrification of all sectors as well as near-complete removal of fossil fuel use. Both situations will affect the climate, though the green route appears to leave a salvageable situation for human survival, whereas the consequences of unchecked emissions are unforeseeable, but will likely lead to the devastation of society as we know it.

1.2 A green solution to a clean future

To mitigate the effects of climate change, such as global warming and extreme weather events, drastic changes in the functioning of our fossil fuel based society are needed to reduce the effective emissions of CO_2. Currently, all sectors of industry are mostly operating on abundantly available fossil fuels like oil, natural gas and coal for transportation, generation of heat and electricity as well as the production of hundreds of products like plastics, solvents, lubricants, pharmaceuticals, tires, shoes and basketballs [8]. In order to achieve a sustainable society, fossil fuels need to be phased out and replaced with renewable alternatives that fulfil their role, whether that is electricity generation or the production of commodity and specialty chemicals. Human ingenuity once again looked at the forces of nature and realized the development of renewable energy systems to generate power in a sustainable manner. By harnessing the energy of the sun in photovoltaic (PV) solar cells, the power of wind through turbines, the heat of the earth through geothermal wells and the flow of water through

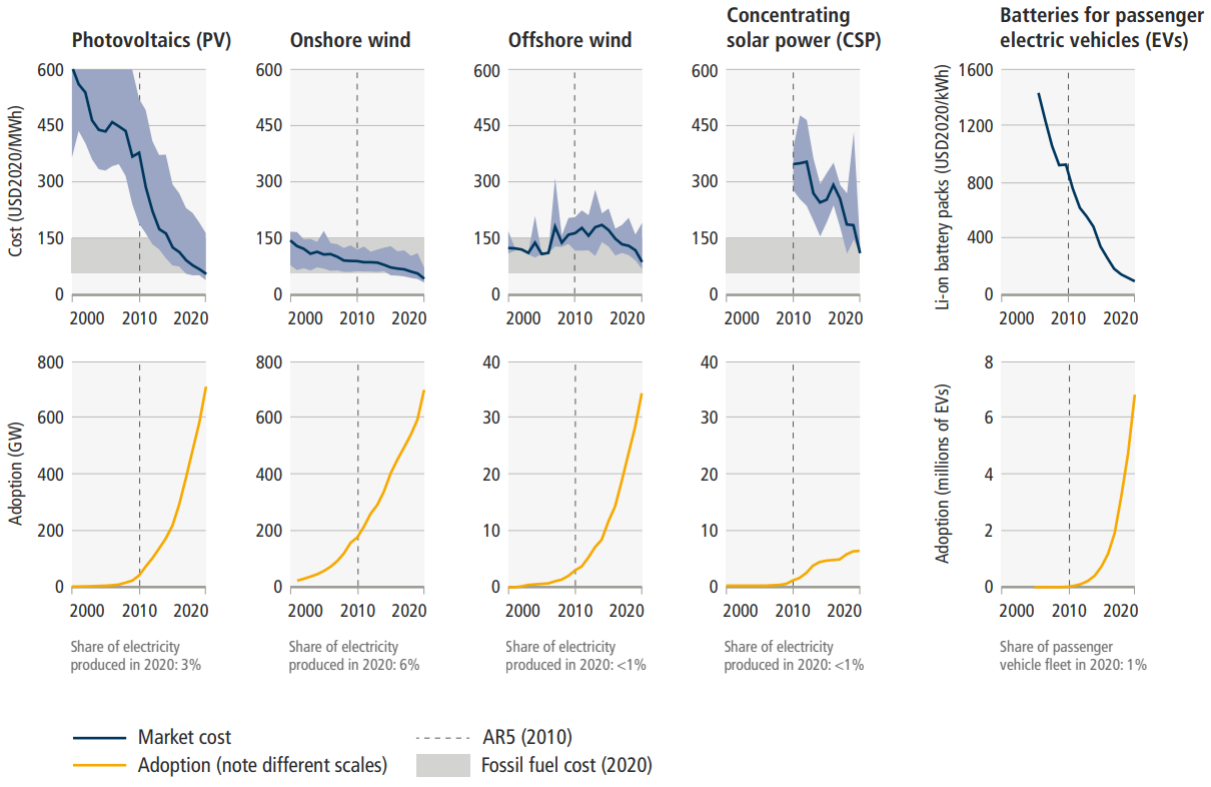

Figure 1.3 Trends for the price and adoption of renewable energy technologies between 2000 and 2020. Improvements in the cost-efficiency of PV and wind energy has caused renewable electricity generation to be cheaper than fossil fuels. As a result of cheap electricity and a demand for more sustainable transportation, Li-ion battery pack followed the same trend leading to the introduction of millions of electric vehicles (EVs). [5]

hydropower dams, we have found the sustainable energy tools needed to reduce greenhouse gas emissions while still providing much needed electricity on a large scale. The energy transition is already underway and has caused the markets associated with each power source to grow in the last decade. In fact, PV and wind have started to compete with fossil fuel prices on a MWh basis, causing a positive feedback loop in both the exponential growth of their implementation and the further decrease of prices as dictated by the economy of scales, displayed in Fig. 1.3.

A new issue that came with the use of renewable energy sources is that generating these types of electricity are intermittent by nature, whereas fossil fuels are used continuously and can be deployed and stored flexibly. This intermittency of power is undesired for a multitude of reasons as society does not want to be reliant on natural cycles in its daily rhythm. In addition, industrial machines tend to be operated in a continuous manner for weeks or months without interruption in order to be more efficient. The imbalance between electricity generation and consumption causes grid instability and requires solar/wind farms to sell at negative prices or to be turned off entirely to prevent overloading of the grid. [9] Currently only a fraction of the total energy landscape has shifted to renewable sources, meaning that the supply-demand imbalance will only grow as the energy transition continues if no mitigation strategy is implemented. Ideally, renewable electricity will always be generated at full capacity, while excess electricity can be stored to mitigate daily and seasonal fluctuations. Battery storage might sound intuitive, though the required capacity and timescale of storage needed to facilitate a nations energy supply and demand makes it difficult due to the low energy density of batteries and their tendency to leak power during a prolonged period of storage.

Through electrochemical conversion, it is possible to store electrical power generated by renewable sources in chemical bonds. This method of energy storage has a dual purpose; Firstly, storing energy in chemicals is more desirable for long term energy storage and secondly, these chemicals produced by renewable energy can be utilized not only to regain energy, but to replace fossil fuel based alternatives used in a wide range of chemical reactions. In the ongoing energy transition, interest in hydrogen is enjoying unprecedented momentum as a substitute energy carrier and chemical building block and is therefore considered a prime candidate for securing energy in the future. [10] Nevertheless, hydrogen comes with its own limitations. Low

energy density makes compressive storage and transportation expensive which challenges hydrogen's ability to be effectively implemented in society. Additionally, while hydrogen is considered a strong alternative as an energy carrier, it does not provide the range of dynamic utility that long carbon chains in fossil fuels have. Here, the future of a potential renewable based chemical process industry has to rely on an alternative method of producing high energy density carbon-carbon bonds (C-C bonds).

A potentially attractive way to deal with all presented issues (CO_2 emissions, an abundance of intermittent electricity and the need for renewable C-C bonds), is through the electrochemical conversion of CO_2. It is possible to electrochemically convert CO_2 into CO and/or hydrocarbons that can function as intermediate building blocks or directly as synthetic fuels. Subsequently, a mixture of CO and H_2, also known as synthesis gas (syngas) can be used in Fischer-Tropsch synthesis [11] to produce hydrocarbons. This conversion method provides a renewable pathway to an artificial substitute for fossil fuels and could be used to close the carbon cycle, store intermittent energy and provide the desired C-C bonds.

While the electrochemical conversion of CO_2 is a promising solution to the aforementioned problems, research has shown a variety of technical limitations that need to be addressed before this technology can be scaled up and implemented. To date, low reaction rates, substantial resistive losses, a lack of uniform product selectivity and troubling long-term stability makes electrochemical CO_2 reduction systems have insufficient economic incentives for society to replace fossil fuels. In order for CO_2 electrolysis to become a pivotal component of the energy transition away from fossil fuels it needs to combine multidisciplinary science with industrial requirements.

1.3 Thesis outline and research questions

The electrochemical conversion of CO_2 appears to be a promising solution to emissions, energy storage and dynamic utility. However, substantial resistive losses, a lack of uniform product selectivity and poor long-term stability of these electrochemical systems are limiting the implementation of this technology into industry. In the past decade research has moved towards gas diffusion electrode systems that allow for conversion rates (>200 mA/cm^2) that are of industrial interest,

however, the transferability of knowledge from traditional aqueous based H-cell electrolysis to the new flow cell and membrane electrode assembly (MEA) reactors is convoluted. This thesis is focused on further understanding the effects of process intensification of a CO_2 electrolysis device, and the overall chapter structure is outlined below.

Chapter 2 – *'The electrochemical conversion of CO_2 – Theory and development'* comprises of a technical introduction to CO_2 electroreduction. The theory behind the CO_2 reduction reaction and the role of catalyst materials is discussed first. Then the shortcomings of H-cells, the original research systems, is used to explain how CO_2 electrolysis systems have developed and the changes that has brought to research and industrial feasibility. Finally, a brief overview and insight into the essential components of an electrochemical cell are laid out.

Chapter 3 – *'Characterizing CO_2 reduction catalysts on gas diffusion electrodes: A direct comparison of the activity, selectivity and stability of transition metal catalysts'* covers the core part of this thesis. In this chapter a range of transition metal catalysts (Ag, Au, Zn, Pd, Cu) are studied in a flow cell environment. Inspired by the benchmarking study of Hori et al. this work focused on having a highly controlled, well documented characterization method and covers the transferability and comparability of electrochemical parameters within and across the tested metals. By increasing the applied current density from the H-cell regime (10 mA/cm^2) to the flow cell regime (>200 mA/cm^2) the effects of electric intensification on activity, selectivity and stability are tested. During the broad empirical study that encompasses this work, the following research questions are to be answered:

- *How transferable are catalyst characteristics when increasing current densities from the H-cell regime to the flow cell regime?*
- *What is comparatively the best performing CO_2-to-CO catalyst at elevated current densities in terms of selectivity, activity and stability?*

During this extensive research, much was learned about the electric intensification on catalysts and in parallel also about operational parameters and system limitations. This sparked motivation for the following projects/chapters.

Chapter 4 – '*Zero-Gap Electrochemical CO_2 Reduction Cells: Challenges and Operational Strategies for Prevention of Salt Precipitation*' takes a dive into the

literature on salt formation and prevention in zero-gap MEA systems. CO_2 reduction electrolysis is developing quickly and one of the main limitations not often discussed is salt formation. While CO_2 reduction is the desired reaction, the presence of CO_2, highly alkaline conditions and supporting cations facilitate the formation of carbonate deposits. This chapter covers the theory behind the precipitation of K_2CO_3 salts and establishes 4 categories of recently published solution strategies on how to prevent the detrimental effects of salts or how to avoid the formation altogether. Here we investigate the question:

- *Can detrimental K_2CO_3 formation be prevented and what solution strategies are available?*

Chapter 5 – *'Bulk layering effects of Ag and Cu in tandem CO_2 electrolysis to adjust C_{2+} selectivity'* is a study on how a robust Cu catalyst might benefit from minute amounts of Ag. In Chapter 3 it was found that increasing the current density on a pure Cu catalyst caused its product selectivity towards ethylene and other C_{2+} products to be enhanced up to a certain amount, while simultaneously decreasing the output of CO. The decrease in CO might indicate that the rate of dimerization of Cu towards C_{2+} products becomes limited by a lack of available CO. In theory, adding a minute amount of Ag to the catalyst layer in tandem should produce additional CO, potentially benefiting the dimerization reaction on the Cu catalyst. On the other hand, it is not guaranteed all CO created on Ag will readsorb at Cu sites and dimerize, effectively increasing the CO concentration of the product stream. To answer these hypotheses the following research questions are addressed:

- *Can a Cu catalyst produce additional C_{2+} products when provided with additional CO through tandem catalysis?*
- *Does Cu independently produce enough CO to satisfy all its dimerization requirements?*

Finally, Chapter 6 – *'Future Outlook'* relays an educated guess on how CO_2 electrolysis can influence the energy landscape of the future and what systemic solutions are needed for it to come to full fruition.

References Chapter 1.

1. *Hint to Coal Consumers*, in *The Selma Times*. 1902: Selma. p. 4.
2. Robinson, E. and R.C. Robbins, *Sources, abundance, and fate of gaseous atmospheric pollutants. Final report and supplement*. 1968, United States: Stanford Research Institute,Menlo Park, CA.
3. Climate, N. *Atmospheric carbon dioxide amounts and annual emmisions (1750-2021)*. 2022 [cited 2023; Available from: https://www.climate.gov/media/14596.
4. IPCC, *Climate Change 2022: Impacts, Adaptation, and Vulnerability*. 2022, IPCC. p. 3056.
5. IPCC, *Climate Change 2022: Mitigation of Climate Change. Contribution of Working Group III* 2022.
6. UNFCCC, *Kyoto Protocol to the United Nations Framework Convention on Climate Change adopted at COP3*. 1997: Kyoto, Japan.
7. UNFCCC, *The Paris Agreement - Publication*. 2018: Paris Climate Change Conference - November 2015.
8. Corporation, R.E. *Products made from petroleum*. 2017 [cited 2022; Available from: https://www.ranken-energy.com/index.php/products-made-from-petroleum/.
9. Bird, L., et al., *Wind and solar energy curtailment: A review of international experience*. Renewable and Sustainable Energy Reviews, 2016. **65**: p. 577-586.
10. IEA, *The Future of Hydrogen - Seizing today's opportunities*. 2019, IEA: Paris.
11. Dag Schanke, E.B., Anders Holmen, *Fischer-tropsch synthesis*, E.E. AS, Editor. 2001.

Chapter 2.

The electrochemical conversion of CO_2

This thesis is focused on the electrochemical conversion of CO_2 to value-added products through the electrochemical CO_2 reduction reaction (CO_2RR). More specifically, by empirically testing and characterizing bulk catalysts the goal is to obtain a greater scientific understanding as to how the CO_2 reduction performs under electrically intensified conditions and to shine a light on what might limit the development of industrially relevant CO_2 electrolyzers. This section provides background on CO_2 reduction reactions and catalyst theory (2.1), the technological evolution of electrolyzer systems (2.2) and a description of the most essential components of an electrochemical cell (2.3).

2.1 Catalysts – Workhorse of the system

As with every electrochemical reaction, the driving force behind any redox reaction is the potential-driven transfer of electrons from one molecule to another in order to create a system that is in thermodynamic equilibrium. To facilitate this, the reaction requires an oxidizing agent, which donates electrons at the anode performing an oxidation reaction, and a reducing agent, which accepts electrons at the cathode performing a reduction reaction. To maintain electroneutrality, these two reactions need to occur simultaneously and are therefore considered half reactions. Here, the CO_2RR represents not one, but an array of reducing electrochemical half reactions, which all have their own minimum required voltage, known as the thermodynamic equilibrium potential. Examples of CO_2 reduction half reactions are shown in Eq. 1-5. [1]. Their thermodynamic potentials are measured at 25 °C vs SHE. This selection of reactions shows the formation of some of the most common CO_2 reduction products, being carbon monoxide, methane, ethylene, ethanol and propanol.

$$CO_2 + H_2O + 2e^- = CO + 2OH- \quad (-0.52V\ vs\ SHE)\ (1)$$

$$CO_2 + 6H_2O + 8e^- = CH_4 + 8OH- \quad (-0.25V\ vs\ SHE)\ (2)$$

$$2CO_2 + 8H_2O + 12e^- = C_2H_4 + 12OH- \quad (-0.34V\ vs\ SHE)\ (3)$$

$$2CO_2 + 9H_2O + 12e^- = C_2H_5OH + 12OH- \quad (-0.33V\ vs\ SHE)\ (4)$$

$$3CO_2 + 13H_2O + 18e^- = C_3H_7OH + 18OH- \quad (-0.32V\ vs\ SHE)\ (5)$$

When going down the list of Eq. 1-5, the half reactions towards more complex products show an increased amount of electron transfers is required, going from 2 electron transfers for CO and formic acid (HCOOH) to 18 electron transfers for propanol (C_3H_7OH). Aside of the reactants and products, each electron transfer leads to the formation of transient ionic intermediates, complicating the reaction pathways. Simultaneously hydroxide ions, equal to the amount of electron transfers, are produced, leading to a highly alkaline environment near the cathode. This will become important when discussing the effects of electric intensification on catalyst selectivity in Chapter 2 and even more so for carbonate salt formation in Chapter 3.

Meanwhile, the thermodynamic equilibrium potentials from Eq. 1-5 show that methane formation (Eq. 2) is the most favorable reaction. In practice, only a fairly small fraction of methane is actually formed during the CO_2RR, due to the nature of how CO_2 conversion takes place. For the rigid CO_2 molecule to be reactive, it needs to

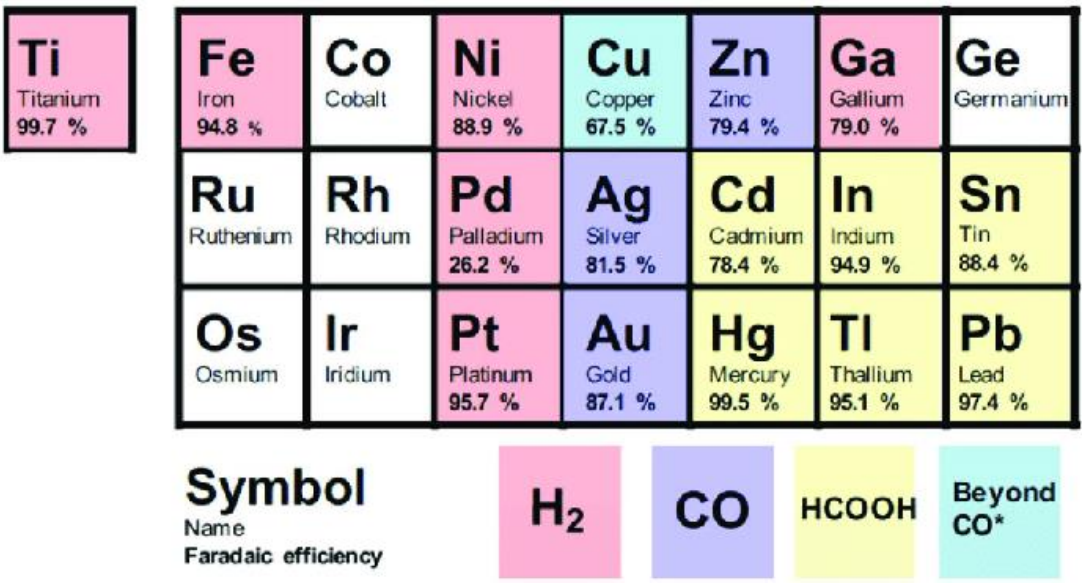

Figure 2.1 A subsection of the periodic table describing the most prominent product obtained under CO_2 reduction conditions. Three categories of catalysts can be identified having an affinity towards producing H_2, CO and HCOO(H). Cu is placed in a fourth category due to its unique interaction with the CO intermediate, allowing it to dimerize into a variety of C_{2+} products. [12]*

be destabilized by temporarily binding to a catalytic site through the insertion of an additional electron, hereby forming the first reaction intermediate, CO_2-*. The CO_2-* molecule can have different modes of binding to the surface, as well as having specific binding strengths for its subsequent intermediates, depending on the catalytic material and environmental conditions. As depicted in Fig 1.4 by analyzing the products formed during CO_2 reduction, some catalytic metals do not bind with the CO_2 molecule (Ti, Pt) or bind it too strongly (Pd), disabling the active site, and instead only producing H_2 through the hydrogen evolution reaction (HER). This reaction is considered a parasitic loss, as it wastes electrons that were supposed to be used to reduce CO_2. Other metals such as Sn and Pb are found to be effective at converting CO_2 to formic acid (HCOOH) and its anionic counterpart formate ($HCOO^-$). A third group of transition metal catalysts, containing Ag and Au effectively strip away one oxygen molecule from CO_2 (Eq. 1), after which a weakly bound CO* intermediate is quickly released, selectively forming CO. One exceptional catalyst, Cu, is able produce CO* and retain it long enough to facilitate protonation and dimerization reactions between multiple CO* molecules, resulting in a range of up to 18 different products on the same catalyst. [2]

The 'best catalyst'

With the goal of finding the illustrious 'best catalyst', researchers from across the world have been studying the CO_2 reduction reaction for decades. In order to quantify what the 'best catalyst' is, a set of three electrochemical parameters need to be assessed.

Firstly, the **activity** describes a relationship between applied voltage and measured current. When measuring current under a constant potential, also known as chronoamperometry, some catalysts are capable of achieving higher current densities than a catalyst that suffers from larger electron transfer resistance and therefore achieve a lower current density. Likewise, in chronopotentiometry, where the potential is measured under a constant applied current, a lower voltage indicates a more efficient conversion of electrons into chemical bonds. For this thesis, all experiments are of chronopotentiometric nature, so that the effects of elevated current densities can be measured and compared.

While efficient electron transfer lowers the cost of operation, it is important to assess what chemicals are produced. Therefore, the second electrochemical parameter is **selectivity**, which is used to assess the effectivity of electron transport to each

product. Selectivity is described by the Faradaic efficiency or F.E. and is calculated by creating a ratio between the equivalent charge that is fixated within the outgoing products and the total electrical charge of the consumed electrons, as shown in Eq. 6.

$$\boldsymbol{F.E.} = \frac{\boldsymbol{electrons_{out}}}{\boldsymbol{electrons_{in}}} * \mathbf{100\%} = \frac{\boldsymbol{z*n*F}}{\boldsymbol{I*t}} * \mathbf{100\%} \qquad \textbf{(6)}$$

Here z is the number of electrons per product *[mol e^-/mol P]*, n is the amount of product *[mol P]*, F is Faraday's constant used to convert molar quantity to total charge *[96485 C/mol e^-]*, I is the applied current *[C/s]* and t is the duration of production *[s]*. Ideally 100% of the implemented electrons are transferred into the CO_2 reduction product of choice, but in reality an array of undesired conversion reactions take place. Facilitated by the non-uniform function of the catalyst and transient local conditions, we find alternative CO_2 reduction reactions as well as the hydrogen evolution reaction (HER) among these parasitic side reactions. Besides the lost electricity, low product selectivity towards the desired product can cause post-process separation cost to increase. Therefore, selectivity is a key parameter in catalyst development.

Last but not least, **stability** needs to be considered. Long term stability is a necessity for any industrially relevant system. In general, stability can be considered as the duration a system can operate before it starts malfunctioning. During CO_2 electrochemistry specifically, stability can be affected in a variety of ways. As will be discussed in Chapter 3, simply increasing the rate of the reaction can alter the activity, selectivity and stability of the catalyst significantly. The catalyst surface can reform or sinter together due to the applied potential and acidity/alkalinity of the environment, changing the interaction of intermediates with the catalyst, or replacing the reaction with HER. Applied potential can also lead to flooding of catalyst supports when using gas-liquid based systems in particular, restricting CO_2 mass transport towards the catalyst. Additionally, accumulation of reactants, products and spectator molecules during rapid electrolysis can ultimately lead to the formation of salt deposits on the surface that can sabotage the entire system, as will be further explored in Chapter 4.

Hori's benchmarking study

By testing all types of metals, organic molecules, mixtures, alloyed compositions and many more under a broad range of conditions, the research community has attempted to find the catalyst with the lowest potential, highest single product selectivity and longest stability. One of the most relevant studies in this category was the research

performed by *Y. Hori et al.* in 1994. [3] Their work addresses how fundamental difficulties related to the CO_2RR cause many confusions and contradictions in the field of electrochemistry. They highlight how metallic impurities in the electrolyte can affect the catalyst performance, how electrochemical equilibria are continuously perturbed due to dissolution of CO_2 and changes in pH at the electrode during electrolysis and how differences in the experimental methods can lead to disagreeing results. The work then continues by describing a meticulous method that was followed to benchmark 17 different planar metal electrodes under identical conditions for their CO_2 reduction capabilities, a summary of which is shown in Table 2.1. These experiments were performed in an H-cell, an electrochemical device that uses two compartments for the electrodes, separated by a membrane. This configuration allows the user to deploy reference electrodes, hereby distinguishing between anode and cathode performance. Section 2.2 will further elaborate on the advantages and disadvantages of the H-cell reactor and how its successors were able to circumvent limitations of the previous systems. The precise work by Hori et al. has become an anchor point for researchers in the past decades not only for improving cathodic catalyst understanding, but also for showing the detail in methodology required to obtain comparable and reliable results.

Faradaic Efficiencies of Products in CO_2 Reduction at Various Metal Electrodes. Electrolyte: 0.1 M $KHCO_3$, T = 18.5 ± 0.5°C. Reprinted from Ref. 23, Copyright (1994) with Permission from Elsevier

Electrode	Potential vs. SHE V	Current density mA cm^{-2}	Faradaic efficiency, %							
			CH_4	C_2H_4	EtOH[a]	PrOH[b]	CO	$HCOO^-$	H_2	Total
Pb	−1.63	5.0	0.0	0.0	0.0	0.0	0.0	97.4	5.0	102.4
Hg	−1.51	0.5	0.0	0.0	0.0	0.0	0.0	99.5	0.0	99.5
Tl	−1.60	5.0	0.0	0.0	0.0	0.0	0.0	95.1	6.2	101.3
In	−1.55	5.0	0.0	0.0	0.0	0.0	2.1	94.9	3.3	100.3
Sn	−1.48	5.0	0.0	0.0	0.0	0.0	7.1	88.4	4.6	100.1
Cd	−1.63	5.0	1.3	0.0	0.0	0.0	13.9	78.4	9.4	103.0
Bi[c]	−1.56	1.2	-	-	-	-	-	77	-	-
Au	−1.14	5.0	0.0	0.0	0.0	0.0	87.1	0.7	10.2	98.0
Ag	−1.37	5.0	0.0	0.0	0.0	0.0	81.5	0.8	12.4	94.6
Zn	−1.54	5.0	0.0	0.0	0.0	0.0	79.4	6.1	9.9	95.4
Pd	−1.20	5.0	2.9	0.0	0.0	0.0	28.3	2.8	26.2	60.2
Ga	−1.24	5.0	0.0	0.0	0.0	0.0	23.2	0.0	79.0	102.0
Cu	−1.44	5.0	33.3	25.5	5.7	3.0	1.3	9.4	20.5	103.5[d]
Ni	−1.48	5.0	1.8	0.1	0.0	0.0	0.0	1.4	88.9	92.4[e]
Fe	−0.91	5.0	0.0	0.0	0.0	0.0	0.0	0.0	94.8	94.8
Pt	−1.07	5.0	0.0	0.0	0.0	0.0	0.0	0.1	95.7	95.8
Ti	−1.60	5.0	0.0	0.0	0.0	0.0	tr.	0.0	99.7	99.7

[a]ethanol; [b]n-propanol; [c]the data are taken from Hori et al.[23] except Bi which is read from an illustration in a paper by Kunugi et al.[117]; [d]the total value contains C_3H_5OH(1.4%), CH_3CHO(1.1%), C_2H_5CHO(2.3%) in addition to the tabulated substances; [e]the total value contains C_2H_6(0.2%)

Table 2.1 The results of the benchmarking performed by Y. Hori showing the electrochemical characterization of various metal electrodes under CO_2 reduction conditions. By keeping identical cleaning, preparation, and testing procedures the tested metals could be compared as fairly as possible in terms of their required potential and product selectivity. [1]

However, the arrival of new systems allowed much faster conversion rates over the same geometric area and with that a divergence from the ideal controlled environments that are available in H-cells. Chapter 3 shows how a similar meticulous style of experimentation is used to obtain an updated version of Hori's benchmark.

2.2 Shapes and sizes of CO_2 electrolyzers

Prior to the rapid development of highly active heterogeneous catalysts we see today, exploratory work on CO_2 reduction catalysts started in aqueous H-cells. The ongoing development of CO_2 reduction electrolysers has been performed primarily in three individual systems, the H-cell, the flow cell and the membrane electrode assembly (MEA), all represented in Fig. 2.2. Here we present several reactor architectures that can be used for electrochemical CO2 reduction and discuss the benefits and shortcomings of each of these configurations.

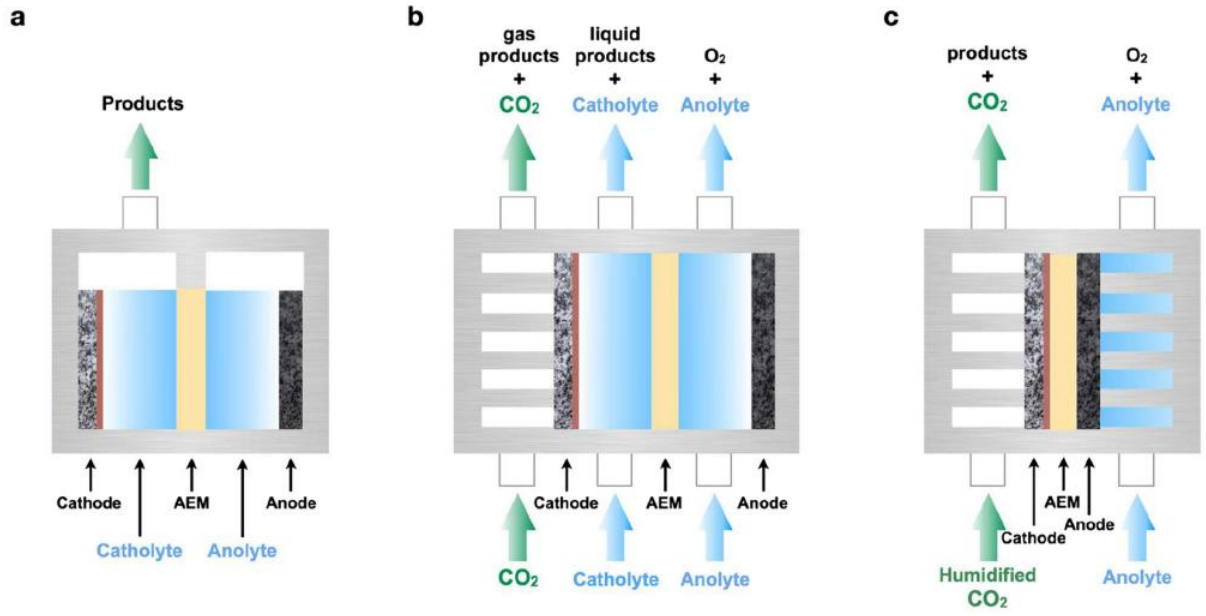

Figure 2.2 Schematic representations of the different electrochemical reactors used to study the CO_2 reduction reaction. (a.) The H-cell with its two liquid compartments would often be operated in batch mode. (b.) a gas diffusion electrode reactor configuration with flowing catholytes and anolytes, and (c.) a membrane electrode assembly with no catholyte and back-fed anolyte. [4]

H-cells and membranes

The first CO2RR experiments were performed in aqueous reactors consisting of two liquid compartments and a separative membrane, called an H-cell, named after its frequently used H-shape. Each side of the H-cell performs one of the complementary half reactions and a membrane is positioned in between the compartments to prevent

the crossover of products. The opposing anode and cathode compartments are filled with an electrolyte solution named after its respective catalyst environment, the catholyte and anolyte (see Fig. 2.2a).

Reference electrodes are often introduced in the anolyte and catholyte compartments, in order to create a 3- or 4-electrode setup with a known reference potential to measure cathodic and anodic current/voltage that take into account resistive losses in electrolyte and membrane. The scientific research that has gone into understanding the CO_2RR has progressed much because of detailed studies that could be performed in the H-cell under highly controlled conditions. By testing finely tuned catalysts and monitoring factors like temperature, electrolyte pH, product concentrations and electrical resistance, the characteristics of the system were identified, resulting in a deeper understanding of onset potentials, resistive losses and chemical side reactions.

The presence of a membrane in between the two compartments prevents products from transferring to the opposing catalyst and thereby performing the reverse redox reactions, effectively consuming the formed products and nullifying the energy put in. While the transfer of products is limited, both compartments still need to communicate in order to close the electrical circuit. The membrane allows for the transport of ionic species across each compartment and can be generally classified in following categories: cation or proton exchange membranes (CEMs/PEMs), anion exchange membranes (AEMs) and bipolar membranes (BPMs). All membranes make use of polymers that contain a carbon backbone that provides mechanical stability, while each membrane has a unique internal structure giving it its characteristic ion transport feature. As the names suggest, the fixed charge groups of that exist within the AEMs (positively charged) and CEMs (negatively charged) allow only oppositely charged ions to pass through, as is schematically shown in Fig. 2.3. BPMs consist of a stacked CEM and AEM in direct contact, combining both functionalities. While limiting the interaction of the catholyte and anolyte, the BPM is able to regulate the dissociation of water into H^+ and OH^- to resupply ions consumed at the electrodes. The BPM has an opportunity to enable individual tuning of both electrolytes to their desired operation, for example, allowing anodic reactions to proceed in more favorable alkaline conditions, while cathodic reactions can be performed at neutral or acidic pH. However, the energy needed to dissociate water internally plus the resistance of the

multi-layered membrane result in a severe increase of required potential, making it an ineffective industrial solution as of yet.

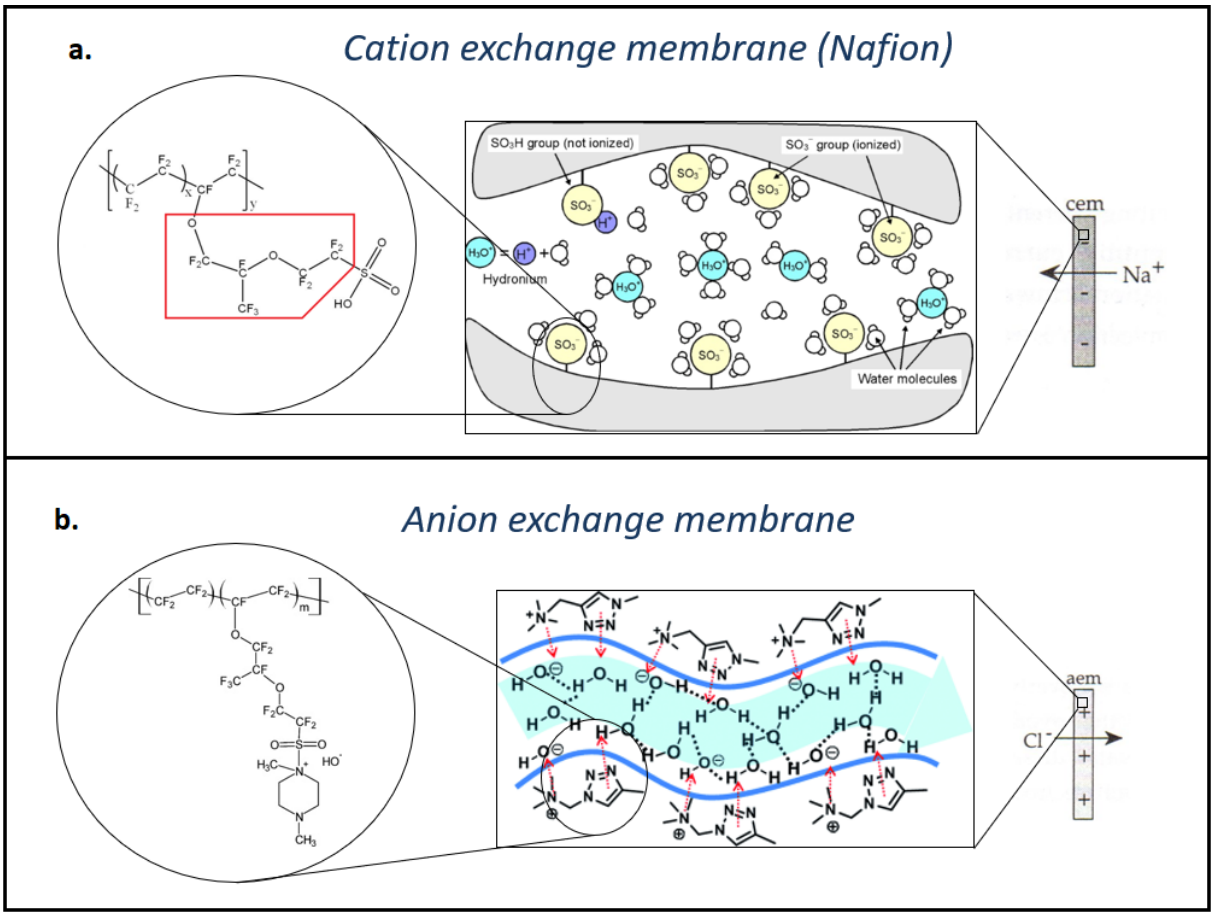

Figure 2.3 Schematic visualization of two mono-polar membranes. The cation exchange membrane facilitates the transport of positively charged species by retaining those momentarily on fixed side groups of negatively charged groups, such as sulfonates (SO_3^-). The anion exchange membrane shown here makes use of quaternary amine (NR_4^+) side groups to attract and conduct negatively charged ions.

Flow cells and membrane electrode assemblies

To perform CO_2 reduction in an H-cell, a gas flow of CO_2 is often introduced into the catholyte compartment directly, dissolving CO_2 until saturation is achieved. The limited diffusivity (D = 0.0016 mm^2/s) and solubility (~33mM) of CO_2 in water causes the CO_2 mobility to be low and the CO_2 reduction activity to be limited to 30-40 mA/cm^2. Designer catalysts are developed to lower the onset potential of the reaction or focus the catalysts performance towards a specific product. These catalysts are often still tested in H-cells at extremely low current densities of <10 mA/cm^2, in which their functionality is proven. While this rate of reaction was adequate for scientific

exploration of catalysts, it would not be sufficient to achieve an economically attractive system. In addition, the thick electrolyte layer between the electrodes resulted a large resistance for the reaction, which further limited the techno-economic feasibility of the system.

In the past decade, CO_2 reduction research has increased significantly. [5] This surge in interest can be ascribed partially to the renewed societal desire to industrialize CO_2 valorization, but more importantly to the introduction of a component in this system that assisted heterogeneous catalysis in achieving this goal, the gas diffusion layer (GDL). The GDL is a conductive sheetlike material that has been functionalized to allow a gas and liquid phase to be in close contact with one another, without the liquid entering into the gas phase or vice-versa. As can be seen in the top-right section of Fig. 2.5, the backing layer of the GDL consists of rigidly compressed carbon fibers that provide mechanical stability, electrical conductivity and adequate porosity to allow the unrestricted flow of gasses. On other side is the Microporous layer (MPL), which prevents liquid from flowing through the GDL and into the gas phase. On this side the GDL is coated in a hydrophobic mixture, preventing water from freely entering the gas phase. [7]

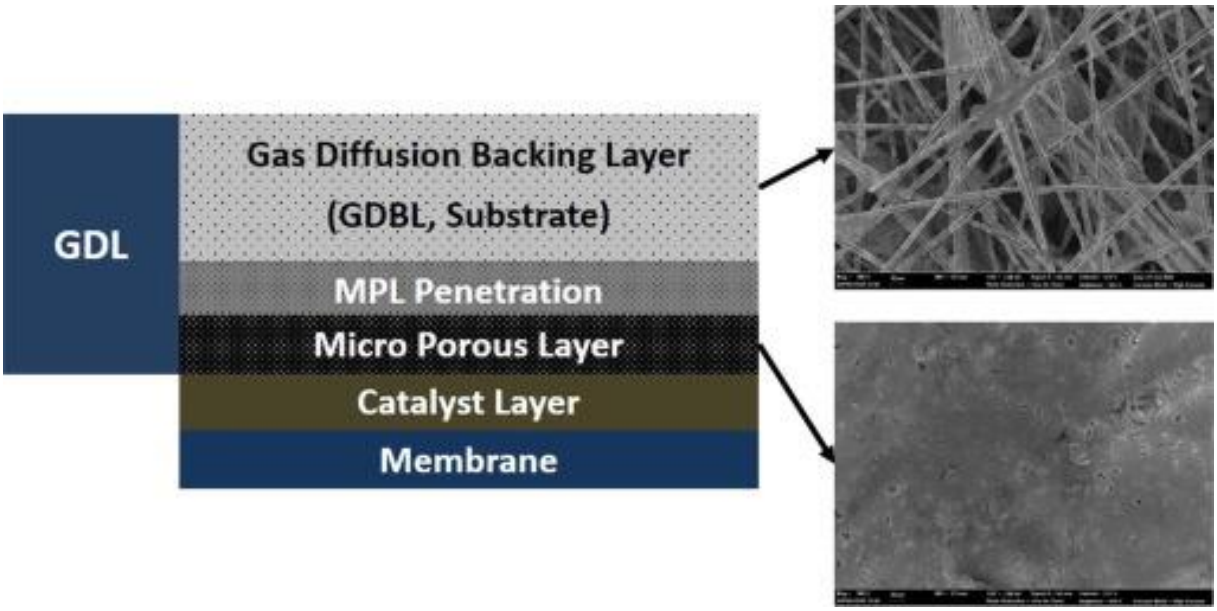

Figure 2.4 The composition of an MEA in steps. A GDL is formed by compressing carbon fibers together to form the backing layer (top-right) and smoothening it with a hydrophobic PTFE/carbon black mixture to form the MPL (bottom-right). A catalyst layer can then be deposited on top of the MPL to

produce a GDE, which can be deployed in a flow cell. Alternatively, the GDE altogether can be fused with the membrane, ultimately creating an MEA. [6]

In the interest of CO_2 electrolysis, a catalyst layer can be deposited on top of the MPL through a variety of deposition methods, such as spray coating, sputtering or hand painting among many others. The combination of a GDL substrate with a catalyst layer is considered a gas diffusion electrode (GDE). The GDE can be placed in a system called a flow cell (see Fig. 2.2b), which in theory works the same as an H-cell, except now the reactant CO_2 gas can be fed to the catalyst from the backside of the GDL and the formed gaseous products could also escape through the backside. Due to the much faster transport of reactants to and products from the catalyst, the flow cell system allows CO_2 electrocatalysis to be performed 1-2 orders of magnitude faster than in H-cells over the same geometric area.

The electrical intensification of the surface is a great push towards industrial implementation, however, the flow cell system still has many shortcomings. While the currents are increased using this configuration, the ohmic losses of the electrolyte that scale with the total current also increase with reaction rate. Further, the GDE is also not able to maintain its hydrophobic characteristic under these highly electrified conditions, as the flow of electrons gradually draw the electrolyte through the MPL. [8] Simultaneously, the flow of liquid and gas close to one another causes a pressure drop over the GDE, making phase separation less stable over time, though this can be omitted by introducing back pressure regulation. In Chapter 3 the flow cell and the electric intensification of the surface will be studied for a range of catalysts. In this thesis we will see how an increase in current density affects the required potential due to increased ohmic losses, we see a change in selectivity as local concentrations of intermediates change, and how the stability of both the gas-liquid interface and the catalyst layer are affected.

The most recent developments of CO_2 electrolysis have been made using a membrane electrode assembly (MEA) (Fig 2.2c). The MEA places the GDE directly against the product-separating membrane (Fig. 2.5), thereby completely removing the catholyte and placing the anode and cathode in close proximity from one-another. This architecture reduces the ohmic losses of the system severely, causing the operational potential to be much closer to the theoretical minimum potential. While allowing a further increase in current density, the MEA also suffers from its own limitations. The

fast reaction rates and high concentration of negative charges at the cathode during operation leads to the detrimental formation of salt deposits on the surface, as will be further explored in Chapter 4.

From a theoretical point of view, the scientific research that has gone into understanding the CO_2RR has come a long way due to detailed studies under highly controlled conditions. By testing finely tuned catalysts at slow reaction rates in H-cells, while optimizing environmental factors like electrolyte concentrations and cation species, the function and operation of various catalysts was understood. The introduction of GDEs has been beneficial to the industrial relevance of CO_2 electrolysis, yet simultaneously causing a large influx of new knowledge. The knowledge of catalyst functionality in H-cells does not linearly translate to the newly introduced flow cell and MEA systems. In addition, the use of GDE systems has made in situ studying of the catalyst much more complex. This thesis focuses on better understanding the transferability of H-cell knowledge to flow cell systems under elevated current densities, and what transient behaviors in activity, selectivity and stability are observed when pushing the GDE system to its limits.

References Chapter 2.

1. Hori, Y., *Electrochemical CO_2 Reduction on Metal Electrodes*, in *Modern Aspects of Electrochemistry*, C.G. Vayenas, R.E. White, and M.E. Gamboa-Aldeco, Editors. 2008, Springer New York: New York, NY. p. 89-189.
2. Kortlever, R., et al., *Catalysts and Reaction Pathways for the Electrochemical Reduction of Carbon Dioxide*. The Journal of Physical Chemistry Letters, 2015. **6**(20): p. 4073-4082.
3. Hori, Y., et al., *Electrocatalytic process of CO selectivity in electrochemical reduction of CO2 at metal electrodes in aqueous media.* Electrochimica Acta, 1994. **39**(11): p. 1833-1839.
4. Hung, S.-F., *Electrochemical flow systems enable renewable energy industrial chain of CO2 reduction*. 2020. **92**(12): p. 1937-1951.
5. Endrődi, B., et al., *Continuous-flow electroreduction of carbon dioxide.* Progress in Energy and Combustion Science, 2017. **62**: p. 133-154.
6. Park, J., et al., *A review of the gas diffusion layer in proton exchange membrane fuel cells: Durability and degradation.* Applied Energy, 2015. **155**: p. 866-880.
7. Schweiss, R., et al., *SIGRACET® Gas Diffusion Layers for PEM Fuel Cells, Electrolyzers and Batteries (White Paper)*. 2016.
8. Yang, K., et al., *Role of the Carbon-Based Gas Diffusion Layer on Flooding in a Gas Diffusion Electrode Cell for Electrochemical CO2 Reduction.* ACS Energy Letters, 2021. **6**(1): p. 33-40.

Chapter 3.

Characterizing CO_2 reduction catalysts on gas diffusion electrodes

Comparing activity, selectivity and stability of transition metal catalysts.

Continued advancements in the electrochemical reduction of CO_2 (CO_2RR) have emphasized that reactivity, selectivity and stability are not explicit material properties, but combined effects of the catalyst, double-layer, reaction environment and system configuration. These realizations have steadily built upon the foundational work performed for a broad array of transition metals performed at 5 mA cm^{-2} which historically guided the research field. To encompass the changing advancements and mindset within the research field, an updated baseline at elevated current densities could then be of value. Here we seek to re-characterize the activity, selectivity and stability of the 5 most utilized transition metal catalysts for CO_2RR (Ag, Au, Pd, Sn and Cu) at elevated reaction rates through electrochemical operation, physical characterization and varied operating parameters to provide a renewed resource and point of comparison. As a basis we have employed a common cell architecture, highly controlled catalyst layer morphologies and thicknesses, and fixed current densities. Through a data set of 88 separate experiments, we provide comparisons between CO producing catalysts (Ag, Au, Pd), highlighting CO limiting current densities on Au and Pd at 72 mA cm^{-2} and 50 mA cm^{-2}, respectively. We further show the instability of Sn in highly alkaline environments, and the convergence of product selectivity at elevated current densities for a Cu catalyst in neutral and alkaline media. Lastly, we reflect upon the use and limits of reaction rates as a baseline metric by comparing catalytic selectivity at 10 vs 200 mA cm^{-2}. We hope the collective work provides a resource for researchers setting up CO_2RR experiments for the first time.

This chapter is based on: Mark Sassenburg, Reinier de Rooij, Nathan Taylor Nesbitt, Recep Kas, Sanjana Chandrashekar, Nienke J. Firet, Kailun Yang, Kai Lui, Marijn A. Blommaert, Martin Kolen, Davide Ripepi, Wilson A. Smith, Thomas Burdyny. ACS Appl. Energy Mater. 2022, 5, 5, 5983–5994. May 3, 2022. Available Online at https://doi.org/10.1021/acsaem.2c00160

3.1 Introduction

Increasing energy demand is having a significantly negative impact on the global environment due to the emissions associated with the extraction, transport and utilization of fossil fuels. Renewable electricity generated from solar or wind and sustainable feedstocks such as air and water are needed to replace fossil fuels and reduce greenhouse gas emissions in the production of important chemicals and fuels. One promising approach can directly utilize atmospheric CO_2 (or CO_2 captured at point sources) and using renewable electricity to drive the electrochemical reduction of CO_2 to valuable chemicals and fuels.

In the past decade the CO_2 reduction reaction (CO_2RR) has received increasing attention due to its potential to supplant fossil fuels in the production of base chemicals and fuels. The field has built upon pivotal work in the 1990's and 2000's by Yoshio Hori et al. which categorized the activity of transition metal catalysts for CO_2RR under well-controlled conditions at current densities of 5 mA cm^{-2} [1]. These works provided a solid foundation for exploratory catalyst development into each metal, giving the research field a fixed current density point of comparison. For CO_2RR to be both economically feasible and environmentally impactful, however, significant progress is now needed to make the process efficient and stable at scale. Specifically, large scale facilities (> MW), high current densities (>100 mA cm^{-2}) and long-term stability (>1000 h) with high energy efficiency and single pass conversion efficiency are needed to achieve these goals, while retaining near-uniform selectivity to reduce downstream separation processes [2]. The necessity for process intensification in particular has now led to the rapid increase in current densities to the realm of 100-1000 mA cm^{-2}, which significantly affects the local reaction environment [3], system design [4], catalytic behavior [5] and overall stability [6]. The original controlled experiments characterizing materials at 5 mA cm^{-2} did not experience these consequences of process intensification, motivating the need for an updated reference of base performance of transition metal catalysts that reflect practical industrial conditions.

The use of gas diffusion electrodes (GDEs) have shown the ability to achieve high current densities (>200 mA cm^{-2}) by having the catalyst supported on a microporous substrate at a gas-liquid interface [7], [8], [9], [10], [11]. As the CO_2RR community begins to use such electrode architectures that allow concentrated gas-phase CO_2 to be fed close to the cathode, greater emphasis has been placed on understanding the

interconnected factors which govern the electrocatalytic performance as the scale and intensity of the system increases. While the electrode potential is ultimately the driving force that allows surface reactions to occur, the reaction environment is heavily influenced by current density and mass transport. For example, recent studies on catalysts deposited on GDEs have shown that an increase of current density [12], [13] and the use of different electrolytes [6], [14], [15], [16], [17] have effects on product selectivity by varying the local reaction environment. The importance of current density dependent effects such as mass transport and homogeneous reactions is also observed in bicarbonate ($KHCO_3$) electrolysis systems where bicarbonate plays a dual role as a proton and CO_2 source. A study on the direct conversion of a bicarbonate electrolyte ($KHCO_3$) to CO for example showed that CO production was largely retained on a GDE while feeding nitrogen gas instead of CO_2 [18]. These examples highlight the importance of the catalyst's surrounding reactor configuration on the measured performance and using fixed current densities to support previous work performed at fixed cathode potentials.

Another complexity within the field is that most reported works do not describe the experimental setups that are used, and these setups can vary widely between groups. As can the testing conditions that are used (e.g., flow rates, electrolyte, membranes). Furthermore, few works present the data for multiple materials within the same paper as was previously done by Hori et al. at 5 mA cm^{-2}. An updated baseline data set of the most commonly used transition metals may then act as a reference for both new and established researchers in the field. In particular a data set where the experimental setup and the catalytic material had been well-defined and compared against other catalysts under the same experimental conditions can provide a common foundation for benchmarking experimental setups.

Within this work we compare the baseline CO_2 reduction performance of Au, Ag, Pd, Sn and Cu catalysts deposited on GDEs at fixed current densities within a representative reactor configuration (Figure 3.1) over a broad parameter space. The electronic, structural and electrochemical properties of the GDEs with different catalysts were characterized before and after 1 hour of electrolysis using 2 electrolytes (1 M $KHCO_3$ and KOH) and at 4 applied current densities (10, 50, 100, 200 mA cm^{-2}). Constant current densities were chosen instead of constant potentials in order to control the overall catalytic conversion rate, thus keeping total diffusion and migration

of the involved species comparable in each case. The data set then supplements works using fixed cathodic voltages. During electrolysis at the applied current densities, the products were collected for analysis and the negative voltage was measured with respect to a Ag/AgCl reference electrode. The combined work provides a wide data set for comparison to literature, highlighting features of each of the metals which cannot be elicited from low current density experiments alone.

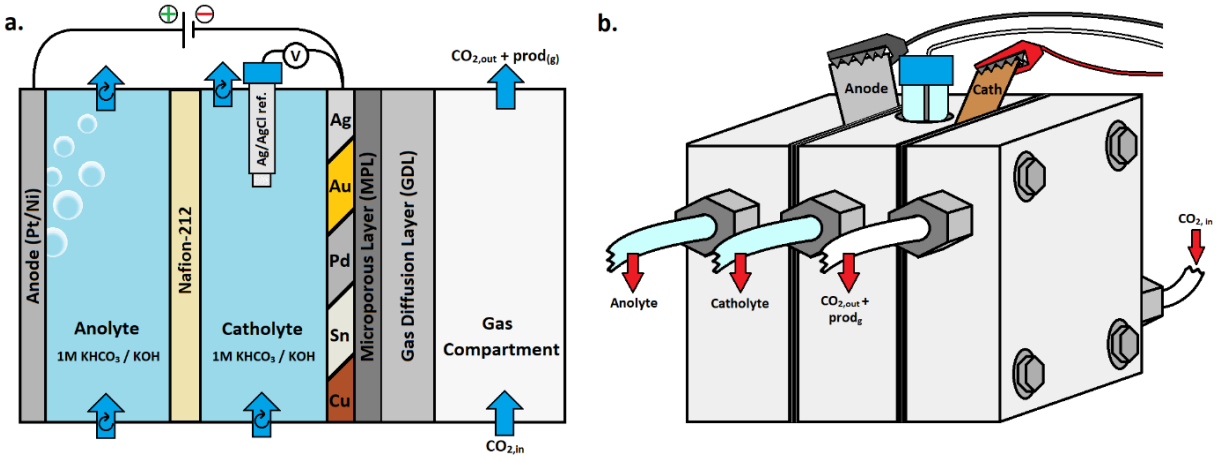

Figure 3.1. Schematic representation of the 3-compartment gas diffusion electrode setup interior (a.) and exterior (b.) used to investigate CO_2 reduction reaction catalysts in neutral and alkaline electrolytes while utilizing a gaseous CO_2 feed.

3.2 Controlled experimental platform and testing conditions

For characterizing the electrochemical performance of the five transition metals, we have chosen to use a fixed cell architecture and catalyst morphology which represents a recognizable baseline for the field. This entails a nanoparticle-based catalyst layer with a nominal catalyst thickness of 100 nm deposited onto a carbon-based gas-diffusion layer with a flowing catholyte configuration (Figure 3.1a). Such an orientation is reflected in a number of publications within the field [19], [20], [21], [22], [23], [24], [16], [25], [26], [27] and such a system acts as a direct comparative baseline for research assessing changes in the type of gas-diffusion layer, catalyst morphology, catalyst loading, electrolyte type, electrolyte concentration and operating conditions (temperature, pressure, current density, voltage). The chosen operating conditions for

our comparisons span a range of current densities (10, 50, 100, 200 mA cm^{-2}) for the two most commonly used electrolytes (1 M $KHCO_3$ and 1 M KOH), thus encompassing common testing conditions in literature.

While the configuration and operating conditions that are chosen for the data set are important, we must make sure that their implementation is extremely well-controlled to ensure both a high level of repeatability of the experimental data, as well as reproducibility of the results by external users. Without providing such regulation and documentation, the baseline cannot function as well as intended. Here we provide large control over both the utilized catalyst, and the testing infrastructure as described below and in detail in the Supporting Information (SI).

To create a repeatable nanoparticle-based catalyst we deposited our 5 metal transition catalysts (Ag, Au, Pd, Sn and Cu) onto a Sigracet 39BB gas diffusion layer (GDL) using magnetron sputtering (AJA International Inc.) to deposit ~100 nm thickness metal catalysts (see detailed description and equipment in SI A). The deposition thickness of the unit was confirmed through profilometry for each individual material. The as-deposited samples then resulted in a nanoparticle layer on the top of the GDL which was similar for each base material as confirmed though scanning electron microscopy (SEM) (JSM-6010LA, JEOL), high resolution SEM imaging (NovaNanoSEM 450, FEI) and AFM (AFM with Icon ScanAsyst, Bruker). The five materials are visualized in Figure S3.21, exhibiting a similar porous structure. Due to the roughness of the GDE and the catalyst layer porosity the thickness of the ensemble is greater than the deposited 100 nm. The elemental composition of the catalyst surface was examined ex-situ by X-ray photoelectron spectroscopy (XPS) (K-Alpha, Thermo Scientific) before and after electrolysis to identify the surface species present on the electrolyte-side of the catalyst layer. Since XPS is performed ex-situ, however, a measure of oxidation from air is expected for surface species for all samples. SEM and XPS analyses allow for the stability of the catalyst layer to be examined from a morphology and contaminant perspective. In order to minimize the influence of residual electrolyte species on the ex-situ SEM and XPS results, a rinsing protocol with DI water and drying was included (See SI A). All catalysts were deposited homogeneously on a 4.4 cm^2 square electrode area, with a geometric active electrode area of 2.25 cm^2 exposed to the electrolyte while placed in the assembled

electrochemical cell. Lastly, a new sample was used for each electrochemical experiment.

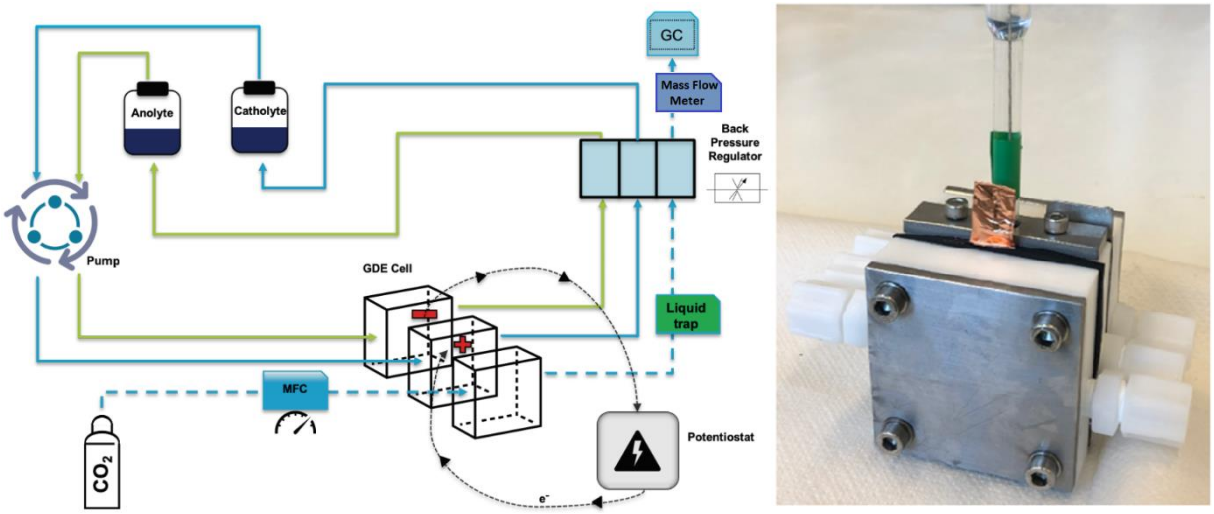

Figure 3.2. Left: schematic drawing highlighting the components of the electrochemical setup. Right: picture of the assembled 3-compartment flow cell.

While control over the catalyst deposition and morphology is of critical importance, so too is the robustness of operating the electrochemical system itself. Operating GDE systems for CO_2 electrolysis are challenging for a number of reasons relating to electrode flooding [28], [29], penetration of CO_2 into the liquid phase, CO_2 consumption by the electrolyte [30], and pressure-imbalances caused by fluid flow and gas chromatography (GC) measurements. Here we demonstrate a system which incorporates back-pressure regulation (to prevent gas/liquid crossover) and mass flow meters (to identify the gas flow into the GC used in calculations) to maintain the gas-liquid environment as consistently as possible during experiments. GC measurements every 5 minutes lead to some gas pressure increase and gas escaping through the liquid phase, but only after injection of the product gas stream. To improve the confidence in the presented results, duplicates of each experiment were performed.

Electrochemical experiments were performed in a 3-compartment GDE system as shown in Figure 3.2. Technical drawings of the cell compartments are available in the SI (Figure S3.57 to S3.60). The electrochemical setup consists of external liquid bottles containing 80 mL each of the respective anolyte and catholyte connected to a peristaltic pump to recirculate the catholyte and anolyte chambers at 10 mL min^{-1}. It is important to note recirculation of electrolyte could induce transient pH effects due to a combination of continuous acidification by $CO_{2,g}$ reacting with hydroxyls and the

production of hydroxyls at the cathode. In general, a $KHCO_3$ bulk pH shift from 7.8 to 8.5 - 8.8 (@ 200mA cm^{-2}, 1h) was measured for $KHCO_3$. For KOH the dissolution of CO_2 was a more significant factor reducing bulk pH from 13.8 to 13.0 - 12.8. CO_2 was provided using a pure CO_2 bottle and regulated by a mass flow controller to feed the cathode gas compartment at 30 mL min^{-1}. The electrochemical measurements were performed utilizing a ParSTAT MC potentiostat (Ametek SI) to perform 1-hour chronopotentiometry on each sample. The electrochemical cell includes a Ag/AgCl reference electrode, positioned in the catholyte chamber to measure cathodic potential. A liquid trap at the gas outlet of the cell is used to protect the GC in case of flooding. All outlets are connected to a back pressure regulator and enable the balancing of gas and liquid pressures at 1220 mbar, hereby promoting gas/liquid separation. The quantity of gas entering the GC was measured again using a mass flow meter (Bronkhorst EL-FLOW Select), since the conversion and dissolution of CO_2 can lead to great disparity between the in- and outflow. The products of electrochemical CO_2 reduction over 1 hour were measured using online gas chromatography (Compact GC 4.0, Global Analyzer Solutions).

While gas products (CO, CH_4, C_2H_4, H_2) were measured by online GC, post experimental analysis of the accumulated liquid products in the catholyte (formate, ethanol, propanol) were performed using an Infinity 1260 II HPLC (Agilent Technologies). A Nafion-212 membrane was deployed to prevent anionic products from crossing over to the anolyte. As validation, anolyte samples were taken from experiments in which large quantities of formate were expected to be formed. During analysis of the anolyte, product signals were less than 0.5% of the catholyte signal and were thus discarded. Data of product analysis and the electrochemical experiments was combined to show the Faradaic Efficiency (F.E.) and partial current density of the products as a function of applied current density, providing two different perspectives of the same data.

The electrode potentials versus a Ag/AgCl reference were also recorded during experiments and converted to RHE but were not iR-corrected. In the system configuration a large ohmic drop exists, which reduces the accuracy of the iR-correction, particularly due to changes in the electrolyte conductivity with current density [44], temperature and experimental time (See SI A. for further details).

3.3 Results

Here, we present the material and electrochemical characterization for the 5 most commonly investigated transition metal catalysts (Ag, Au, Pd, Sn, Cu) for CO2R. For each of the 5 metals and 2 electrolytes, duplicates of four current densities were tested. In some cases, extra experiments were added to extend observed trends (for Au/Pd) and where stability issues were observed (for Sn). In this work, 88 GDE samples were then fabricated and characterized with chronopotentiometry, product analysis, SEM imaging, XPS, and with that a substantial data set was obtained. For the sake of brevity, only the most relevant data is presented in the following sections, with the most critical findings given greater emphasis. All obtained data is available in *SI B. Characterization Data,* categorized by characterization technique, for use in further studies and comparisons.

While all electrochemical experiments were run for 1-hour, the data presented here uses the selectivity vs current density after the first 20 minutes of operation, averaged over the duplicate experiments. This time was chosen as it simultaneously allowed for the stabilization of product curves from the GC and does not conflate catalyst stability over time with the selectivity of the original catalyst and configuration (e.g., Sn dissolution over time). The stability of the catalyst over the full-length of experiments are however discussed.

Silver

Silver (Ag) is a promising electrocatalyst for the selective conversion of CO_2 to CO and has previously been studied in H-cell [31], [32], [33], [34] as well as in GDE architectures [35], [16]. The selectivity of Ag to produce CO from CO_2 is largely due to the weak binding energy that CO has with Ag surfaces, though there are minor differences with facet/site composition and coordination. A recent study found that 20-30% of the selectivity of Ag towards CO can be tuned towards formate ($HCOO^-$) by increasing the pressure and electrolyte alkalinity without affecting the catalyst stability [36]. When this work was compared to other Ag-GDE studies it showed that CO/ $HCOO^-$ selectivities and energy efficiencies at equal current densities were non-uniform across separate studies, implying the presence of unique parameters for each configuration.

In our work, for all tested current densities Ag shows >80-90 % selectivity towards CO with a gradual shift towards formate as the current density increased (Figure 3.3 a-b). The $HCOO^-$ formation increasing at higher current densities has been previously reported to be an effect of high local pH which favors $HCOO^-$ formation at the expense of CO [37]. Despite the high selectivity of these electrodes, the surface morphology exhibited significant changes in both electrolytes after 1 hour of electrolysis. SEM images (Figure 3.3 c-e), show that after electrolysis in either electrolyte, large (>20 μm) features emerge in fractal-like structures, indicating that electrons are being scattered or absorbed in greater amounts. XPS characterization of these features primarily consist of potassium and oxygen, suggesting that they may be related to salt formation from the electrolytes during or after operation. Ion beam etching was performed on these electrodes and showed pristine Ag under this top layer of K/O *(See SI B: HR-SEM)*. Although the selectivity was minimally affected during the

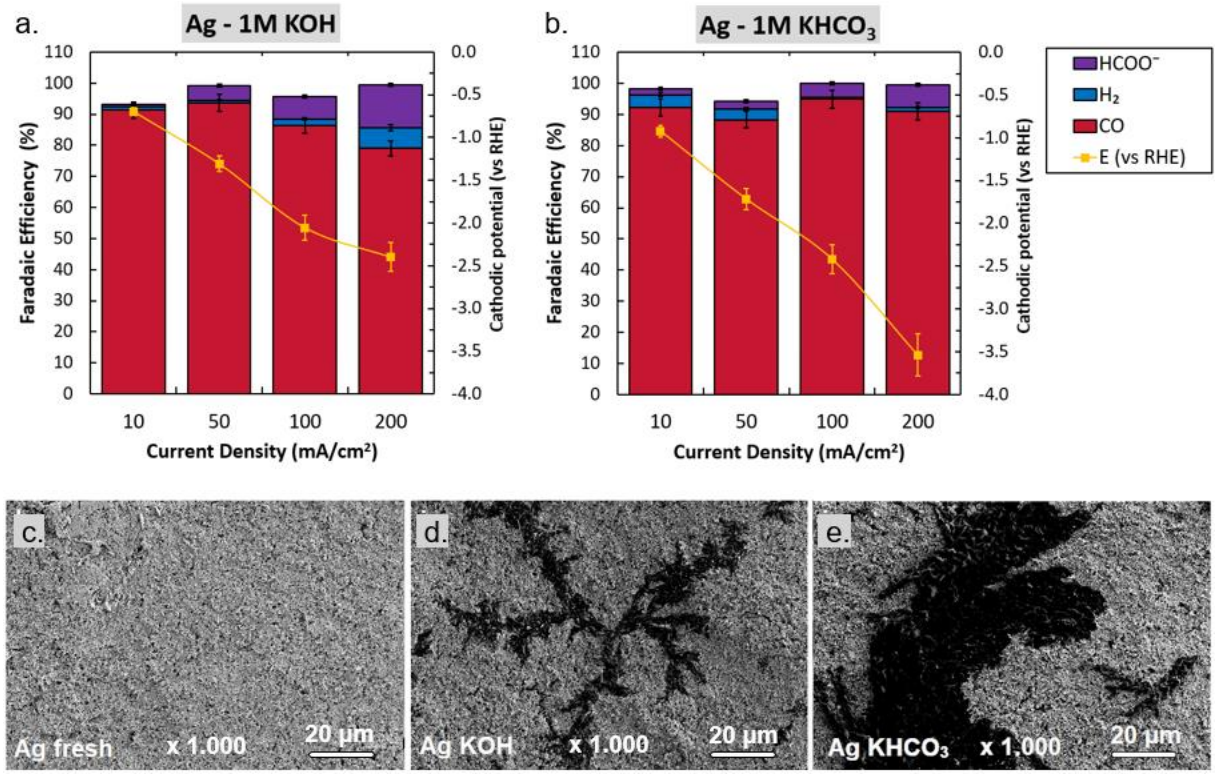

Figure 3.3. Characterization of Ag coated electrodes. Faradaic efficiency as a function of activity with cathodic potentials in 1 M KOH (a.) and 1 M $KHCO_3$ (b.). Error bars in panels a. and b. represent the data points from two separate experiments. SEM images before (c.) and after both 200 mA cm^{-2} experiments (d. - e.) show dark surface coverages.

1h experiments, continuation of electrolysis under these conditions will likely lead to large salt crystals forming on the surface, eventually blocking gas flow and/or rupturing the substrate. A recent paper on the surface coverage and the effects of

electrolyte concentration on K-salt growth has shown similar features which are directly attributed to be potassium carbonate (K_2CO_3) and resulted in a rapid decrease of selectivity to CO after 50% of the surface was covered [38].

From the performed experiments it can be concluded that Ag is an effective CO producing electrocatalyst with high selectivity and low overpotential compared to other catalyst materials presented here. Such a result is not unexpected given silver's prevalence in GDE-based CO2R. Overall, the selectivity for Ag to CO was retained over the evaluated current density range. Increasing current density to 200 mA/cm2 caused the local reaction conditions to become more alkaline over time, promoting the production of formate.

Gold

Gold (Au) has historically been shown to be the best performing CO reduction catalyst in aqueous based H-cells due to its low onset potential for the CO_2RR and high selectivity towards CO [39], [40], [41], [42]. Although Au has shown the ability to lower the initial energy barrier in the CO2RR, increasing current densities above the H-cell regime show a continuous loss of selectivity towards CO while H_2 evolution is promoted. Subsequently, gold is comparatively un-utilized in GDE configurations compared to H-cell systems. In examples where gold has been used in GDEs, low partial current densities towards CO are observed before the hydrogen evolution reaction begins to dominate [43].

Within our experimental data set, we observe a similar limitation from the gold catalysts. Specifically, the 1 M KOH experiments depict a clear downward trend in CO selectivity with increasing current density which occurs earlier than the mass transport limited currents achievable. Plotting the same data as a partial current density instead (Figure 3.4c.), it can be seen that the CO production rate becomes limited to j_{CO} = 72 mA cm^{-2}. In experiments conducted in $KHCO_3$, CO also begins to plateau in the tested range. Comparing material characterization before and after the reaction, XPS scans (Figure S3.41-3.43) show no changes in Au peak intensity and SEM images show no mesoscopic changes to the surface. However, post-experimental XPS results do show peaks for potassium (K 2p) and oxygen (O 1s), due to the formation of (bi)carbonate on the catalyst surface similar in nature to the peaks observed for the Ag catalyst, but in lower quantities.

Aside from the decaying selectivity towards CO, the most interesting Au result is the observed limiting current density of 72 mA cm^{-2} in 1 M KOH. To assess whether the limitation was due to surface site availability we doubled the sample thickness to 200 nm nominal thickness and tested over the same range of current densities. At this thickness the entire catalyst layer should still have ample access to CO_2. However, these 200 nm samples showed near identical results to the thinner 100 nm samples (see dotted line in Figure 3.4c.). Similar studies on pure Au resulted in limiting current densities of j_{CO} = 35 mA cm^{-2} [13] and to 100 mA cm^{-2} [43]. Further research is required to determine whether this limitation towards CO is intrinsic to Au and to better understand which conditions might affect the value of the plateau current.

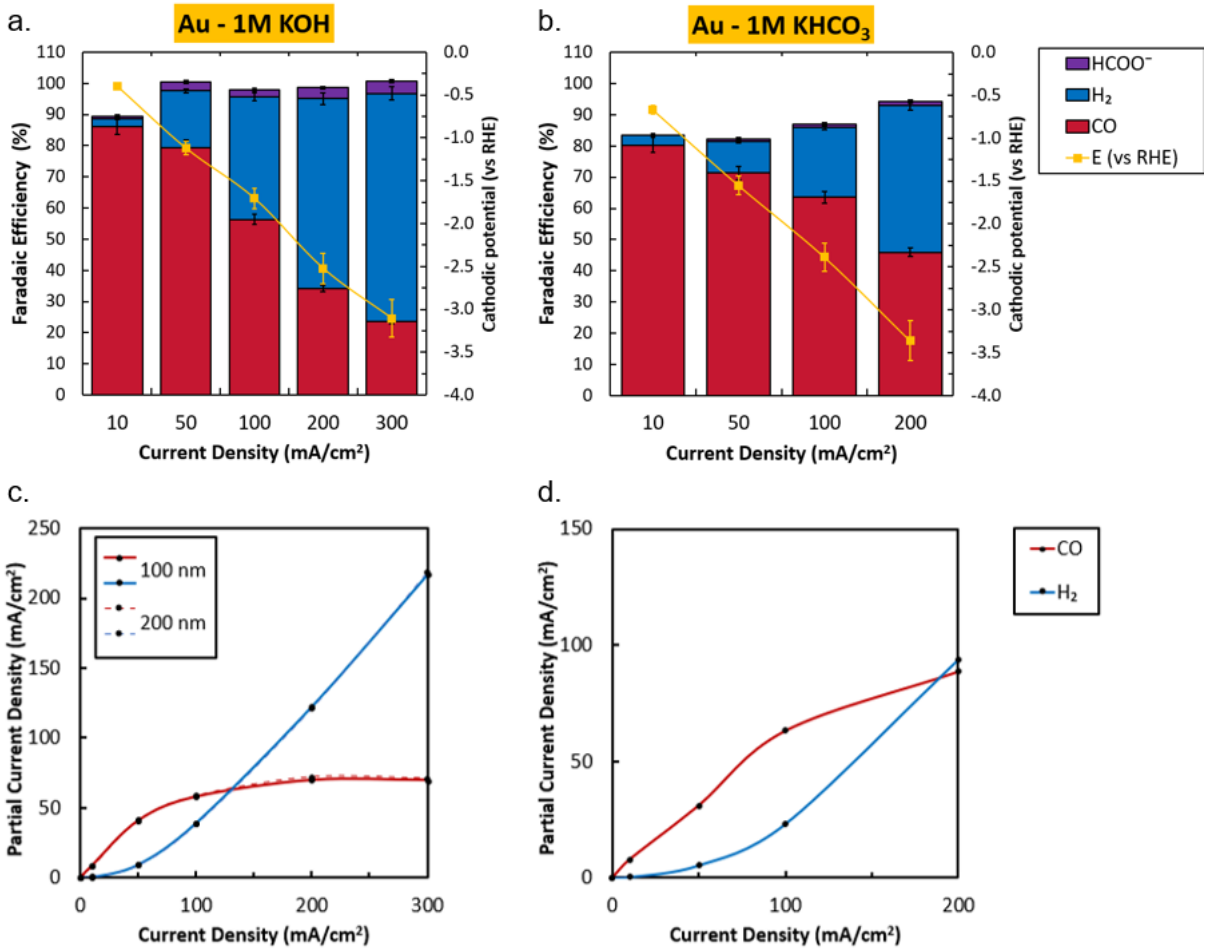

Figure 3.4. Characterization of Au coated electrodes. Faradaic efficiency as a function of activity with cathodic potentials in 1 M KOH (a.) and 1 M $KHCO_3$ (b.). Error bars in panels a. and b. represent the data points from two separate experiments. The correlated partial current density for 1 M KOH on 100 and 200 nm Au (c.) show a limiting CO current density of 72 mA cm^{-2}. The partial current density of Au in 1 M $KHCO_3$ (d.) can be seen to level off at a slightly higher value. Blue and red lines are added to visualize the limiting trend of CO and the gradual increase of H_2.

Palladium

Palladium (Pd) has been studied as a single crystal electrode for CO_2 reduction [45] and as a nanoparticle catalyst [46], [47], [48], in which CO and formate were found as the main carbon containing products at different electrode potentials. Within our experiments shown in Figure 3.5, Pd exhibits high initial selectivity towards CO at 10 mA cm^{-2}, but shows steadily increasing HER selective behavior as a function of current density, similar to what was seen for Au, and only trace amounts of formate. Minimal amounts of formate were found for all the experiments across the entire applied current range. Similar to what was observed for gold, the partial current densities indicate a limiting current density to CO of approximately 50 mA cm^{-2}. XPS results reveal that during the experiments potassium accumulates on the surface accompanied

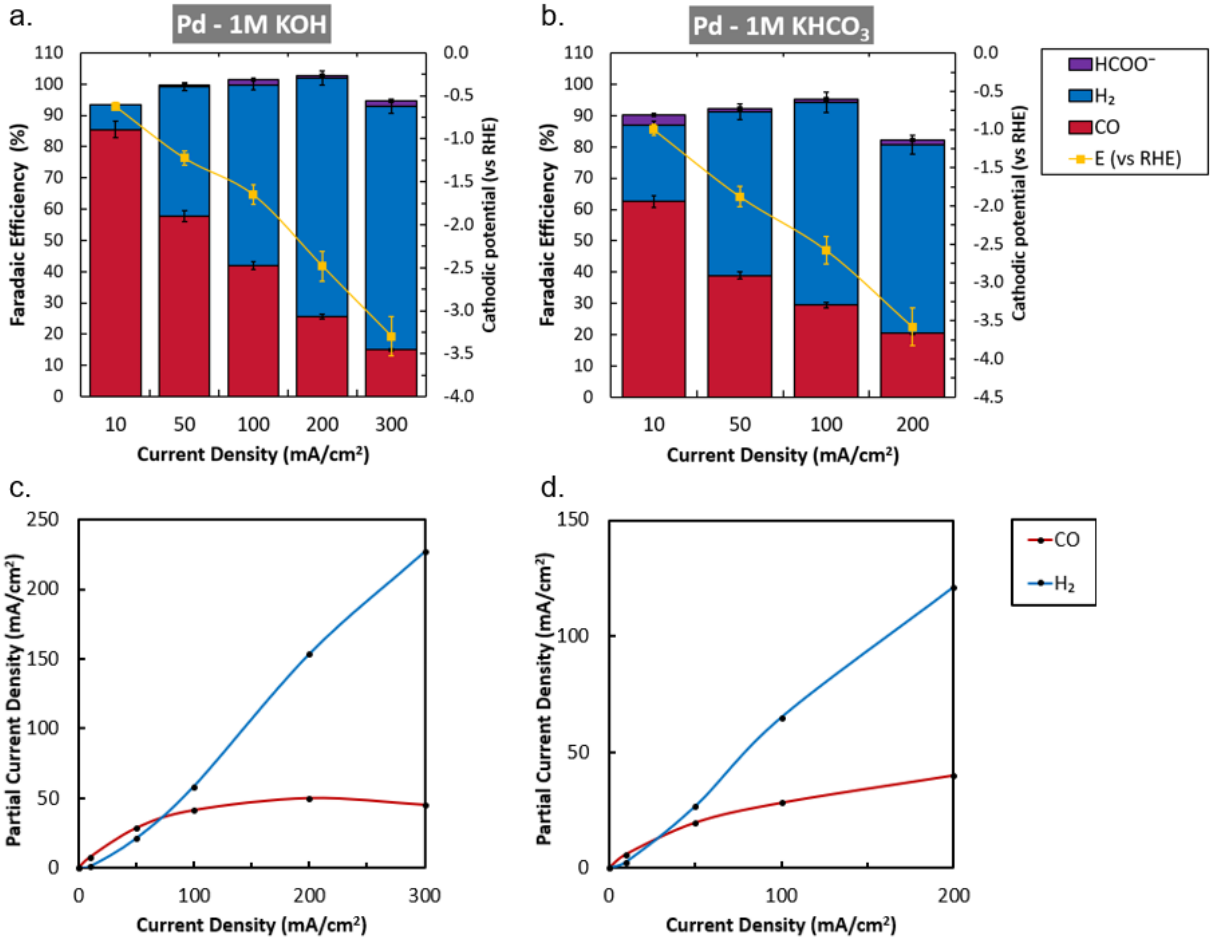

Figure 3.5. Characterization of Pd coated electrodes. Faradaic efficiency as a function of activity with cathodic potentials in 1 M KOH (a.) and 1 M $KHCO_3$ (b.). Error bars in panels a. and b. represent the data points from two separate experiments. The correlated partial current density for Pd in 1 M KOH (c.) show a limiting CO current density around 50 mA cm^{-2}. The partial current density of Pd in 1 M $KHCO_3$ (d.) levels off at a slightly lower value while the HER continually increases. Blue and red lines are added to visualize the limiting trend of CO and the gradual increase of H_2.

by a slight decrease in Pd 3d signal, indicating partial coverage. Before electroreduction the Pd catalyst already showed oxygen content comparable to after the experiment, however, a peak shift towards slightly lower binding energies is witnessed after both KOH and $KHCO_3$ experiments, indicating a change in the role of oxygen. SEM images before and after applying current seem relatively stable for $KHCO_3$, except for localized impurities. Additional SEM images for the electrodes operating in KOH at intermediate current densities (especially at 100, 200 mA cm^{-2}, see SI B) show a wide variety of drastic morphological surface changes.

Unlike Au, previous literature performed at lower current densities suggests that Pd experiences a plateau current density for CO due to surface poisoning by CO at lower overpotentials [49], [50], [51]. Here, at the elevated operating potentials, it is however unclear if this is limiting its performance. From the results here the overall high level of H_2 formation and the relatively large required overpotentials make pure Pd nanoparticles an inadequate catalyst for large scale utilization in its present form. Alternatively, Pd might find its use as a bimetallic co-catalyst, as past studies have shown it to be an interesting metal to tune dimerization to multi-carbon products [52], [53] due to its strong binding with CO.

Tin

Tin (Sn) is a catalyst studied for its highly selective formation of formate [55], [56], [57], [58], [59]. Finding a highly selective formate ($HCOO^-$) catalyst can be helpful for the development and implementation of CO_2 reduction technologies. Alongside CO, formate is another chemical building block that can be used as a reactant in further downstream synthesis, but can also be used as a renewable feedstock in biosynthesis towards fine chemicals [54]. Sn does suffer from poor stability, leading some researchers to investigate alloying and adding ionomers and binders to protect the Sn catalyst [60], [61], [62], [63].

Here, GDEs deposited with Sn show high selectivity towards formate throughout all experiments across the entire applied current range. At an applied current density of 200 mA cm^{-2} the system lost selectivity towards carbon containing products, reflected by the increase in hydrogen evolution over the duration of the experiment. An explanation for this is provided by observing the XPS spectra, where a scan of the Sn 3d peaks show a significant decrease of Sn after the $KHCO_3$ experiment and near-

complete disappearance after 1h operation in KOH, indicating the loss of Sn during electrolysis due to dissolution in the highly alkaline conditions, as described by the Sn Pourbaix diagram. The O 1s peaks also show decreased signal, following the trend of Sn 3d. Potassium uptake is relatively low for these samples, as is displayed by less prominent K 2p peaks (right peaks of Figure 3.6 c). SEM images of Sn samples after reaction in $KHCO_3$ show no clear morphological changes, aside of slight bleaching near GDL native cracks (as shown in zoomed out SI images). Crystals (different from the earlier seen (bi)carbonate) were also found in KOH experiments. These crystals were likely formed by a combination of the dissolution of Sn in the highly alkaline environment, while the applied potential caused localized redeposition in a more stable agglomerated form.

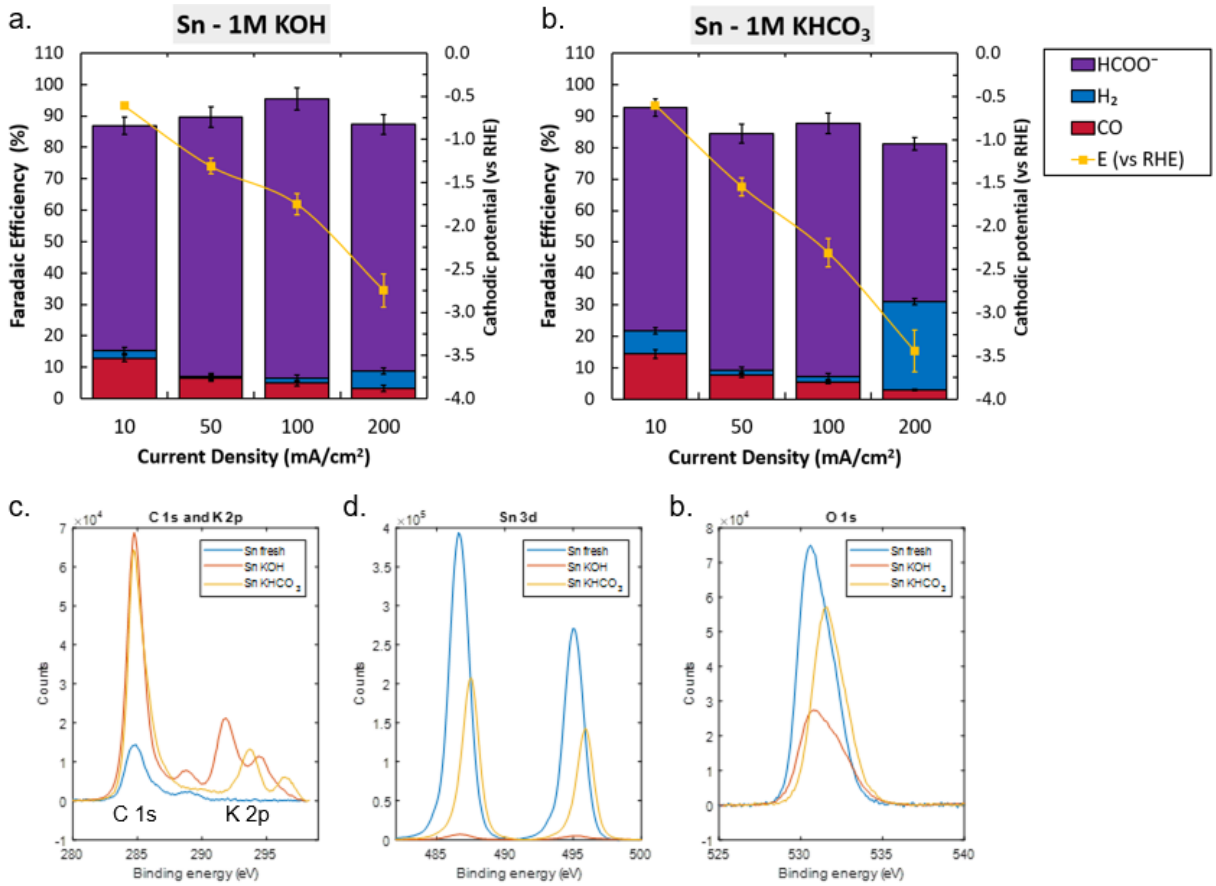

Figure 3.6. Characterization of Sn coated electrodes. Faradaic efficiency as a function of activity with cathodic potentials in 1 M KOH (a.) and 1 M $KHCO_3$ (b.). Error bars in panels a. and b. represent the data points from two separate experiments. XPS results for C 1s and K 2p (c.), Sn 3d (d.) and O 1s (e.) scans before and after the 200 mA cm^{-2} experiment in both electrolytes.

Overall Sn has shown to be an effective catalyst for the selective production of $HCOO^-$ throughout many years of prior research, and this trend is confirmed here.

However, the lack of stability at elevated current densities of a sputter deposited Sn catalyst showed that it is vital to find techniques to stabilize the catalyst and prevent the Sn dissolution through the use of nanoparticles, binding agents, co-catalysts or ionomers in order to ensure long term stability.

Copper

Copper (Cu) has received significant attention by CO_2 reduction researchers due to its unique ability to convert CO_2 into at least 16 different products [64]. Numerous studies focused on improving the activity and selectivity of Cu through morphological enhancements [65], [66], facet dependent behavior [67], [68] and local environment control [69], [70]. Some of the mechanistic pathways behind the formation of various products are still debated [71], [72], but it has become clear that the specific binding strength of Cu to CO allows for dimerization of adsorbed CO and CHO species, resulting in multicarbon (C_{2+}) product formation. In GDE experiments, Cu and Cu-alloys have shown promising selective behavior towards prominently ethylene at elevated current densities [73].

In our work, sputter deposited Cu GDEs show highly-varied product selectivities with changing current densities, as reported elsewhere. At an applied current density of 10 mA cm^{-2}, the Cu GDEs produce a mixture of H_2, CO and formate at low overpotentials. At an applied current density of 50 mA cm^{-2} methane, ethylene and ethanol are detected as well. Further increasing the current density shows a shift in the product distribution towards ethylene while CO production plateaus. Comparing XPS results before and after experiments show that, besides a slightly higher degree of oxidation and the presence of potassium in the case of KOH (while decreasing the Cu 2p signal), the composition remains consistent. In contrast, SEM imaging does show significant restructuring of the surface in most experiments. The 200 mA cm^{-2} case showed that the specific conditions and applied potential resulted in the formation of Cu nanoneedles and cubes. The post-electrolysis HR-SEM image of $KHCO_3$ (Figure 3.7 d/S3.37) show that the Cu catalyst has restructured under the applied potential, favoring cubic shapes.

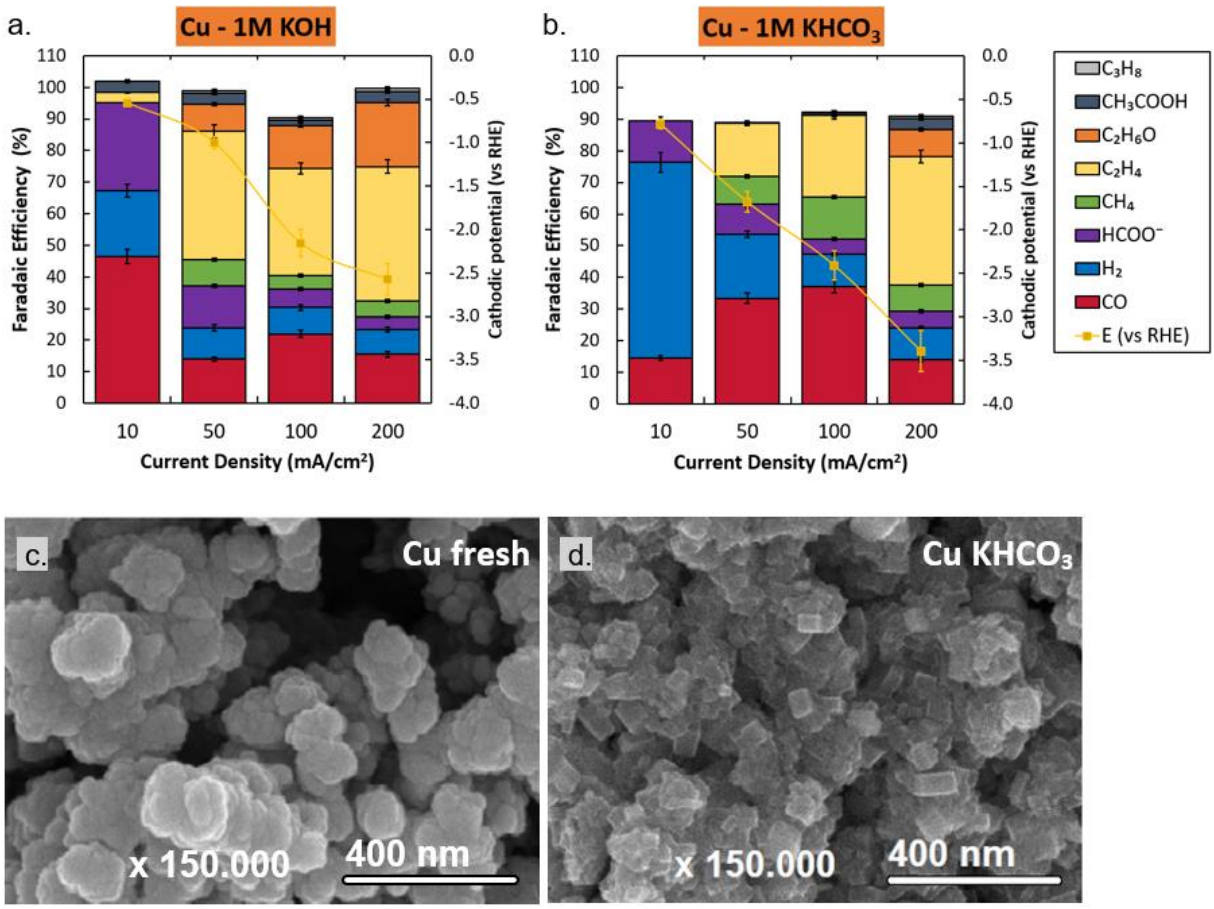

Figure 3.7. Characterization of Cu coated electrodes. Faradaic efficiency as a function of activity with cathodic potentials in 1 M KOH (a.) and 1 M $KHCO_3$ (b.). Error bars in panels a. and b. represent the data points from two separate experiments. HR-SEM images of fresh Cu (c.) and after 1h electrolysis in $KHCO_3$ (d.) show a cubic faceting of the catalyst.

3.4 Comparison of low and high reaction rate selectivities

Through the presented experiments, we were able to observe trends for the different catalysts as a function of applied current density. Of the five assessed transition metals only silver maintained its selectivity towards CO_2 reduction products over a broad current density range, while Au, Sn and Pd tended towards H_2 as a primary product as current densities were increased. Cu maintained its total CO_2 reduction selectivity, with product distributions growing at higher reaction rates. These results highlight how low vs high current density testing conditions change the observed product selectivities through variations in the local reaction environment, changes to catalyst

stability and the increased applied potentials which influence the relative activity of each product at different current densities.

One observation that needs to be highlighted is the limiting current density of Au and Pd towards CO, whereas Ag did not observe such a limit under the same conditions. Here the production of H_2 on Ag remains low up to 200 mA cm^{-2}, allowing for high CO selectivities to be maintained. Conversely on Au, hydrogen formation increases with current density while CO plateaus. A detailed study into the intrinsic limit of converting CO_2 could help determine which of these metals can effectively be used for industrial purposes, and why gold is a less favorable CO_2R catalyst at higher potentials and current densities.

For Sn the effect of electrolyte composition was more impactful than current density in the conversion of CO_2 to formate. We found that Sn experiments in $KHCO_3$ lead to mild catalyst restructuring, while in KOH structural instabilities damaged the catalyst

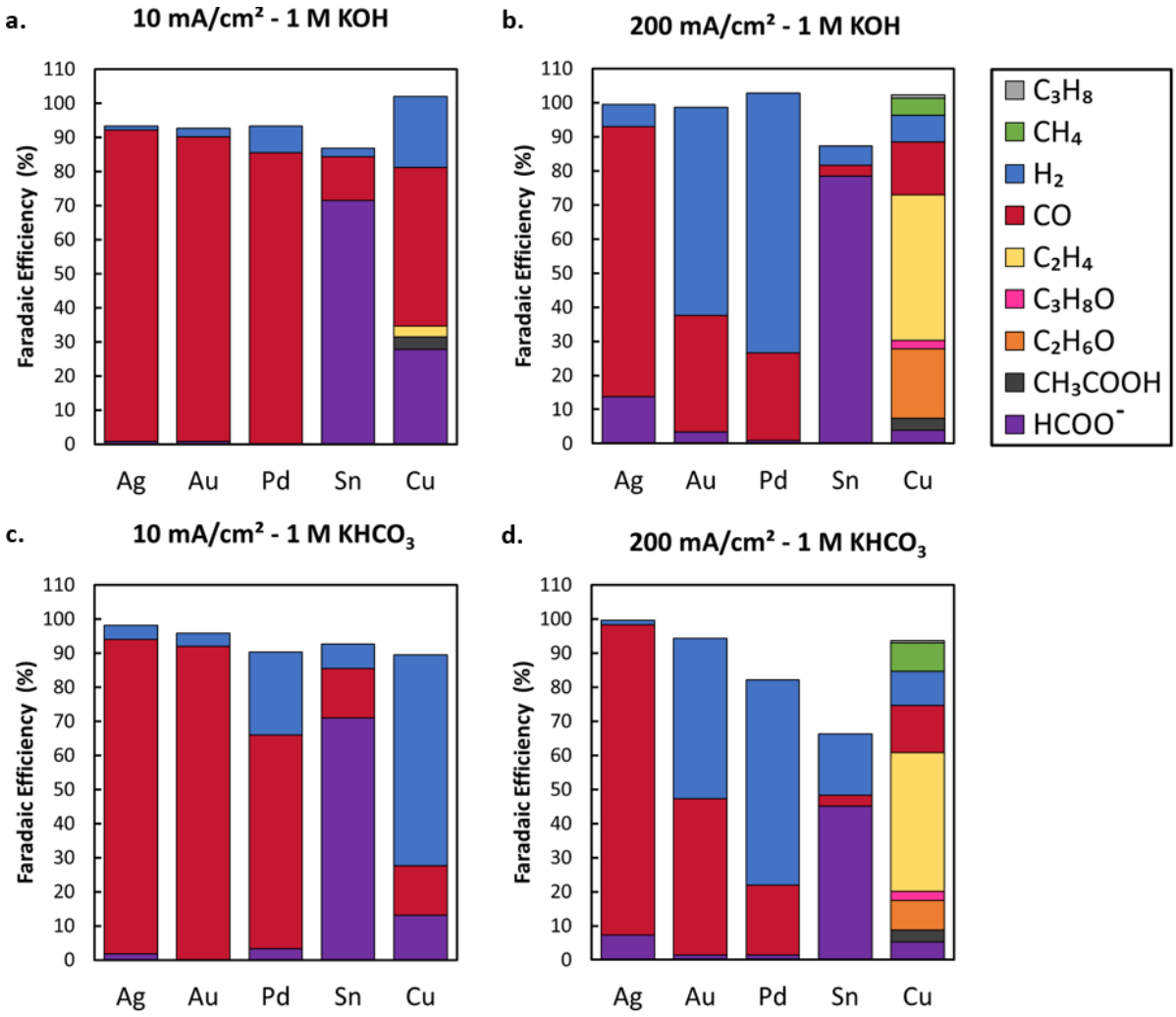

Figure 3.8. Selectivity comparison of transition metal catalysts in 1 M KOH at 10 mA cm^{-2} (a.) and 200 mA cm^{-2} (b.) and in 1 M $KHCO_3$ at 10 mA cm^{-2} (c.) and 200 mA cm^{-2} (d.).

surface irreversibly. During the 1 hr electrolysis the effects of restructuring were not clearly expressed through product distributions yet, but it became apparent that increasing current densities led to enhanced surface reformation and more frequent flooding issues. These trends highlight the necessity of applied current density and electrolyte composition when comparing or benchmarking the electrochemical performance of catalysts on gas diffusion electrodes.

To this end here we briefly provide a direct side-by-side comparison of the selectivity at low (10 mA cm^{-2}) and higher (200 mA cm^{-2}) current density as a reflection to the baseline work previously performed in an H-cell [1]. Shown in Figure 3.8 we compare these current densities in 1 M KOH and 1 M $KHCO_3$. The differences between the two electrolytes that are prevalent at lower current densities (Figure 3.8a, c) are much less impactful when going to 200 mA cm^{-2} (Figure 3.8b, d). The elevated rate of formed OH^- and consumed CO_2 gradually close the gap between both starting conditions. As a

result, the product distribution of the catalyst homogenizes as its activity is increased, regardless of the electrolyte. We can also more clearly see that some metals match their product selectivity at higher current densities consistently with little variation, while others start favoring the HER or an alternative carbon product.

Importantly, comparing the 10 mA cm^{-2} flow cell results against the 5 mA cm^{-2} H-cell benchmark for CO_2 reduction shows mostly similarities in applied potential and product selectivity, highlighting that reaction rate is a more prominent performance indicator at lower current densities than the choice between H-cell and flow cells. This is likely because the reaction environment remains similar, and a difference in available surface area is less likely to be limiting.

3.5 Conclusion

The main focus of this work is to provide a comparison of elemental catalysts by creating a controlled system and identifying the effect of current density on activity, selectivity and stability while moving from the H-cell regime (10 mA cm^{-2}) up to the mass transport capabilities of the GDE regime (200 mA cm^{-2}). Emphasis was placed on comparability of metals by producing 100 nm thick samples, and performing electrochemical and material characterization, and assessing collected data according to a detailed protocol. Although such a protocol allows for correlating catalysts without bias, a downside of this approach is that only a singular experimental configuration is screened. None-the-less we have strived to perform this analysis in a well-described and controlled testing environment for the confirmation and reproducibility of new and existing researchers within the field. Changes in performance due to varying catalysts, configurations and operating conditions are then grounded by a common point of comparison.

References Chapter 3.

1. Hori, Y., Electrochemical CO_2 Reduction on Metal Electrodes. In *Modern Aspects of Electrochemistry*, Vayenas, C. G.; White, R. E.; Gamboa-Aldeco, M. E., Eds. Springer New York: New York, NY, 2008; pp 89-189.
2. Verma, S.; Kim, B.; Jhong, H. M.; Ma, S.; Kenis, P. J. A., A Gross-Margin Model for Defining Technoeconomic Benchmarks in the Electroreduction of CO2. *ChemSusChem* **2016,** *9* (15), 1972-1979.
3. Bohra, D.; Chaudhry, J. H.; Burdyny, T.; Pidko, E. A.; Smith, W. A., Modeling the electrical double layer to understand the reaction environment in a CO2 electrocatalytic system. *Energy Environ. Sci.* **2019,** *12* (11), 3380-3389.
4. Park, S.; Wijaya, D. T.; Na, J.; Lee, C. W., Towards the Large-Scale Electrochemical Reduction of Carbon Dioxide. *Catalysts* **2021,** *11* (2), 253.
5. Zhang, X.; Li, J.; Li, Y.; Jung, Y.; Kuang, Y.; Zhu, G.; Liang, Y.; Dai, H., Selective and High Current CO2 Electro-Reduction to Multicarbon Products in Near-Neutral KCl Electrolytes. *J. Am. Chem. Soc.* **2021,** *143* (8), 3245-3255.
6. Vennekötter, J.; Scheuermann, T.; Sengpiel, R.; Wessling, M., The electrolyte matters: Stable systems for high rate electrochemical CO2 reduction. *Journal of CO2 Utilization* **2019,** *32*, 202-213.
7. Burdyny, T.; Smith, W. A., CO_2 Reduction on Gas-Diffusion Electrodes and Why Catalytic Performance Must be Assessed at Commercially-Relevant Conditions. *Energy Environ. Sci.* **2019,** *12* (5), 1442-1453.
8. Weng, L.; Bell, A. T.; Weber, A. Z., Modeling Gas-Diffusion Electrodes for CO_2 Reduction. *Phys. Chem. Chem. Phys.* **2018,** *20* (25), 16973-16984.
9. Salvatore, D. A.; Weekes, D. M.; He, J.; Dettelbach, K. E.; Li, Y. C.; Mallouk, T. E.; Berlinguette, C. P., Electrolysis of Gaseous CO2 to CO in a Flow Cell with a Bipolar Membrane. *ACS Energy Lett.* **2018,** *3* (1), 149-154.
10. Dinh, C.; Burdyny, T.; Kibria, M. G.; Seifitokaldani, A.; Gabardo, C. M.; García de Arquer, F. P.; Kiani, A.; Edwards, J. P.; De Luna, P.; Bushuyev, O. S.; Zou, C.; Quintero-Bermudez, R.; Pang, Y.; Sinton, D.; Sargent, E. H., CO_2 Electroreduction to Ethylene via Hydroxide-Mediated Copper Catalysis at an Abrupt Interface. *Science* **2018,** *360* (6390), 783-787.
11. Nitopi, S.; Bertheussen, E.; Scott, S. B.; Liu, X.; Engstfeld, A. K.; Horch, S.; Seger, B.; Stephens, I. E. L.; Chan, K.; Hahn, C.; Nørskov, J. K.; Jaramillo, T. F.; Chorkendorff, I., Progress and Perspectives of Electrochemical CO2 Reduction on Copper in Aqueous Electrolyte. *Chem. Rev.* **2019**, 119, 12, 7610–7672.

12. Jhong, H. M.; Tornow, C. E.; Smid, B.; Gewirth, A. A.; Lyth, S. M.; Kenis, P. J. A., A Nitrogen-Doped Carbon Catalyst for Electrochemical CO2 Conversion to CO with High Selectivity and Current Density. *ChemSusChem* **2017,** *10* (6), 1094-1099.

13. Verma, S.; Hamasaki, Y.; Kim, C.; Huang, W.; Lu, S.; Jhong, H.-R. M.; Gewirth, A. A.; Fujigaya, T.; Nakashima, N.; Kenis, P. J. A., Insights into the Low Overpotential Electroreduction of CO_2 to CO on a Supported Gold Catalyst in an Alkaline Flow Electrolyzer. *ACS Energy Lett.* **2018,** *3* (1), 193-198.

14. Sebastián-Pascual, P.; Mezzavilla, S.; Stephens, I. E. L.; Escudero-Escribano, M., Structure-sensitivity and Electrolyte Effects in CO2 Electroreduction: From Model Studies to Applications. *ChemCatChem* **2019,** 11, 1-21.

15. Pang, Y.; Burdyny, T.; Dinh, C..; Kibria, M. G.; Fan, J. Z.; Liu, M.; Sargent, E. H.; Sinton, D., Joint tuning of nanostructured Cu-oxide morphology and local electrolyte programs high-rate CO2 reduction to C2H4. *Green Chem.* **2017,** *19* (17), 4023-4030.

16. Verma, S.; Lu, X.; Ma, S.; Masel, R. I.; Kenis, P. J. A., The effect of electrolyte composition on the electroreduction of CO2 to CO on Ag based gas diffusion electrodes. *Phys. Chem. Chem. Phys.* **2016,** *18* (10), 7075-7084.

17. Wu, J.; Risalvato, F. G.; Ke, F.; Pellechia, P. J.; Zhou, X.-D., Electrochemical Reduction of Carbon Dioxide I. Effects of the Electrolyte on the Selectivity and Activity with Sn Electrode. *J. Electrochem. Soc.* **2012,** *159* (7), F353-F359.

18. Li, T.; Lees, E. W.; Goldman, M.; Salvatore, D. A.; Weekes, D. M.; Berlinguette, C. P., Electrolytic Conversion of Bicarbonate into CO in a Flow Cell. *Joule* **2019,** *3* (6), 1487-1497.

19. De Gregorio, G. L.; Burdyny, T.; Loiudice, A.; Iyengar, P.; Smith, W. A.; Buonsanti, R., Facet-Dependent Selectivity of Cu Catalysts in Electrochemical CO2 Reduction at Commercially Viable Current Densities. *ACS Catal.* **2020,** *10* (9), 4854-4862.

20. Luo, W.; Zhang, J.; Li, M.; Züttel, A., Boosting CO Production in Electrocatalytic CO2 Reduction on Highly Porous Zn Catalysts. *ACS Catal.* **2019,** *9* (5), 3783-3791.

21. García de Arquer, F. P.; Dinh, C.; Ozden, A.; Wicks, J.; McCallum, C.; Kirmani, A. R.; Nam, D.; Gabardo, C.; Seifitokaldani, A.; Wang, X.; Li, Y. C.; Li, F.; Edwards, J.; Richter, L. J.; Thorpe, S. J.; Sinton, D.; Sargent, E. H., CO2; electrolysis to multicarbon products at activities greater than 1 A cm<sup>−2</sup&gt. *Science* **2020,** *367* (6478), 661.

22. Dinh, C.; Burdyny, T.; Kibria, M. G.; Seifitokaldani, A.; Gabardo, C. M.; García de Arquer, F. P.; Kiani, A.; Edwards, J. P.; De Luna, P.; Bushuyev, O. S.; Zou, C.; Quintero-Bermudez, R.; Pang, Y.; Sinton, D.; Sargent, E. H., CO2; electroreduction to ethylene via hydroxide-mediated copper catalysis at an abrupt interface. *Science* **2018,** *360* (6390), 783.

23. Wang, Y.; Shen, H.; Livi, K. J. T.; Raciti, D.; Zong, H.; Gregg, J.; Onadeko, M.; Wan, Y.; Watson, A.; Wang, C., Copper Nanocubes for CO2 Reduction in Gas Diffusion Electrodes. *Nano Lett.* **2019,** *19* (12), 8461-8468.

24. Chen, X.; Chen, J.; Alghoraibi, N. M.; Henckel, D. A.; Zhang, R.; Nwabara, U. O.; Madsen, K. E.; Kenis, P. J. A.; Zimmerman, S. C.; Gewirth, A. A., Electrochemical CO2-to-ethylene conversion on polyamine-incorporated Cu electrodes. *Nat. Catal.* **2021,** *4* (1), 20-27.
25. Salvatore, D.; Berlinguette, C. P., Voltage Matters When Reducing CO2 in an Electrochemical Flow Cell. *ACS Energy Lett.* **2020,** *5* (1), 215-220.
26. Song, J. T.; Song, H.; Kim, B.; Oh, J., Towards Higher Rate Electrochemical CO2 Conversion: From Liquid-Phase to Gas-Phase Systems. *Catalysts* **2019,** *9* (3), 224.
27. Ma, M.; Kim, S.; Chorkendorff, I.; Seger, B., Role of ion-selective membranes in the carbon balance for CO2 electroreduction via gas diffusion electrode reactor designs. *Chemical Science* **2020,** *11* (33), 8854-8861.
28. Yang, K.; Kas, R.; Smith, W. A.; Burdyny, T., Role of the Carbon-Based Gas Diffusion Layer on Flooding in a Gas Diffusion Electrode Cell for Electrochemical CO2 Reduction. *ACS Energy Lett.* **2021,** *6* (1), 33-40.
29. Leonard, M. E.; Clarke, L. E.; Forner-Cuenca, A.; Brown, S. M.; Brushett, F. R., Investigating Electrode Flooding in a Flowing Electrolyte, Gas-Fed Carbon Dioxide Electrolyzer. *ChemSusChem* **2020,** *13* (2), 400-411.
30. Ma, M.; Clark, E. L.; Therkildsen, K. T.; Dalsgaard, S.; Chorkendorff, I.; Seger, B., Insights into the carbon balance for CO2 electroreduction on Cu using gas diffusion electrode reactor designs. *Energy Environ. Sci.* **2020,** *13* (3), 977-985.
31. Hatsukade, T.; Kuhl, K. P.; Cave, E. R.; Abram, D. N.; Jaramillo, T. F., Insights into the electrocatalytic reduction of CO2 on metallic silver surfaces. *Phys. Chem. Chem. Phys.* **2014,** *16* (27), 13814-13819.
32. Firet, N. J.; Smith, W. A., Probing the Reaction Mechanism of CO2 Electroreduction over Ag Films via Operando Infrared Spectroscopy. *ACS Catal.* **2016,** *7* (1), 606-612.
33. Singh, M. R.; Kwon, Y.; Lum, Y.; Ager, J. W.; Bell, A. T., Hydrolysis of Electrolyte Cations Enhances the Electrochemical Reduction of CO_2 over Ag and Cu. *J. Am. Chem. Soc.* **2016,** *138* (39), 13006-13012.
34. Rosen, J.; Hutchings, G. S.; Lu, Q.; Rivera, S.; Zhou, Y.; Vlachos, D. G.; Jiao, F., Mechanistic Insights into the Electrochemical Reduction of CO2 to CO on Nanostructured Ag Surfaces. *ACS Catal.* **2015,** *5* (7), 4293-4299.
35. Ma, S.; Luo, R.; Gold, J. I.; Yu, A. Z.; Kim, B.; Kenis, P. J. A., Carbon nanotube containing Ag catalyst layers for efficient and selective reduction of carbon dioxide. *J. Mater. Chem. A* **2016,** *4* (22), 8573-8578.
36. Gabardo, C. M.; Seifitokaldani, A.; Edwards, J. P.; Dinh, C.; Burdyny, T.; Kibria, M. G.; O'Brien, C. P.; Sargent, E. H.; Sinton, D., Combined high alkalinity and pressurization enable efficient CO2 electroreduction to CO. *Energy Environ. Sci.* **2018,** *11* (9), 2531-2539.

37. Seifitokaldani, A.; Gabardo, C. M.; Burdyny, T.; Dinh, C.; Edwards, J. P.; Kibria, M. G.; Bushuyev, O. S.; Kelley, S. O.; Sinton, D.; Sargent, E. H., Hydronium-Induced Switching between CO2 Electroreduction Pathways. *J. Am. Chem. Soc.* **2018,** *140* (11), 3833-3837.

38. Cofell, E. R.; Nwabara, U. O.; Bhargava, S. S.; Henckel, D. E.; Kenis, P. J. A., Investigation of Electrolyte-Dependent Carbonate Formation on Gas Diffusion Electrodes for CO2 Electrolysis. *ACS Appl. Mater. Interfaces* **2021,** *13* (13), 15132-15142.

39. Hori, Y.; Wakebe, H.; Tsukamoto, T.; Koga, O., Electrocatalytic process of CO selectivity in electrochemical reduction of CO2 at metal electrodes in aqueous media. *Electrochim. Acta* **1994,** *39* (11), 1833-1839.

40. Hara, K.; Kudo, A.; Sakata, T., Electrochemical reduction of carbon dioxide under high pressure on various electrodes in an aqueous electrolyte. *J. Electroanal. Chem.* **1995,** *391* (1), 141-147.

41. Yoshio, H.; Katsuhei, K.; Shin, S., Production of CO and CH4 in Electrochemical Reduction of CO2 at Metal Electrodes in Aqueous Hydrogencarbonate Solution. *Chem. Lett.* **1985,** *14* (11), 1695-1698.

42. Zhu, W.; Michalsky, R.; Metin, Ö.; Lv, H.; Guo, S.; Wright, C. J.; Sun, X.; Peterson, A. A.; Sun, S., Monodisperse Au Nanoparticles for Selective Electrocatalytic Reduction of CO_2 to CO. *J. Am. Chem. Soc.* **2013,** *135* (45), 16833-16836.

43. Ozden, A.; Liu, Y.; Dinh, C.-T.; Li, J.; Ou, P.; García de Arquer, F. P.; Sargent, E. H.; Sinton, D., Gold Adparticles on Silver Combine Low Overpotential and High Selectivity in Electrochemical CO2 Conversion. *ACS Appl. Energy Mater.* **2021,** *4* (8), 7504-7512.

44. Liu, K.; Smith, W. A.; Burdyny, T., Introductory Guide to Assembling and Operating Gas Diffusion Electrodes for Electrochemical CO2 Reduction. *ACS Energy Letters* **2019,** *4* (3), 639-643.

45. Hoshi, N.; Noma, M.; Suzuki, T.; Hori, Y., Structural effect on the rate of CO2 reduction on single crystal electrodes of palladium. *J. Electroanal. Chem.* **1997,** *421* (1), 15-18.

46. Klinkova, A.; De Luna, P.; Dinh, C.; Voznyy, O.; Larin, E. M.; Kumacheva, E.; Sargent, E. H., Rational Design of Efficient Palladium Catalysts for Electroreduction of Carbon Dioxide to Formate. *ACS Catal.* **2016,** *6* (12), 8115-8120.

47. Zhu, W.; Zhang, L.; Yang, P.; Hu, C.; Luo, Z.; Chang, X.; Zhao, Z.-J.; Gong, J., Low-Coordinated Edge Sites on Ultrathin Palladium Nanosheets Boost Carbon Dioxide Electroreduction Performance. *Angew. Chem.* **2018,** *130* (36), 11718-11722.

48. Gao, D.; Zhou, H.; Wang, J.; Miao, S.; Yang, F.; Wang, G.; Wang, J.; Bao, X., Size-Dependent Electrocatalytic Reduction of CO2 over Pd Nanoparticles. *J. Am. Chem. Soc.* **2015,** *137* (13), 4288-4291.

49. Zhang, H.; Wang, S.; Jiang, K.; André, T.; Cai, W., In situ spectroscopic investigation of CO accumulation and poisoning on Pd black surfaces in concentrated HCOOH. *J. Power Sources* **2012,** *199*, 165-169.

50. O'Brien, C. P.; Lee, I. C., CO Poisoning and CO Hydrogenation on the Surface of Pd Hydrogen Separation Membranes. *J. Phys. Chem. C* **2017,** *121* (31), 16864-16871.

51. Min, X.; Kanan, M. W., Pd-Catalyzed Electrohydrogenation of Carbon Dioxide to Formate: High Mass Activity at Low Overpotential and Identification of the Deactivation Pathway. *J. Am. Chem. Soc.* **2015,** *137* (14), 4701-4708.

52. Kortlever, R.; Peters, I.; Balemans, C.; Kas, R.; Kwon, Y.; Mul, G.; Koper, M. T. M., Palladium–gold catalyst for the electrochemical reduction of CO2 to C1–C5 hydrocarbons. *Chem. Commun.* **2016,** *52* (67), 10229-10232.

53. Feng, R.; Zhu, Q.; Chu, M.; Jia, S.; Zhai, J.; Wu, H.; Wu, P.; Han, B., Electrodeposited Cu–Pd bimetallic catalysts for the selective electroreduction of CO2 to ethylene. *Green Chem.* **2020,** *22* (21), 7560-7565.

54. Mura, M. G.; Luca, L. D.; Giacomelli, G.; Porcheddu, A., Formic Acid: A Promising Bio-Renewable Feedstock for Fine Chemicals. *Adv. Synth. Catal.* **2012,** *354* (17), 3180-3186.

55. Kapusta, S.; Hackerman, N., The Electroreduction of Carbon Dioxide and Formic Acid on Tin and Indium Electrodes. *J. Electrochem. Soc.* **1983,** *130* (3), 607-613.

56. Chen, Y.; Kanan, M. W., Tin Oxide Dependence of the CO2 Reduction Efficiency on Tin Electrodes and Enhanced Activity for Tin/Tin Oxide Thin-Film Catalysts. *J. Am. Chem. Soc.* **2012,** *134* (4), 1986-1989.

57. Zhang, S.; Kang, P.; Meyer, T. J., Nanostructured Tin Catalysts for Selective Electrochemical Reduction of Carbon Dioxide to Formate. *J. Am. Chem. Soc.* **2014,** *136* (5), 1734-1737.

58. Wang, Q.; Dong, H.; Yu, H., Development of rolling tin gas diffusion electrode for carbon dioxide electrochemical reduction to produce formate in aqueous electrolyte. *J. Power Sources* **2014,** *271*, 278-284.

59. Sen, S.; Skinn, B.; Hall, T.; Inman, M.; Taylor, E. J.; Brushett, F. R., Pulsed Electrodeposition of Tin Electrocatalysts onto Gas Diffusion Layers for Carbon Dioxide Reduction to Formate. *MRS Advances* **2016,** *2* (8), 451-458.

60. Choi, S. Y.; Jeong, S. K.; Kim, H. J.; Baek, I.; Park, K. T., Electrochemical Reduction of Carbon Dioxide to Formate on Tin–Lead Alloys. *ACS Sustainable Chem. Eng.* **2016,** *4* (3), 1311-1318.

61. Sarfraz, S.; Garcia-Esparza, A. T.; Jedidi, A.; Cavallo, L.; Takanabe, K., Cu–Sn Bimetallic Catalyst for Selective Aqueous Electroreduction of CO2 to CO. *ACS Catal.* **2016,** *6* (5), 2842-2851.

62. Dong, W. J.; Yoo, C. J.; Lee, J.-L., Monolithic Nanoporous In–Sn Alloy for Electrochemical Reduction of Carbon Dioxide. *ACS Appl. Mater. Interfaces* **2017,** *9* (50), 43575-43582.

63. Li, Q.; Fu, J.; Zhu, W.; Chen, Z.; Shen, B.; Wu, L.; Xi, Z.; Wang, T.; Lu, G.; Zhu, J.-j.; Sun, S., Tuning Sn-Catalysis for Electrochemical Reduction of CO2 to CO via the Core/Shell Cu/SnO2 Structure. *J. Am. Chem. Soc.* **2017.** *139* (12), 4290–4293.

64. Kuhl, K. P.; Cave, E. R.; Abram, D. N.; Jaramillo, T. F., New Insights into the Electrochemical Reduction of Carbon Dioxide on Metallic Copper Surfaces. *Energy Environ. Sci.* **2012,** *5* (5), 7050-7059.

65. Kas, R.; Kortlever, R.; Milbrat, A.; Koper, M. T. M.; Mul, G.; Baltrusaitis, J., Electrochemical CO2 reduction on Cu2O-derived copper nanoparticles: controlling the catalytic selectivity of hydrocarbons. *Phys. Chem. Chem. Phys.* **2014,** *16* (24), 12194-12201.

66. Ma, M.; Djanashvili, K.; Smith, W. A., Controllable Hydrocarbon Formation from the Electrochemical Reduction of CO_2 over Cu Nanowire Arrays. *Angew. Chem. Int. Ed.* **2016,** *55* (23), 6680-6684.

67. Mariano, R. G.; McKelvey, K.; White, H. S.; Kanan, M. W., Selective Increase in CO_2 Electroreduction Activity at Grain-Boundary Surface Terminations. *Science* **2017,** *358* (6367), 1187-1192.

68. Luo, W.; Nie, X.; Janik, M. J.; Asthagiri, A., Facet Dependence of CO2 Reduction Paths on Cu Electrodes. *ACS Catal.* **2016,** *6* (1), 219-229.

69. Lim, C. F. C.; Harrington, D. A.; Marshall, A. T., Effects of mass transfer on the electrocatalytic CO2 reduction on Cu. *Electrochim. Acta* **2017,** *238*, 56-63.

70. Wang, L.; Nitopi, S. A.; Bertheussen, E.; Orazov, M.; Morales-Guio, C. G.; Liu, X.; Higgins, D. C.; Chan, K.; Nørskov, J. K.; Hahn, C.; Jaramillo, T. F., Electrochemical Carbon Monoxide Reduction on Polycrystalline Copper: Effects of Potential, Pressure, and pH on Selectivity toward Multicarbon and Oxygenated Products. *ACS Catal.* **2018,** *8* (8), 7445-7454.

71. Kortlever, R.; Shen, J.; Schouten, K. J. P.; Calle-Vallejo, F.; Koper, M. T. M., Catalysts and Reaction Pathways for the Electrochemical Reduction of Carbon Dioxide. *J. Phys. Chem. Lett.* **2015,** *6* (20), 4073-4082.

72. Schouten, K. J. P.; Qin, Z.; Gallent, E. P.; Koper, M. T. M., Two Pathways for the Formation of Ethylene in CO Reduction on Single-Crystal Copper Electrodes. *J. Am. Chem. Soc.* **2012,** *134* (24), 9864-9867.

73. Han, L.; Zhou, W.; Xiang, C., High-Rate Electrochemical Reduction of Carbon Monoxide to Ethylene Using Cu-Nanoparticle-Based Gas Diffusion Electrodes. *ACS Energy Lett.* **2018**, 855-860.

Chapter 3. Supporting Information

Characterizing CO_2 reduction catalysts on gas diffusion electrodes

Comparing activity, selectivity and stability of transition metal catalysts.

SI A. Protocols

In order to obtain comparable results amongst both different materials and researchers it is necessary to streamline our methodologies (production, characterization and performance) for performing all planned experiments. It is of utmost importance that our individual approaches to each experiment are as similar as possible. To equally treat all samples our researchers specialized in certain characterization methods. Building of the cell for performance experiments was explained by one person to ensure practical details (e.g., ref. electrode spacing, cathode/anode fixation and cell tilt) to be uniform as well. This protocol will give the main guidelines to obtain comparable results for each technique and to allow reproduction of results.

Sample production

Samples were produced by means of **magnetron sputtering deposition**. To compare the parameters of different materials it is best to have similar thickness and structural morphology. It is assumed uniform, comparable structures are obtained by using continuous rotation, **20 sccm Ar** at **3 µbar** and similar deposition rates. **DC power of 50 W** was used for Au, Ag, Cu and Pd. More volatile Sn was produced at 20 W. To obtain the correct thickness the deposition rate will first be calculated by measuring the depth profile of a glass piece after 10 min sputtering. After determining the deposition rate for each material, the deposition time to make 100 nm (calculated on glass) will be used to make the GDE samples. It is assumed the error in glass-to-GDE transferability is similar between different materials. See Profilometry for more details about the thickness determination. For the sputtering deposition we will make use of the AJA2 as shown in Figure S3.1 on the left-end side of the AJA system.

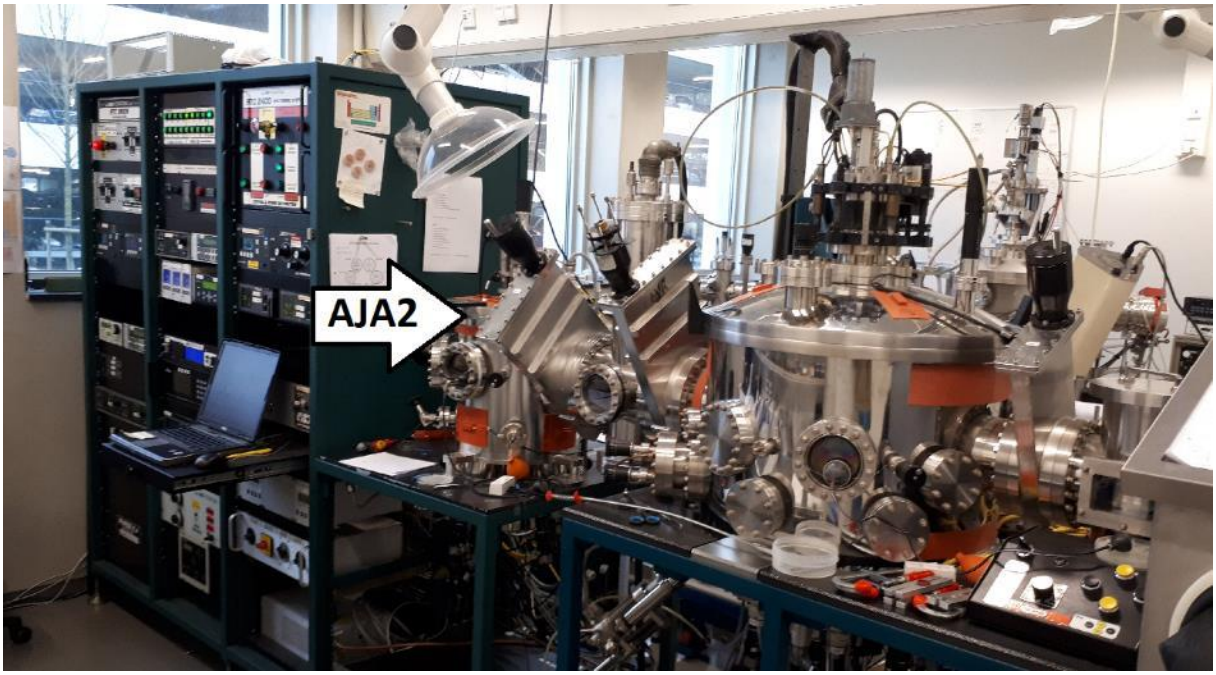

Figure S3.3. AJA, magnetron sputter. For our materials we will make use of the leftmost chamber (AJA2).

Material Characterization

Most material characterization techniques can be performed by one person, which makes executing the experiments and producing comparable results much easier. Nevertheless, everyone should understand how and why we perform each technique and discuss the results of each method.

(High Resolution) Scanning Electron Microscopy – (HR)SEM

SEM (Figure S3.2) and **HR-SEM** are used to obtain information about **surface morphology**, thereby tracking whether its structure changes after 1h operation. Found abnormalities like clusters, deformation, crystals or exposed MPL could indicate poor stability. To be able to compare materials (HR-)SEM images are used to show similar morphologies across different metals as a result of sputtering. The HR-SEM is located in a cleanroom. Images are made at the following magnifications:

Figure S3.4. JEOL, JSM-6010LA Scanning electron microscope.

-SEM (Figure S3.2): x 50, 100, 500, 1000, 5000

-HR-SEM (cleanroom): x 50k, 100k, 150k

Figure S5.3. Bruker, Atomic Force Microscope with Dimension Icon ScanAsyst.

Atomic Force Microscopy – AFM

AFM (Figure S3.3) is another surface probing technique in addition to the SEM. This technique will give information on **surface topography and phase separation**. For AFM we make use of TESPA-v2 probes. Height and phase images of the catalyst surface at a magnification of **500 x 500 nm** and **1000 x 1000 nm** are taken**.** Some parameters of the AFM can be sample specific and need to be optimized during operation.

Profilometry

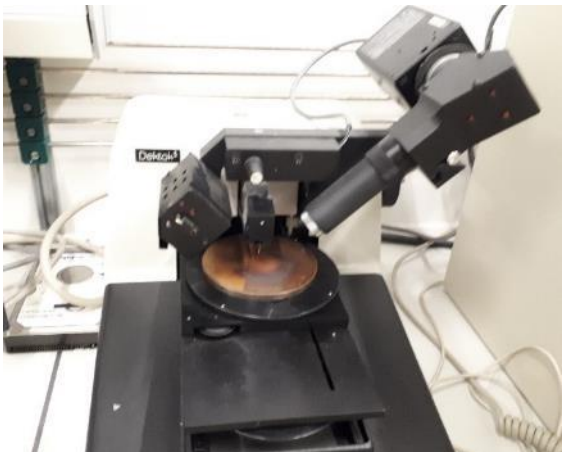

Figure S3.6. INRF, Dektak 3 profilometer.

Profilometry (Figure S3.4) is a simple technique that measures the **thickness** of the samples by comparing the height to a reference point. The coarseness of the microporous layer is ±1 μm and the sputtered thickness we aim for is **100 nm**. Because of this coarseness, profilometry will be performed on a piece of Menzel glass, added to each sputtering procedure. By partially Scotch-taping the glass surface and peeling the tape away after sputtering, an abrupt interface between sputtered and non-sputtered glass is created. This interface is easily measured by profilometry, giving the thickness with a ±5 nm error. Although the porosity of catalysts on GDEs is higher than on glass, which results in a thicker layer on GDE, it is assumed that the translation of catalyst layer thickness between glass and GDE is constant over the range of materials. In the end the importance of this characterization is not the exact thickness, but to ensure similar thicknesses are present amongst all samples to obtain comparable mass transport properties.

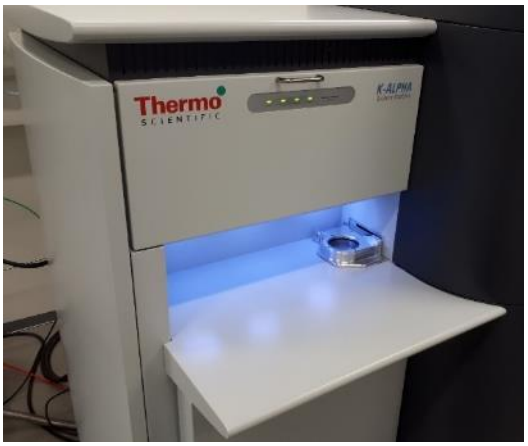

Figure S3.7. ThermoFisher Sci., K-Alpha XPS.

X-ray Photoelectron Spectroscopy – XPS

XPS (Figure S3.5) gives clear information about the **purity and oxidation state** of the samples. This way we can exclude or take into account the effects of impurities and oxidation of the catalyst. For each catalyst a survey scan is performed first. Elements of interest are scanned separately to obtain more accurate data. A C 1s scan shows the presence of substrate carbon (and some omnipresent surface carbon). This peak will hint at if the substrate became more or less exposed after operation. Very close to the C 1s peak is the K 2p peak used to identify potassium, which can deposit from the electrolyte on the surface during operation. A respective metal scan (e.g., Au 4f for Au) is used to see change in the catalysts abundance and oxidation. Finally, an O 1s scan is used to measure the degree of oxidation.

Sample handling and rinsing

While producing, installing and ex-situ measuring GDE samples it is important to avoid any direct contact with the MPL/catalyst layer. Due to the powder like structure of the Sigracet 38 BC MPL this layer gives off its catalyst and carbon black easily. In such a case a new sample needed to be deployed, since this could have affected the homogeneity, loading and pore size distribution. Therefore, it is important to have proper handling strategies. During the experiments samples were only touched on the sturdy GDL backside or along the edges of the catalyst side using tweezers (outside of the active area). After placing a sample between two gaskets a mask was placed over to prevent any contaminations. During ex-situ experiments this care was also taken and it was made sure only the active area was studied.

During the reaction with the potassium containing electrolytes, it is likely that at the cathode secondary reactions with the potassium ions in solution would occur. In order to prevent post-reaction salt-crusting or residual oxidations a rigorous rinsing protocol was deployed. After each experiment the catholyte and anolyte streams were switched with a 250 mL DI water solution that was continuously recirculated through the cell for approx. 5 minutes to remove any residual $KHCO_3$/KOH electrolyte species. Afterwards the cell was opened and the sample was taken out with tweezers and sprayed again with bottled DI water for 30 seconds and subsequently dried using an abundant nitrogen stream. After this the samples were stored until ex-situ characterization was performed.

Performance Characterization

A major component of this comparison is the reproducibility of the experimental procedure. This section documents the details of the setup.

Cell construction and parameters

The experimental setup and the internal electrochemical cell will be built according to Figure S3.6 and S3.7:

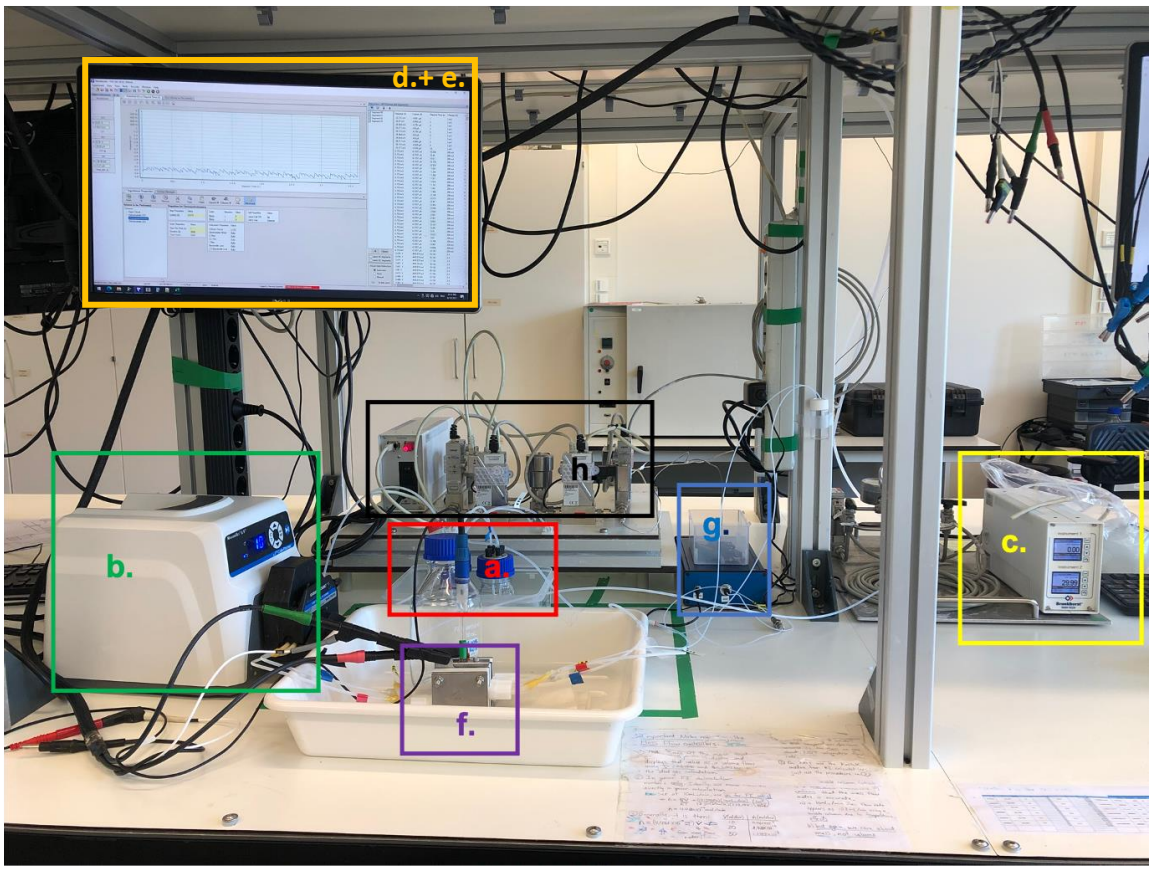

Figure S3.8. Practical experimental setup. a. External electrolyte compartments. b. Peristaltic pump (10 mL min^{-1}). c. MFC for CO_2 (30 sccm). d.+ e. Potentiostat, BPR and GC control. f. PTFE flow cell. g. Liquid trap. h. Back pressure regulator.

The external setup consists of 2 external electrolyte compartments (80 mL electrolyte each) from which the pump (Cole-Parmer Masterflex L/S, φ_{pump} = 10 mL min^{-1}) transported the anolyte and catholyte to the lower cell inlets. The corresponding upper outlets go back to the electrolyte compartments from the outlets. The cell is tilted slightly to aid in the transport of anode formed oxygen out from the top of the anolyte compartment, hereby reducing potential fluctuations. The CO_2 MFC (Bronkhorst EL-flow, φ_{MFC} = 30 sccm) is connected to the gas inlet of the cell and the outlet is connected directly to the GC once measurements are taken. During circulation of both liquid and gas an overpressure of 80-100 mbar is witnessed on the MFC pressure gauge. GC injections close the gas pathway temporarily (2-3 seconds) and cause overpressure to shortly spike to ~200 mbar, leading to minor gas crossover into the catholyte and subsequently leaving through the external compartment. The loss of gas has a minor effect on the gaseous product collection, but since this only occurs after every injection the system has a 4-minute time window to equilibrate before the following injection takes place.

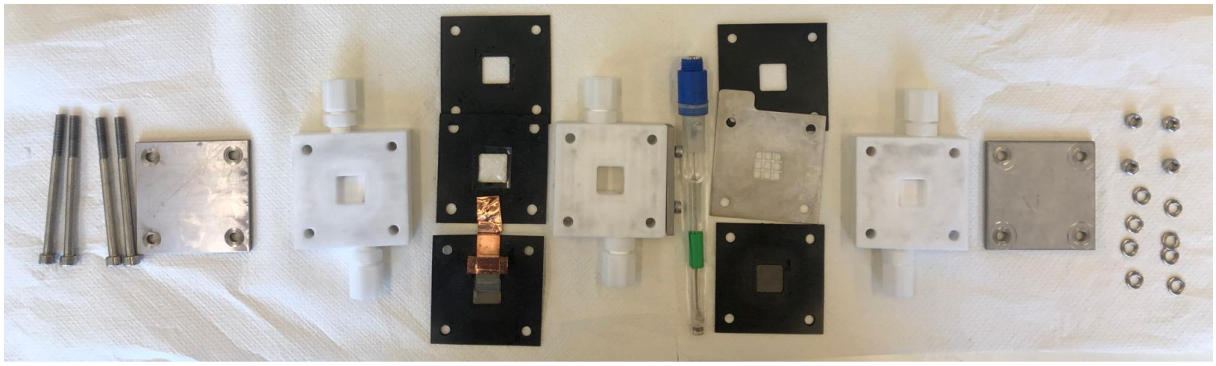

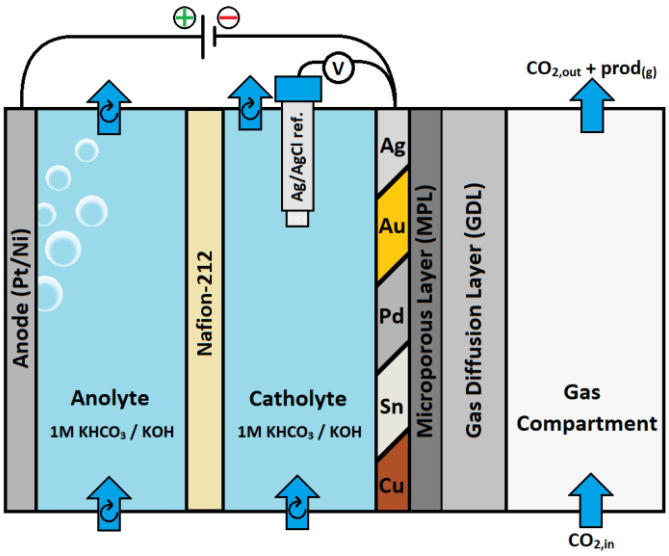

Figure S3.7. Exploded view of the 3-compartment cell (top) and schematic drawing of the cell interior (right).

From left to right: Anode (Ni mesh in 1 M KOH/Pt wire in 1 M $KHCO_3$) inside a recirculating anolyte compartment. Nafion-212 cation exchange membrane. Recirculating catholyte compartment with reference electrode. GDE with respective cathode catalyst layer on the microporous layer MPL facing the catholyte. CO_2 gas compartment. Between the anode and cathode, the counter and working electrode are connected respectively applying a negative current. Between the working electrode and the Ag/AgCl reference potential is measured.

Between the anolyte and catholyte compartments the anode and membrane are positioned in a sandwich of gaskets. This sandwich consists of 5 parts: a gasket, the anode (bent away from the membrane and taped to the first gasket for electrical connection), a second gasket, the Nafion-212 cation exchange membrane and a third gasket. The sputtered GDE sample is also squished between two gaskets alongside a current collector. A more detailed description can be found in a paper by Liu et al. on assembly and operation of GDE cells [1].

Table S1. Setup conditions for alkaline and neutral experiments.

Electrolyte type	**Alkaline**	**Neutral**
Starting pH	13.8 – 14.0	7.8 - 8.0
Anolyte	1M KOH *(>85% pellets, Sigma Aldrich)*	1M $KHCO_3$ *(ACS reag. 99.7%)*
Catholyte	1M KOH *(>85% pellets, Sigma Aldrich)*	1M $KHCO_3$ *(ACS reag. 99.7%)*
OER Anode	Ni mesh	Pt wire
Membrane	Nafion-212	Nafion-212
Ref. electrode	XR310 Radiometer Analytical	XR310 Radiometer Analytical

Potentiostat

All potentiostatic measurements are performed with the **ParStat 4000** (Figure S3.8) or **ParStat MC.**

pH is measured before and after experiments. By combining pH and EIS results, the measured potential can be converted to RHE:

$$E_{(RHE)} = E_{cath} + 0.0591\ pH + E^{o}_{Ag/AgCl} - iR_{drop}$$

Figure S8. Ametek, Princeton Applied Research, ParStat 4000 Potentiostat /Galvanostat/EIS analyser.

Where E_{cath} is the measured negative potential between the reference and the cathode, $E^{o}_{Ag/AgCl}$ is the standard reference potential ($E^{o}_{Ag/AgCl}$ = 0.1976V vs RHE @ 25 °C) and iR_{drop} the negative current times measured resistance. Unfortunately, it was not possible to accurately determine the iR drop through EIS at elevated current densities due to the long path of electrolyte between cathode and reference. More details on this can be found in SI B. Electrochemical impedance spectroscopy. Instead, all reported potentials are iR-uncorrected as described by the following formula:

$$E_{(uncorr.\ vs\ RHE)} = E_{cath} + 0.0591\ pH + E^{o}_{Ag/AgCl}$$

Chronopotentiometry experiments are the core part of this research. By keeping the current density (C.D.) constant and combining this with gas and liquid analysis we are able to determine the product selectivity at a certain production rate as well as the stability over time. The planar active surface area is 2.25 cm², so the potentiostat input are adapted as shown in brackets. Chronopotentiometry measurements are taken for 1 hour at the following currents:

- 10 mA/cm² (comparable C.D. to H-cell activity) [= - 22.5 mA]
- 50 mA/cm² [= - 112.5 mA]
- 100 mA/cm² [= - 225 mA]
- 200 mA/cm² [= - 450 mA]
- 300 mA/cm² [= - 675 mA]

After an experiment catholyte samples are taken and analyzed by HPLC for liquid products.

Gas Chromatography (GC)

GC (Figure S3.9) measurements are taken every 4 minutes from the gas phase outlet during all chronopotentiometry experiments to measure the concentration of gaseous products. Before each measurement 3 injections without applied potential are performed as a second check of the baseline after flushing the system. It is important to perform regular calibration checks to ensure measurements are accurate. The gas products CO, H_2 and C_2H_4 are calibrated at 3 levels (10, 100, 1000 ppm).

Figure S3.9. Global Analyser Solutions, CompactGC 4.0 gas chromatograph.

High Performance Liquid Chromatography (HPLC)

Figure S3.10. Agilent Technologies, 1260 Infinity II HPLC.

After each chronopotentiometry experiment a sample of catholyte will be taken to the Agilent Technologies 1260 Infinity II **HPLC** (Figure S3.10) equipped with VWD (dual wavelength: 210 nm and 280 nm) and RID (T = 40 °C) to measure the concentration of liquid carbon containing species on basis of their retention times in an Hi-Plex H column (T = 50 °C). Main products of interest here are formic acid, acetic acid, acetaldehyde, ethanol and propanol. 10 levels of calibration were performed (10-10000 ppm, R^2 > 99.9 %)

SI B. Characterization data

This section displays the results of the performed experiments. Data is collected via chronopotentiometry, electrochemical impedance spectroscopy (EIS), gas and liquid product analysis (GC/HPLC), (high resolution-) scanning electron microscopy (SEM & HR-SEM imaging), X-ray photoelectron spectroscopy (XPS) and atomic force microscopy (AFM).

Electrochemical impedance spectroscopy – EIS

Electrochemical impedance spectroscopy can be used to determine the resistance between the reference and working electrode and consecutively correct the measured potential for any resistive losses. During this series of experiments an EIS measurement was performed before and after each experiment. It was found that the configuration of our system had a significant drawback: Due to the relatively large distance between the reference electrode and the GDE cathode (~8 mm) the measured resistance was **3-4 Ω** for 1 M KOH and **7-8 Ω** for 1 M $KHCO_3$. This extremely large correction factor caused the iR corrections to lower the voltage significantly. To illustrate: 8 Ω * 450 mA = 3.6 V of ohmic drop. Furthermore, it was found that correcting potentials at 100/200 mA cm^{-2} with said resistance caused overcompensation. For instance, the corrected potential at 200 mA cm^{-2} in 1 M $KHCO_3$ was lower than the corrected potential at 50 mA cm^{-2}. In some cases the iR-drop even exceeded the applied potential, indicating that the resistance during operation at elevated currents was actually lower than we were able to measure during 'offline', no-current EIS.

Concluding, it was decided to not correct the measured potential for its resistive losses. This was done to avoid confusion about the measured potentials due to changing electrolyte conductivities throughout the length of the experiment, and to evade overcompensation of unrealistic resistances.

Chronopotentiometry

Below V_{cat}-t chronopotentiometry diagrams of all metal-electrolyte combinations are shown as measured against an Ag/AgCl reference electrode without corrections for iR-drop (Figure S3.11 – S3.15). Most of the high current experiments show diverging from the patterns. These values indicate the instabilities of the system at elevated activities, due to bubble formation in the electrolytes resulting in issues such as GDE flooding and gas crossover.

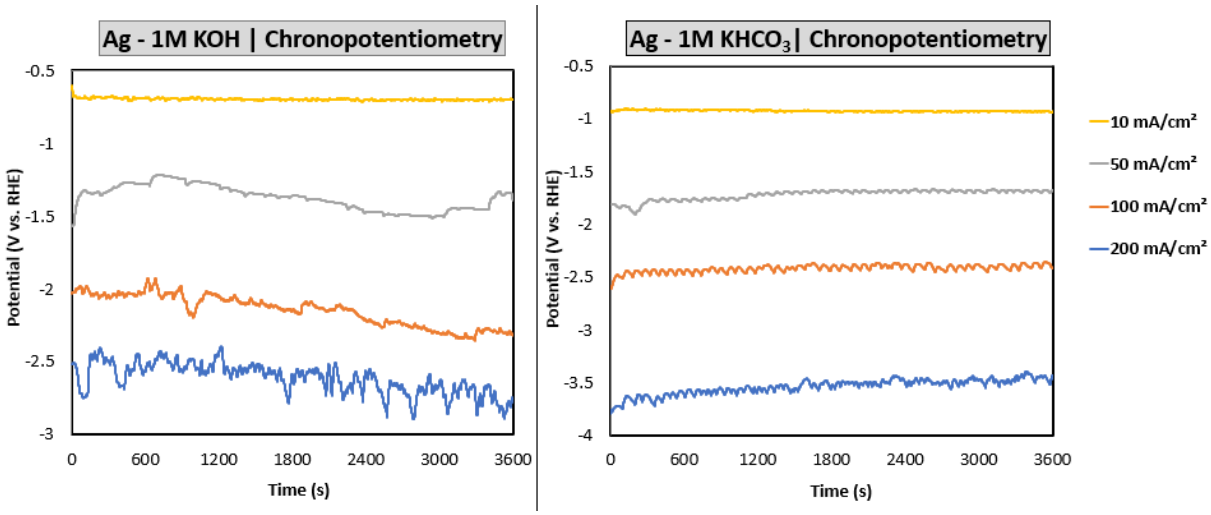

Figure S3.11. Chronopotentiometry measurements for Ag in 1 M KOH and $KHCO_3$.

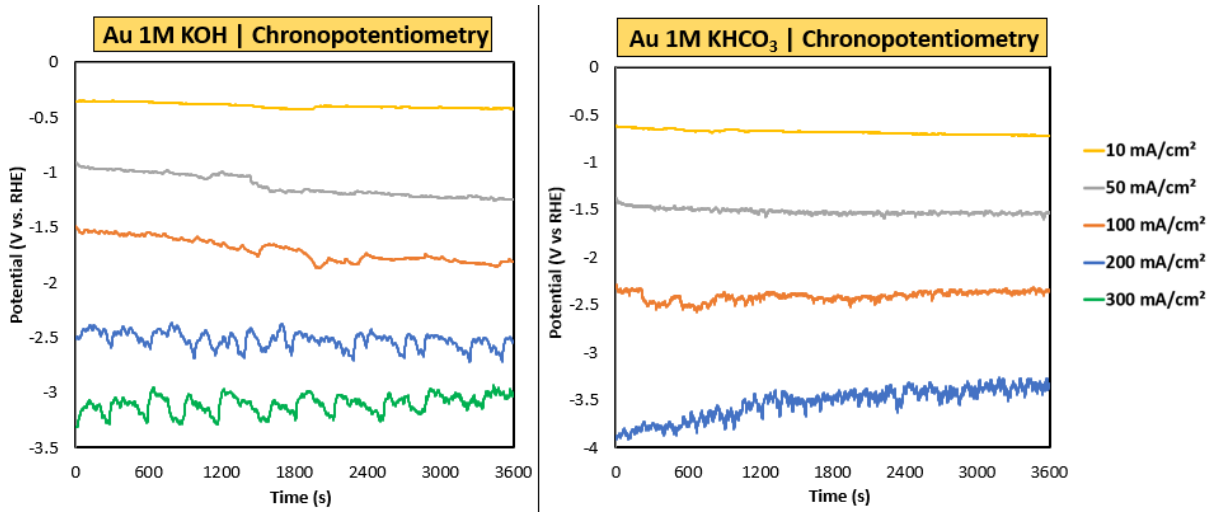

Figure S3.12. Chronopotentiometry measurements for Au in 1 M KOH and $KHCO_3$.

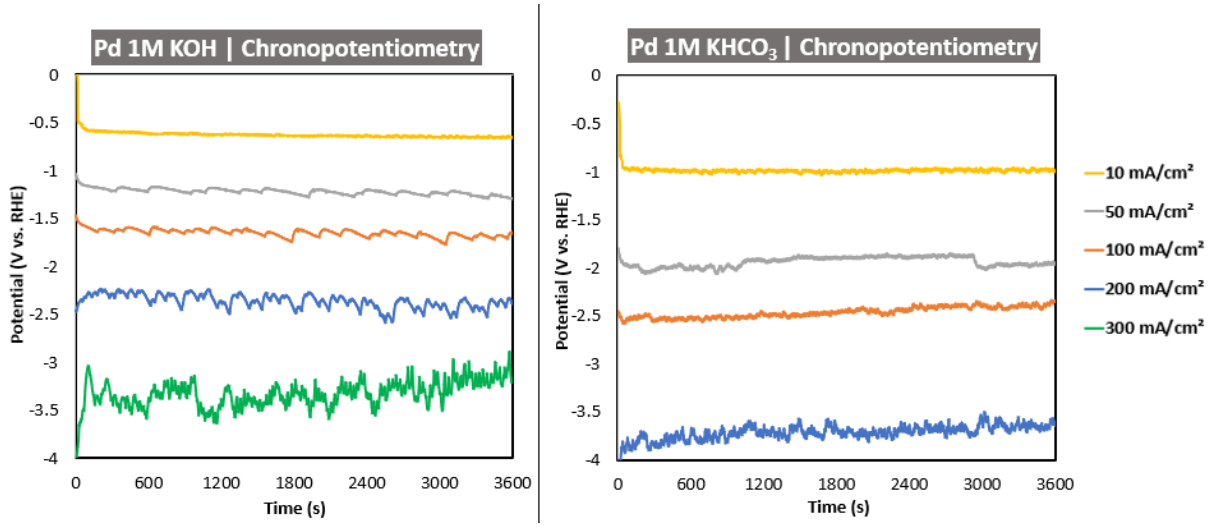

Figure S3.13. Chronopotentiometry measurements for Pd in 1 M KOH and $KHCO_3$.

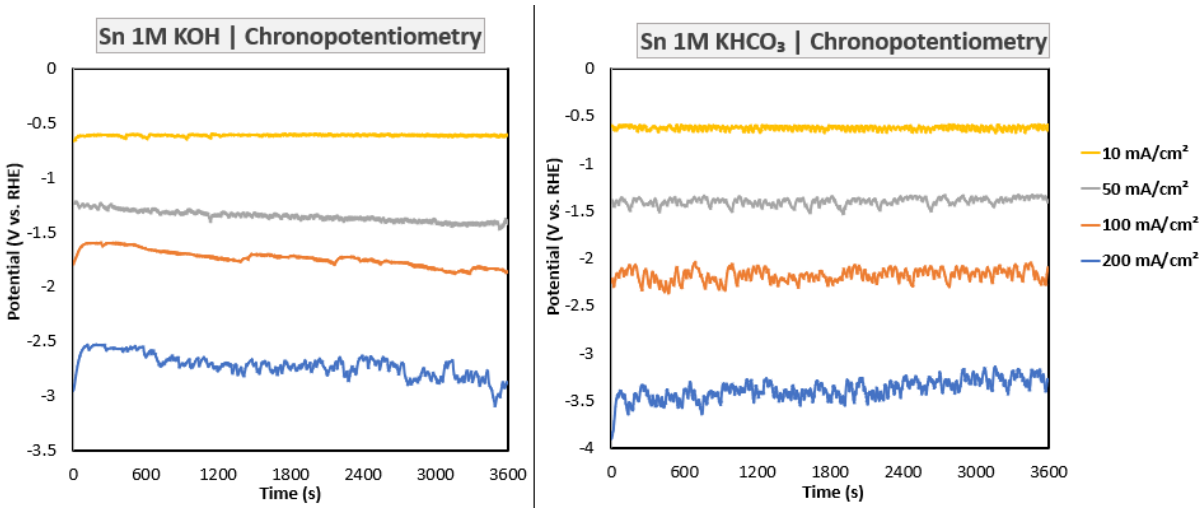

Figure S3.14. Chronopotentiometry measurements for Sn in 1 M KOH and $KHCO_3$.

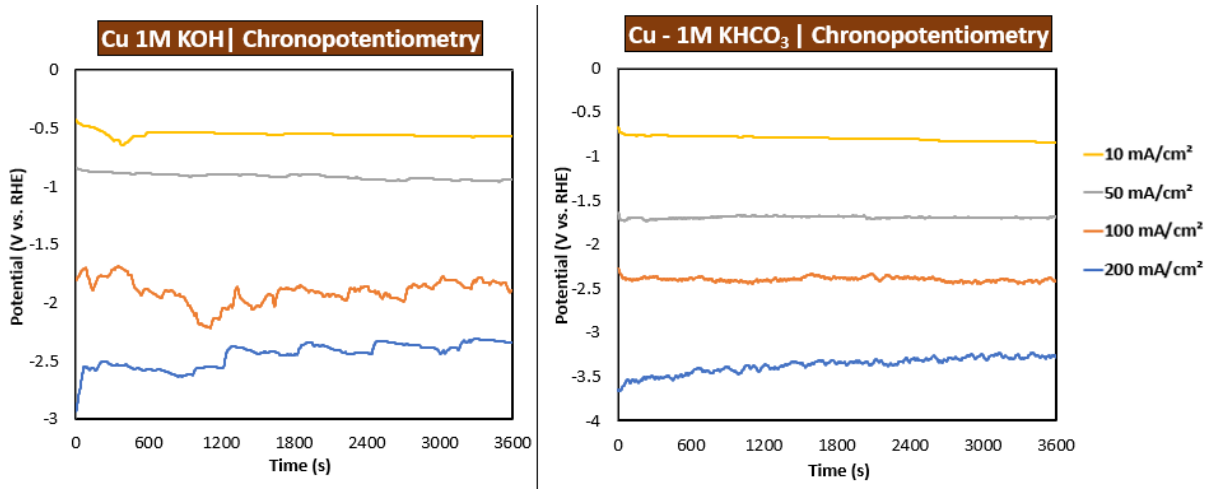

Figure S3.15. Chronopotentiometry measurements for Cu in 1 M KOH and $KHCO_3$.

Time-dependent Faradaic efficiencies - FE

During all experiments GC samples were taken every 4 minutes. The measured signal is converted into a concentration. Liquid analysis by HPLC is only performed when the experiment is completed after which the production is averaged over the duration. The following formula is used to calculate and plot the time-dependent Faradaic efficiencies (Figure S3.16 – S3.20). $\boldsymbol{FE_n}$ is the Faradaic efficiency of product n, $\boldsymbol{z_n}$ the number of electrons per formed molecule of product n, $\boldsymbol{F}$ the Faraday constant, $\boldsymbol{c_n}$ the concentration of n measured by the GC, $\boldsymbol{\varphi_{CO_2}}$ the molar flowrate of CO_2 and $\boldsymbol{I_{tot}}$ the total current going through the system.

$$FE_n = \frac{z_n F (c_n * \varphi_{CO_2})}{I_{tot}}$$

Products are H_2 (z = 2), CO (z = 2), CH_4 (z = 8) and C_2H_4 (z = 12) [mol_e/mol_n]. $\boldsymbol{F}$ = 96485 [C/mol_e], $\boldsymbol{c_n}$ [mol_n/mol_{CO2}], $\boldsymbol{\varphi_{CO_2}}$ (=30 mL/min) = 4,46*10^{-5} [mol_{CO2}/s].

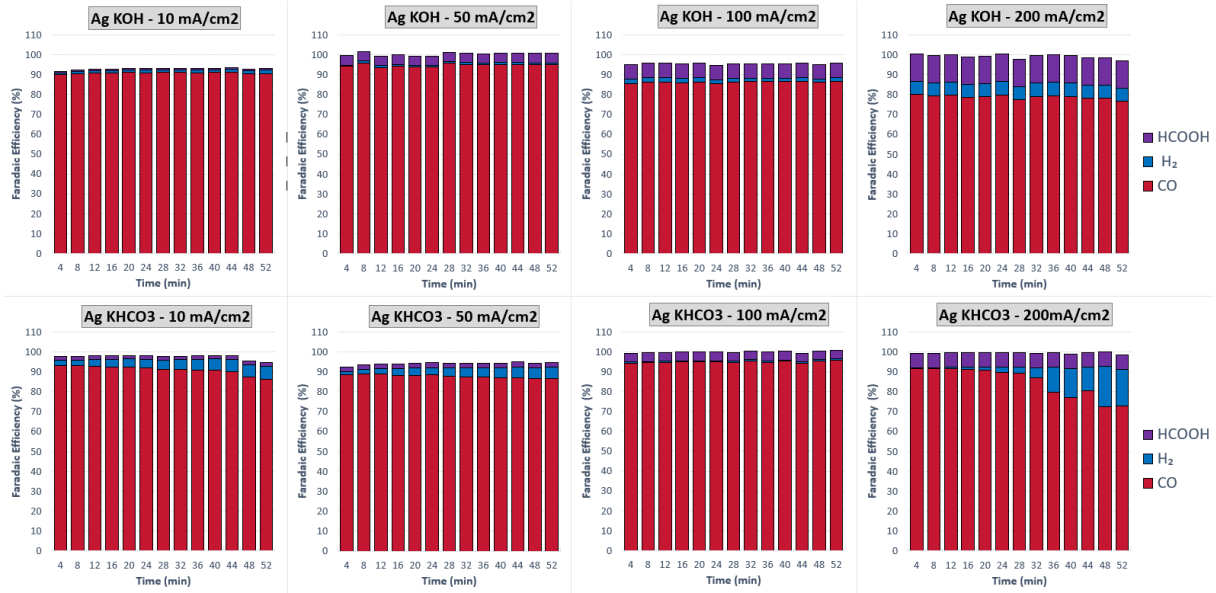

Figure S3.16. Time-dependent FE of products for a 100 nm Ag GDE.

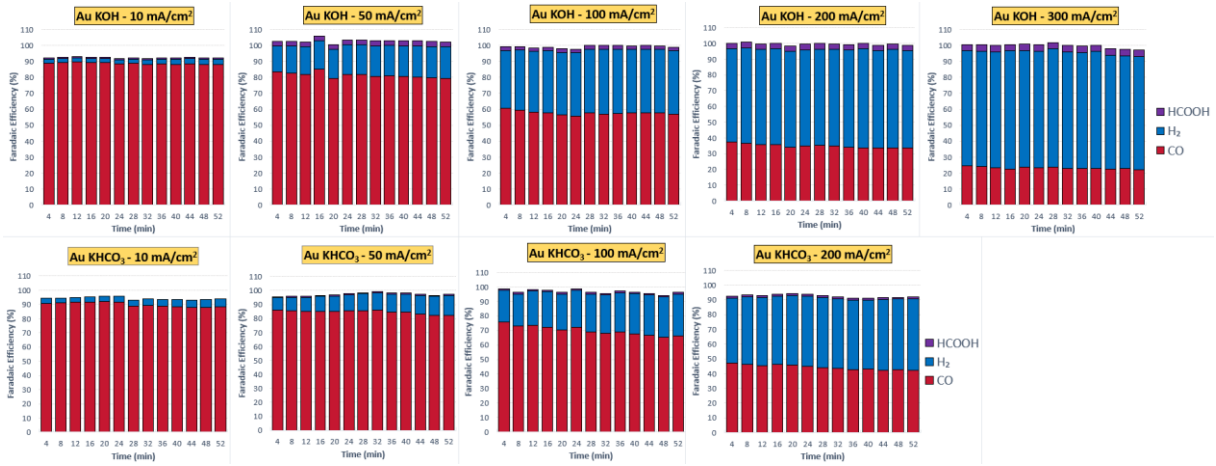

Figure S3.17. Time-dependent FE of products for a 100 nm Au GDE.

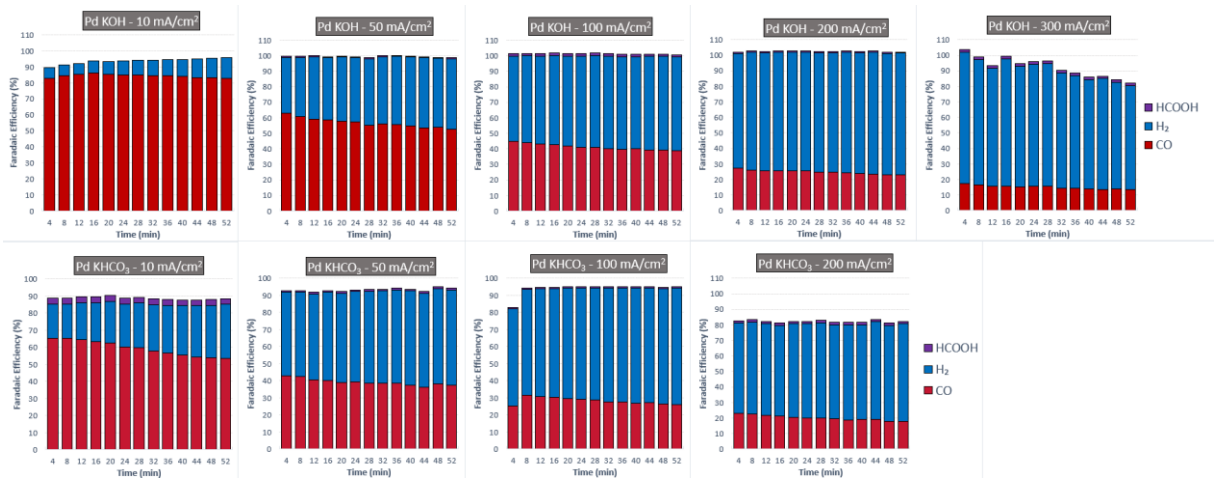

Figure S3.18. Time-dependent FE of products for a 100 nm Pd GDE.

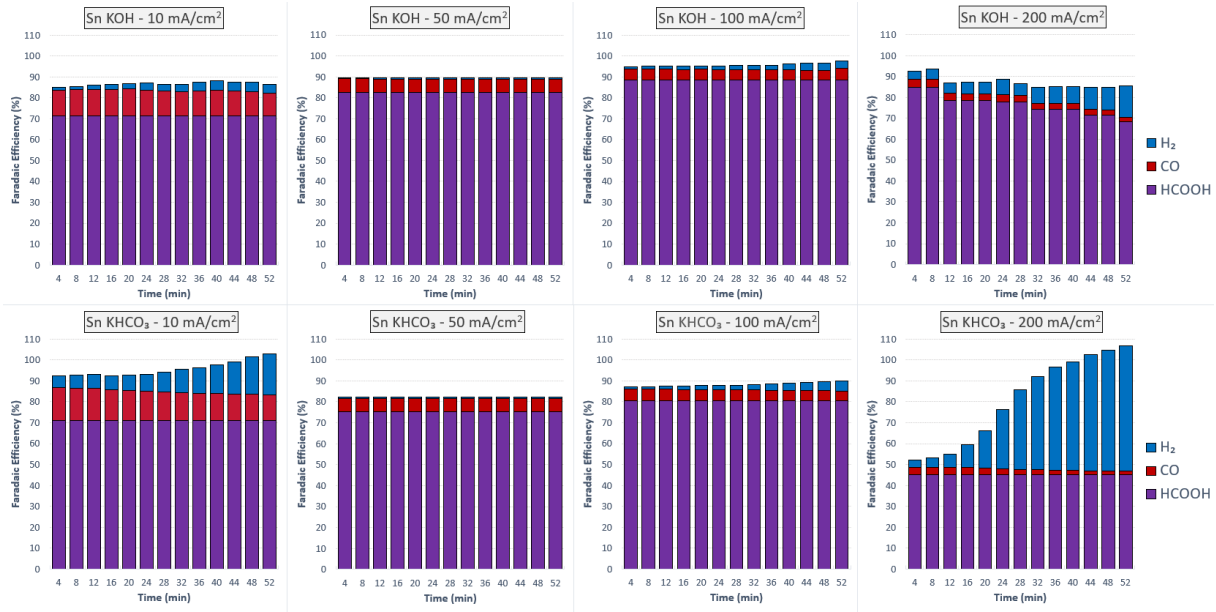

Figure S3.19. Time-dependent FE of products for a 100 nm Sn GDE.

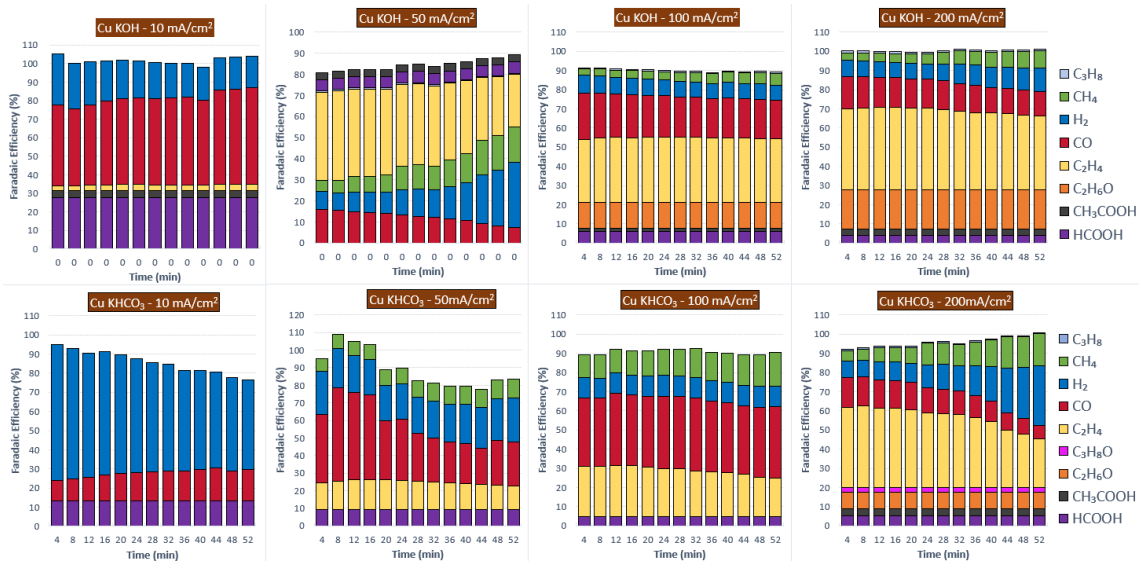

Figure S3.20. Time-dependent FE of products for a 100 nm Cu GDE.

Scanning electron microscopy – SEM

In Figure S3.21 below HR-SEM images of the as-deposited catalysts are displayed. All catalysts show similar porosity and catalyst coverage on the GDE. Sn shows slightly increased agglomeration of the catalysts due to the more volatile nature of the metal *(Note: the deposition power of Sn was 20 W as compared to 50 W for the other metals.)*

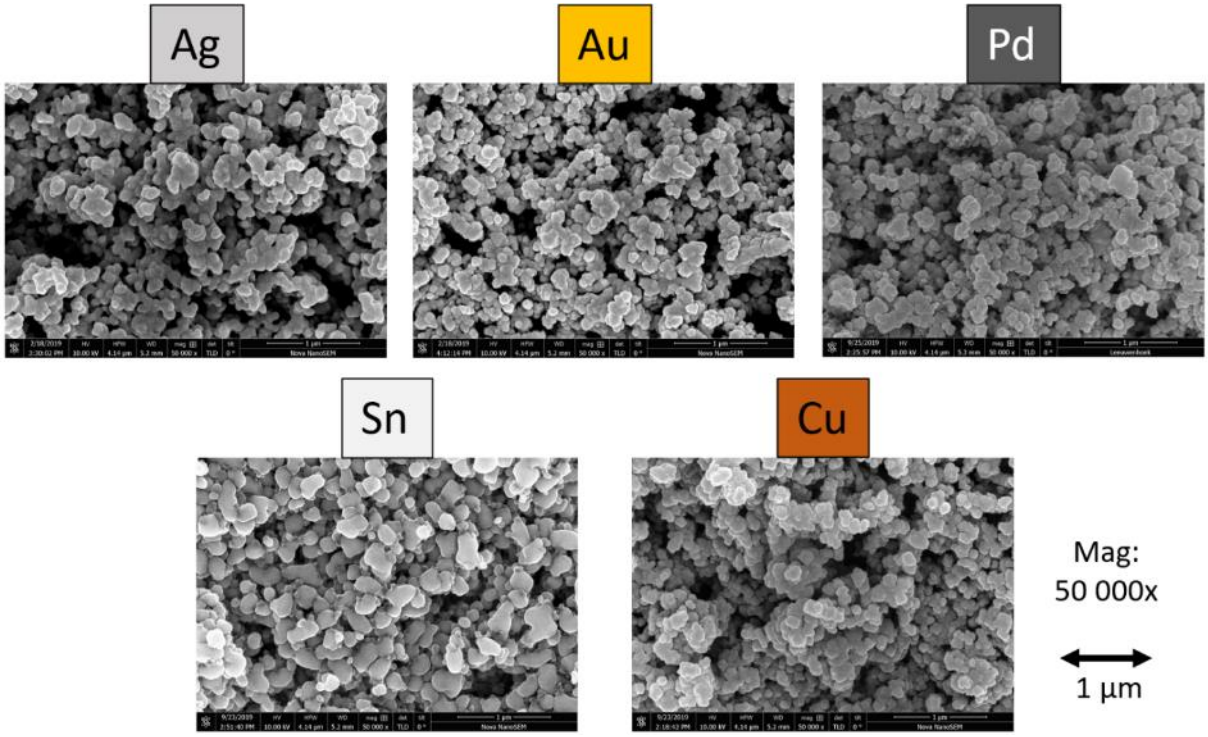

Figure S3.21. HR-SEM images of all 5 as-deposited catalysts. Throughout a similar porosity and particle size can be observed.

The remainder of this section contains scanning electron microscopy images taken from a bare Sigracet 38 BC GDL (Figure S3.22) as well as fresh and used samples (Figure S3.23 – S3.32). Initially 500 mA cm^{-2} (=1.125 A) experiments were also attempted, but due to the limiting compliance voltage of our potentiostat (ΔU_{max} = 12 V_{cell}) alongside the high resistance of the wide cell, it was not possible to achieve the requested current. Instead, the physical effects of 12 V total cell potential can be witnessed, at which current densities between 300-500 mA cm^{-2} were achieved. SEM images of these experiments do show interesting features of potassium depositions, catalyst reconstruction and a continuation of the earlier observed surface changes to a greater extent.

Magnifications and total dimensional image sizes

Magnification: **x 50** **~2.6 x 1.7 mm**	Magnification: **x 100** **~1.3 x 0.85 mm**	Magnification: **x 500** **~260 x 170 µm**	Magnification: **x 1000** **~130 x 85 µm**	Magnification: **x 5000** **~26 x 17 µm**

Bare gas diffusion layer (GDL)

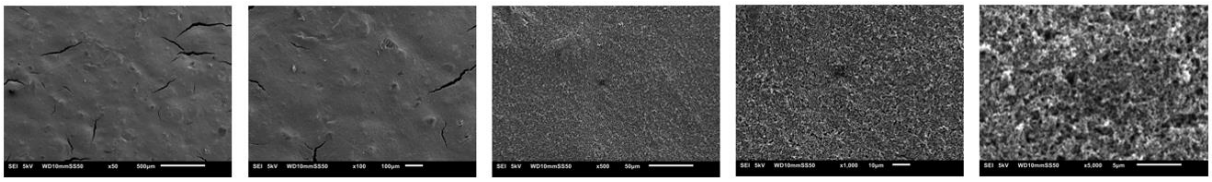

Figure S3.22. SEM images of a bare gas diffusion layer (Sigracet 38 BC)

Ag – KOH

100nm Ag - 10mA/cm^2 – 1M KOH

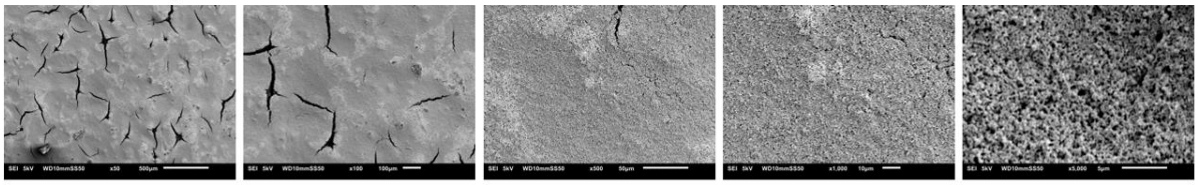

100nm Ag - 50mA/cm^2 – 1M KOH

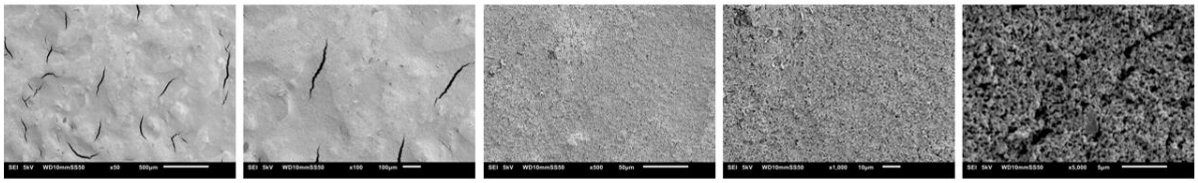

100nm Ag – 100mA/cm^2 – 1M KOH

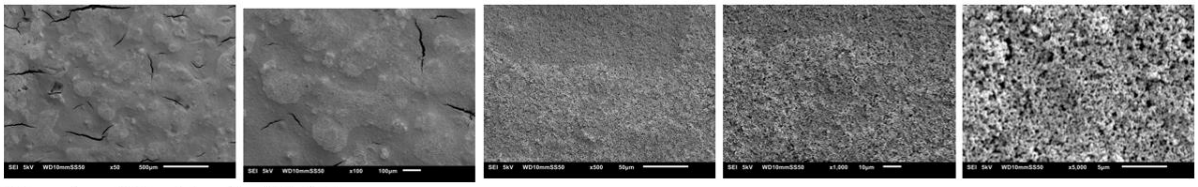

100nm Ag - 200mA/cm^2 – 1M KOH

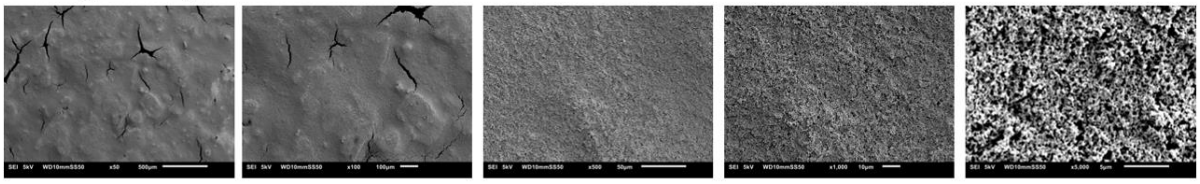

100nm Ag - 12 V_{cell} – 1M KOH

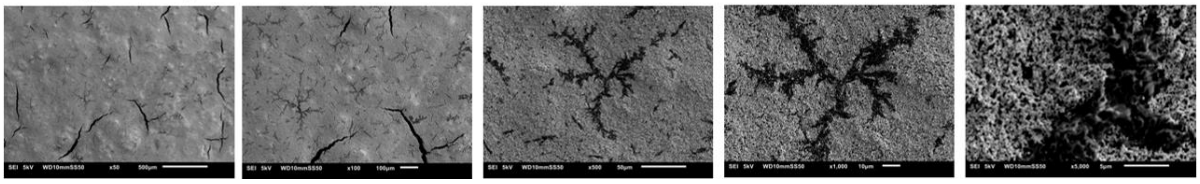

Figure S3.23. SEM images of 100 nm Ag on GDE after 1 hour reaction in 1M KOH at various current densities. Overall, this system seems stable up to 200 mA cm^{-2}. At 500 mA cm^{-2} the surface displays branched coverage, which was identified to mainly contain increased amounts of potassium and oxygen. It is likely the high overpotentials initiated a growing deposition of potassium from the electrolyte.

x 50 ~2.6 x 1.7 mm	x 100 ~1.3 x 0.85 mm	x 500 ~260 x 170 µm	x 1000 ~130 x 85 µm	x 5000 ~26 x 17 µm

Ag – $KHCO_3$

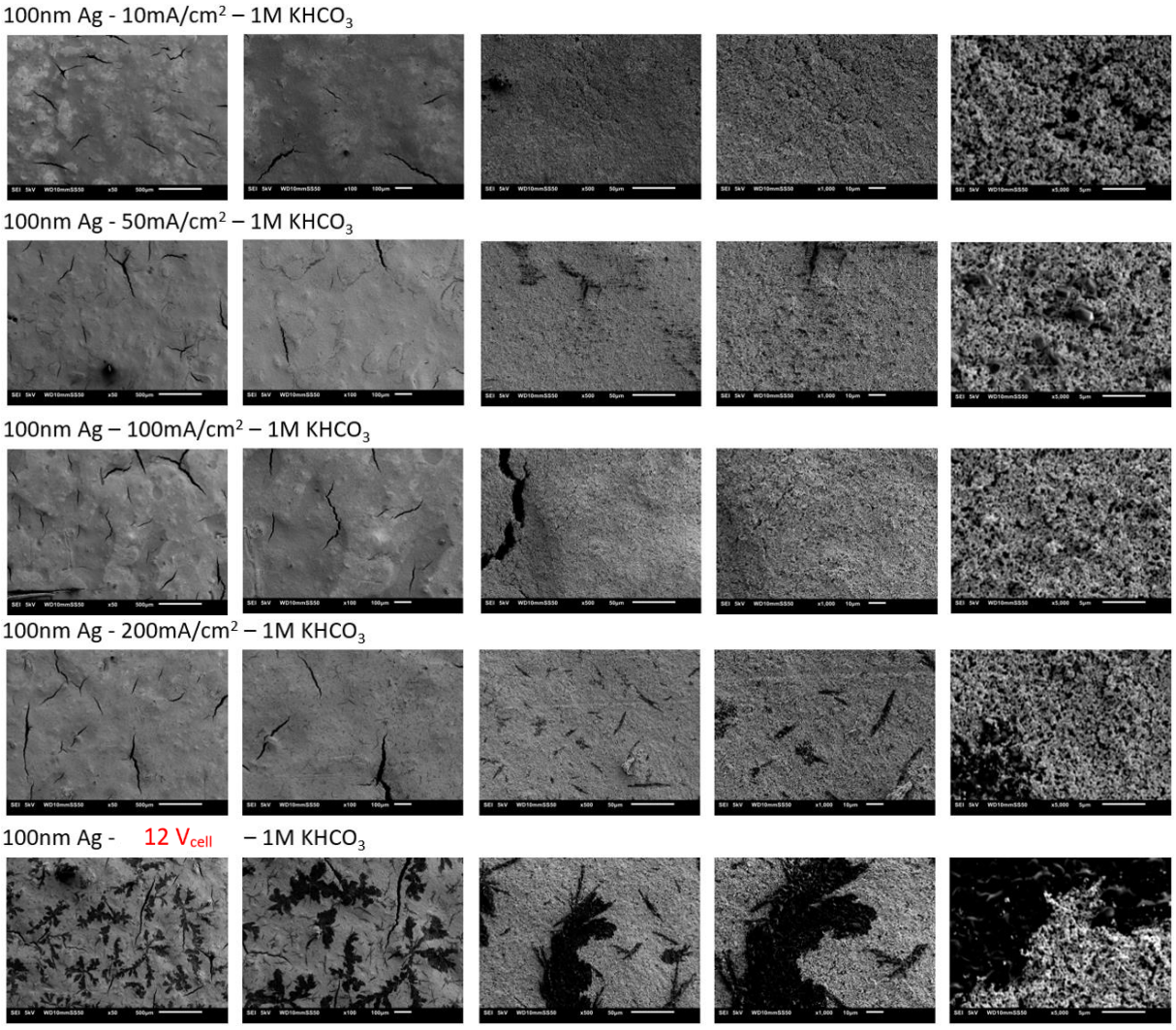

Figure S3.24. SEM images of 100 nm Ag on GDE after 1 hour reaction in 1M $KHCO_3$ at various current densities. At 50 and 100 mA cm^{-2} minor crystals are visible in the x5.000 magnification images. Even higher currents show exponential growth of these crystals. At 12 V the surface is largely covered by this black deposition, with features reaching up to 1-2 mm in length. Again, potassium and oxygen were found in increased quantities in these areas.

x 50 ~2.6 x 1.7 mm	x 100 ~1.3 x 0.85 mm	x 500 ~260 x 170 µm	x 1000 ~130 x 85 µm	x 5000 ~26 x 17 µm

Au – KOH

100nm Au - 10mA/cm^2 – 1M KOH

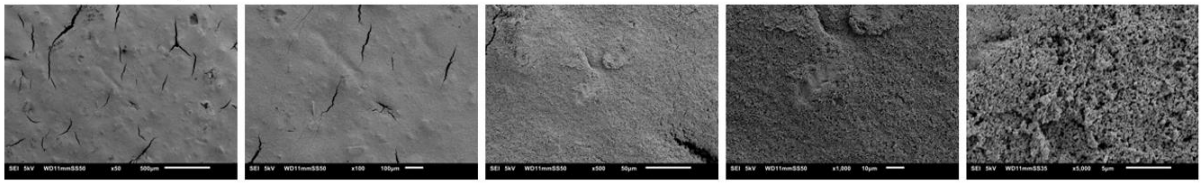

100nm Au - 50mA/cm^2 – 1M KOH

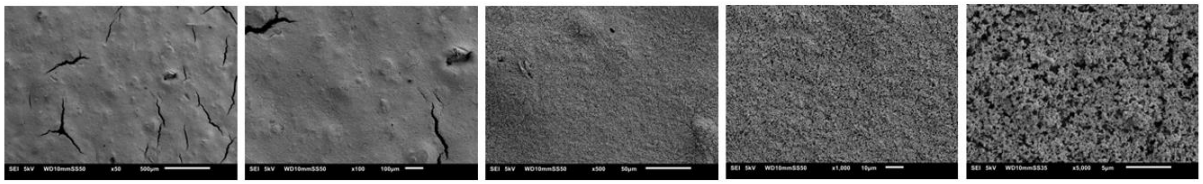

100nm Au – 100mA/cm^2 – 1M KOH

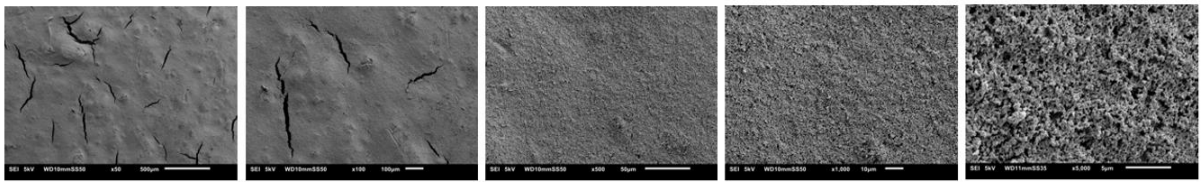

100nm Au - 200mA/cm^2 – 1M KOH

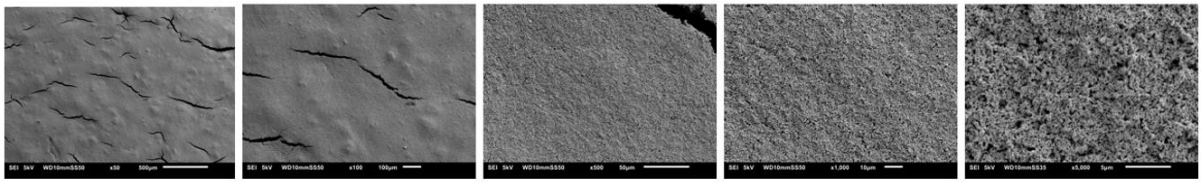

100nm Au - 12 V_{cell} – 1M KOH

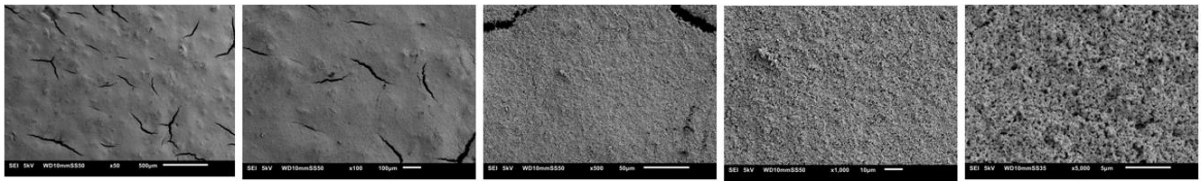

Figure S3.25. SEM images of 100 nm Au on GDE after 1 hour reaction in 1 M KOH at various current densities. Au is stable and no apparent changes across all 5 samples are found under these conditions.

x 50 ~2.6 x 1.7 mm	x 100 ~1.3 x 0.85 mm	x 500 ~260 x 170 µm	x 1000 ~130 x 85 µm	x 5000 ~26 x 17 µm

Au – $KHCO_3$

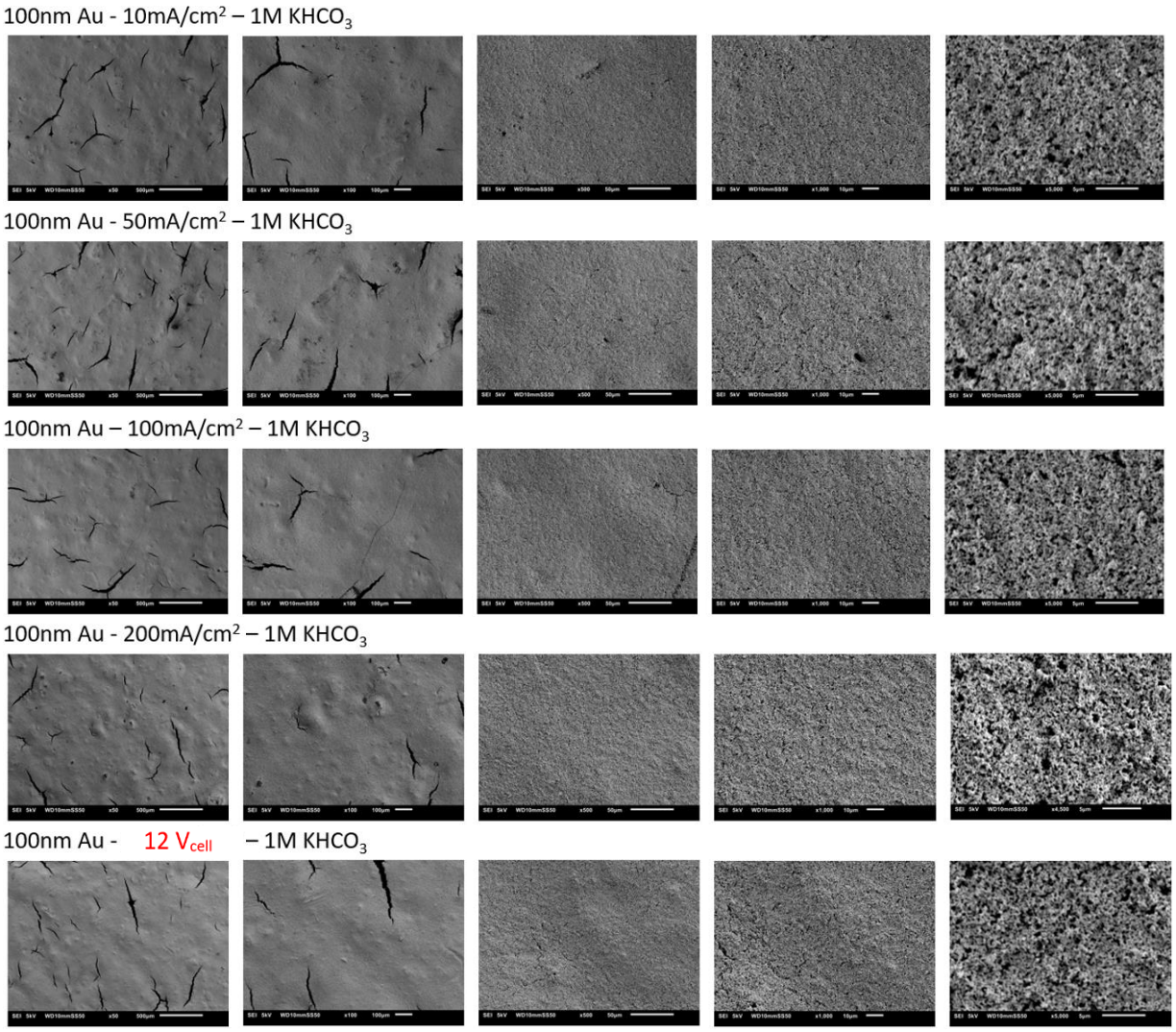

Figure S3.26. SEM images of 100 nm Au on GDE after 1 hour reaction in 1 M $KHCO_3$ at various current densities. Au is stable and no apparent changes across all 5 samples are found under these conditions.

x 50 ~2.6 x 1.7 mm	x 100 ~1.3 x 0.85 mm	x 500 ~260 x 170 µm	x 1000 ~130 x 85 µm	x 5000 ~26 x 17 µm

Pd – KOH

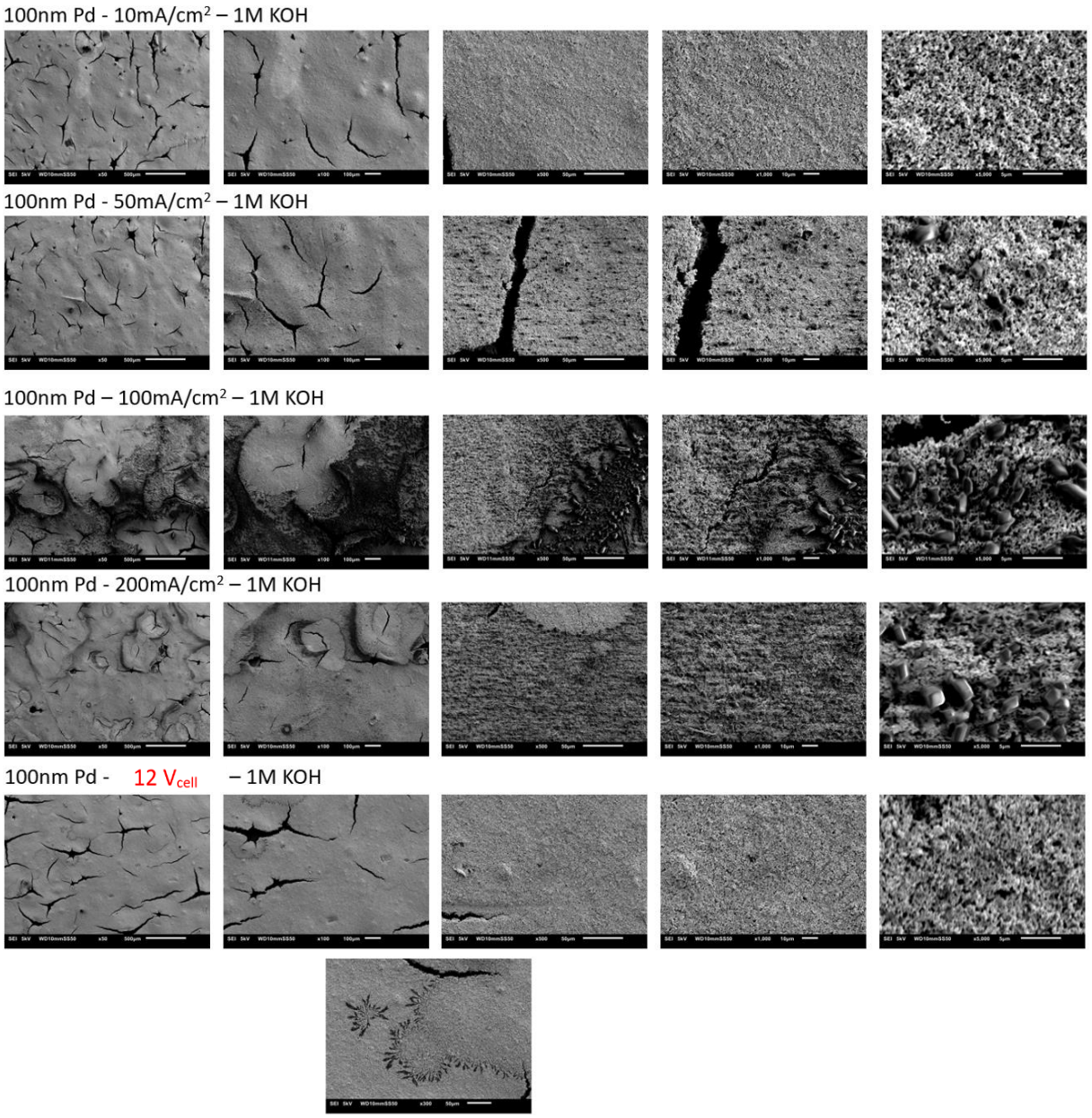

Figure S3.27. SEM images of 100 nm Pd on GDE after 1 hour reaction in 1 M KOH at various current densities. All current densities above the lowest (10 mA cm^{-2}) show surface instability and coverages to different extent. The surface seems to change the most at 100 mA cm^{-2}, after which higher currents and potentials show a lesser disrupting effect.

x 50 ~2.6 x 1.7 mm	x 100 ~1.3 x 0.85 mm	x 500 ~260 x 170 µm	x 1000 ~130 x 85 µm	x 5000 ~26 x 17 µm

Pd – $KHCO_3$

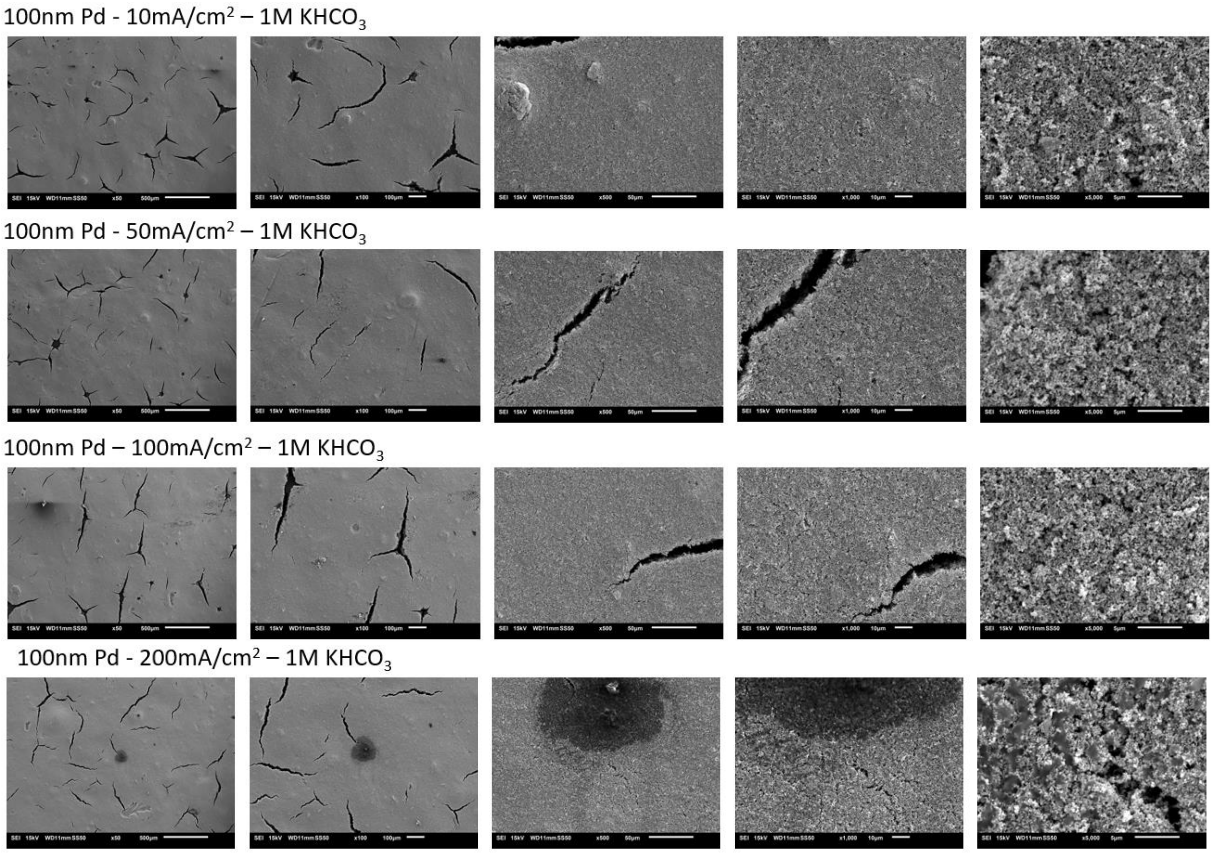

Figure S3.28. SEM images of 100 nm Pd on GDE after 1 hour reaction in 1 M $KHCO_3$ at various current densities. In comparison to the 1 M KOH case these samples show much better stability with a small fraction of the surface being altered.

x 50 ~2.6 x 1.7 mm	x 100 ~1.3 x 0.85 mm	x 500 ~260 x 170 µm	x 1000 ~130 x 85 µm	x 5000 ~26 x 17 µm

Sn – KOH

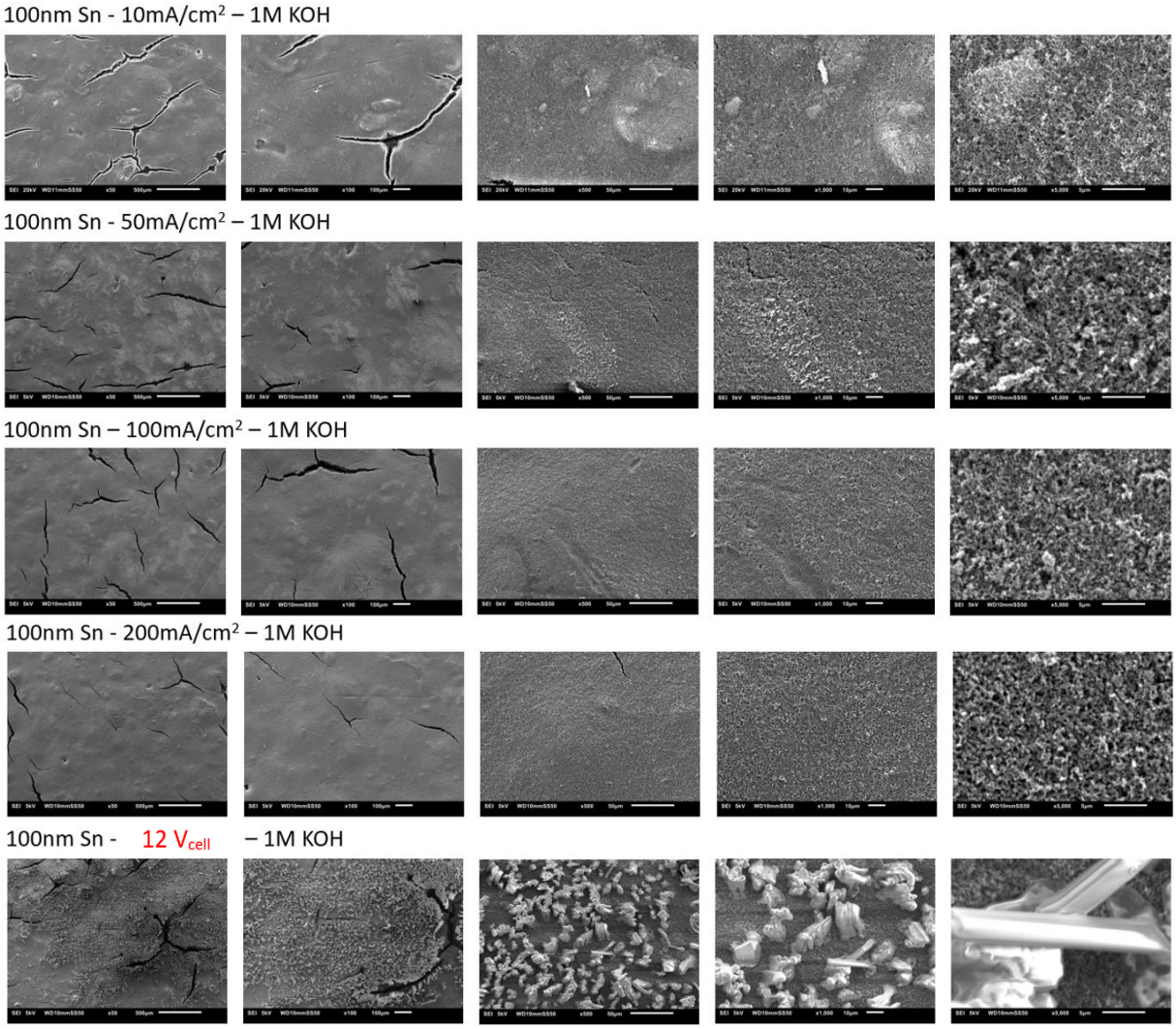

Figure S3.29. SEM images of 100 nm Sn on GDE after 1 hour reaction in 1 M KOH at various current densities. Overall, the Sn samples seems rather stable at low and moderate activities. The x5000 image of the 200 mA cm^{-2} case showed 'thinner' GDE structures, indicating minor dissolution of the catalyst. Looking at the samples exposed to 12 V_{cell} a remarkable sight was obtained. The surface of the GDE was for a large part covered in potassium containing crystals.

x 50 ~2.6 x 1.7 mm	x 100 ~1.3 x 0.85 mm	x 500 ~260 x 170 µm	x 1000 ~130 x 85 µm	x 5000 ~26 x 17 µm

Sn – $KHCO_3$

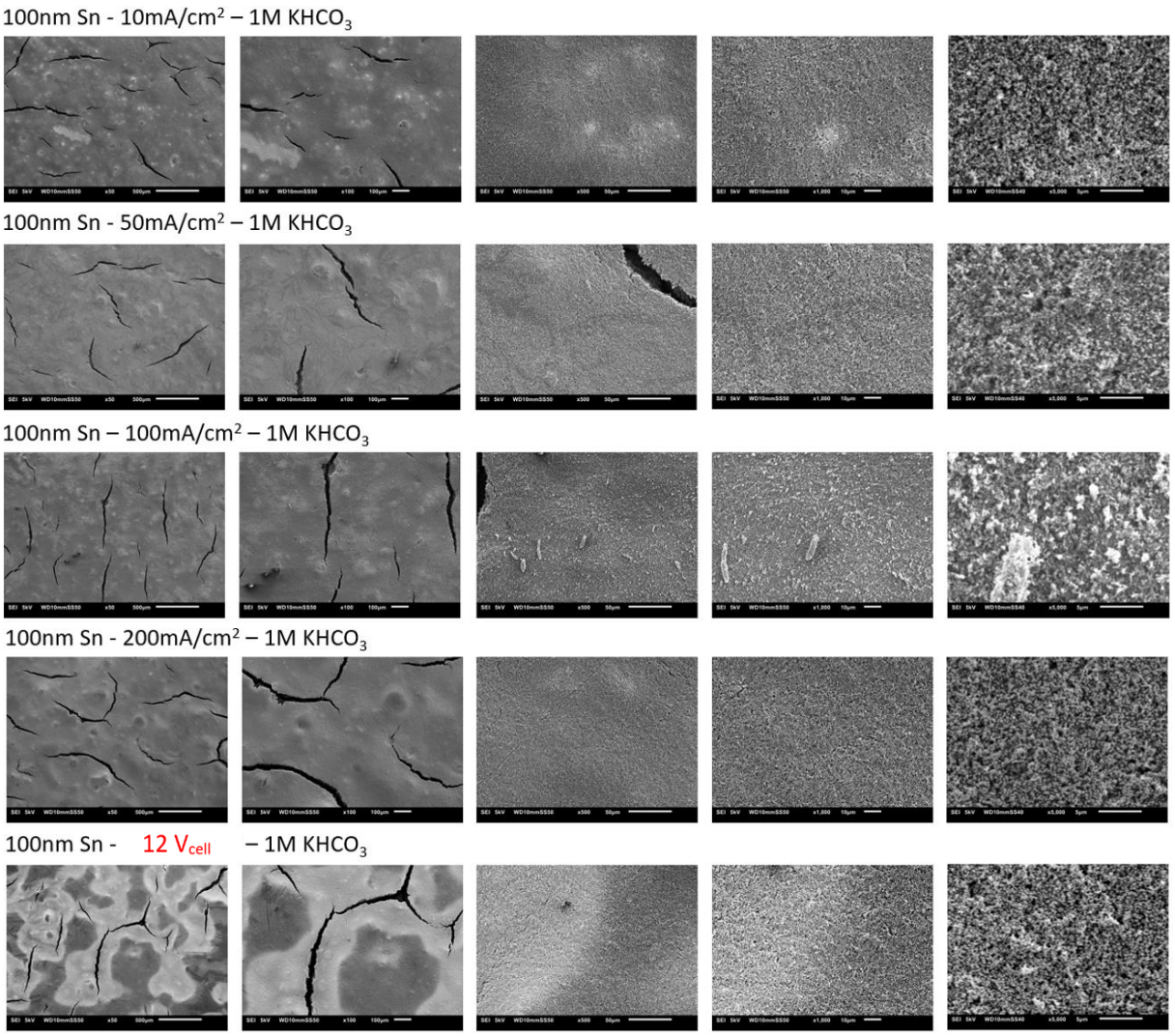

Figure S3.30. SEM images of 100 nm Sn on GDE after 1 hour reaction in 1 M $KHCO_3$ at various current densities. Whereas the KOH experiments showed significant instabilities induced through alkaline conditions, the less extreme environment of $KHCO_3$ only showed a change in color when increasing activity. No distinct differences of what the nature of the decoloring could be was found when looking into elemental mapping.

x 50 ~2.6 x 1.7 mm	x 100 ~1.3 x 0.85 mm	x 500 ~260 x 170 µm	x 1000 ~130 x 85 µm	x 5000 ~26 x 17 µm

Cu – KOH

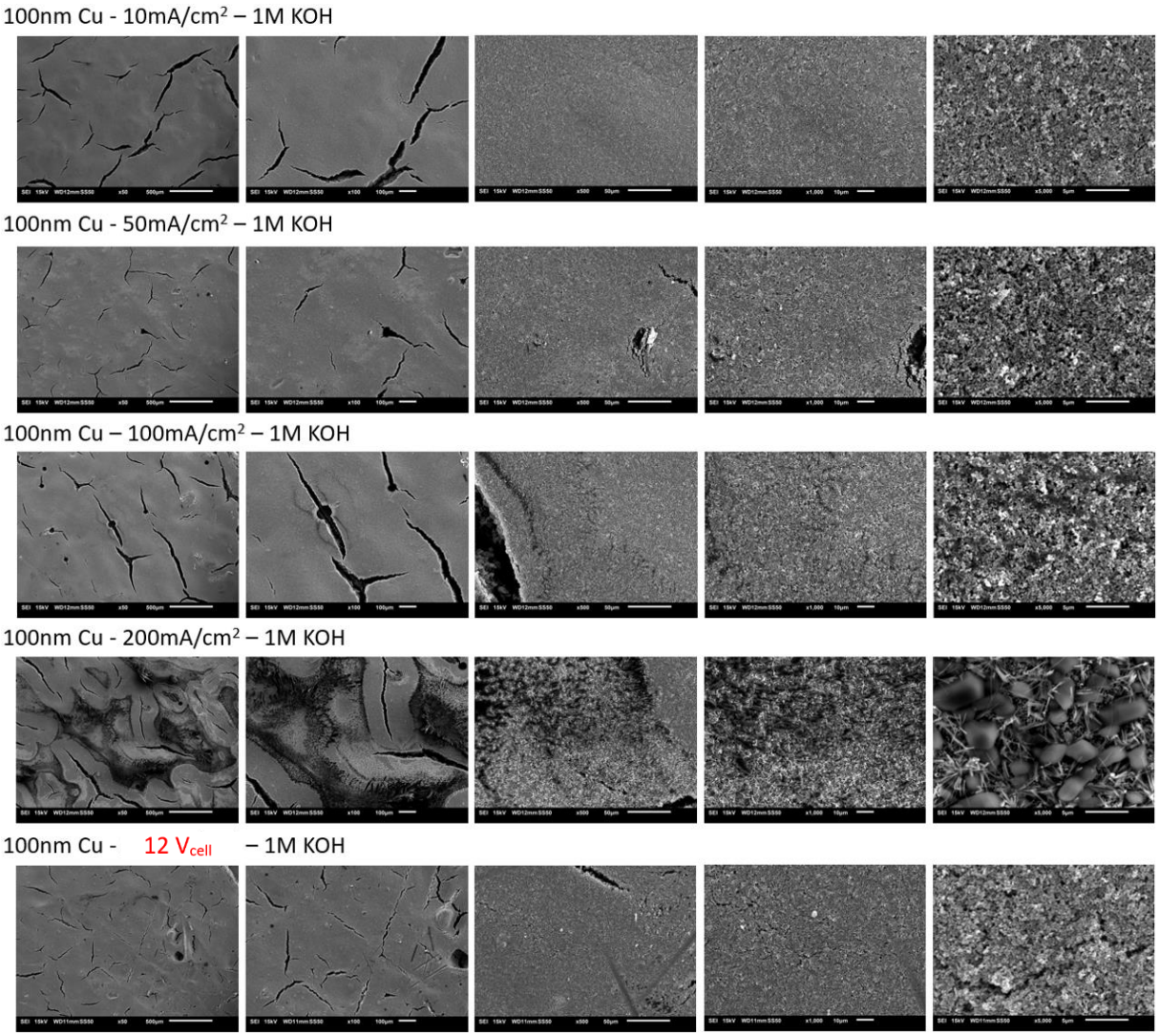

Figure S3.31. SEM images of 100 nm Cu on GDE after 1 hour reaction in 1 M KOH at various current densities. Minor restructuring is observed at 50, 100 and 500 mA cm^{-2}. The 200 mA cm^{-2} appears to supply the surface with a very specific environment that allows the growth of both facetted potassium-containing crystals as well as Cu nanoneedles.

x 50 ~2.6 x 1.7 mm	x 100 ~1.3 x 0.85 mm	x 500 ~260 x 170 µm	x 1000 ~130 x 85 µm	x 5000 ~26 x 17 µm

Cu – $KHCO_3$

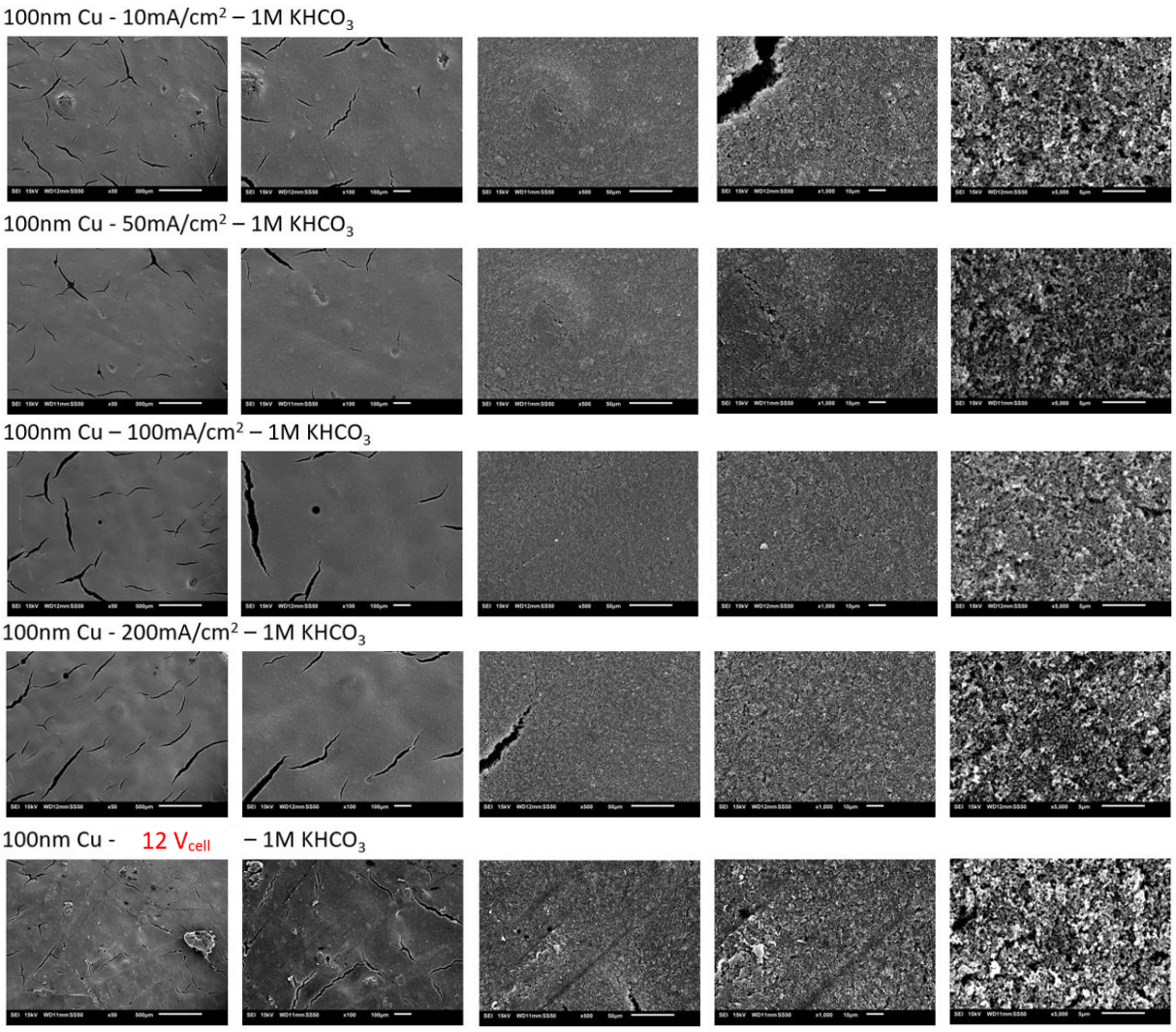

Figure S3.32. SEM images of 100 nm Cu on GDE after 1 hour reaction in 1 M $KHCO_3$ at various current densities. Throughout all experiments no significant changes were found on the surface structure. The darkening in some images is caused by a change of SEM brightness settings.

High-resolution scanning electron microscopy - HR-SEM

This section contains three magnifications of high resolution scanning electron microscopy (HR-SEM) images of the 5 metals as deposited and after electroreduction for 1 hour in 1 M KOH and 1 M $KHCO_3$ at V_{cell} = 12 V (Figure S3.33 – S3.37. Above the images the used magnification can be found. Between the sputtered and used samples differences such as agglomeration, clustering, smoothening, deposition and reformation can be found.

Magnif.	**x 15.000**	**x 50.000**	**x 150.000**
Size	**9,0 x 13,5 µm**	**2,7 x 4,1 µm**	**0,9 x 1,35 µm**

Ag – sputtered

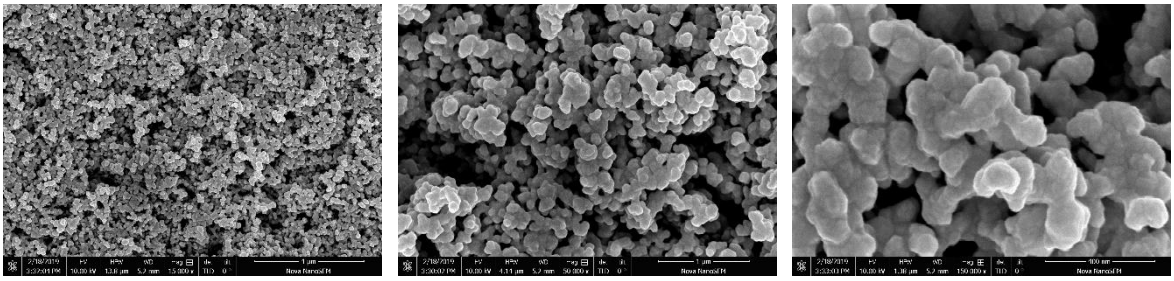

Ag – 1 M KOH

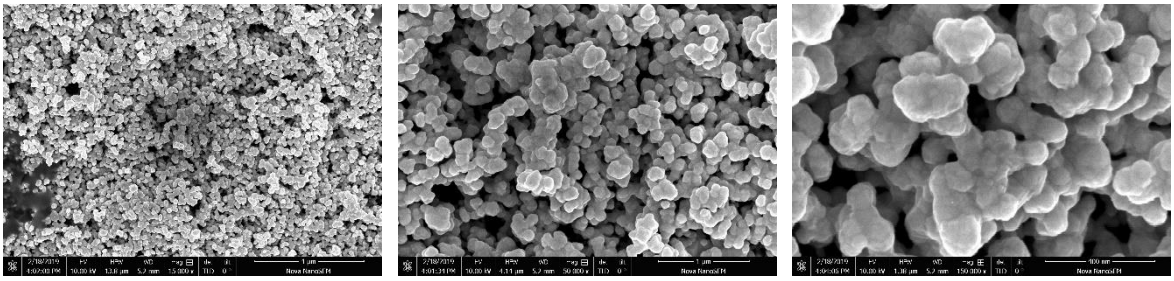

Ag – $KHCO_3$

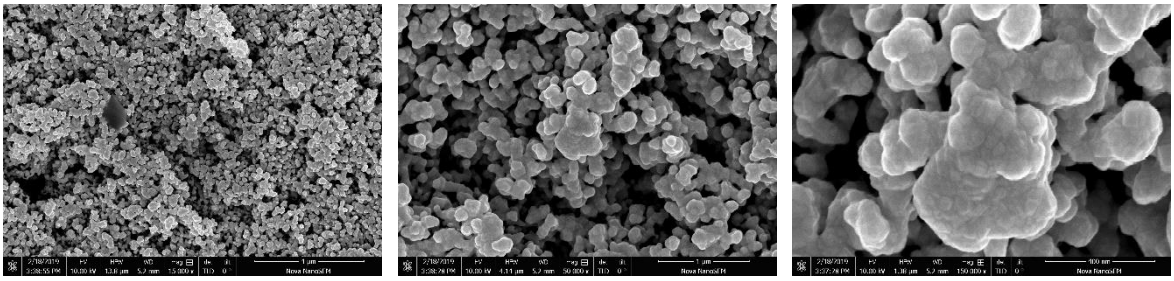

Figure S3.33. HR-SEM images of 100 nm Ag on GDE before and after 1 hour reaction. The catalyst layer itself seems to be unaffected by the reaction.

Magnif.	x 5.000	x 50.000	x 150.000
Size	27 x 41 µm	2,7 x 4,1 µm	0,9 x 1,35 µm

Au – sputtered

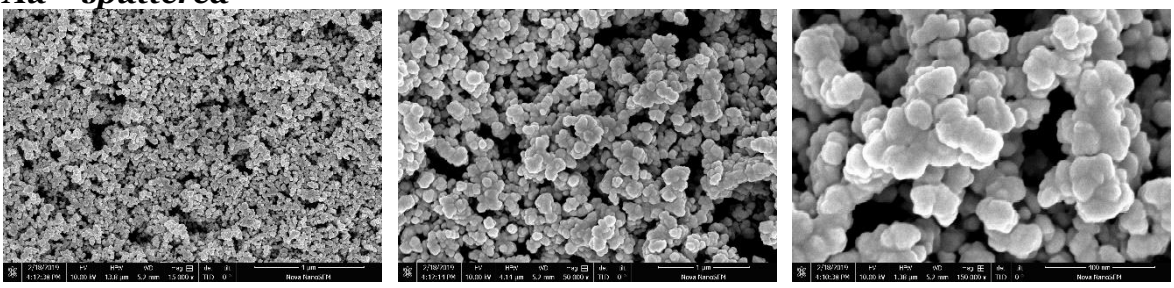

Au – KOH

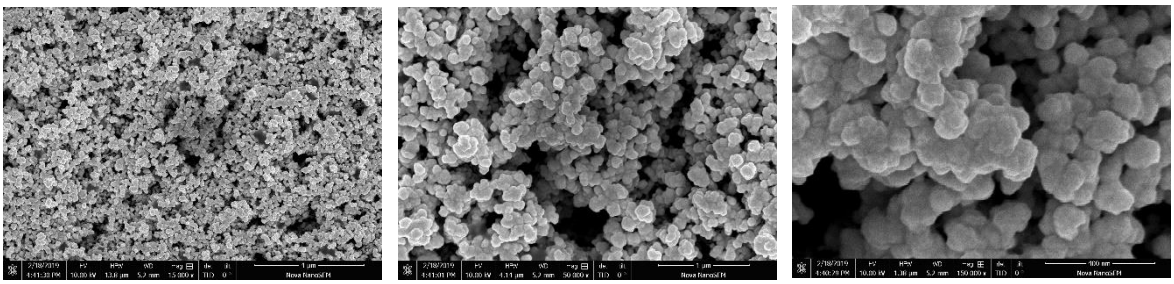

Au – $KHCO_3$

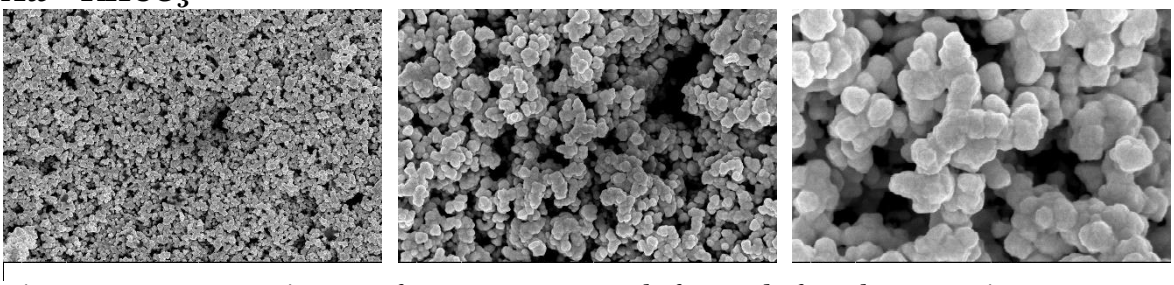

Figure S3.34. HR-SEM images of 100 nm Au on GDE before and after 1 hour reaction.

Pd – sputtered

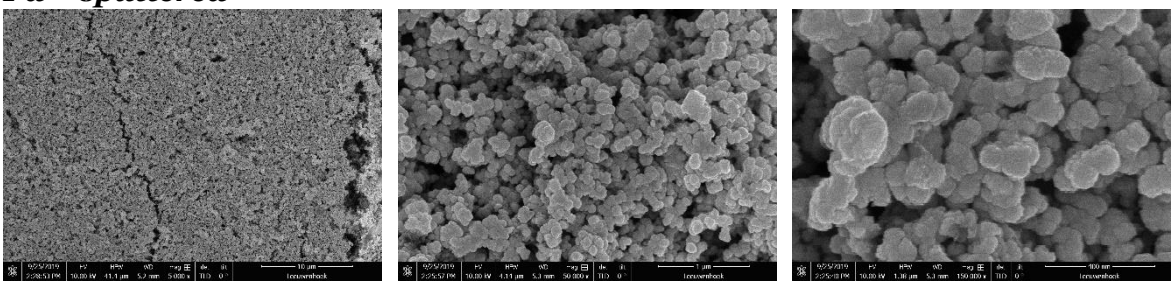

Pd – KOH

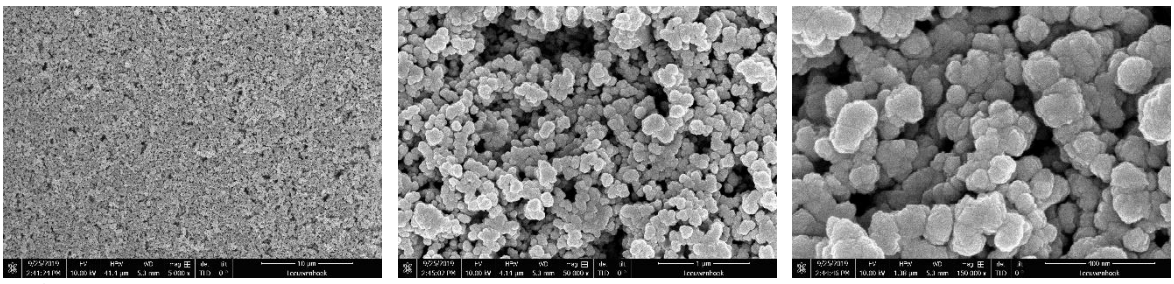

Pd – $KHCO_3$

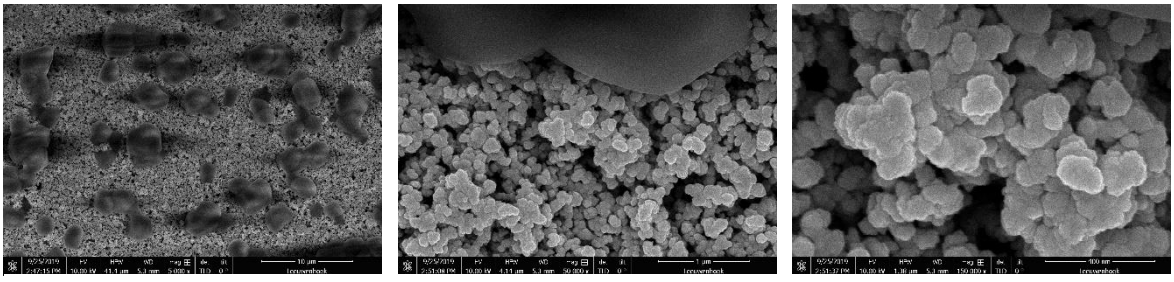

Figure S3.35. HR-SEM images of 100 nm Pd on GDE before and after 1 hour reaction.

Magnif.	x 5.000	x 50.000	x 150.000
Size	27 x 41 µm	2,7 x 4,1 µm	0,9 x 1,35 µm

Sn – sputtered

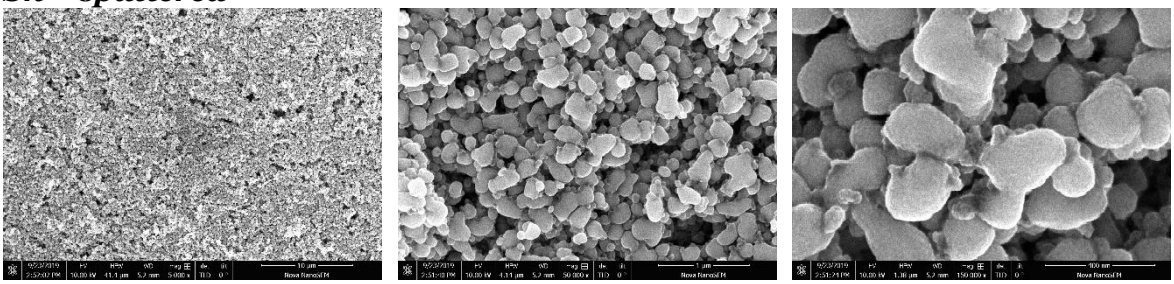

Sn – KOH

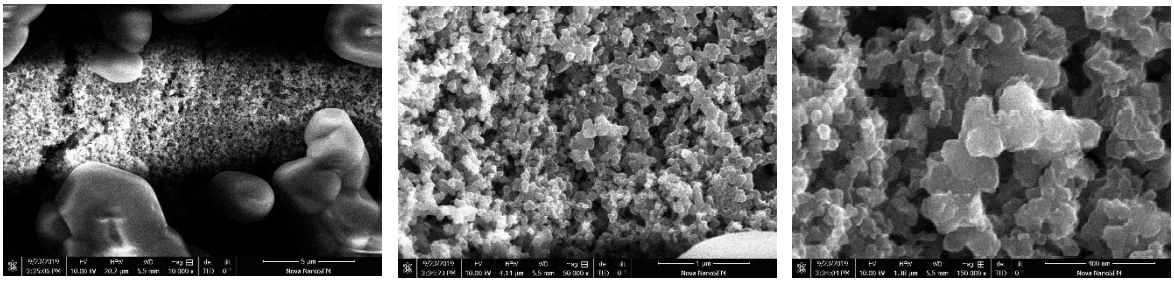

Sn – $KHCO_3$

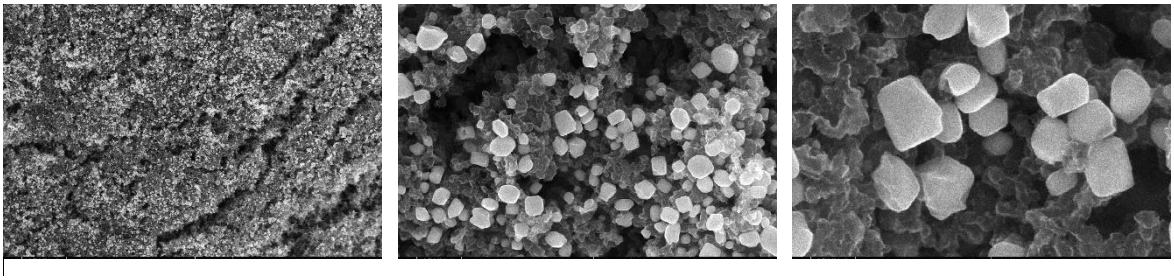

Figure S3.36. HR-SEM images of 100 nm Sn on GDE before and after 1 hour reaction.

Cu – sputtered

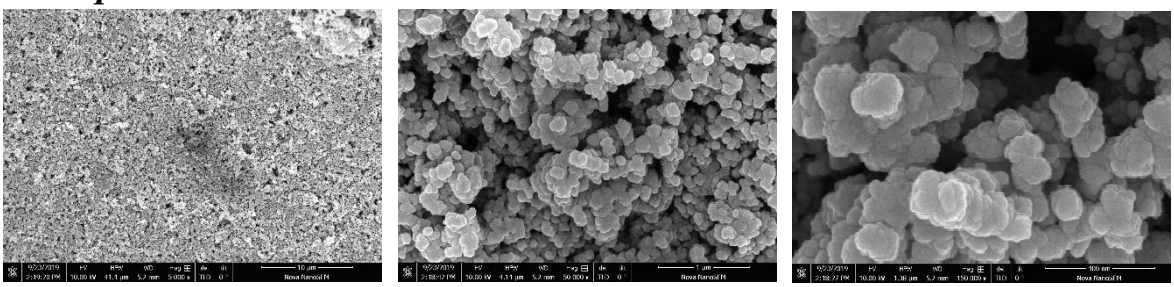

Cu – KOH

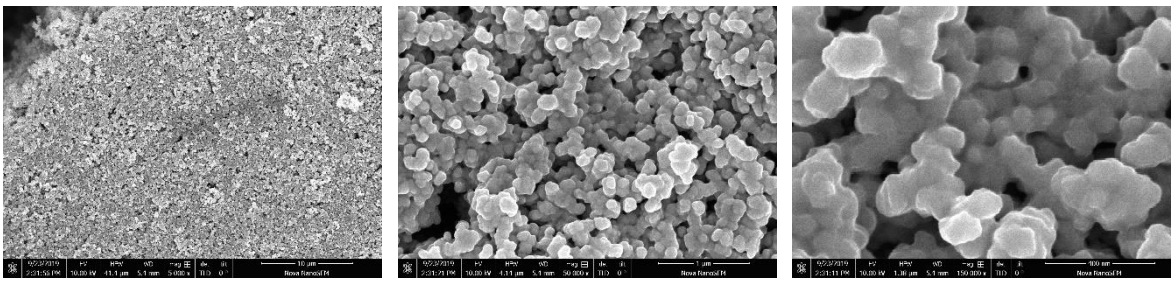

Cu – $KHCO_3$

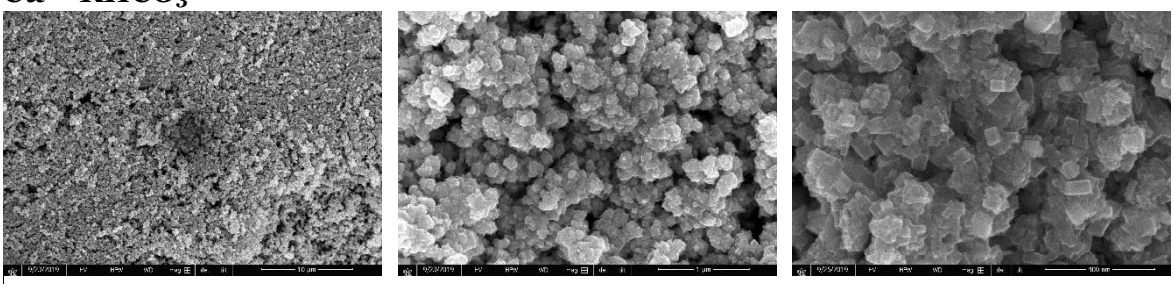

Figure S3.37. HR-SEM images of 100 nm Cu on GDE before and after 1 hour reaction.

X-ray photoelectron spectroscopy – XPS

This section contains all XPS scans of the 5 metals as deposited and after electroreduction at 200 mA/cm^2 for 1 hour in both KOH and $KHCO_3$ (Figure S3.38 – S52). During XPS the following scans were performed for each of these samples:

1. **A survey scan** between 1350 and 0 eV
2. **A respective metal element scan** (Ag/Au/Pd/Sn/Cu)
3. **A valence band scan** [in some cases]
4. **A carbon (C) scan** between 298 and 279 eV
5. **An oxygen (O) scan** between 545 and 525 eV
6. **A potassium (K) scan** between 305 and 287 eV

Corresponding to the numbers above the following format is used:

[Metal] [Condition]

1.	**2.**	**[3.]**
4.	**5.**	**6.**

The survey and respective metal elements give us information on the stability of the metal, for instance, in the Sn fresh vs Sn KOH/$KHCO_3$ case there is a significant signal drop-off of the Sn3d peak (~99% for KOH, ~50% for $KHCO_3$) after testing, indicating its instability.

To obtain additional information on the presence and stability of the GDE the carbon (and fluorene) peaks are looked into. Each scan is performed on and averaged over 2 separate locations (random spots, not on substrate native crevices).

Ag fresh

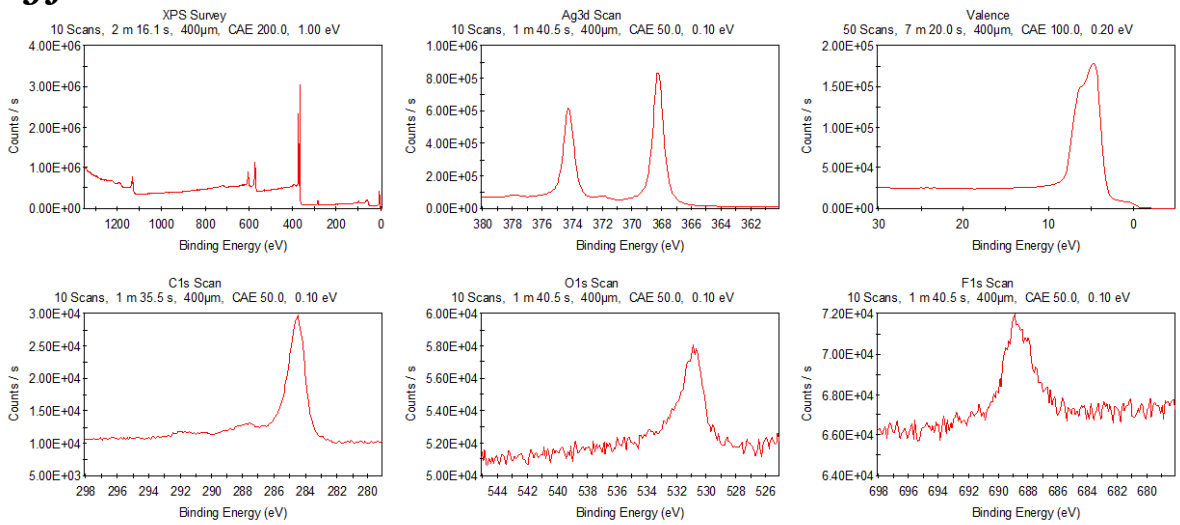

Figure S3.38. XPS spectra of a fresh Ag sample.

Ag KOH

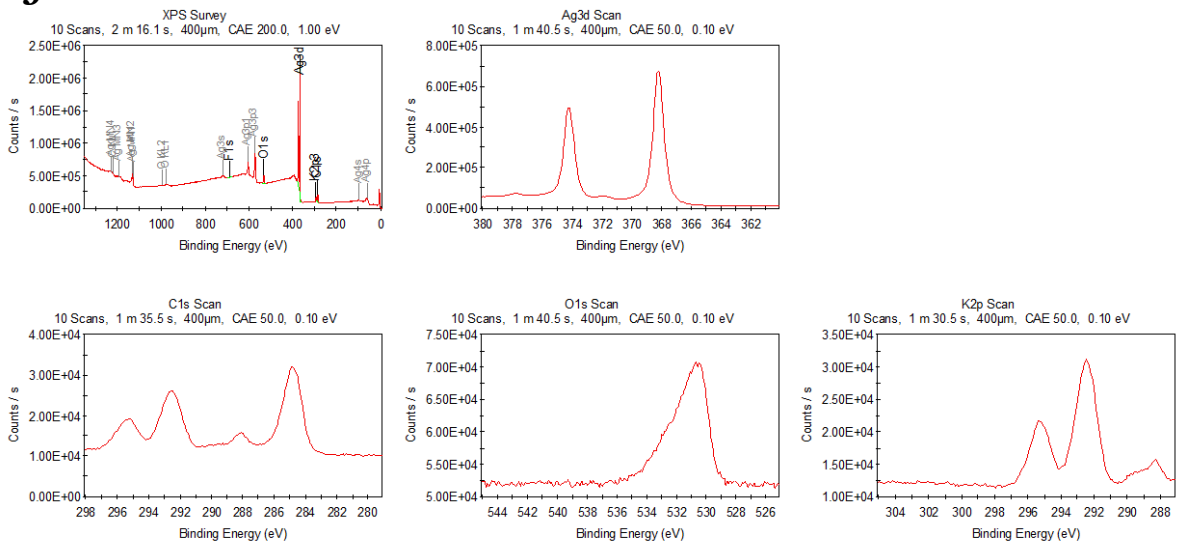

Figure S3.39. XPS spectra of a Ag sample after 1 hr electrolysis at 200 mA cm^{-2} in 1 M KOH.

Ag $KHCO_3$

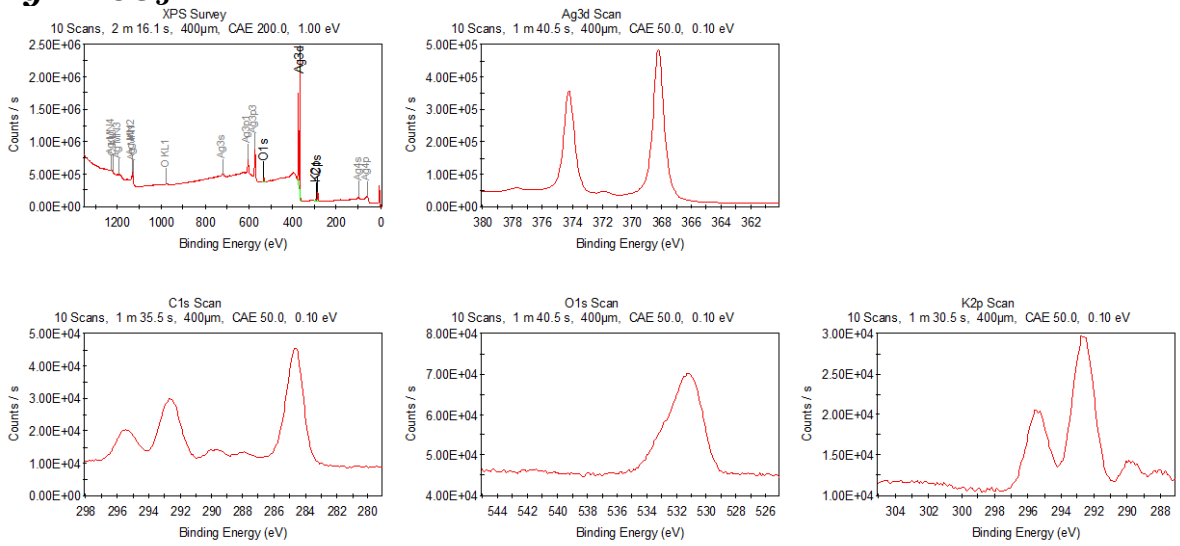

Figure S3.40. XPS spectra of a Ag sample after 1 hr electrolysis at 200 mA cm^{-2} in 1 M $KHCO_3$.

Au fresh

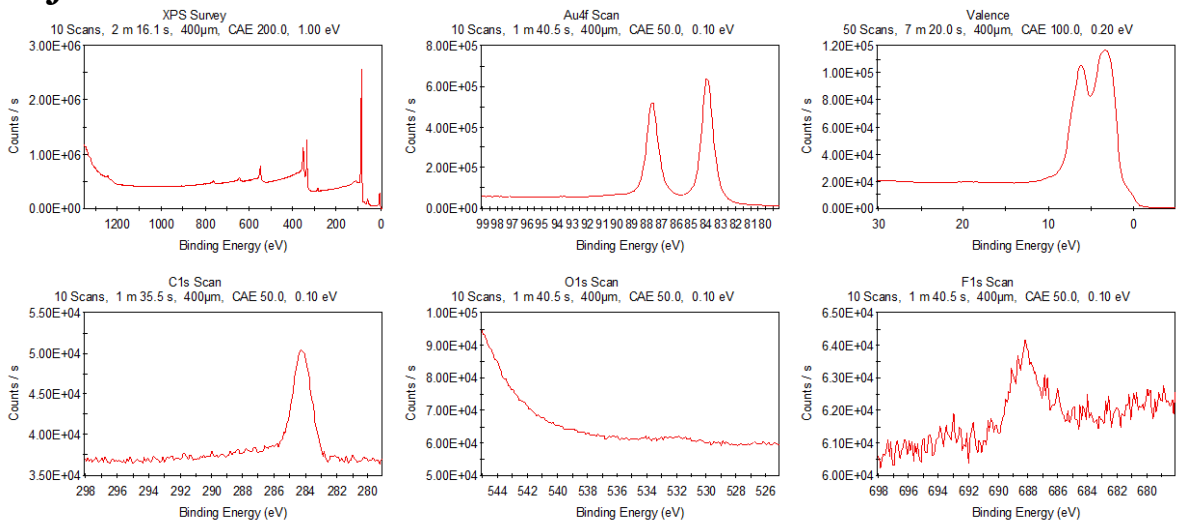

Figure S3.41. XPS spectra of a fresh Au sample.

Au KOH

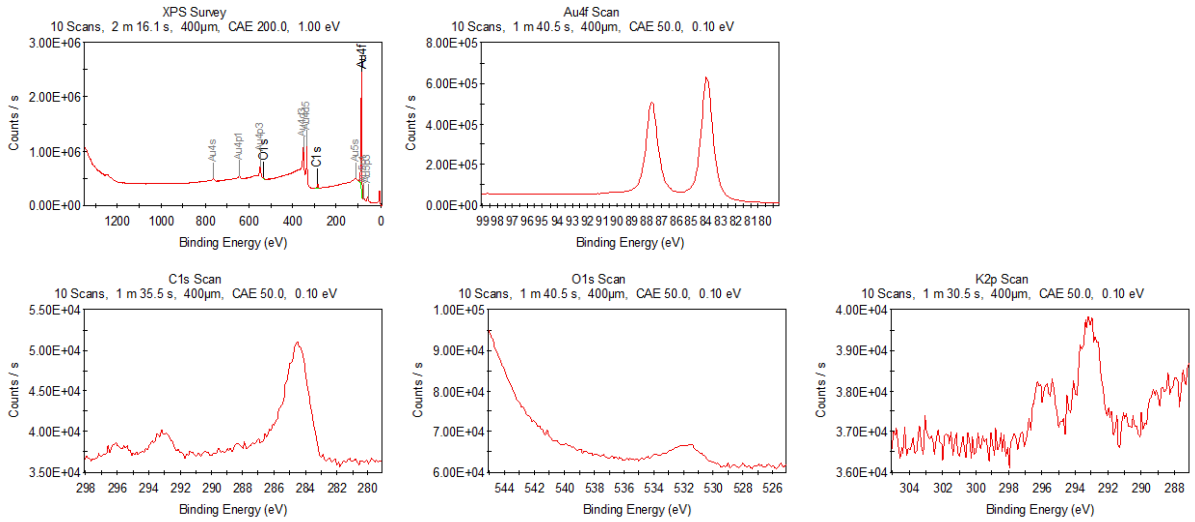

Figure S3.42. XPS spectra of a Au sample after 1 hr electrolysis at 200 mA cm^{-2} in 1 M KOH.

Au $KHCO_3$

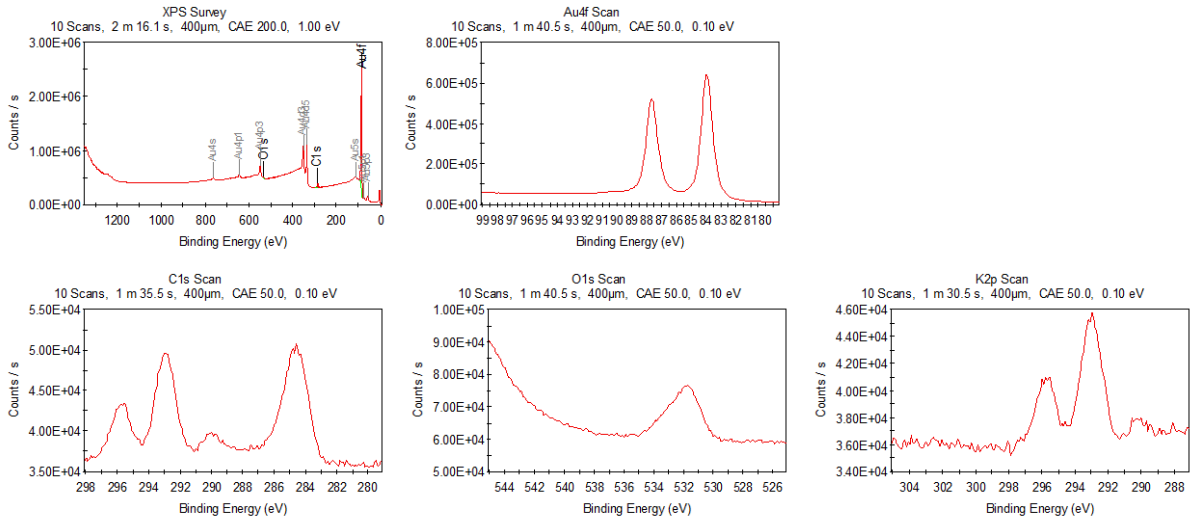

Figure S3.43. XPS spectra of a Au sample after 1 hr electrolysis at 200 mA cm^{-2} in 1 M $KHCO_3$.

Pd fresh

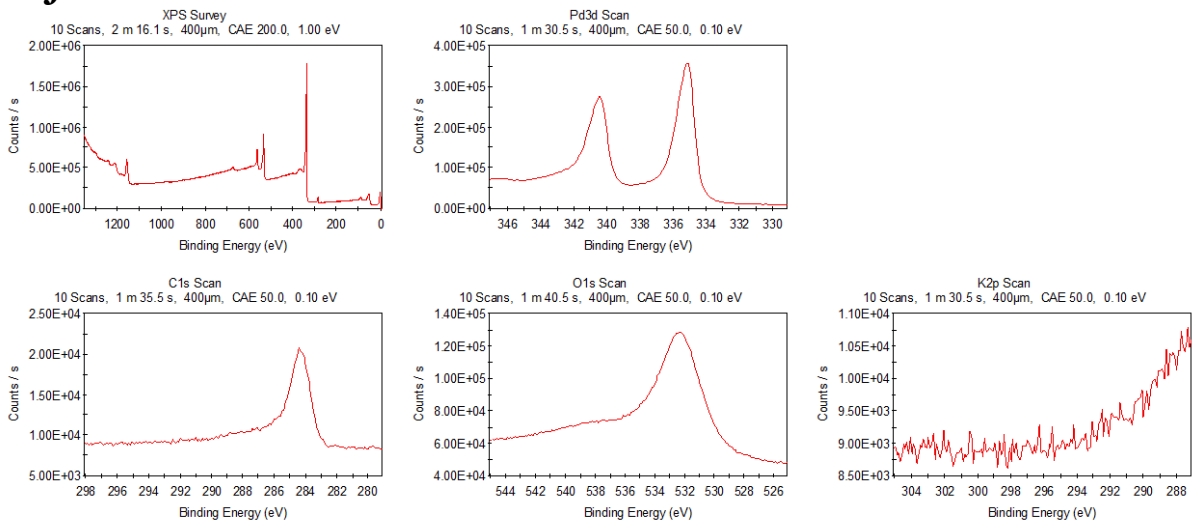

Figure S3.44. XPS spectra of a fresh Pd sample.

Pd KOH

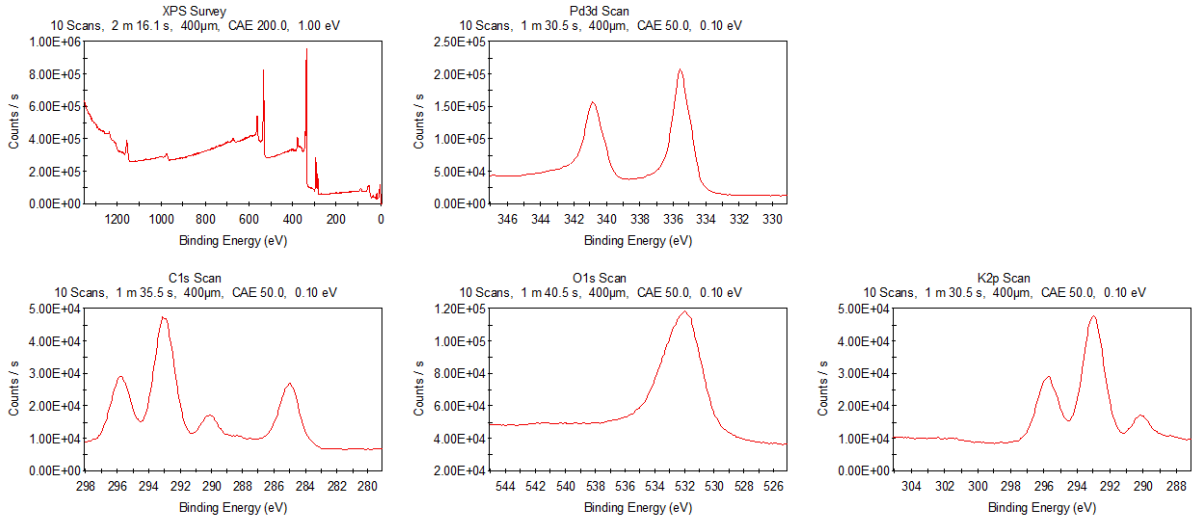

Figure S3.45. XPS spectra of a Pd sample after 1 hr electrolysis at 200 mA cm^{-2} in 1 M KOH.

Pd $KHCO_3$

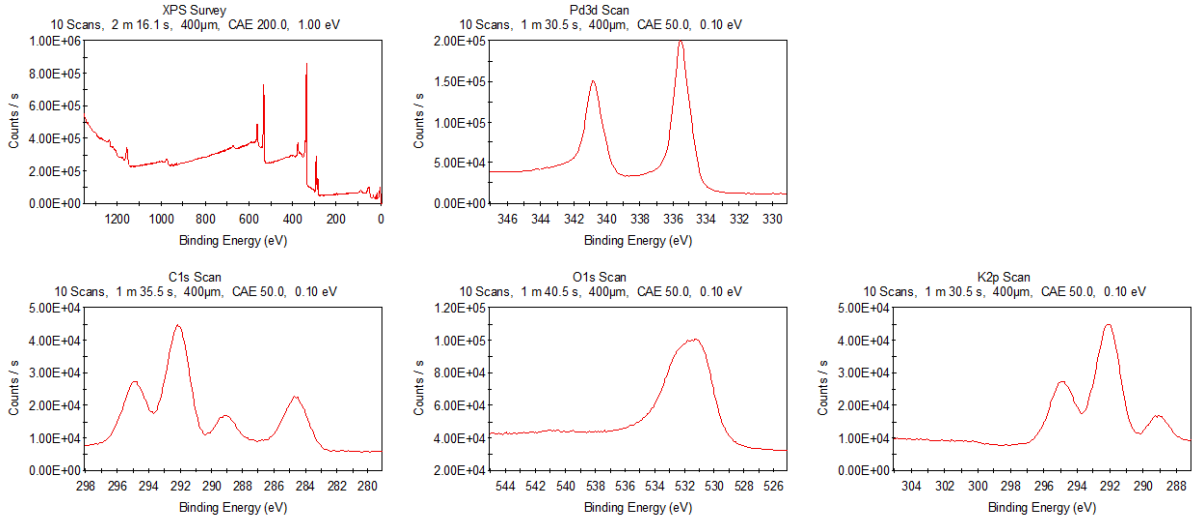

Figure S3.46. XPS spectra of a Pd sample after 1 hr electrolysis at 200 mA cm^{-2} in 1 M $KHCO_3$.

Sn fresh

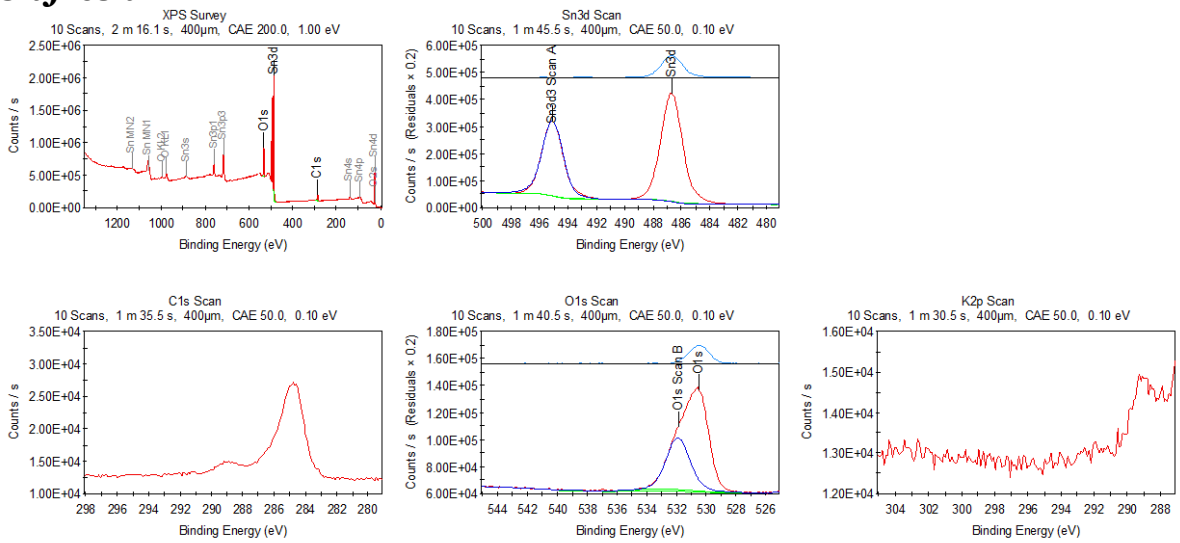

Figure S3.47. XPS spectra of a fresh Sn sample.

Sn KOH

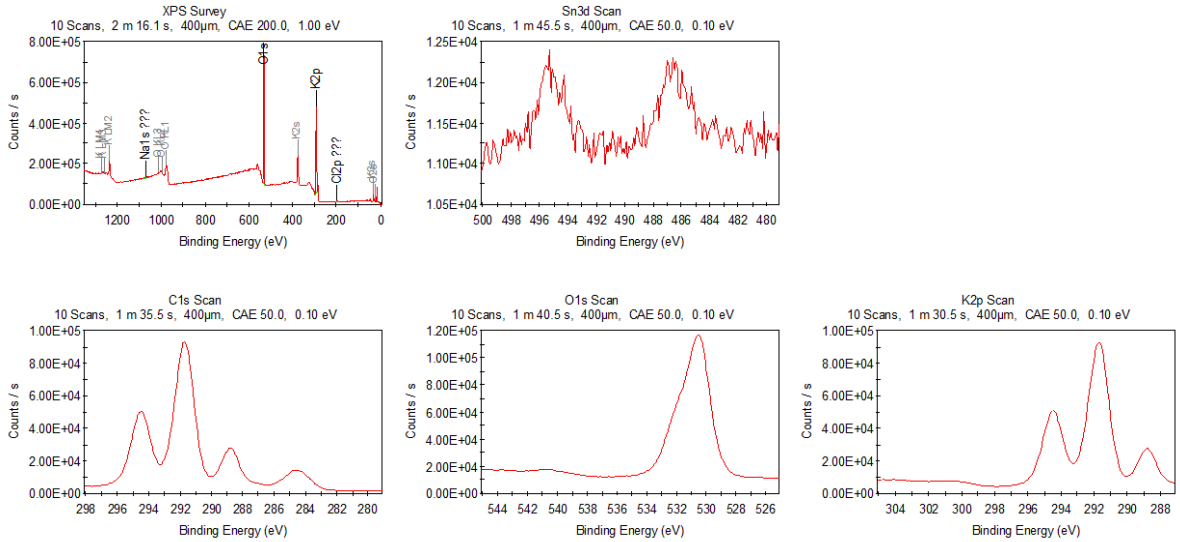

Figure S3.48. XPS spectra of a Sn sample after 1 hr electrolysis at 200 mA cm^{-2} in 1 M KOH.

Sn $KHCO_3$

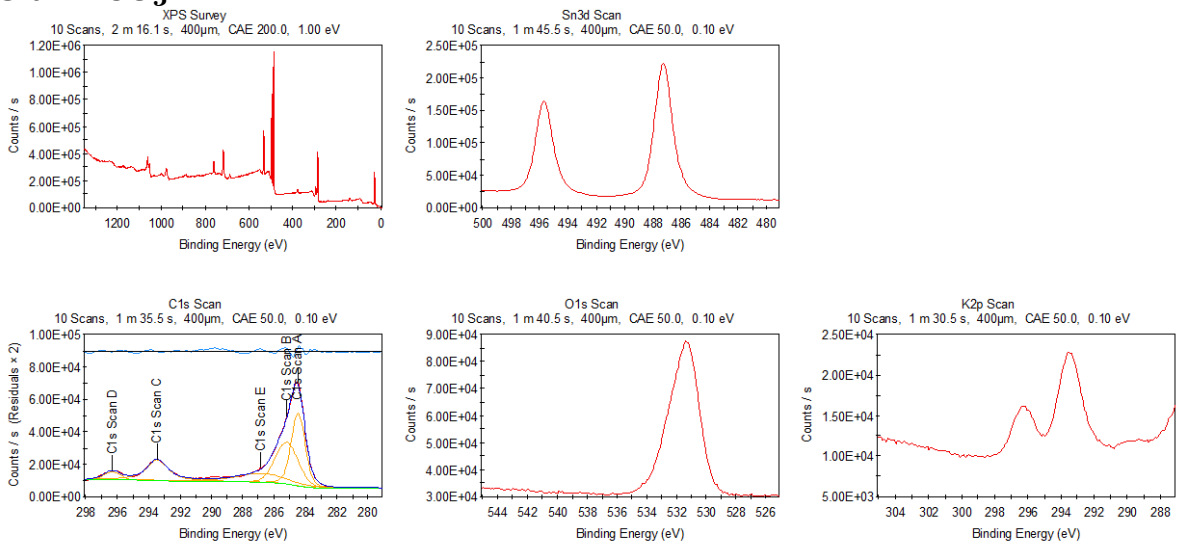

Figure S3.49. XPS spectra of a Sn sample after 1 hr electrolysis at 200 mA cm^{-2} in 1 M $KHCO_3$.

Cu fresh

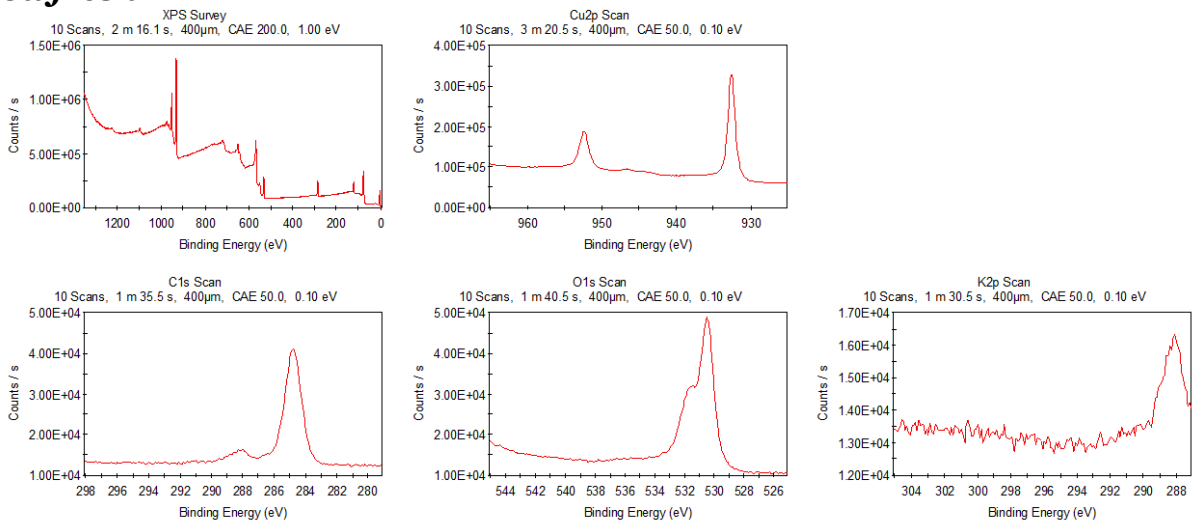

Figure S3.50. XPS spectra of a fresh Cu sample.

Cu KOH

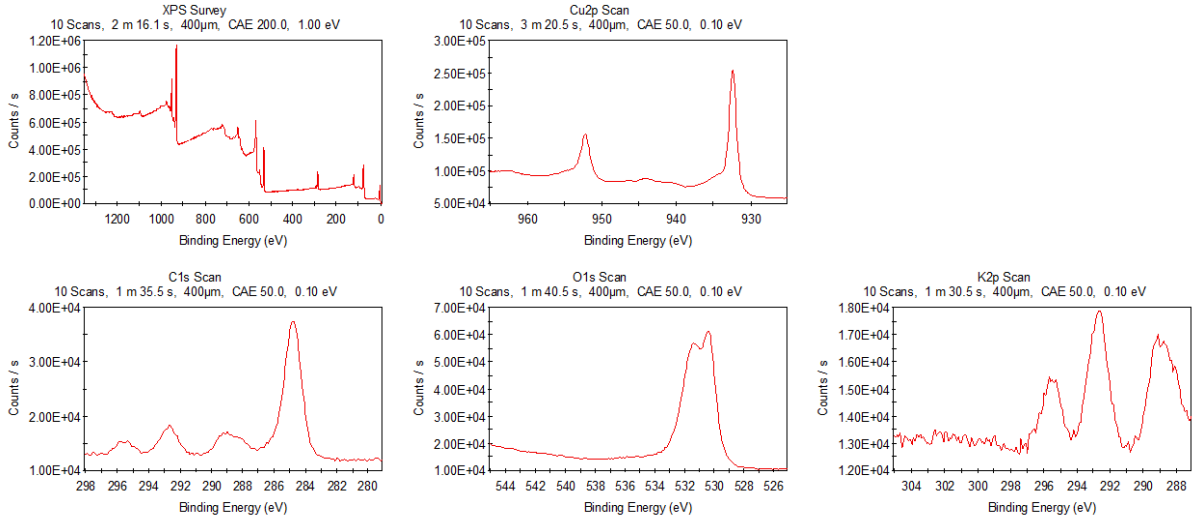

Figure S3.51. XPS spectra of a Cu sample after 1 hr electrolysis at 200 mA cm^{-2} in 1 M KOH.

Cu $KHCO_3$

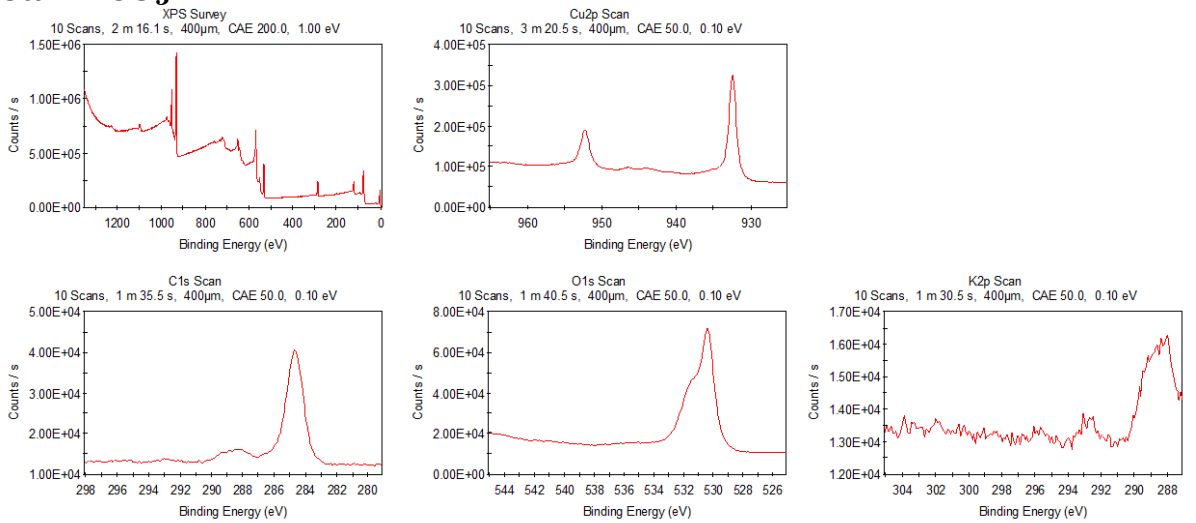

Figure S3.52. XPS spectra of a Cu sample after 1 hr electrolysis at 200 mA cm^{-2} in 1 M $KHCO_3$.

Atomic force microscopy – AFM

Atomic Force Microscopy (AFM) is a powerful tool to look into the smallest details of the reactive surface. Below µm size topography heightmaps of a bare GDE sample can be found as well as of before and after catalysis samples of Ag, Au, Sn and Cu (Figure S53 – S57). The Z-axis of in the 1 µm x 1 µm heightmaps has an aspect ratio of 1:1:0.3 (the 2 µm x 2 µm 'Bare GDE' sample has a normal 1:1:1 ratio). Although it is hard to compare AFM images, it gives an idea of what the surface looks like on the nano- and microscale.

Bare GDE

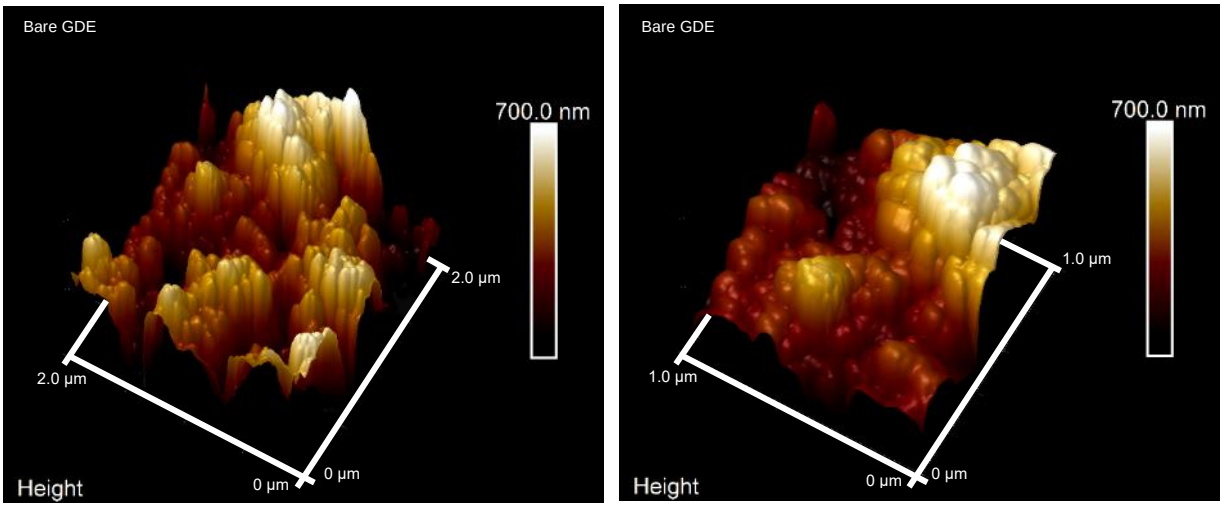

Figure S3.53. Two AFM images of a bare GDE substrate (left 2.0 x 2.0 µm, right 1.0 x 1.0 µm). The roughness of the surface ranges over 700 nm.

Ag

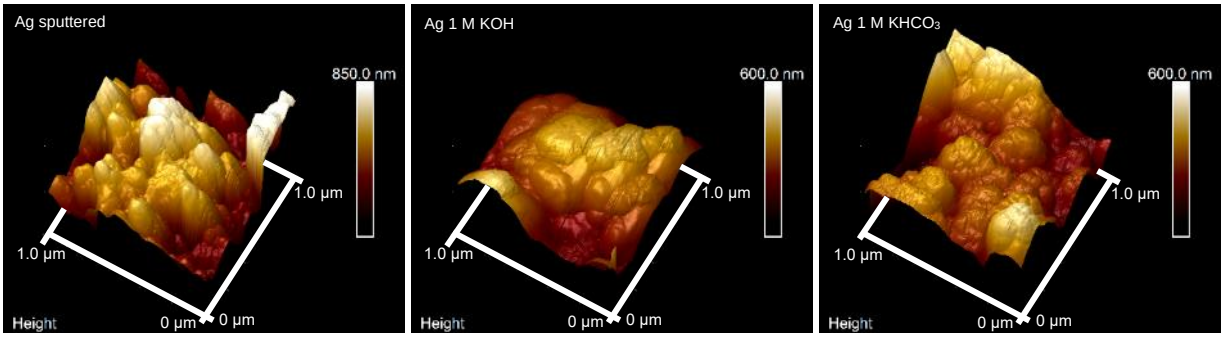

Figure S3.54. AFM images of Ag before and after electrolysis.

Au

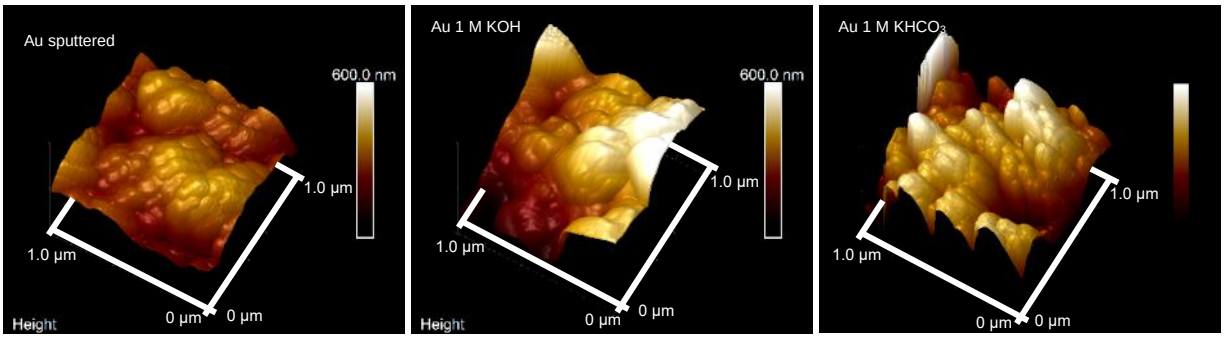

Figure S3.55. AFM images of Au before and after electrolysis.

Sn

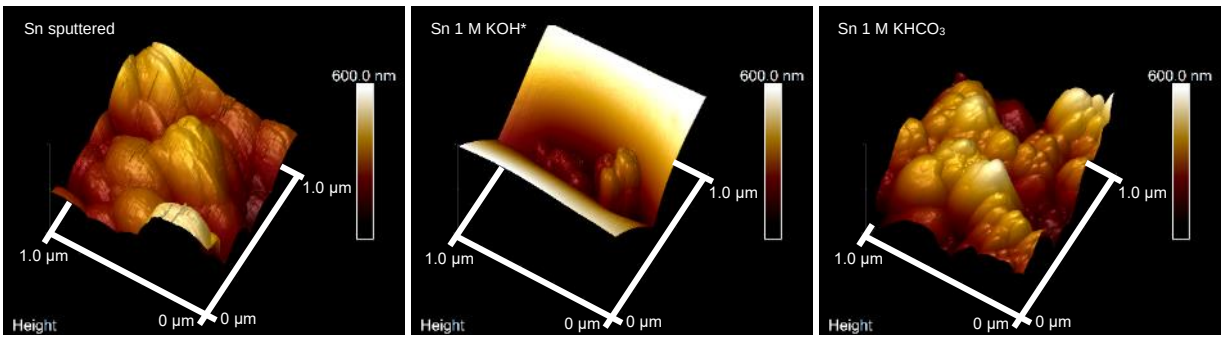

Figure S3.56. AFM images of Sn before and after electrolysis. For the Sn 1M KOH, SEM images were covered in bright crystals. The KOH AFM measurement was performed in a sharp valley between two crystals where only a small area of the GDE was visible.

Cu

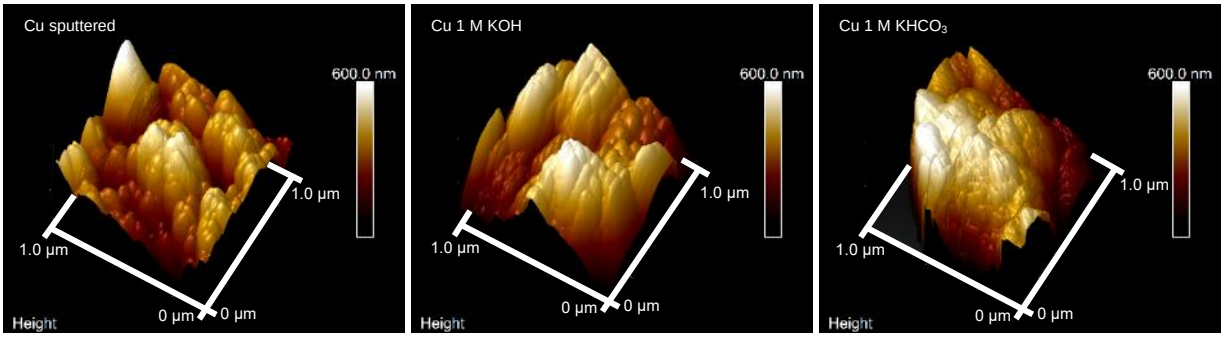

Figure S3.57. AFM images of Cu before and after electrolysis.

PTFE Cell design

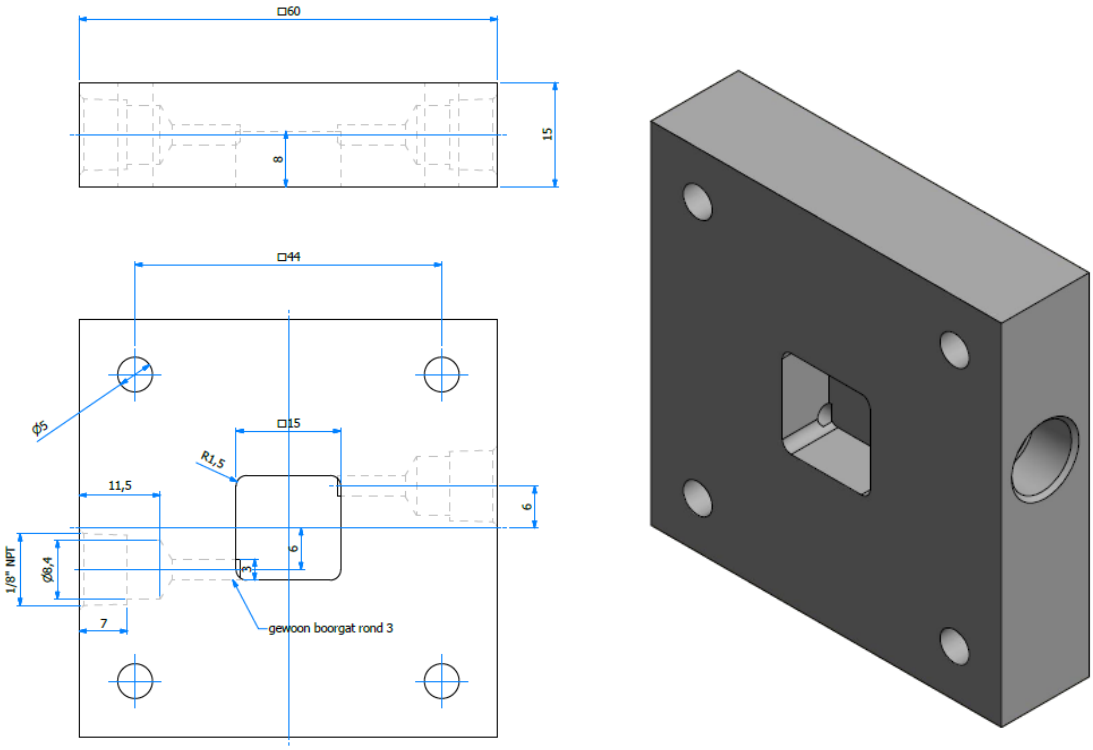

Figure S3.58 Dimensions of the CO2 gas channel for the electrochemical cell.

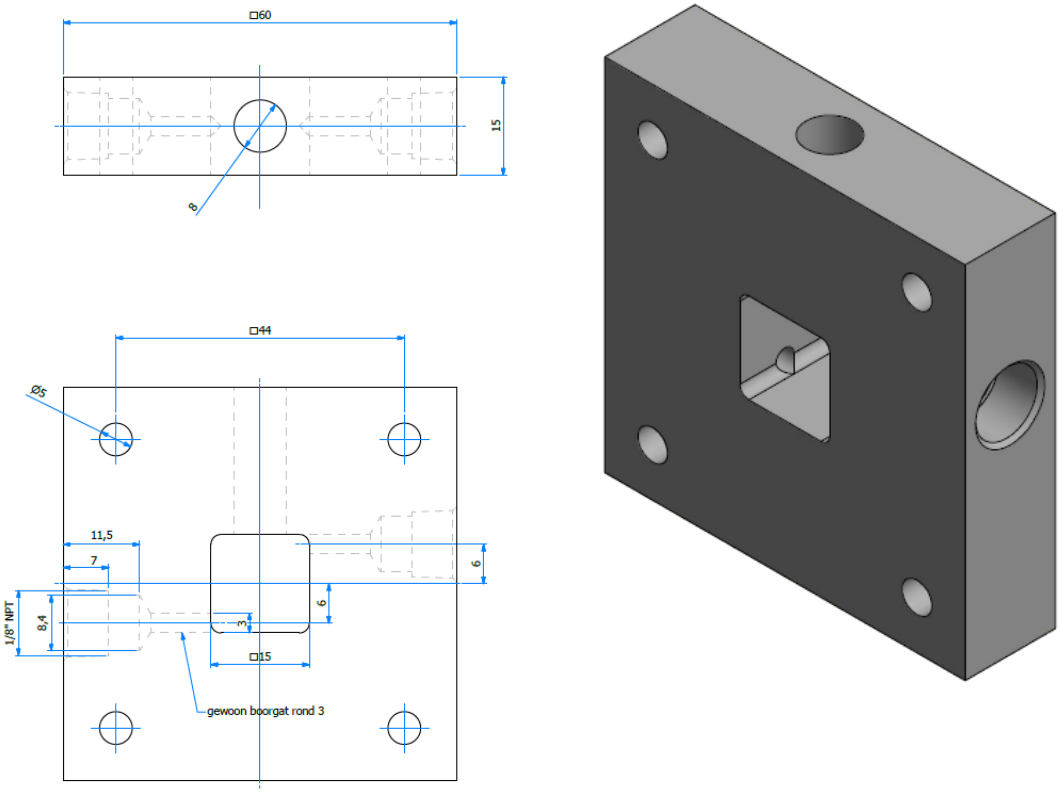

Figure S3.59 Dimensions of the electrochemical catholyte chamber.

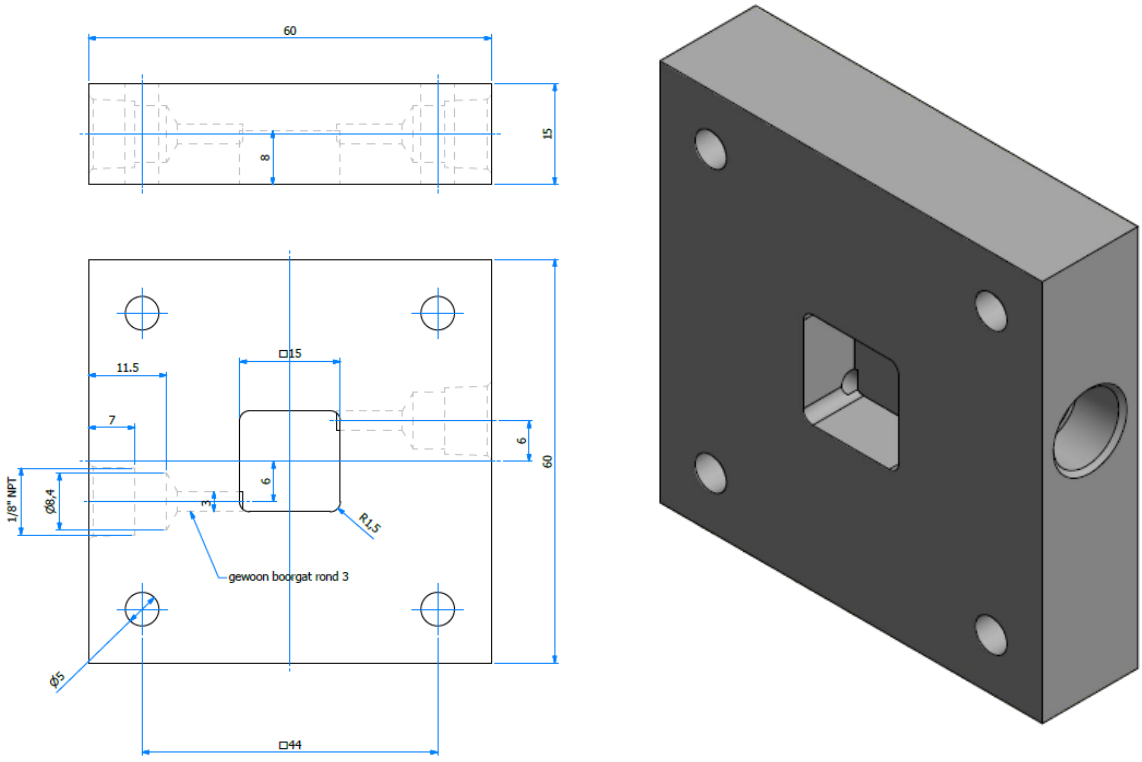

Figure S3.60 Dimensions of the electrochemical anolyte chamber.

References Chapter 3 SI.

1. Liu, K., W.A. Smith, and T. Burdyny, *Introductory Guide to Assembling and Operating Gas Diffusion Electrodes for Electrochemical CO2 Reduction*. ACS Energy Letters, 2019. **4**(3): p. 639-643.

Chapter 4.

Zero-gap electrochemical CO2 reduction cells: Challenges and operational strategies for prevention of salt precipitation

Salt precipitation is a problem in electrochemical CO_2 reduction electrolyzers that limits their long-term durability and industrial applicability by reducing active area, causing flooding and hindering gas transport. Salt crystals form when hydroxide generation from electrochemical reactions interacts homogeneously with CO_2 to generate substantial quantities of carbonate. In the presence of sufficient electrolyte cations, the solubility limits of these species are reached, resulting in 'salting out' conditions in cathode compartments. Detrimental salt precipitation is regularly observed in membrane electrode assemblies, especially when operated at high current densities. This Perspective briefly discusses the mechanisms for salt formation, and recently reported strategies for preventing or reversing salt formation in CO_2 reduction membrane electrode assemblies. We link these approaches to the solubility limit of potassium carbonate within the electrolyzer, and describe how each strategy separately manipulates water, potassium and carbonate concentrations to prevent (or mitigate) salt formation (Fig 4.1).

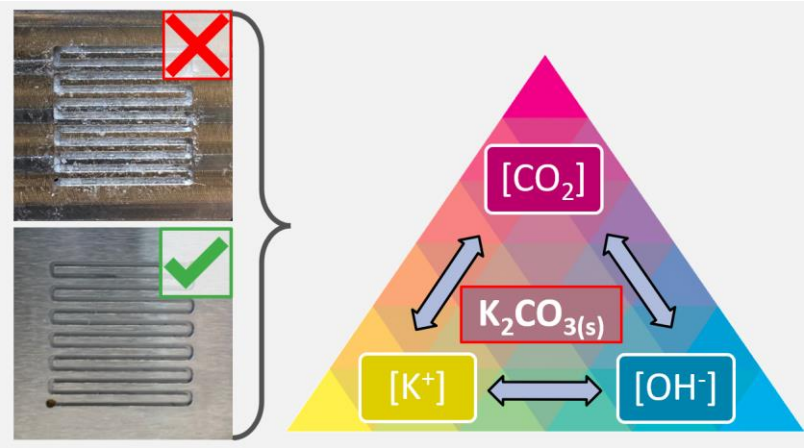

Figure 4.9 *Salt formation in CO_2 electrolysers occurs because of the interplay of K^+, CO_2 and OH^- concentrations and is able to limit or block the flow through the gas channel.*

This chapter is based on: Mark Sassenburg, Maria Kelly, Siddhartha Subramanian, Wilson A. Smith, and Thomas Burdyny. *ACS Energy Letters* **2023** *8* (1), 321-331. Dec 5, 2022. Available online at: https://pubs.acs.org/doi/10.1021/acsenergylett.2c01885

4.1 The formation of carbonate salts

The electrochemical CO_2 reduction reaction (CO_2RR) provides a pathway towards a more CO_2 neutral society. Although still in its infancy, the potential for this technology to develop further has led to improvements in the product selectivity, activity and stability of CO_2RR electrolyzers. Much has been adopted from the already matured electrochemical hydrogen evolution reaction (HER) field, where performance metrics such as >1 A cm^{-2} conversion and >10,000 hr lifetime are easily surpassed.[1] By adopting technical features like the gas diffusion electrode (GDE)[2–6] and membrane electrode assembly (MEA)[7] cell architecture, the field of CO_2 reduction has achieved industrially relevant current densities (>200 mA cm^{-2}) while retaining selective conversion. These improvements were in part realized by utilizing highly alkaline electrolytes, such as KOH, to limit the competing HER[4,8–10] and humidifying the CO_2 gas stream to manage water availability to the cathode and membrane.[11,12] However, since being incorporated into more industrial reactors, additional challenges have been found which impact the long term stability and economic feasibility of CO_2RR. In particular, the precipitation of salts within the reactor leads to operational failures which diminish the potential impact of this technology. In higher energy efficiency MEA architectures where a liquid catholyte is removed, salt precipitation is common and highly-disruptive to steady performance.

An exchange MEA is the most common MEA architecture used in CO_2RR electrolyzers. The cathode side uses a porous GDE and is fed with a gaseous stream of CO_2 that can be dry or humidified. The anode of the exchange MEA contacts a liquid anolyte that provides reactants for the anode reaction (typically oxygen evolution) and serves as a water source for the membrane.[12] MEAs with a gaseous anode feed (also known as full MEAs) have been demonstrated for CO_2RR[13–16] but reports on these systems are limited and fall outside the primary scope of this Perspective.

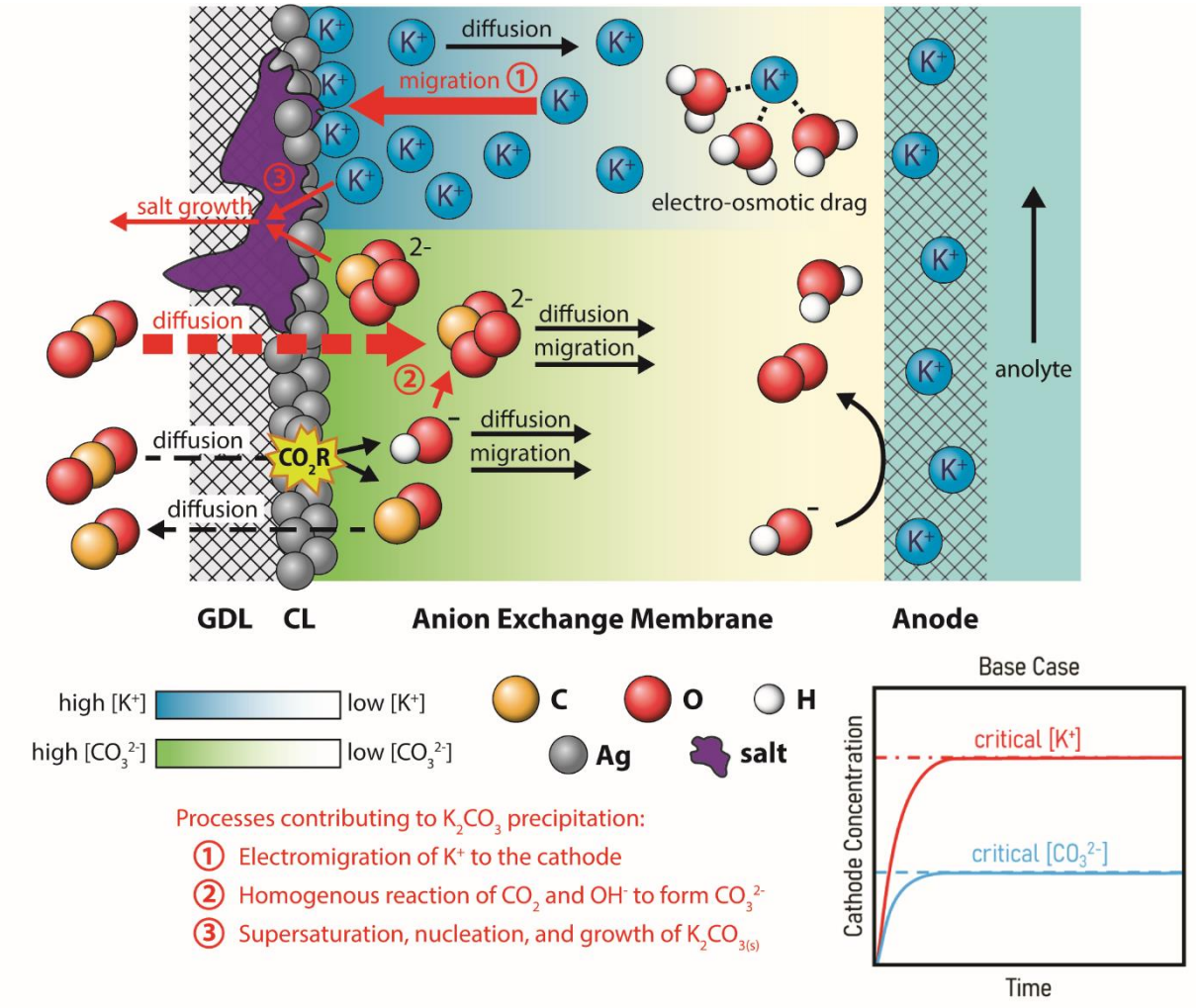

Figure 4.2 *Schematic representation of the cascade of reactions and ion transport in an exchange MEA leading to salt formation on the cathode composed of a catalyst layer (CL) and gas-diffusion layer (GDL). The inserted graph shows the change in ion concentrations occurring near the cathode. After both CO_3^{2-} and K^+ concentrations reach critical levels, the precipitation of K_2CO_3 starts to occur.*

The use of GDEs in MEAs is the feature which enables elevated current densities by reducing the liquid diffusion length of CO_2 from the gas phase to the catalyst surface. However, the production of hydroxide as a byproduct of CO_2RR during water-splitting, and the use the KOH as an anolyte, result in a highly alkaline local environment[17–19] in the cathode compartment of the electrolyzer. The excess CO_2 which is enabled by the gas-diffusion layer then simultaneously provides a route towards salt formation through the production of (bi)carbonates (Fig. 4.2).

In MEAs, these carbonate salts can form in the cathode flow field, on the gas side of the cathode, within the GDE, and on the membrane side of the electrode in systems using both alkaline and near-neutral anolytes.[7,12,20,21] The deposits block the initially

porous GDE and cause the pressure within the cathode chamber to increase as gas flow is progressively restricted by the salts.[20,22] The presence and formation of salt also restricts access of CO_2 to the catalyst, leading to increased hydrogen Faradaic efficiencies. Although salt precipitation has been observed in other alkaline electrochemical systems,[23,24] its prevalence in CO_2 reduction electrolyzers comes from the interplay of 3 components essential to CO_2RR: the reactant CO_2 gas, the proton-source (H_2O or HCO_3^-)[25–27] and a cation that assists in catalysis.[28–30] Several citations used in the work presented here make use of 3 compartment flow cells[22,31,32,41,56] and even fully aqueous setups[25-30, 47], in which mass transport can be quantitatively different. Nevertheless, the underlying principles of local alkalinity, water and ion transport, can generally be translated to MEA systems.

Several operational approaches have been deployed in literature to maintain long-term CO_2 electrolysis without salt formation. In essence, however, each of these strategies work towards a similar goal and separately prevent salt formation by lowering either [K^+], [CO_3^{2-}] or [K_2CO_3] in the cathode compartment. Some are "active" approaches that require a periodic change in the operational state of the electrolyzer. Others are "passive" approaches that are in effect at all times. Here, we group the strategies presented in literature into four general categories.

1. **Passive Anolyte Approach** - The anolyte concentration is decreased, or the cation identity is changed, to keep the accumulation of cations at the cathode surface below the critical salting out concentration.
2. **Dissolution Approach** - The cathode is periodically pulsed with water or an equivalent solvent to dissolve accumulated salts and increase water availability. Alternatively, while feeding a deionized water anolyte, the cathode is periodically flushed with an "activation" solution to provide cations near the cathode surface.
3. **Active Pulse Approach** - The MEA is operated in a pulsed electrolysis mode where periodically switching to a low applied potential allows accumulated cations and carbonate ions to diffuse away from the cathode, thereby keeping their concentration below critical levels.
4. **Passive Membrane Approach** - The MEA membrane and its components are chosen to reduce ion migration to and accumulation at the cathode.

This Perspective reflects on these operational strategies for avoiding or reversing salt formation in CO_2 electrolyzers. We discuss each of these approaches in-depth next to the phenomena causing salt formation to highlight that all strategies work towards the same goal of avoiding the solubility limits of carbonate salts, each by targeting either the cation, anion or water concentrations.

Firstly, to explain how salt formation takes place, we look at the conversion of CO_2-to-CO on a Ag catalyst in an alkaline environment. During electrolysis, some of the CO_2 fed into the system is converted to CO as described by the cathodic half reaction:

$$\boldsymbol{CO_2(aq) + H_2O(l) + 2\,e^- \rightarrow CO(aq) + 2\,OH^-(aq)} \quad [1]$$

For each converted CO_2 molecule, two hydroxide ions are produced when in a neutral or alkaline pH environment. In addition to making the environment more alkaline, OH^- also participates in the unwanted homogeneous conversion of CO_2 to bicarbonate and carbonate (depending on the exact pH):

$$\boldsymbol{CO_2(g) + 2\,OH^-(aq) \underset{pKa=6.4}{\leftrightharpoons} HCO_3^-(aq) + OH^-(aq) \underset{pKa=10.3}{\leftrightharpoons} CO_3^{2-}(aq) + H_2O(l)} \quad [2]$$

Since CO_2 gas is abundantly present and hydroxides are continuously produced, the effectively utilized amount of CO_2 gas for CO_2RR can drop down to ~30% due to dissolution, while up to ~70% of CO_2 is converted into carbonates that can fuel salt formation. [31,32] Multiphysics models developed by Weng *et al.* and Kas *et al.* have also determined the maximum CO_2 utilization efficiency to be ~50% for an exchange MEA system and a GDE with a flowing catholyte, respectively.[33,34] While this is a significant problem on its own in terms of CO_2 utilization efficiency, another issue is the accumulation of carbonate at the cathode due to reaction [2].

The third reaction to consider is the combination of accumulating carbonate ions near the gas-liquid interface and the cations (i.e., K^+) that are used to improve ionic conductivity and stabilize CO_2 reduction intermediates. Since the cathode is negatively charged during electrolysis and hydroxide ions are being produced, migration of cations from the anolyte past the membrane lead to a gradually increasing concentration near the cathode to maintain charge neutrality within the system. Ultimately the high concentrations of cations and carbonates exceed the solubility limit (1096 g/L or 7.93 M K_2CO_3 at 20 °C in pure water)[35] and lead to the formation of salts:

$$\boldsymbol{CO_3^{2-}(aq) + 2\,K^+(aq) \leftrightharpoons K_2CO_3(s)} \quad [3]$$

It is most accurate to use the solubility product constant (K_{sp}) to define the conditions for K_2CO_3 precipitation. However, K_2CO_3 is highly soluble, and at saturation the solution would deviate from ideal solution behavior. For simplicity, the remainder of this review, the solubility of K_2CO_3 in units of molarity will be used to describe the conditions for precipitation with the disclaimer that greater concentrations of potassium and carbonate could lead to earlier than described salt formation. For this reason, operational strategies should aim to keep both **K^+ < 15.86 M** and **CO_3^{2-} < 7.93 M** to avoid the solubility product from exceeding the solubility limit.

In addition to K_2CO_3, $KHCO_3$ and $K_4H_2(CO_3)_3 \cdot 1.5H_2O$[20] have also been detected by ex situ XRD in MEA cathodes. $KHCO_3$ and $K_4H_2(CO_3)_3 \cdot 1.5H_2O$ can form by CO_2 sorption of solid K_2CO_3, so it is proposed that K_2CO_3 initially precipitates then reacts with excess CO_2 in the gas stream to form other carbonate salts.[20,36]

Many studies have examined the effect of different salt cations on the performance of CO_2RR systems, but here we focus on the implications of K^+ as it is the most studied salt cation. These conclusions can be generalized to other cations, albeit with different solubility limits potentially changing the primary location of salt formation in the cathode compartment.

While the chemical reactions in Eqs. 1-3 describe how ions are formed and precipitate into salts, the Nernst-Planck equation then describes the transport and accumulation of ions across the electrochemical system:

$$\boldsymbol{J(x) = -D\frac{\partial C(x)}{\partial x} + \frac{-zF}{RT}DC\frac{\partial \varphi(x)}{\partial x} + Cv(x)} \qquad [4]$$

$$\boldsymbol{Flux = Diffusion + Migration + Convection}$$

Where J(x) is the flux of an ionic species, D is its diffusivity constant, dC/dx is the concentration gradient, z is its electronic charge, F is Faraday's constant, R is the ideal gas constant, T is the temperature, dϕ/dx is the electrical potential gradient, and v(x) is the fluid velocity. Near the electrode surface where the fluid velocity v is negligible ($Cv(0) = 0$), this equation states that in a steady state system where there is no net flux of ionic species ($J(x) = 0$), the electromigration of potassium ions towards the negative cathode has to equalize with the diffusion of high concentrations back to the (relatively) low concentration bulk.

Within a zero-gap system the concentrations of ionic species are then determined by the applied reaction rate, the anolyte concentration and the diffusion, migration and convection driven ionic transport through the cathode region, membrane and anode region. While carbonate forms easily as gaseous CO_2 reacts with the OH^- product (Eqn 2), a zero-gap system typically has limited potassium ions initially at the cathode. Moreover, the majority of reported zero-gap systems utilize anion exchange membranes, which should be repellant to cations.[37] Driven by the high concentration of negative charges at the cathode, counterion transport of potassium across the anion exchange membrane is facilitated through electro-osmotic drag as depicted in Fig 4.2. In conjunction with water transport, partially neutralized potassium ions are able to cross the membrane and accumulate at the cathode.

In order to avoid potassium carbonate precipitation in a strongly alkaline system, the concentrations of both CO_3^{2-} and K^+ must be kept below 7.93 M and 15.86 M, respectively. Although these concentrations are much higher than the ~1 M K^+ of typical CO_2RR electrolytes, the substantial production of hydroxide and carbonate at elevated current densities create such an environment, as was computationally hypothesized by several catalyst layer concentration models.[17,38,39]

The experiences of rapid salt formation at industrially relevant current densities (e.g. 50 minutes for a 2 M KOH anolyte operating at 100 mA cm^{-2})[40] indicate that the migration term of cations towards the cathode is larger than the diffusion term in equation 4. Once salting out conditions are met nucleation occurs and rapid growth of crystals is observed into the cathode pores and flow field until salts block gas flow altogether.

To achieve an operational lifetime in the range of hydrogen electrolyzers (>10,000 hours), methods for the prevention (or reversal) of salt formation in CO_2RR MEA systems need to be developed and improved. However, MEA designs to prevent carbonate precipitation faces several challenges with various tradeoffs for performance and durability. Any change made to suppress salt formation often contributes to other negative effects such as electrolyte flooding[41], loss of CO_2RR selectivity over HER [42], increase in cell voltage[43], or increased down time of the reactor for cleaning or pulsed electrolysis modes[44]. Thus, implementation of engineering and design methods for precipitation prevention results in a complex optimization problem of many MEA operational factors.

In the last decade of CO_2RR research, salt precipitation in CO_2 electrolyzers with GDEs has not been studied extensively despite being a commonly observed phenomenon. Only a few papers have mentioned salt formation and its importance in operations, while fewer provide empirical engineering solutions to obtain longer stability. By analyzing the research that has sought to overcome salt precipitation we were able to identify 4 main categories of engineering solutions. These approaches include (i) passively modifying the anolyte concentration and composition, (ii) actively dissolving salts at the cathode, (iii) pulsing the electrolyzer, and (iv) passively modifying the MEA. Collectively, these strategies tackle the same issue of preventing potassium and carbonate from simultaneously reaching their critical concentrations.

4.2 Passive Anolyte Approach – Cation Concentration and Identity

The first option presented to reduce salt formation is to decrease the concentration of cations in the electrolyte or eliminate them entirely from the system (illustrated in Fig. 4.3). From a mass transport perspective, a lower bulk concentration of K^+ in the anolyte reduces the transport effects of ion migration from the anode to the cathode. Migration is then balanced by diffusion of cations from the cathode to the anode. Combined, the accumulation of potassium at the cathode is maintained below the solubility limit of K_2CO_3 thereby preventing salt precipitation (Fig. 4.3a).

Liu *et al.* showed that reducing the anolyte concentration to 10 mM $KHCO_3$ instead of the typical 1 M concentration allowed stable operation for 3800 hours (200 mA cm^{-2}, 3 V_{cell}).[43] In this situation, the diffusion and migration terms equalize and keep the potassium concentration below the critical salting out condition. However, the use of a lower anolyte concentration also increased the overall cell resistance, leading to higher cell potentials. Similarly, Endrődi *et al.* observed decreasing the electrolyte concentration prolongs electrolyzer operation at the expense of current density. When operating an MEA at 3.1 V_{cell}, the current density with a 0.1 M KOH anolyte was 300 mA cm^{-2}, but dropped to 100 mA cm^{-2} in a deionized water anolyte.[20] The drop in current density when using a pure water feed can again be attributed to its low conductivity: electrochemical impedance spectra of both cells indicated a 3 to 4 times larger charge transfer resistance in the MEA fed with pure water compared to 0.1 M KOH. Reyes et al. highlighted that aside the importance of cation regulation, gas-fed

CO_2 electrolysers also depend strongly on managing the hydration of the catalyst and membrane.[68]

However, the performance of CO_2RR MEAs using a pure water anolyte has been improved using novel membranes and ionomers that reduce the ionic resistance and improve its permselective behavior (the ability to conduct H^+ over K^+).[69] For example, Yin *et al.* used a quaternary ammonia poly(*N*-methyl-piperidine-*co*-*p*-terphenyl) polymer as both anion exchange membrane and cathode ionomer in an MEA operating with pure water anolyte. The system achieved 100 mA cm^{-2} at 2.25 V for over 100 hr with CO FE consistently greater than 90%.[45] The same system reached 500 mA cm^{-2} and ~90% FE at 3V and 60 °C, although long term durability at this current density was not reported. By avoiding the use of an alkaline electrolyte and introduction of metal cations, the authors were able to prevent salt precipitation entirely. Notably, it is necessary to have small amounts of alkali metal cations to increase the system conductivity and stabilize the CO_2RR intermediates,[29] so the mechanisms for CO_2RR in systems with deionized water anolytes should be further investigated. O'Brien *et al.* suggests such systems without a mobile cation can still achieve high CO_2RR selectivity because the fixed positive charges in the anion exchange membrane stabilize the intermediates instead.[46] These examples demonstrate the tradeoff between salt

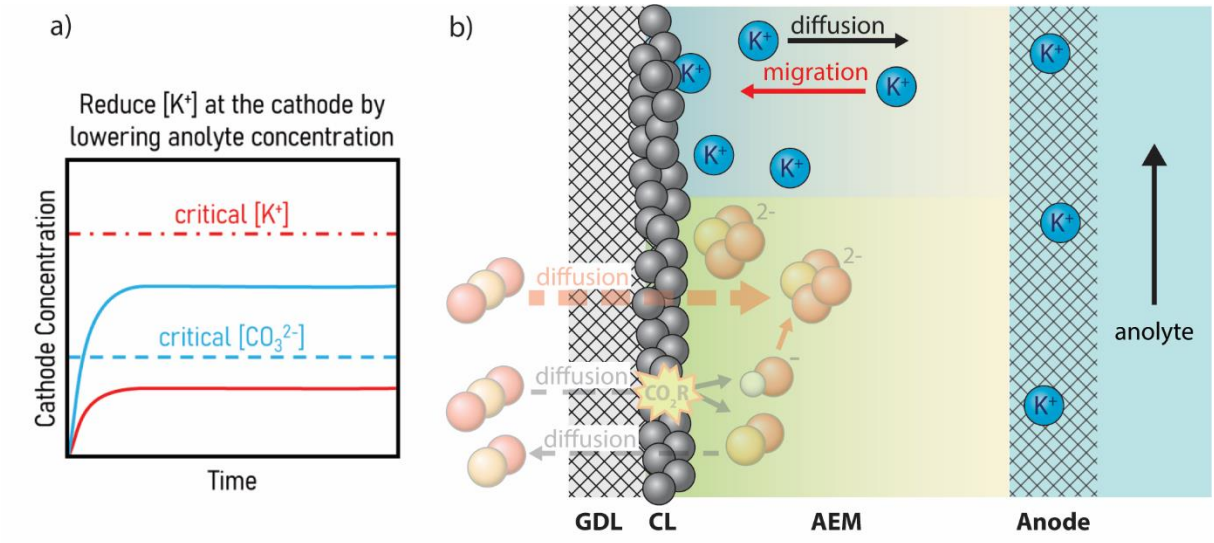

Figure 4.3 *(a) Plot of assumed cathode concentration versus time showing the general trends of K^+ and CO_3^{2-} concentrations at the cathode when the anolyte concentration is reduced. (b) Schematic depiction of a lower concentration of K^+ in the anolyte solution resulting in reduced electromigration. This enables the balancing between migration and diffusion of K^+, keeping the total concentration below its solubility limit.*

precipitation and cell voltage. Thus, for the issue of salt prevention, the question is whether it is economically beneficial to prevent salt precipitation by using dilute electrolytes that will increase the overall cell potential. As more data on long-term testing of CO_2RR electrolyzers becomes available, technoeconomic analyses should consider the tradeoff between cell potential and cell lifetime which is influenced by salt precipitation.

Salt precipitation may also be controlled by the chemical composition of the electrolyte. Cofell *et al.* observed that switching the electrolyte from KOH to CsOH in a flow cell resulted in smaller, well-dispersed bicarbonate crystal deposits and a slowing of the performance degradation caused by the precipitation of carbonate salts.[4] By contrast, the bicarbonate deposits formed from KOH electrolyte covered much larger areas of the cathode and formed fractal-like patterns. Chiacchiarelli *et al.* also noted the effect of cation identity on slowing the formation of deposits on an electrode.[47] In their work, a rotating Sn electrode was submerged in a 0.1 M $KHCO_3$ electrolyte purged with N_2. Subsequent electrolysis resulted in several degradation modes, including alkali deposits from the electrolyte. The amount of the deposits decreased based on the cation identity in the order $Na^+ > K^+ > Cs^+$. This trend could be explained by the solubility change with cation identity (Table 1). For carbonates, the solubility (in units of molarity) increases in the order $Na^+ < K^+ \approx Cs^+$, and for bicarbonates, the trend is $Na^+ < K^+ < Cs^+$.[35] Additionally, differences in ionic radius, ion hydration, and ion diffusivity have all been suggested to affect the rate of cation transport to the cathode surface and the energies required to nucleate and grow a carbonate salt.[4,47] These effects of cation identity on salt precipitate morphology merit further investigation and have yet to be shown in an MEA architecture.

Table 1: *Solubility of (bi)carbonate species for Na^+, K^+ and Cs^+ cations.*

Salt	**Solubility (M at 20 °C)**
$NaHCO_3$	1.14
$KHCO_3$	2.24
$CsHCO_3$	3.49
Na_2CO_3	2.06
K_2CO_3	7.93
Cs_2CO_3	8.01

4.3 Dissolution Approach – Adding solvents to the Cathode

The second approach to reduce the consequences of salt precipitation works by actively adding solvents to the cathode region to dissolve and remove precipitates and elevated salt concentrations from near the cathode surface. While preventing salt formation is ideal, this second strategy demonstrates how operational performance can be regained after salts have precipitated in a CO_2RR system. Importantly this strategy takes advantage of the fact that the most detrimental effect of salt formation is blockages of the CO_2 diffusion pathways, and not necessarily the nucleation of salt crystals themselves. If the salt crystals at the cathode can then be removed through the timely introduction of a secondary flow, the operational lifetime of the system can be increased (Fig. 4.4). Additionally, preventative addition of water to the cathode region can periodically lower ion concentrations prior to salt formation occurring.

Endrődi *et al.* performed two experiments to remove the accumulation of K_2CO_3 salts in the cathode.[42] In the first experiment, the cathode gas feed was humidified and heated to 85 °C to increase the water vapour in the cathode flow field and salt solubility. This approach allowed for stable operation for at least 8 hours (at 200 mA cm^{-2}, 3 V_{cell}), but lowered the selective CO conversion to 65 - 70% due to the increased water content which promoted HER. In the second experiment, the cathode chamber was flushed once per hour with 50 cm^3 deionized water (T_{cell} = 60°C). During CO_2RR, a continuously decaying current (275 – 200 mA cm^{-2}) was obtained, which the authors attributed to the formation of K_2CO_3. After each dissolution step, the reduced current returned to its initial value after which a new 'decay cycle' was initiated. The combination of lower temperature and salt dissolution resulted in a continuous selectivity of 85% CO_2-to-CO. The empirically chosen value of 50 cm^3 deionized water shows that this method of regeneration is possible, but also far from optimized. Later work by the same group cast doubt on cathode rinsing as a viable long-term technique for removing precipitates since significant pressure is necessary to penetrate the hydrophobic cathode and effectively clean out the precipitated salts.[20] Currently, carbon based GDEs commonly used for CO_2RR are only mechanically robust enough to withstand pressure differences up to 100 mbar prior to flooding.[41,48] Moreover, droplets that remain in the GDL after rinsing can promote HER and limit the free accessibility of CO_2 to the catalyst. The two aforementioned effects indicate the limited feasibility of dissolution as a viable technique to overcome salt formation.

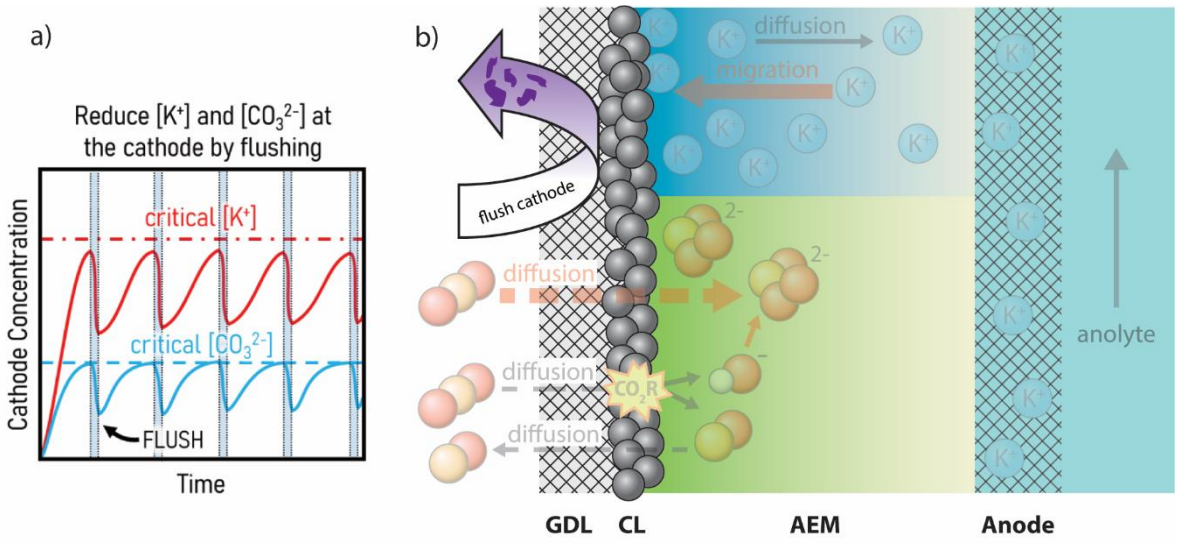

Figure 4.4 *(a) Plot of cathode concentration versus time showing the general trends of K^+ and CO_3^{2-} concentrations at the cathode during active flushing of the cathode compartment. (b) Schematic depiction of actively mitigating the buildup of ions and nucleation of crystal seeds on the catalyst by dissolving and removing salt from the cathode with water or a regenerative solution.*

Instead of using water to periodically dissolve and flush out already formed salts, increasing the water availability has also been shown as a technique to prevent salt precipitation. In one case, De Mot *et al.* introduced more liquid water to a Sn-based MEA for formate production by injecting a constant stream of water with the cathode gas feed.[40] The water injection rate was calculated by conducting a water balance on the cathode compartment, and the authors determined 0.15 mL/min of additional water was necessary to prevent salt precipitation. This calculation was in good agreement with their experimental results which found that at 0.2 mL/min of water injection, there was no visible salt formation within 1 h (although potassium was detected in the electrode pores by ICP-MS). For comparison, at a 0.1 mL/min water injection rate, the MEA failed after 50 minutes because of salt precipitation. Further increasing the water injection rate decreased the amount of K^+ detected in the cathode GDE, but also diluted the concentration of formate in the product stream. Typically, concentrated product streams are desired for downstream processing steps, so this work highlights the potential negative impact of water (and salt) management schemes on product dilution.

In a separate work, Wheeler *et al.* humidified the cathode gas feed to reduce the formation of salt precipitates.[12] When water is supplied through the gas stream, less water is drawn across the anion exchange membrane to facilitate CO_2RR. This means

that co-ion transport of K^+ across the membrane is reduced, mitigating the accumulation of K^+ at the cathode. However, Mardle *et al.* noted that humidifying the gas feed lowers selectivity for CO_2RR at higher current densities because of flooding of the cathode. Thus, water management is key to not only CO_2RR performance but also salt precipitation.[49] Conversely, others suggest that salt formation is initially *caused by* flooding of the electrolyte into the GDE and then drying of the electrolyte to leave behind salt crystals that subsequently pump more liquid into the GDE.[36] So the question remains whether salt formation in the cathode GDE is caused by flooding and drying of the electrolyte, by salt crystals first forming and then pulling liquid in to flood the electrode, or a combination of both processes.[6,50]

The examples discussed above all use a liquid anolyte containing KOH or $KHCO_3$ and rely on introducing more water to the cathode to flush out salts or limit co-ion migration. Recently, Endrődi *et al.* have successfully mitigated salt precipitation by taking the opposite approach: feeding the cell with a pure water anolyte and periodically "activating" the cathode by injecting a small volume of alkali cation containing solutions (10 cm^3 of 0.5 M KOH) into the cathode feed.[20] These solutions were 1:3 isopropanol/water mixtures (to help the solution penetrate the hydrophobic GDE) and were injected every 12 hours of operation. At a constant cell potential of 3.2 V, initial introduction of the activation solution increased j_{CO} from 120 mA cm^{-2} to 350 mA cm^{-2}. Over the course of 224 hours, j_{CO} stabilized to 420 ± 50 mA cm^{-2} and no salt precipitation was observed in the cells; however, stable operation over thousands of hours using this technique has not yet been demonstrated.

4.4 Active Pulse Approach – Pulsed electrolysis

A third approach to overcome salt precipitation is the use of a periodic regeneration voltage to redistribute ions within the MEA. In this approach the device voltage is ramped up and down in a predefined duty cycle, which lowers the operating current density and temporarily reduces the formation of byproduct hydroxide. During the lower voltage cycle the transport of ions in the system is maintained, however (Fig. 4.5). Migration of K^+ from the anolyte is then decreased, while CO_3^{2-} has additional time to move to the anode, collectively decreasing the concentrations of both ions and preventing salt formation.

Xu *et al.* demonstrated the benefits of a recurring regeneration step where the

potential was alternated between -3.8 V_{cell} during operation and -2.0 V_{cell} during regeneration. Stable operation was maintained for 236 hours (out of which 157 hours were at an operational voltage).[44] When the same setup ran without a regeneration voltage, the system broke down after ~10 hours due to salt formation. Subsequent modelling of these two systems indicated that electromigration (instead of diffusion) of carbonate ions during the regeneration step is responsible for the long-term stability of the pulsed electrolyzer. These works indicate that active manipulation of applied current or voltage are viable methods of controlling the pH and ion distribution in an MEA to mitigate salt precipitation.

Due to the low number of case studies on altering operational and regenerative voltages as well as cycle durations, there is plenty of room for further investigation using this approach. To complement the relevance of this direction of research, future CO_2 electrolyzers are likely required to operate intermittently to account for fluctuating power generation from renewable sources.[51] However, there may then be too many operational constraints from both the electrolyzer and system perspective to optimize both fully.[52]

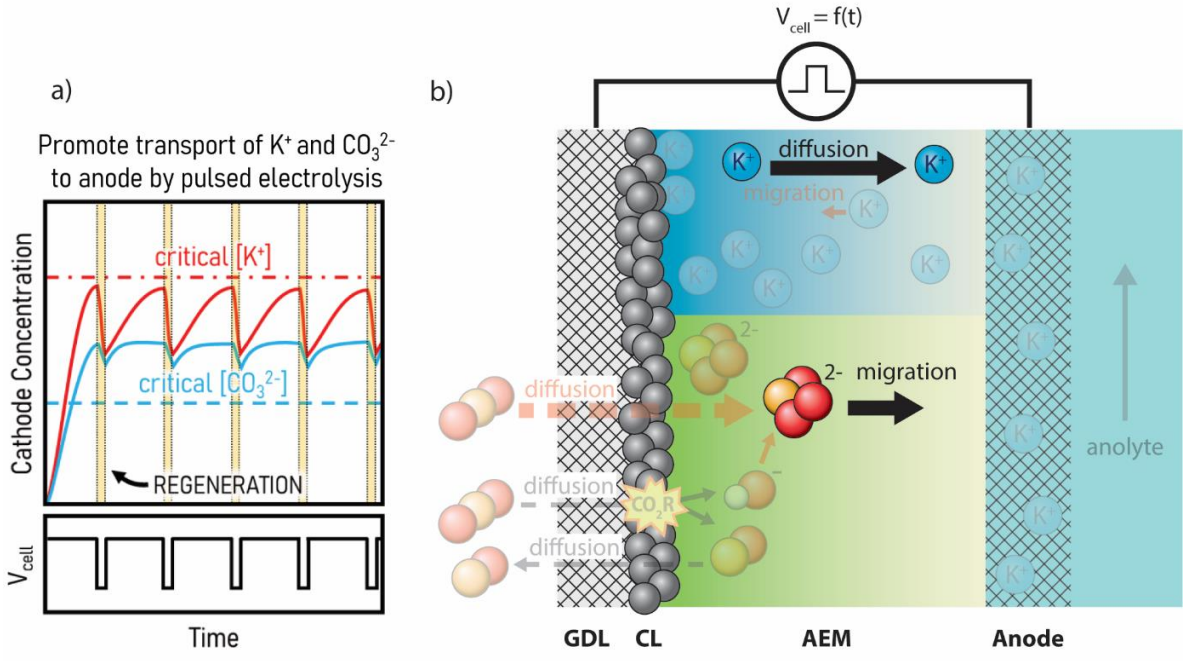

Figure 4.5 *(a) Plots of cathode concentration and cell voltage versus time showing the general trends of K^+ and CO_3^{2-} concentrations at the cathode during pulsed electrolysis. (b) Schematic depiction of ion-transport during a 'pulse' of lower voltage. At the lower regeneration voltage, the reaction slows down and migration of carbonates and K^+ allow the system to partially homogenize before returning to the operational voltage.*

4.5 Passive Membrane Approach – Membranes and Materials

The previous three approaches, while viable to maintain steady operation, all allowed for the excess formation of carbonate species. The operational approaches then provide an engineering solution rather than a fundamental solution to the problem of salt formation. The final approach described here aims to reconvert any formed (bi)carbonates back into CO_2 by providing protons to the cathode chamber through the use of a bipolar membrane (BPM) instead of a monopolar membrane (Fig. 4.6).[53–56] Such an approach then adjusts the physical and chemical components of the MEA itself which differs from the previous operational approaches.

A BPM is composed of both a cation exchange layer and an anion exchange layer that are affixed to one another. Upon the application of a reversed bias (where the cation exchange layer is closest to the cathode and the anion exchange layer is closest to the anode), water inside the membrane is split into H^+ and OH^- molecules which migrate to the cathode and anode, respectively. By using a BPM in a MEA for CO_2 electrolysis salt formation is then reduced through two different approaches. First, the H^+ generated in the BPM migrates to the cathode and chemical interacts with (bi)carbonates to regenerate CO_2, effectively offsetting the hydroxide that was generated in Eq. 1.[57–59] And second, as H^+ becomes the primary charge carrier, the migration of the co-ion K^+ from the anolyte is greatly reduced. Both [K^+] and [CO_3^{2-}] are then reduced using a BPM operating in reversed bias as compared to a monopolar membrane. A large factor in the success of using BPMs to prevent salt formation resides in the ability to prevent co-ion crossover of potassium from the anolyte. Such BPM properties have been examined by Blommaert et al. who showed that under reversed-bias conditions water dissociation will dominate K^+ co-ion crossover at current densities >10 mA cm^{-2}.[60] In fact, beyond current densities of 1 mA cm^{-2}, the flux of K^+ was shown to be fixed almost independent of the applied current density, and constituted less than 3% of the charge transported across the membrane. Thus, a BPM is likely to greatly slow salt precipitation by limiting potassium transport to the cathode, but by itself will not clearly avoid precipitation. Alternatively, operating a BPM in forward bias (where the cationic AEM is pressed against the catalyst), can assist the reaction by either regenerating CO_2 from the bicarbonate or directly reducing bicarbonate instead.[70] Simultaneously, in this configuration the implementation of quarternary ammonium cations at the catalyst-membrane interface replaced the need

for mobile cations. When Xu et al. deployed this method, stable operation for 200 hours was achieved while limiting the lost CO_2 to 3%.[71]

In principle a monopolar CEM can also be used to transport H^+ ions towards the cathode using an acidic anolyte solution. The acidity of the cathode needs to be balanced, however, to avoid excessive proton concentrations which would cause HER to dominate CO2 electrolysis.[61]

In literature the BPM approach has been used in a number of scenarios with the primary intent to increase CO_2 utilization within CO_2 electrolysis systems.[62] If a higher fraction of CO_2 is used for the electrochemical reaction, then less CO_2 can be converted into carbonate salts. During operation the BPM provides the cathode with sufficient H^+, neutralizing the produced OH^- at the cathode. The BPM approach allowed for stable operation of >12[53] and 24[54] hours, whereas the use of a Nafion CEM in the same 12 hr experiment setup revealed an increase of cell potential by 300 mV over 12 hr due to increasing anolyte pH. Using BPMs, however, results in greater membrane resistances and increased potentials due to the need to dissociate water. Designing effective bipolar membranes might help in overcoming the higher cell voltages

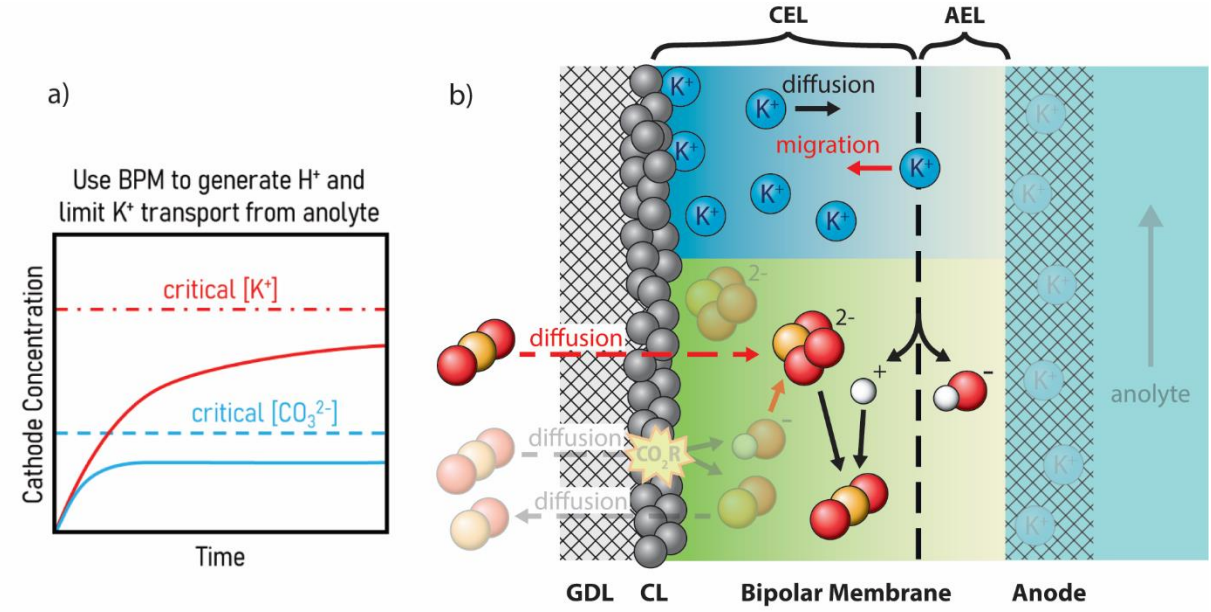

Figure 4.6 *(a) Plot of cathode concentration versus time showing the general trends of K^+ and CO_3^{2-} concentrations at the cathode when a BPM is used. (b) Schematic showing effects of a BPM on K^+-comigration past the membrane by limiting free ion transport and electro-osmotic drag. Additionally, CO_3^{2-} concentrations are reduced by combining with H^+ formed at the BPM junction to regenerate CO_2. While changing the MEA recipe delays the accumulation of ions, it does not necessarily prevent critical concentrations from being reached.*

encountered in commercially available BPMs.[63] Promising results by Oener et al. showed optimization of the BPM through lower thickness, increased AEM/CEM interface area and an additional water dissociation catalyst led to overpotentials as low as 10 mV (@20 mA/cm^2).[72]

4.6 Conclusion

A common challenge for CO_2RR research is controlling the environment close to the catalyst such that the core performance metrics of voltage, current density, selectivity and stability can all be maintained. The issue of salt precipitation in MEA systems is no exception and requires consideration of the electrochemical and chemical reactions occurring in the system, as well as mass transport within each component. Herein we identified several mechanisms that lead to salt formation and reviewed four operational techniques for salt precipitation prevention in neutral and alkaline CO_2RR MEAs, all with the goal of lowering cation and/or carbonate concentrations near the cathode.

The outlook for each of the presented approaches are promising given the relatively few papers that have tried to directly address salt formation, leaving room for greater advancements. For example, there remains a large amount of operating conditions left to be tested and combining a subset of the approaches above is likely to allow for salt formation failure to be prevented indefinitely. It is also worth noting that the challenges associated with salt and carbonate formation were only noted a few years prior to this article, and there are now several proposed solutions, highlighting progress in a short period of time. Notably for each of the presented cases, however, is that system stability was improved at the cost of decreases in other performance metrics. For example, decreasing the anolyte concentration or using a BPM is penalized by higher cell voltages, while periodic operation lowers the capacity factor of the electrolyzer. Future work then needs to evaluate which trade-offs are acceptable at the expense of other metrics.

Looking to the future, we note that operational strategies are not the only methods available to stop salt precipitation, and we expect materials selection and development to also play a role. Recent reports in flow cells have demonstrated the ability of ionomer binders, monolayers and bilayers to control local concentrations of ions in the catalyst layer and influence salt precipitation.[5,64] When developing solutions to overcome salt

precipitation for CO_2RR, researchers can also look to other fields for inspiration. Research on durable membranes for water filtration applications has extensively studied materials design strategies (i.e. controlling surface charge, roughness, hydrophobicity, etc.) to mitigate membrane fouling by inorganic salts (primarily $CaCO_3$, SiO_2 and $BaSO_4$).[65] The formation of carbonate salts at gas-liquid-solid boundaries is also of interest to geological carbon storage applications whereby CO_2 is injected into saline aquifers for sequestration.[66] Further study into salt nucleation and growth mechanisms under CO_2RR conditions by *operando* or *in situ* characterization techniques (i.e. atomic force microscopy, nano- or micro-computed tomography, x-ray diffraction, etc.) will also inform the development of both materials-based and operational salt prevention strategies. Lastly, the emerging field of CO_2RR under acidic conditions provides another avenue to avoid the issue of salt precipitation entirely, as the reduction of hydroxide concentrations leads to significantly less homogenous formation of salts.[67] Future works should weigh the advantages and disadvantages of CO_2RR in acidic and alkaline environments to determine which system is most desirable for a durable and selective electrolyzer operating at industrially relevant current densities, that also maintain overall high energy and carbon efficiency.

Salt precipitation is one of the major limitations for the selective and long-term operation of neutral and alkaline MEA CO_2RR electrolyzers. This issue is difficult to avoid because the three essential components for CO_2RR (CO_2 gas, a proton source, and an alkali cation) also directly influence the local concentrations of ions that can precipitate into salt deposits. Here mechanisms for salt formation are discussed, and four operational approaches to prevent or reverse salt precipitation are presented, which can be broken down into either passive system changes or active mediation. Several of these strategies are successful over the course of tens to hundreds of hours; however, none demonstrate selective system operation on the order of tens of thousands of hours. We encourage researchers to report longer term electrolysis studies using these salt precipitation prevention methods and analyze their feasibility for commercial systems. A combination of operational solutions will likely need to be deployed to solve the salt precipitation problem.

References Chapter 4.

(1) Buttler, A.; Spliethoff, H. Current Status of Water Electrolysis for Energy Storage, Grid Balancing and Sector Coupling via Power-to-Gas and Power-to-Liquids: A Review. *Renew. Sustain. Energy Rev.* **2018**, *82*, 2440–2454. https://doi.org/10.1016/j.rser.2017.09.003.

(2) Lv, J.-J.; Jouny, M.; Luc, W.; Zhu, W.; Zhu, J.-J.; Jiao, F. A Highly Porous Copper Electrocatalyst for Carbon Dioxide Reduction. *Adv. Mater.* **2018**, *30* (49), 1803111. https://doi.org/10.1002/adma.201803111.

(3) Verma, S.; Hamasaki, Y.; Kim, C.; Huang, W.; Lu, S.; Jhong, H.-R. M.; Gewirth, A. A.; Fujigaya, T.; Nakashima, N.; Kenis, P. J. A. Insights into the Low Overpotential Electroreduction of CO_2 to CO on a Supported Gold Catalyst in an Alkaline Flow Electrolyzer. *ACS Energy Lett.* **2018**, *3* (1), 193–198. https://doi.org/10.1021/acsenergylett.7b01096.

(4) Cofell, E. R.; Nwabara, U. O.; Bhargava, S. S.; Henckel, D. E.; Kenis, P. J. A. Investigation of Electrolyte-Dependent Carbonate Formation on Gas Diffusion Electrodes for CO_2 Electrolysis. *ACS Appl. Mater. Interfaces* **2021**, *13* (13), 15132–15142. https://doi.org/10.1021/acsami.0c21997.

(5) Nwabara, U. O.; Hernandez, A. D.; Henckel, D. A.; Chen, X.; Cofell, E. R.; de-Heer, M. P.; Verma, S.; Gewirth, A. A.; Kenis, P. J. A. Binder-Focused Approaches to Improve the Stability of Cathodes for CO_2 Electroreduction. *ACS Appl. Energy Mater.* **2021**, *4* (5), 5175–5186. https://doi.org/10.1021/acsaem.1c00715.

(6) Pham, T. H. M.; Zhang, J.; Li, M.; Shen, T.-H.; Ko, Y.; Tileli, V.; Luo, W.; Züttel, A. Enhanced Electrocatalytic CO2 Reduction to C2+ Products by Adjusting the Local Reaction Environment with Polymer Binders. *Adv. Energy Mater. n/a* (n/a), 2103663. https://doi.org/10.1002/aenm.202103663.

(7) de Jesus Gálvez-Vázquez, M.; Moreno-García, P.; Xu, H.; Hou, Y.; Hu, H.; Montiel, I. Z.; Rudnev, A. V.; Alinejad, S.; Grozovski, V.; Wiley, B. J.; Arenz, M.; Broekmann, P. Environment Matters: CO_2 RR Electrocatalyst Performance Testing in a Gas-Fed Zero-Gap Electrolyzer. *ACS Catal.* **2020**, *10* (21), 13096–13108. https://doi.org/10.1021/acscatal.0c03609.

(8) Dinh, C.-T.; Burdyny, T.; Kibria, M. G.; Seifitokaldani, A.; Gabardo, C. M.; García de Arquer, F. P.; Kiani, A.; Edwards, J. P.; De Luna, P.; Bushuyev, O. S.; Zou, C.; Quintero-Bermudez, R.; Pang, Y.; Sinton, D.; Sargent, E. H. CO2 Electroreduction to Ethylene via Hydroxide-Mediated Copper Catalysis at an Abrupt Interface. *Science* **2018**, *360* (6390), 783–787. https://doi.org/10.1126/science.aas9100.

(9) Garg, S.; Li, M.; Z. Weber, A.; Ge, L.; Li, L.; Rudolph, V.; Wang, G.; E. Rufford, T. Advances and Challenges in Electrochemical CO 2 Reduction Processes: An Engineering and Design Perspective Looking beyond New Catalyst Materials. *J. Mater. Chem. A* **2020**, *8* (4), 1511–1544. https://doi.org/10.1039/C9TA13298H.

(10) Burdyny, T.; A. Smith, W. CO 2 Reduction on Gas-Diffusion Electrodes and Why Catalytic Performance Must Be Assessed at Commercially-Relevant Conditions. *Energy Environ. Sci.* **2019**, *12* (5), 1442–1453. https://doi.org/10.1039/C8EE03134G.

(11) Ge, L.; Rabiee, H.; Li, M.; Subramanian, S.; Zheng, Y.; Lee, J. H.; Burdyny, T.; Wang, H. Electrochemical CO2 Reduction in Membrane-Electrode Assemblies. *Chem* **2022**. https://doi.org/10.1016/j.chempr.2021.12.002.

(12) Wheeler, D. G.; Mowbray, B. A. W.; Reyes, A.; Habibzadeh, F.; He, J.; Berlinguette, C. P. Quantification of Water Transport in a CO2 Electrolyzer. *Energy Environ. Sci.* **2020**, *13* (12), 5126–5134. https://doi.org/10.1039/D0EE02219E.

(13) Wang, G.; Pan, J.; Jiang, S. P.; Yang, H. Gas Phase Electrochemical Conversion of Humidified CO2 to CO and H2 on Proton-Exchange and Alkaline Anion-Exchange Membrane Fuel Cell Reactors. *J. CO2 Util.* **2018**, *23*, 152–158. https://doi.org/10.1016/j.jcou.2017.11.010.

(14) Shironita, S.; Karasuda, K.; Sato, M.; Umeda, M. Feasibility Investigation of Methanol Generation by CO2 Reduction Using Pt/C-Based Membrane Electrode Assembly for a Reversible Fuel Cell. *J. Power Sources* **2013**, *228*, 68–74. https://doi.org/10.1016/j.jpowsour.2012.11.097.

(15) Pérez-Rodríguez, S.; Barreras, F.; Pastor, E.; Lázaro, M. J. Electrochemical Reactors for CO2 Reduction: From Acid Media to Gas Phase. *Int. J. Hydrog. Energy* **2016**, *41* (43), 19756–19765. https://doi.org/10.1016/j.ijhydene.2016.06.130.

(16) Kriescher, S. M. A.; Kugler, K.; Hosseiny, S. S.; Gendel, Y.; Wessling, M. A Membrane Electrode Assembly for the Electrochemical Synthesis of Hydrocarbons from CO2(g) and H2O(g). *Electrochem. Commun.* **2015**, *50*, 64–68. https://doi.org/10.1016/j.elecom.2014.11.014.

(17) Bohra, D.; H. Chaudhry, J.; Burdyny, T.; A. Pidko, E.; A. Smith, W. Modeling the Electrical Double Layer to Understand the Reaction Environment in a CO 2 Electrocatalytic System. *Energy Environ. Sci.* **2019**, *12* (11), 3380–3389. https://doi.org/10.1039/C9EE02485A.

(18) Yang, K.; Kas, R.; Smith, W. A. In Situ Infrared Spectroscopy Reveals Persistent Alkalinity near Electrode Surfaces during CO $_2$ Electroreduction. *J. Am. Chem. Soc.* **2019**, *141* (40), 15891–15900. https://doi.org/10.1021/jacs.9b07000.

(19) Lu, X.; Zhu, C.; Wu, Z.; Xuan, J.; Francisco, J. S.; Wang, H. In Situ Observation of the PH Gradient near the Gas Diffusion Electrode of CO $_2$ Reduction in Alkaline Electrolyte. *J. Am. Chem. Soc.* **2020**, *142* (36), 15438–15444. https://doi.org/10.1021/jacs.0c06779.

(20) Endrődi, B.; Samu, A.; Kecsenovity, E.; Halmágyi, T.; Sebők, D.; Janáky, C. Operando Cathode Activation with Alkali Metal Cations for High Current Density Operation of Water-Fed Zero-Gap Carbon Dioxide Electrolysers. *Nat. Energy* **2021**, *6* (4), 439–448. https://doi.org/10.1038/s41560-021-00813-w.

(21) Yang, K.; Li, M.; Subramanian, S.; Blommaert, M. A.; Smith, W. A.; Burdyny, T. Cation-Driven Increases of CO2 Utilization in a Bipolar Membrane Electrode Assembly for CO2 Electrolysis. *ACS Energy Lett.* **2021**, 4291–4298. https://doi.org/10.1021/acsenergylett.1c02058.

(22) Vennekötter, J.-B.; Scheuermann, T.; Sengpiel, R.; Wessling, M. The Electrolyte Matters: Stable Systems for High Rate Electrochemical CO2 Reduction. *J. CO2 Util.* **2019**, *32*, 202–213. https://doi.org/10.1016/j.jcou.2019.04.007.

(23) Schröder, D.; Sinai Borker, N. N.; König, M.; Krewer, U. Performance of zinc air batteries with added K2CO3 in the alkaline electrolyte. *J. Appl. Electrochem.* **2015**, *45* (5), 427–437. https://doi.org/10.1007/s10800-015-0817-0.

(24) Naughton, M. S.; Brushett, F. R.; Kenis, P. J. A. Carbonate Resilience of Flowing Electrolyte-Based Alkaline Fuel Cells. *J. Power Sources* **2011**, *196* (4), 1762–1768. https://doi.org/10.1016/j.jpowsour.2010.09.114.

(25) Wuttig, A.; Yoon, Y.; Ryu, J.; Surendranath, Y. Bicarbonate Is Not a General Acid in Au-Catalyzed CO2 Electroreduction. *J. Am. Chem. Soc.* **2017**, *139* (47), 17109–17113. https://doi.org/10.1021/jacs.7b08345.

(26) Zeng, J. S.; Corbin, N.; Williams, K.; Manthiram, K. Kinetic Analysis on the Role of Bicarbonate in Carbon Dioxide Electroreduction at Immobilized Cobalt Phthalocyanine. *ACS Catal.* **2020**, *10* (7), 4326–4336. https://doi.org/10.1021/acscatal.9b05272.

(27) Chen, Y.; Wrubel, J. A.; Vise, A. E.; Intia, F.; Harshberger, S.; Klein, E.; Smith, W. A.; Ma, Z.; Deutsch, T. G.; Neyerlin, K. C. The Effect of Catholyte and Catalyst Layer Binders on CO2 Electroreduction Selectivity. *Chem Catal.* **2022**, *2* (2), 400–421. https://doi.org/10.1016/j.checat.2022.01.011.

(28) Chen, L. D. Cations Play an Essential Role in CO2 Reduction. *Nat. Catal.* **2021**, *4* (8), 641–642. https://doi.org/10.1038/s41929-021-00667-1.

(29) Monteiro, M. C. O.; Dattila, F.; Hagedoorn, B.; García-Muelas, R.; López, N.; Koper, M. T. M. Absence of CO2 Electroreduction on Copper, Gold and Silver Electrodes without Metal Cations in Solution. *Nat. Catal.* **2021**, *4*, 654–662. https://doi.org/10.1038/s41929-021-00655-5.

(30) Moura de Salles Pupo, M.; Kortlever, R. Electrolyte Effects on the Electrochemical Reduction of CO2. *ChemPhysChem* **2019**, *20* (22), 2926–2935. https://doi.org/10.1002/cphc.201900680.

(31) Rabinowitz, J. A.; Kanan, M. W. The Future of Low-Temperature Carbon Dioxide Electrolysis Depends on Solving One Basic Problem. *Nat. Commun.* **2020**, *11* (1), 5231. https://doi.org/10.1038/s41467-020-19135-8.

(32) Ma, M.; L. Clark, E.; T. Therkildsen, K.; Dalsgaard, S.; Chorkendorff, I.; Seger, B. Insights into the Carbon Balance for CO 2 Electroreduction on Cu Using Gas Diffusion Electrode Reactor Designs. *Energy Environ. Sci.* **2020**, *13* (3), 977–985. https://doi.org/10.1039/D0EE00047G.

(33) Weng, L.-C.; Bell, A. T.; Weber, A. Z. Towards Membrane-Electrode Assembly Systems for CO2 Reduction: A Modeling Study. *Energy Environ. Sci.* **2019**, *12* (6), 1950–1968. https://doi.org/10.1039/C9EE00909D.

(34) Kas, R.; Star, A. G.; Yang, K.; Van Cleve, T.; Neyerlin, K. C.; Smith, W. A. Along the Channel Gradients Impact on the Spatioactivity of Gas Diffusion Electrodes at High Conversions during CO2 Electroreduction. *ACS Sustain. Chem. Eng.* **2021**, *9* (3), 1286–1296. https://doi.org/10.1021/acssuschemeng.0c07694.

(35) *CRC Handbook of Chemistry and Physics*, 103rd ed.; Rumble Jr., J. R., Ed.; CRC Press/Taylor & Francis: Boca Raton, FL, 2022.

(36) Leonard, M. E.; Clarke, L. E.; Forner-Cuenca, A.; Brown, S. M.; Brushett, F. R. Investigating Electrode Flooding in a Flowing Electrolyte, Gas-Fed Carbon Dioxide Electrolyzer. *ChemSusChem* **2020**, *13* (2), 400–411. https://doi.org/10.1002/cssc.201902547.

(37) Garg, S.; Rodriguez, C. A. G.; Rufford, T. E.; Varcoe, J. R.; Seger, B. How Membrane Characteristics Influence the Performance of CO2 and CO Electrolysis. *Energy Environ. Sci.* **2022**. https://doi.org/10.1039/D2EE01818G.

(38) Lees, E. W.; Bui, J. C.; Song, D.; Weber, A. Z.; Berlinguette, C. P. Continuum Model to Define the Chemistry and Mass Transfer in a Bicarbonate Electrolyzer. *ACS Energy Lett.* **2022**, *7* (2), 834–842. https://doi.org/10.1021/acsenergylett.1c02522.

(39) Hawks, S. A.; Ehlinger, V. M.; Moore, T.; Duoss, E. B.; Beck, V. A.; Weber, A. Z.; Baker, S. E. Analyzing Production Rate and Carbon Utilization Trade-Offs in CO2RR Electrolyzers. *ACS Energy Lett.* **2022**, *7* (8), 2685–2693. https://doi.org/10.1021/acsenergylett.2c01106.

(40) De Mot, B.; Ramdin, M.; Hereijgers, J.; Vlugt, T. J. H.; Breugelmans, T. Direct Water Injection in Catholyte-Free Zero-Gap Carbon Dioxide Electrolyzers. *ChemElectroChem* **2020**, *7* (18), 3839–3843. https://doi.org/10.1002/celc.202000961.

(41) Baumgartner, L. M.; Koopman, C. I.; Forner-Cuenca, A.; Vermaas, D. A. Narrow Pressure Stability Window of Gas Diffusion Electrodes Limits the Scale-Up of CO2 Electrolyzers. *ACS Sustain. Chem. Eng.* **2022**, *10* (14), 4683–4693. https://doi.org/10.1021/acssuschemeng.2c00195.

(42) Endrődi, B.; Kecsenovity, E.; Samu, A.; Darvas, F.; Jones, R. V.; Török, V.; Danyi, A.; Janáky, C. Multilayer Electrolyzer Stack Converts Carbon Dioxide to Gas Products at High Pressure with High Efficiency. *ACS Energy Lett.* **2019**, *4* (7), 1770–1777. https://doi.org/10.1021/acsenergylett.9b01142.

(43) Liu, Z.; Yang, H.; Kutz, R.; Masel, R. I. CO2 Electrolysis to CO and O2 at High Selectivity, Stability and Efficiency Using Sustainion Membranes. *J. Electrochem. Soc.* **2018**, *165* (15), J3371. https://doi.org/10.1149/2.0501815jes.

(44) Xu, Y.; Edwards, J. P.; Liu, S.; Miao, R. K.; Huang, J. E.; Gabardo, C. M.; O'Brien, C. P.; Li, J.; Sargent, E. H.; Sinton, D. Self-Cleaning CO2 Reduction Systems: Unsteady Electrochemical Forcing Enables Stability. *ACS Energy Lett.* **2021**, *6* (2), 809–815. https://doi.org/10.1021/acsenergylett.0c02401.

(45) Yin, Z.; Peng, H.; Wei, X.; Zhou, H.; Gong, J.; Huai, M.; Xiao, L.; Wang, G.; Lu, J.; Zhuang, L. An Alkaline Polymer Electrolyte CO2 Electrolyzer Operated with Pure Water. *Energy Environ. Sci.* **2019**, *12* (8), 2455–2462. https://doi.org/10.1039/C9EE01204D.

(46) O'Brien, C. P.; Miao, R. K.; Liu, S.; Xu, Y.; Lee, G.; Robb, A.; Huang, J. E.; Xie, K.; Bertens, K.; Gabardo, C. M.; Edwards, J. P.; Dinh, C.-T.; Sargent, E. H.; Sinton, D. Single Pass CO2 Conversion Exceeding 85% in the Electrosynthesis of Multicarbon Products via Local CO2 Regeneration. *ACS Energy Lett.* **2021**, *6* (8), 2952–2959. https://doi.org/10.1021/acsenergylett.1c01122.

(47) Chiacchiarelli, L. M.; Zhai, Y.; Frankel, G. S.; Agarwal, A. S.; Sridhar, N. Cathodic Degradation Mechanisms of Pure Sn Electrocatalyst in a Nitrogen Atmosphere. *J. Appl. Electrochem.* **2012**, *42* (1), 21–29. https://doi.org/10.1007/s10800-011-0367-z.

(48) Legrand, U.; Lee, J. K.; Bazylak, A.; Tavares, J. R. Product Crossflow through a Porous Gas Diffusion Layer in a CO2 Electrochemical Cell with Pressure Drop Calculations. *Ind. Eng. Chem. Res.* **2021**, *60* (19), 7187–7196. https://doi.org/10.1021/acs.iecr.1c01316.

(49) Mardle, P.; Cassegrain, S.; Habibzadeh, F.; Shi, Z.; Holdcroft, S. Carbonate Ion Crossover in Zero-Gap, KOH Anolyte CO2 Electrolysis. *J. Phys. Chem. C* **2021**, *125* (46), 25446–25454. https://doi.org/10.1021/acs.jpcc.1c08430.

(50) Li, M.; Idros, M. N.; Wu, Y.; Burdyny, T.; Garg, S.; Zhao, X. S.; Wang, G.; Rufford, T. E. The Role of Electrode Wettability in Electrochemical Reduction of Carbon Dioxide. *J. Mater. Chem. A* **2021**, *9* (35), 19369–19409. https://doi.org/10.1039/D1TA03636J.

(51) Samu, A. A.; Kormányos, A.; Kecsenovity, E.; Szilágyi, N.; Endrődi, B.; Janáky, C. Intermittent Operation of CO2 Electrolyzers at Industrially Relevant Current Densities. *ACS Energy Lett.* **2022**, *7* (5), 1859–1861. https://doi.org/10.1021/acsenergylett.2c00923.

(52) Huesman, A. Integration of Operation and Design of Solar Fuel Plants: A Carbon Dioxide to Methanol Case Study. *Comput. Chem. Eng.* **2020**, *140*, 106836. https://doi.org/10.1016/j.compchemeng.2020.106836.

(53) Li, Y. C.; Zhou, D.; Yan, Z.; Gonçalves, R. H.; Salvatore, D. A.; Berlinguette, C. P.; Mallouk, T. E. Electrolysis of CO2 to Syngas in Bipolar Membrane-Based Electrochemical Cells. *ACS Energy Lett.* **2016**, *1* (6), 1149–1153. https://doi.org/10.1021/acsenergylett.6b00475.

(54) Salvatore, D. A.; Weekes, D. M.; He, J.; Dettelbach, K. E.; Li, Y. C.; Mallouk, T. E.; Berlinguette, C. P. Electrolysis of Gaseous CO2 to CO in a Flow Cell with a Bipolar Membrane. *ACS Energy Lett.* **2018**, *3* (1), 149–154. https://doi.org/10.1021/acsenergylett.7b01017.

(55) Chen, Y.; Vise, A.; Klein, W. E.; Cetinbas, F. C.; Myers, D. J.; Smith, W. A.; Deutsch, T. G.; Neyerlin, K. C. A Robust, Scalable Platform for the Electrochemical Conversion of CO2 to Formate: Identifying Pathways to Higher Energy Efficiencies. *ACS Energy Lett.* **2020**, *5* (6), 1825–1833. https://doi.org/10.1021/acsenergylett.0c00860.

(56) Yang, H.; Kaczur, J. J.; Sajjad, S. D.; Masel, R. I. Performance and Long-Term Stability of CO2 Conversion to Formic Acid Using a Three-Compartment Electrolyzer Design. *J. CO2 Util.* **2020**, *42*, 101349. https://doi.org/10.1016/j.jcou.2020.101349.

(57) Li, Y. C.; Lee, G.; Yuan, T.; Wang, Y.; Nam, D.-H.; Wang, Z.; García de Arquer, F. P.; Lum, Y.; Dinh, C.-T.; Voznyy, O.; Sargent, E. H. CO2 Electroreduction from Carbonate Electrolyte. *ACS Energy Lett.* **2019**, *4* (6), 1427–1431. https://doi.org/10.1021/acsenergylett.9b00975.

(58) Ma, M.; Kim, S.; Chorkendorff, I.; Seger, B. Role of Ion-Selective Membranes in the Carbon Balance for CO2 Electroreduction via Gas Diffusion Electrode Reactor Designs. *Chem. Sci.* **2020**, *11* (33), 8854–8861. https://doi.org/10.1039/D0SC03047C.

(59) Kim, J. Y. 'Timothy'; Zhu, P.; Chen, F.-Y.; Wu, Z.-Y.; Cullen, D. A.; Wang, H. Recovering Carbon Losses in CO2 Electrolysis Using a Solid Electrolyte Reactor. *Nat. Catal.* **2022**, *5* (4), 288–299. https://doi.org/10.1038/s41929-022-00763-w.

(60) Blommaert, M. A.; Verdonk, J. A. H.; Blommaert, H. C. B.; Smith, W. A.; Vermaas, D. A. Reduced Ion Crossover in Bipolar Membrane Electrolysis *via* Increased Current Density, Molecular Size, and Valence. *ACS Appl. Energy Mater.* **2020**, *3* (6), 5804–5812. https://doi.org/10.1021/acsaem.0c00687.

(61) Shafaque, H. W.; Lee, C.; Fahy, K. F.; Lee, J. K.; LaManna, J. M.; Baltic, E.; Hussey, D. S.; Jacobson, D. L.; Bazylak, A. Boosting Membrane Hydration for High Current Densities in Membrane Electrode Assembly CO2 Electrolysis. *ACS Appl. Mater. Interfaces* **2020**, *12* (49), 54585–54595. https://doi.org/10.1021/acsami.0c14832.

(62) Blommaert, M. A.; Subramanian, S.; Yang, K.; Smith, W. A.; Vermaas, D. A. High Indirect Energy Consumption in AEM-Based CO2 Electrolyzers Demonstrates the Potential of Bipolar Membranes. *ACS Appl. Mater. Interfaces* **2022**, *14* (1), 557–563. https://doi.org/10.1021/acsami.1c16513.

(63) Xie, K.; Miao, R. K.; Ozden, A.; Liu, S.; Chen, Z.; Dinh, C.-T.; Huang, J. E.; Xu, Q.; Gabardo, C. M.; Lee, G.; Edwards, J. P.; O'Brien, C. P.; Boettcher, S. W.; Sinton, D.; Sargent, E. H. Bipolar Membrane Electrolyzers Enable High Single-Pass CO2 Electroreduction to Multicarbon Products. *Nat. Commun.* **2022**, *13* (1), 3609. https://doi.org/10.1038/s41467-022-31295-3.

(64) Bui, J. C.; Digdaya, I.; Xiang, C.; Bell, A. T.; Weber, A. Z. Understanding Multi-Ion Transport Mechanisms in Bipolar Membranes. *ACS Appl. Mater. Interfaces* **2020**, *12* (47), 52509–52526. https://doi.org/10.1021/acsami.0c12686.

(65) Zhao, S.; Liao, Z.; Fane, A.; Li, J.; Tang, C.; Zheng, C.; Lin, J.; Kong, L. Engineering Antifouling Reverse Osmosis Membranes: A Review. *Desalination* **2021**, *499*, 114857. https://doi.org/10.1016/j.desal.2020.114857.

(66) Miri, R.; Hellevang, H. Salt Precipitation during CO2 Storage—A Review. *Int. J. Greenh. Gas Control* **2016**, *51*, 136–147. https://doi.org/10.1016/j.ijggc.2016.05.015.

(67) Huang, J. E.; Li, F.; Ozden, A.; Rasouli, A. S.; Arquer, F. P. G. de; Liu, S.; Zhang, S.; Luo, M.; Wang, X.; Lum, Y.; Xu, Y.; Bertens, K.; Miao, R. K.; Dinh, C.-T.; Sinton, D.; Sargent, E. H. CO2 Electrolysis to Multicarbon Products in Strong Acid. *Science* **2021**, *372* (6546), 1074–1078. https://doi.org/10.1126/science.abg6582.

(68) Reyes, A., et al., Managing Hydration at the Cathode Enables Efficient CO2 Electrolysis at Commercially Relevant Current Densities. ACS Energy Letters, 2020. 5(5): p. 1612-1618.

(69) Geise, G.M., M.A. Hickner, and B.E. Logan, Ionic Resistance and Permselectivity Tradeoffs in Anion Exchange Membranes. ACS Applied Materials & Interfaces, 2013. 5(20): p. 10294-10301.

(68) Reyes, A., et al., Managing Hydration at the Cathode Enables Efficient CO2 Electrolysis at Commercially Relevant Current Densities. ACS Energy Letters, 2020. 5(5): p. 1612-1618.

(69) Geise, G.M., M.A. Hickner, and B.E. Logan, Ionic Resistance and Permselectivity Tradeoffs in Anion Exchange Membranes. ACS Applied Materials & Interfaces, 2013. 5(20): p. 10294-10301.

(70) Li, T., et al., Electrolytic Conversion of Bicarbonate into CO in a Flow Cell. Joule, 2019. 3(6): p. 1487-1497.

(71) Xu, Y., et al., A microchanneled solid electrolyte for carbon-efficient CO2 electrolysis. Joule, 2022. 6(6): p. 1333-1343.

(72) Oener, S.Z., M.J. Foster, and S.W. Boettcher, *Accelerating water dissociation in bipolar membranes and for electrocatalysis*. Science, 2020. **369**(6507): p. 1099-1103.

Chapter 5.

Bulk layering effects of Ag and Cu in tandem CO_2 electrolysis to adjust C_{2+} selectivity

5.1 Introduction

Carbon dioxide (CO_2) emissions are one of the main causes of climate change and are a direct result of the fossil fuel-based economy that has driven the development of modern society. One promising solution to mitigate further climate disaster is to use renewable energy to drive the electrochemical reduction of CO_2 (CO_2RR) to value added products. Several decades of research of CO_2RR has shown a relationship between the composition of catalysts having a significant effect on which products are formed [1]. Two of the most promising catalysts are silver (Ag) and copper (Cu) [2]. Ag catalysts are well-known for effectively converting CO_2 into carbon monoxide (CO) with near unity selectivity (>90%) [3], [4]. When CO is combined with hydrogen (H_2) it can then be upgraded into longer carbon chains using Fisher-Tropsch synthesis [5]. Alternatively, Cu catalysts are unique in CO_2RR as they are able to produce multi-carbon products such as ethylene (C_2H_4) and ethanol (C_2H_5OH), in addition to single-carbon compounds such as CO, formate and methane[6]. The multi-carbon products have higher energetic and economic value and utilization potential as chemical building blocks and energy dense fuels. However, one key challenge is to be able to form only one major product and minimize the formation of unwanted side products in order to reduce downstream separations costs.

This chapter is based on a manuscript by Mark Sassenburg, Wilson A. Smith and Thomas Burdyny that is currently under internal revision.

The ability for Cu to produce multi-carbon products stems from the intermediate binding energy of *CO after being reduced from CO_2. [7], [8] CO is a key intermediate in CO2RR for allowing C-C coupling to occur on a catalyst surface, where the binding energy is strong enough to allow the reaction to proceed further, while not being weak enough to desorb and form a product. This optimal binding energy allows for both the dimerization of two bound *CO intermediates through a Langmuir-Hinshelwood mechanism, but also for the reaction between an aqueous CO species with a surface bound *CO intermediate [9]. Such reaction mechanisms are also why Cu is able to further perform the CO reduction reaction (CORR) with a similar product spectrum but a moderately higher ethanol/acetate-to-ethylene ratio [10], [11], [12], [13]. Since many of the achievable CO_2 reduction products have different amounts of electron transfers and unique binding energies, finetuning of the surface and the optimal cathode potential became attractive field of research. Combining Cu with other elements led to a bifurcation of research branches; Alloying and layering. With alloying two (or more) elements are homogeneously mixed in an atomistic sense, hereby tuning the binding energy of the surface. This can be done to for instance extend the binding duration of CO to promote dimerization, or to weaken the bond of a desired product in order to promote earlier release. With layering of elements, two different catalytic materials are deposited in tandem (henceforth this type of reaction will be called tandem catalysis), in which each material specializes in an unique role. Cu based tandem catalysis aims to make the initial step from CO_2 to CO easier on a secondary catalyst, after which Cu can benefit from the CO enriched environment in which dimerization is more favorable than in a pure CO_2 environment. This brings us to the research question: Can the excess production of CO from one catalytic site allow for overall enhanced CO_2RR to multi-carbon products? To answer this question we focus on tandem catalysis and compare it to the performance of their pure metal counterparts.

In order to try and improve the selectivity of CO2RR to multicarbon products, many researchers have used multi-component catalysts, both intermetallic and alloys, to promote CO formation on one site (typically Ag) and place this next to a CO coupling site (typically Cu). In these cases, Cu is either doped with Ag or bimetallic nanoparticle clusters are formed with the intention of providing a spillover effect of CO produced on the Ag catalyst towards the Cu catalyst. When looking specifically into AgCu bimetallic

catalysts, it was found that depending on the method of preparation, the combination of Ag and Cu could increase catalytic activity towards CO [14], allow control over the syngas composition normally produced by Ag [15], improve the Faradaic efficiency (FE) towards methane (CH_4) [16], ethylene (C_2H_4) [17], [18], acetate (CH_3COO^-) and ethanol (C_2H_5OH) [19], [20], [21], [22], [23]. The amount of Ag used in these bimetallic catalysts can also be used to tune the overall C_{2+} selectivity [24], [25]. These studies have given us insight in the possible synergies between Ag and Cu.

Similarly, controlled atomic mixing of Ag in the Cu matrix has also been shown to be an avenue to affect catalyst performance. Whereas the aforementioned works make use of a spillover effect, the incorporation of Ag directly into the bulk lattice of Cu can be used to promote the CO_2-to-CO step [26] [27] and stabilize the intermediate [28]. It has been theorized and shown that introduction of monoatomic Ag in small quantities can also be used to create compressive surface strain in the Cu host matrix, modifying the electronic structure to suppress H_2 evolution and favor the formation of multi-carbon oxygenates [29]. While the presented AgCu bimetallic materials are proven to be effective in tuning the product distribution, many of these tests were performed under highly controlled conditions and reaction rates limited to a few mA/cm^2.

In recent years CO_2 reduction research has shifted to using gas diffusion electrodes (GDEs) to allow for higher reaction rates by increasing the CO_2 concentration near the catalyst [30]. By deploying these GDEs in gas-liquid fed systems like a flow cell or a membrane electrode assembly (MEA), catalyst materials can be studied in a manner more applicable to the desired industrial performance. It was found that the selectivity of Cu and AgCu bimetallics was highly dependent on the reaction rate, despite using the same initial catalysts. As the current density increased, an increase in ethylene and ethanol selectivity was observed, while the CO selectivity decreased [31], [32]. Though C_{2+} products increased significantly, the reduced amount of CO coming out of the system implies a limit to the secondary dimerization reaction, limiting the performance of the Cu catalyst. If this were to be the case, the addition of Ag as a co-catalyst could be beneficial in providing additional CO to the Cu catalyst, circumventing this limitation.

In this research article, we study the tandem catalysis of Ag and Cu in a zero-gap membrane electrode assembly and compare it to the performance different layering

orders, layer thicknesses and its pure metal counterparts. Knowing that CO is an intermediate product towards ethylene we would like to assess whether **the Cu catalyst could produce more C_{2+} products when provided with additional CO through tandem catalysis**, or whether **Cu independently produces enough CO to satisfy all its dimerization requirements**. To test this hypothesis, we compare the selectivity of a pure Ag catalyst to perform CO_2-to-CO reduction (Fig. 5.1a), a pure Cu catalyst capable of dimerization (Fig. 5.1b) and a range of sequentially layered Cu | Ag systems that performs both functions and possibly benefit from a CO enriched environment for further CO-to-C_{2+} dimerization on Cu (Fig. 5.1c).

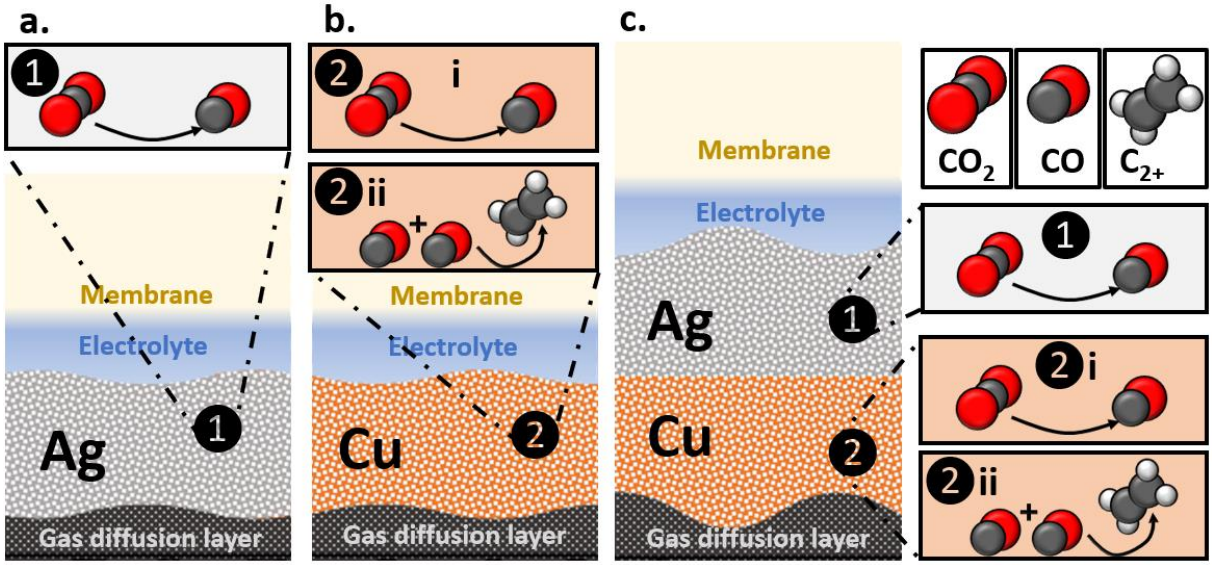

Figure 5.10 Schematic representation of the electrochemical CO_2 reduction reactions in differently catalyzed systems. ***a.*** *Pure Ag mainly promotes CO_2-to-CO conversion (❶).* ***b.*** *a pure Cu catalyst, facilitating both the CO_2-to-CO conversion (❷* **i***), and retaining the formed CO to allow further CO-to-C_{2+} dimerization (❷* **ii***).* ***c.*** *A sequentially layered GDE | Cu | Ag system, where aside of the Cu reactions, the CO_2-to-CO conversion on Ag (❶) can provide the Cu catalyst with a richer CO environment, influencing reaction* ❷**ii**.

5.2 Results and Discussion

To distinguish the effects of catalyst composition and relative structure on electrochemical performance, electrodes were fabricated by DC sputtering of Ag and Cu onto gas diffusion layers (GDLs), as shown in Fig. 5.2a. First, we compared the four electrode structures; *1.)* 100 nm Ag (GDE | Ag_{100}), *2.)* 50 nm Ag with 50 nm Cu on top (GDE | Ag_{50} | Cu_{50}), *3.)* the inversely deposited 50 nm Cu with 50 nm Ag on top (GDE | Cu_{50} | Ag_{50}) and *4.)* 100 nm Cu (GDE | Cu_{100}). *(Henceforth, these systems will*

be labeled according to their deposition order, e.g., 1.) (GDE | Ag_{100}) will be Ag_{100} and 2.) (GDE | Ag_{50} | Cu_{50}) will be $Ag_{50}Cu_{50}$, etc.). Here the overall catalyst layer thickness was fixed to ensure similar CO_2 transport properties from the gas-diffusion layer through the initially constructed catalyst systems. Sample characterization and a detailed experimental methodology have been added to the SI (Fig. S5.1, S5.2). We then performed electrochemical characterization of the electrodes through chronopotentiometry at a fixed current density of 200 mA/cm². This current density was chosen as it represents peak C_{2+} product selectivity for the Cu control case in our zero-gap membrane electrode assembly configuration consisting of a Ni-mesh anode, 1 M KOH anolyte, an anion exchange membrane (Sustainion X37-50) and a Sigracet 38BB GDL substrate. The cathode gas effluent was analyzed every 5 minutes to measure product selectivity.

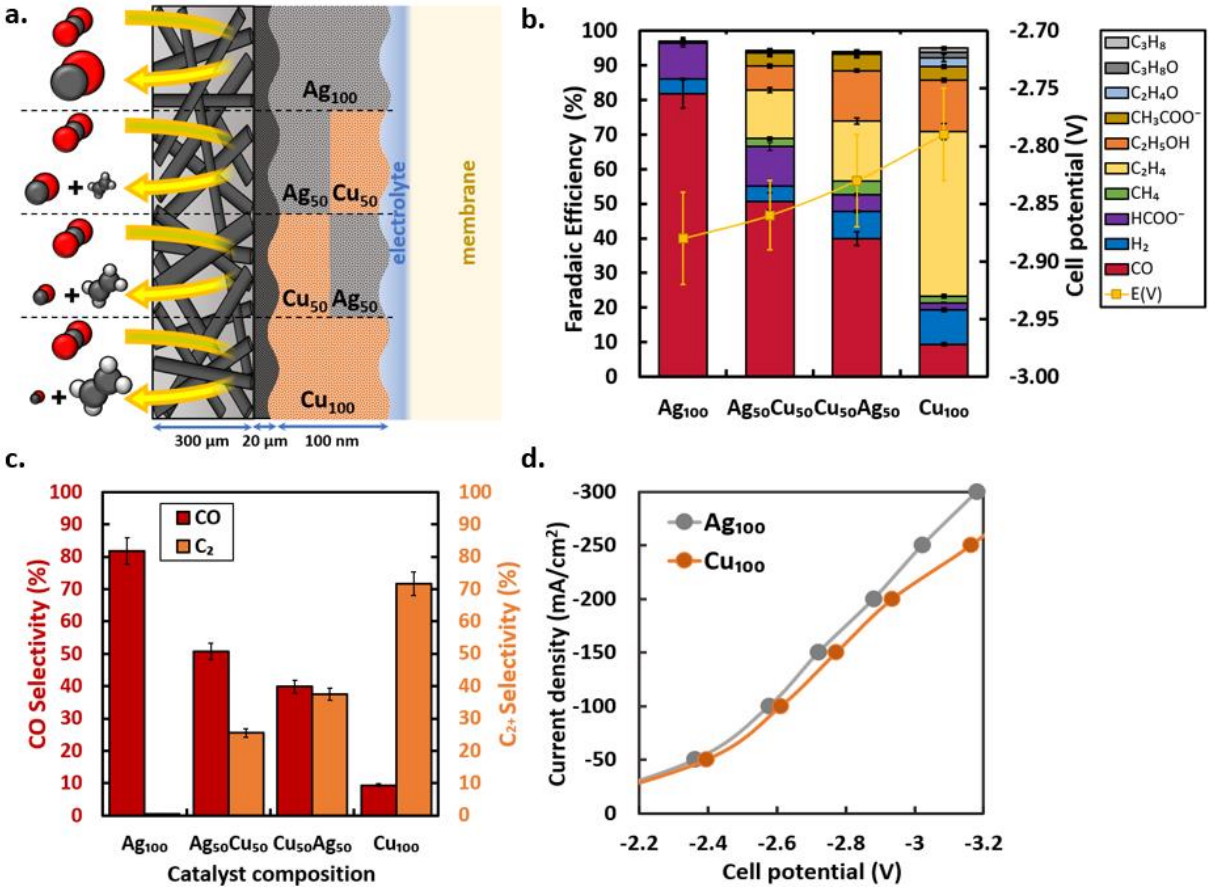

Figure 5.2 ***a.*** *Schematic representation of the four different 100 nm catalysts in a zero-gap MEA. Sizes of the shown molecules indicate the expected trends in conversion tendency.* ***b.*** *Product distributions of electrochemical conversion at 200 mA/cm² show that for the mixed systems, the material closest to the CO_2 gas phase has a more pronounced effect in selectivity and cell potential.* ***c.*** *A comparison of partial current densities for CO and C_2 products.* ***d.*** *I-V curves for Ag_{100} and Cu_{100} samples. Displayed values are taken from triplicate experiments averaged between minute 5 and 60, with error depicting the standard deviation over the duration of the experiment.*

Fig. 5.2a depicts the schematic catalyst compositions within the zero-gap MEA configuration, and Fig. 5.2b shows the measured Faradaic efficiencies for each of the four electrodes. When comparing the product distribution and applied potential of the $Ag_{50}Cu_{50}$ and $Cu_{50}Ag_{50}$ samples with Ag_{100} and Cu_{100} (Fig 5.2b.) it can be seen that the bimetallic systems represent a combination of the pure metals. Looking closely into the differences between the two bimetallic systems the effect of the catalyst layer closest to the CO_2 rich gas phase has the most pronounced contribution, which can be attributed to a less restricted pathway for CO_2 gas to reach the closest catalyst layer. This effect is most prominently observed when looking at the CO selectivity decrease from FE_{CO} = 50.7% to 39.9% and the C_{2+} selectivity increase from FE_{C2} = 25.5% to 37.5% for $Ag_{50}Cu_{50}$ and $Cu_{50}Ag_{50}$, respectively (Fig 5.2c.). Additionally, the potential required to run both tandem catalysts at 200 mA/cm² seems to follow a similar trend where $Cu_{50}|Ag_{50}$ performs more similar to Cu_{100} and $Ag_{50}|Cu_{50}$ more like Ag_{100}. When observing the minor product formation across electrodes, a slight increase in methane (CH_4) and acetate (CH_3COO^-) for the bimetallic electrodes as compared to Cu_{100} is observed, which might indicate that an increased amount of CO produced on Ag is further reduced downstream on the Cu catalyst.

The results presented in Fig. 5.2 show the presence of a layering effect, but these samples were, due to the high fraction of Ag, excessively selective towards CO, whereas the goal was to improve C_{2+} selectivity. It was found that the catalyst closest to the gas phase had the most prominent effect on the total catalyst performance. Alongside the knowledge that only Cu can effectively dimerize CO molecules, this information implies that a small fraction of Ag positioned closest to the liquid phase might be able to slightly promote CO production, which can subsequently be utilized on the Cu bulk catalyst. In order to see whether Ag can have a beneficial effect in this configuration a series of 100 nm Cu samples were prepared with an additional 5, 10 and 15 nm of Ag deposited on top (Cu_{100}, $Cu_{100}Ag_5$, $Cu_{100}Ag_{10}$ and $Cu_{100}Ag_{15}$) were produced and tested. The layer of Ag deposited on the membrane side of the thicker Cu layer can be seen in both SEM and macroscopic images as shown in Fig. SI5.3. As can be seen from Fig. 5.3b the increasing Ag thickness of the samples led to an increase in CO production from 9.4 % on Cu_{100} to 16.7 % on $Cu_{100}Ag_{15}$ and formate (from 2.0 % on Cu_{100} to 4.6 % on $Cu_{100}Ag_{15}$), which was to be expected, as these are the main carbon based products of CO_2 reduction on Ag. However, an increase in selectivity towards products that are

conventionally converted from CO_2 over a Cu catalyst (methane, acetaldehyde, acetate and ethanol) was observed for the samples with a Ag coating. To compensate for the various increases in selectivity, a drastic decrease in ethylene selectivity was seen where the Ag content went up. This decreased the overall C_{2+} selectivity from 75.4% for Cu_{100}

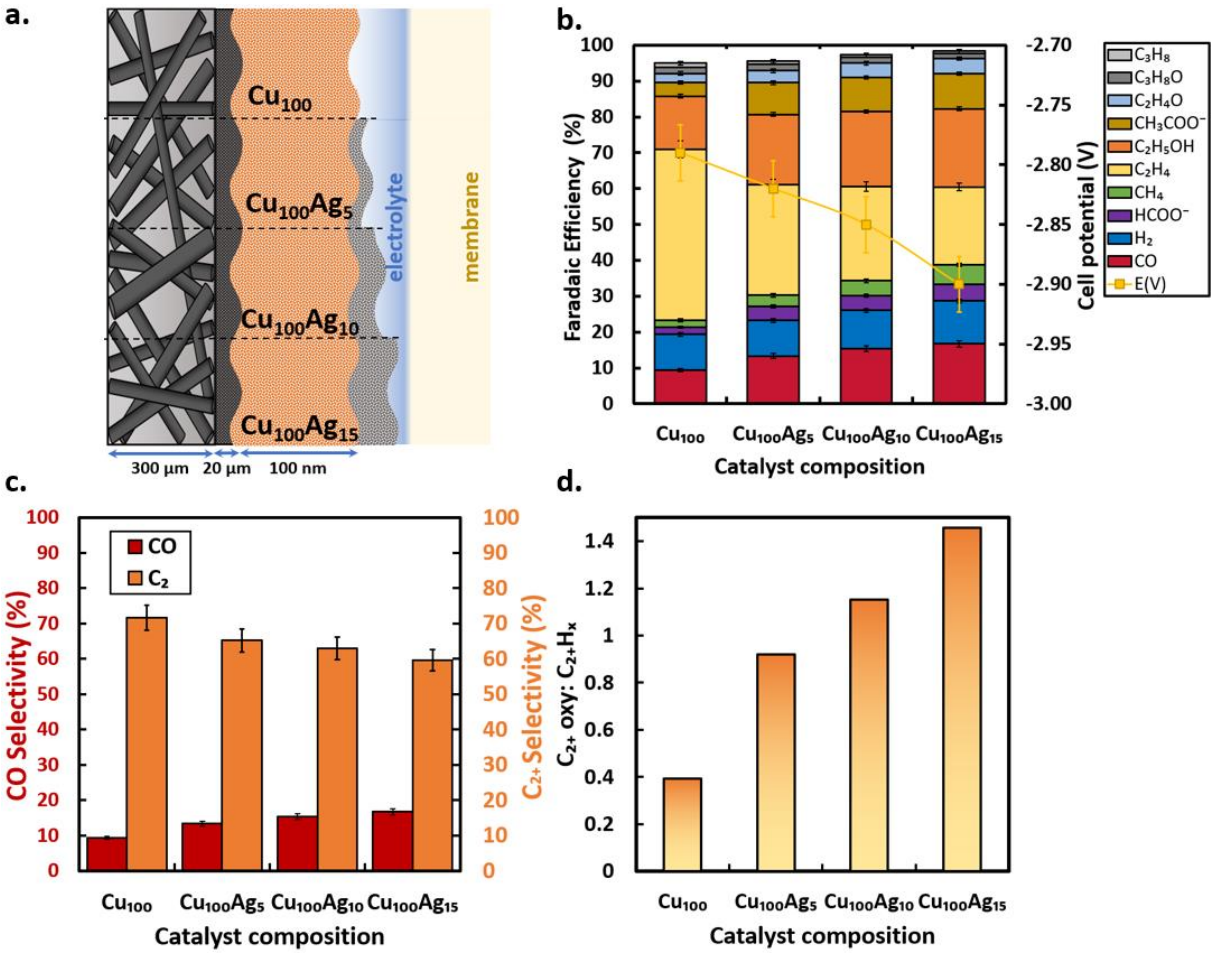

Figure 5.3 ***a.*** *Schematic representation of the four 100 nm Cu catalysts with varying Ag_x contents.* ***b.*** *Product distributions at 200 mA/cm² show a strong decrease of ethylene with increasing Ag. Simultaneously CO, ethanol and acetate increase.* ***c.*** *A comparison of partial current densities for CO and C_{2+} products show a gradual diminish of total C_{2+} selectivity, though the rise in CO selectivity does not fully compensate.* ***d.*** *The ratio between multicarbon oxygenates (C_{2+} oxy) and C_{2+} hydrocarbons ($C_{2+}H_x$) indicates a shift in the overall function of Cu. Displayed values are taken from triplicate experiments averaged between minute 5 and 60, with error depicting the standard deviation over the duration of the experiment.*

to 60.6% for $Cu_{100}Ag_{15}$ (Fig. 5.3c). A final observation that can be taken from the selectivities is the ratio of C_{2+} oxygenates versus C_{2+} hydrocarbons (with no oxygen content). Jouny et al. [33] showed that during similar high-rate electroreduction this selectivity ratio fluctuates when comparing a Cu catalyst for CO_2R and for direct CO reduction (COR) between ~0.3 and ~1.0, respectively. Here, despite not applying direct

COR, the multicarbon oxygenate : hydrocarbon ratio becomes 0.39 for Cu_{100} and 1.45 for $Cu_{100}Ag_{15}$. Although these are different systems, the similarity of these ratios show that the $Cu_{100}Ag_{15}$ sample starts behaving more like Cu in a COR environment. Although mass transport is incomparable to H-cell experiments, a high ratio of C_2 oxygenates (acetate and ethanol) to ethylene has also been shown in various aqueous COR studies, where primarily the formation of acetate is ascribed to a higher local pH [11], [34], [35]. In the system presented here, the additional feed of CO from the Ag catalyst might cause a similar pH increase due to reduced CO_2 acidification.

After the electrochemical experiments, visual inhomogeneities were observed for all Cu containing samples (See Fig. SI5.4 of samples before and after reaction). When further looking into these inhomogeneities using scanning electron microscopy

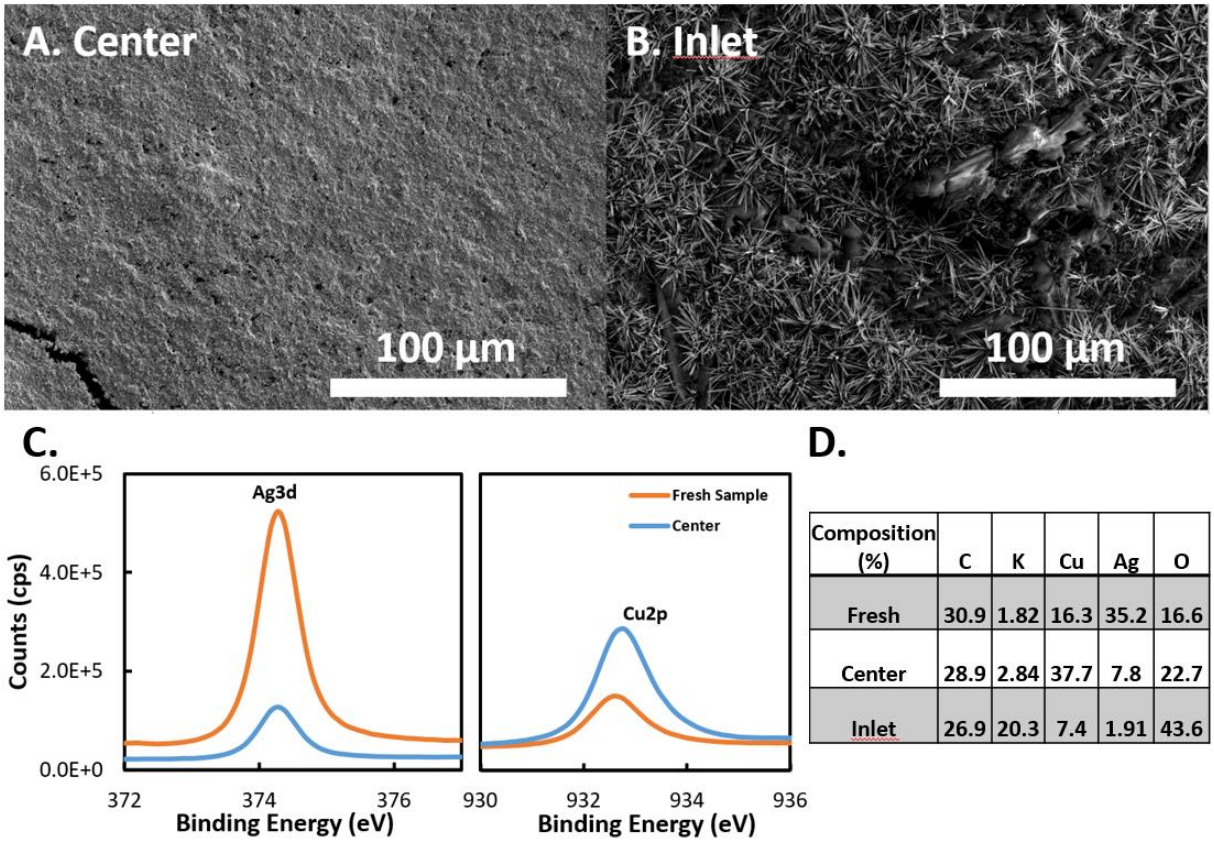

Composition (%)	C	K	Cu	Ag	O
Fresh	30.9	1.82	16.3	35.2	16.6
Center	28.9	2.84	37.7	7.8	22.7
Inlet	26.9	20.3	7.4	1.91	43.6

Figure 5.4 Scanning electron microscopy images of a $Cu_{100}Ag_{15}$ sample near the center of the sample (A.) and near the CO_2 inlet (B.) after 1 hr electrolysis in 1M KOH. While the SEM image near the inlet shows a homogenous Cu|Ag surface, the image near the CO_2 inlet displays strong reformation of the catalyst surface in the form of needle growth, as well as salt deposits. XPS results of a fresh and used sample near the center (C.) show a strong decrease in Ag and increase in Cu on the surface after reaction. The elemental compositions (E.) show the loss of surface Ag, while near the inlet a large uptake of oxidized potassium is detected.

(JEOL-6010A SEM) it was found that while the center and lower end of the 5 cm^2 samples, located further down the CO_2 channel (Fig 5.4A.) showed little to no reformation after operation, the surface of the catalyst near the CO_2 inlet was heavily reformed (Fig. 5.4B), showing clusters of needle like Cu-based structures alongside covering deposits. To see whether the composition and designed layering was affected by the reaction, surface X-ray photoelectron spectroscopy (Thermo-Fisher, K-Alpha) was performed on a fresh sample, and after the experiment from the center and inlet location of the sample. Comparing the homogenous bulk of the fresh sample to the center of the used catalyst (Fig. 5.4C) showed the Ag signal decreased 4-fold over the reaction, while the Cu signal at the surface simultaneously became twice as prominent. The overall Cu:Ag ratio shifted from 1:2 to 4:1. When looking at the elemental compositions of the three (Fig. 5.4D) it was found that the inlet of the used sample had a similar catalytic composition ratio to the center, although this was greatly overshadowed by the strong presence of potassium carbonate (K, C, and O covered 90% of the total signal). The surface instability detected for all performed experiments

5.3 Conclusion

In this study we looked at tandem CO_2 electrolysis over a layered AgCu bulk catalyst in a zero-gap MEA configuration, with the idea that the availability of CO at the Cu surface could be enhanced by providing additional CO_2-to-CO conversion over a Ag catalyst, hereby increasing the total C_{2+} yield. It was found through initial screening of bulk catalysts that the order of deposition affects the potential and product selectivity of the catalytic system altogether. Here we saw that the catalyst deposited closest to the gas phase had the most pronounced effect, though the excessive amount of Ag used initially led to excessive CO production for the overall catalytic system. When depositing minute amounts of 5, 10 and 15 nm of Ag on top of the 100 nm bulk Cu catalyst it was found that the total CO_2-to-C_{2+} conversion decreased in all cases that Ag was deployed and was therefore an ineffective addition as compared to a sample without Ag. It was found, however, that the ratio of multicarbon oxygenates to multicarbon hydrocarbons increased from 0.39 to 1.45 when adding the 15 nm of Ag, indicating that an increased concentration of CO at the Cu bulk led to a shift in its environment. In this particular system the addition of a layered catalyst was not fruitful in terms of getting closer to an ideal mono-selective multicarbon catalyst, though this is just one tested system in a wide field of possibilities. Future study on various

parameters like thicknesses, electrolytes and activities should be explored to find such a holy grail of electrochemistry.

References Chapter 5.

1. Hori, Y., *Electrochemical CO_2 Reduction on Metal Electrodes*, in *Modern Aspects of Electrochemistry*, C.G. Vayenas, R.E. White, and M.E. Gamboa-Aldeco, Editors. 2008, Springer New York: New York, NY. p. 89-189.
2. Jouny, M., W. Luc, and F. Jiao, *General Techno-Economic Analysis of CO2 Electrolysis Systems.* Industrial & Engineering Chemistry Research, 2018. **57**(6): p. 2165-2177.
3. Lee, W.H., et al., *Highly selective and scalable CO2 to CO - Electrolysis using coral-nanostructured Ag catalysts in zero-gap configuration.* Nano Energy, 2020. **76**: p. 105030.
4. Lee, J., et al., *Electrochemical CO2 reduction using alkaline membrane electrode assembly on various metal electrodes.* Journal of CO2 Utilization, 2019. **31**: p. 244-250.
5. Anderson, R.B., *Fischer-Tropsch Synthesis.* 1984.
6. Kortlever, R., et al., *Catalysts and Reaction Pathways for the Electrochemical Reduction of Carbon Dioxide.* The Journal of Physical Chemistry Letters, 2015. **6**(20): p. 4073-4082.
7. Bagger, A., et al., *Catalytic CO2/CO Reduction: Gas, Aqueous, and Aprotic Phases.* ACS Catalysis, 2022. **12**(4): p. 2561-2568.
8. Xiao, H., et al., *Cu metal embedded in oxidized matrix catalyst to promote CO2 activation and CO dimerization for electrochemical reduction of CO2.* Proceedings of the National Academy of Sciences, 2017. **114**(26): p. 6685-6688.
9. Wang, X., et al., *Mechanistic reaction pathways of enhanced ethylene yields during electroreduction of CO2–CO co-feeds on Cu and Cu-tandem electrocatalysts.* Nature Nanotechnology, 2019. **14**(11): p. 1063-1070.
10. Heenen, H.H., et al., *The mechanism for acetate formation in electrochemical CO(2) reduction on Cu: selectivity with potential, pH, and nanostructuring.* Energy & Environmental Science, 2022. **15**(9): p. 3978-3990.
11. Luc, W., et al., *Two-dimensional copper nanosheets for electrochemical reduction of carbon monoxide to acetate.* Nature Catalysis, 2019. **2**(5): p. 423-430.
12. Wang, L., *A happy couple makes acetate from CO.* Nature Catalysis, 2022. **5**(4): p. 240-241.
13. Calle-Vallejo, F. and M.T.M. Koper, *Theoretical Considerations on the Electroreduction of CO to C2 Species on Cu(100) Electrodes.* Angewandte Chemie International Edition, 2013. **52**(28): p. 7282-7285.

14. Choi, J., et al., *Electrochemical CO2 reduction to CO on dendritic Ag–Cu electrocatalysts prepared by electrodeposition.* Chemical Engineering Journal, 2016. **299**: p. 37-44.

15. Yan, W.-Y., C. Zhang, and L. Liu, *Hierarchically Porous CuAg via 3D Printing/Dealloying for Tunable CO2 Reduction to Syngas.* ACS Applied Materials & Interfaces, 2021. **13**(38): p. 45385-45393.

16. Dong, W.J., et al., *Grain Boundary Engineering of Cu–Ag Thin-Film Catalysts for Selective (Photo)Electrochemical CO2 Reduction to CO and CH4.* ACS Applied Materials & Interfaces, 2021. **13**(16): p. 18905-18913.

17. Huang, J., et al., *Structural Sensitivities in Bimetallic Catalysts for Electrochemical CO2 Reduction Revealed by Ag–Cu Nanodimers.* Journal of the American Chemical Society, 2019. **141**(6): p. 2490-2499.

18. Wang, J., et al., *Silver/Copper Interface for Relay Electroreduction of Carbon Dioxide to Ethylene.* ACS Applied Materials & Interfaces, 2019. **11**(3): p. 2763-2767.

19. Dutta, A., et al., *Activation of bimetallic AgCu foam electrocatalysts for ethanol formation from CO2 by selective Cu oxidation/reduction.* Nano Energy, 2020. **68**: p. 104331.

20. Lee, S., G. Park, and J. Lee, *Importance of Ag–Cu Biphasic Boundaries for Selective Electrochemical Reduction of CO2 to Ethanol.* ACS Catalysis, 2017. **7**(12): p. 8594-8604.

21. Ting, L.R.L., et al., *Enhancing CO2 Electroreduction to Ethanol on Copper–Silver Composites by Opening an Alternative Catalytic Pathway.* ACS Catalysis, 2020. **10**(7): p. 4059-4069.

22. Iyengar, P., et al., *Theory-Guided Enhancement of CO2 Reduction to Ethanol on Ag–Cu Tandem Catalysts via Particle-Size Effects.* ACS Catalysis, 2021. **11**(21): p. 13330-13336.

23. Li, Y.C., et al., *Binding Site Diversity Promotes CO2 Electroreduction to Ethanol.* Journal of the American Chemical Society, 2019. **141**(21): p. 8584-8591.

24. Kuhn, A.N., et al., *Engineering Silver-Enriched Copper Core-Shell Electrocatalysts to Enhance the Production of Ethylene and C2+ Chemicals from Carbon Dioxide at Low Cell Potentials.* Advanced Functional Materials, 2021. **31**(26): p. 2101668.

25. Zhang, S., et al., *Electrochemical Reduction of CO2 Toward C2 Valuables on Cu@Ag Core-Shell Tandem Catalyst with Tunable Shell Thickness.* Small, 2021. **17**(37): p. 2102293.

26. Kottakkat, T., et al., *Electrodeposited AgCu Foam Catalysts for Enhanced Reduction of CO2 to CO.* ACS Applied Materials & Interfaces, 2019. **11**(16): p. 14734-14744.

27. Martić, N., et al., *Ag2Cu2O3 – a catalyst template material for selective electroreduction of CO to C2+ products.* Energy & Environmental Science, 2020. **13**(9): p. 2993-3006.

28. Wang, H., et al., *Surface restructuring in AgCu single-atom alloy catalyst and self-enhanced selectivity toward CO2 reduction.* Electrochimica Acta, 2022. **426**: p. 140774.

29. Clark, E.L., et al., *Electrochemical CO2 Reduction over Compressively Strained CuAg Surface Alloys with Enhanced Multi-Carbon Oxygenate Selectivity.* Journal of the American Chemical Society, 2017. **139**(44): p. 15848-15857.

30. Burdyny, T., K. Liu, and W. Smith, *How Local Reaction and Process Conditions Influence CO2 Reduction to Multicarbon Products on Copper Gas-Diffusion Electrodes.* ECS Meeting Abstracts, 2020. **MA2020-01**(36): p. 1515.

31. Sassenburg, M., et al., *Characterizing CO2 Reduction Catalysts on Gas Diffusion Electrodes: Comparing Activity, Selectivity, and Stability of Transition Metal Catalysts.* ACS Applied Energy Materials, 2022. **5**(5): p. 5983-5994.

32. Niu, D., et al., *Cu(2)O-Ag Tandem Catalysts for Selective Electrochemical Reduction of CO(2) to C(2) Products. LID - 10.3390/molecules26082175 [doi] LID - 2175.* (1420-3049 (Electronic)).

33. Jouny, M., W. Luc, and F. Jiao, *High-rate electroreduction of carbon monoxide to multi-carbon products.* Nature Catalysis, 2018. **1**(10): p. 748-755.

34. Malkani, A.S., M. Dunwell, and B. Xu, *Operando Spectroscopic Investigations of Copper and Oxide-Derived Copper Catalysts for Electrochemical CO Reduction.* ACS Catalysis, 2019. **9**(1): p. 474-478.

35. Verdaguer-Casadevall, A., et al., *Probing the Active Surface Sites for CO Reduction on Oxide-Derived Copper Electrocatalysts.* Journal of the American Chemical Society, 2015. **137**(31): p. 9808-9811.

Chapter 5. Supporting Information

Bulk layering effects of Ag and Cu in tandem CO_2 electrolysis to adjust C_{2+} selectivity

Metal catalysts were deposited on the microporous layer (MPL) of a 39BB Sigracet GDL using DC-magnetron sputtering at 50 W. After production, the catalysts were placed in a Dioxide Materials™ MEA cell, with 2.25 x 2.25 cm (5.06 cm^2) active area (Figure S5.1). A Sustainion® X37-50 anion exchange membrane and Ni foam OER catalyst were deployed. 100 mL of 1M KOH anolyte (45% sol., Sigma Aldrich®) was recirculated through the system at 20 mL/min by peristaltic pump (McMaster-Carr®). Pure CO_2 (>99.99%, Linde Plc) was humidified by bubbling through a vial of DI water and fed in excess to the cathode gas compartment at 50 mL/min. The system configuration is shown in Figure S5.2. To account for CO_2 consumption and dissolution, a mass flow meter (El-Flow, Bronckhorst®) measured the exact flow before analysis in the gas chromatograph (CompactGC-4.0, Global Analyser Solutions™). After each experiment liquid samples were taken in duplo and analyzed by HPLC (1260 Infinity II LC, Agilent Technologies, Inc.™). All electrochemical experiments were performed *in triplo* at 200 mA/cm^2 for 60 minutes using a potentiostat (ParSTAT MC, Ametek® SI). The results shown here are averaged over the duration of the experiment, except for the initial GC injection, which was taken while the system was stabilizing.

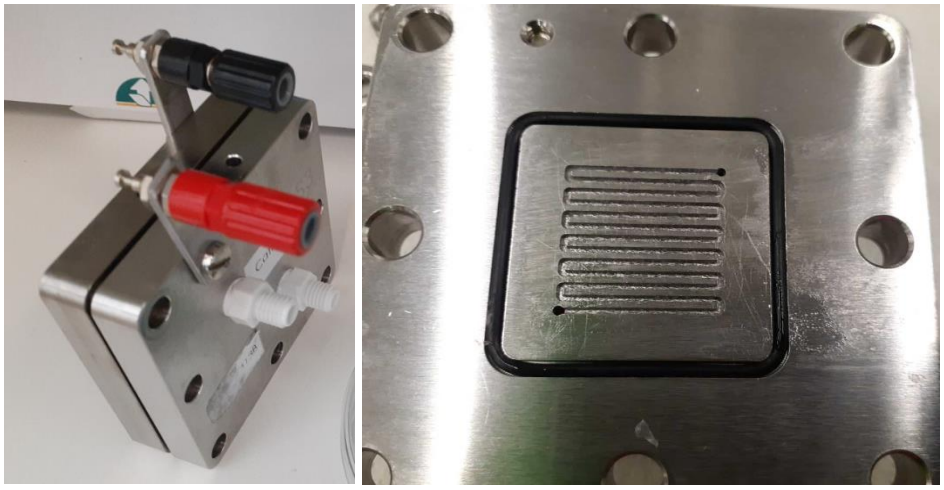

Figure S5.1. Dioxide Materials 5cm^2 electrochemical cell. External appearance and flow channel.

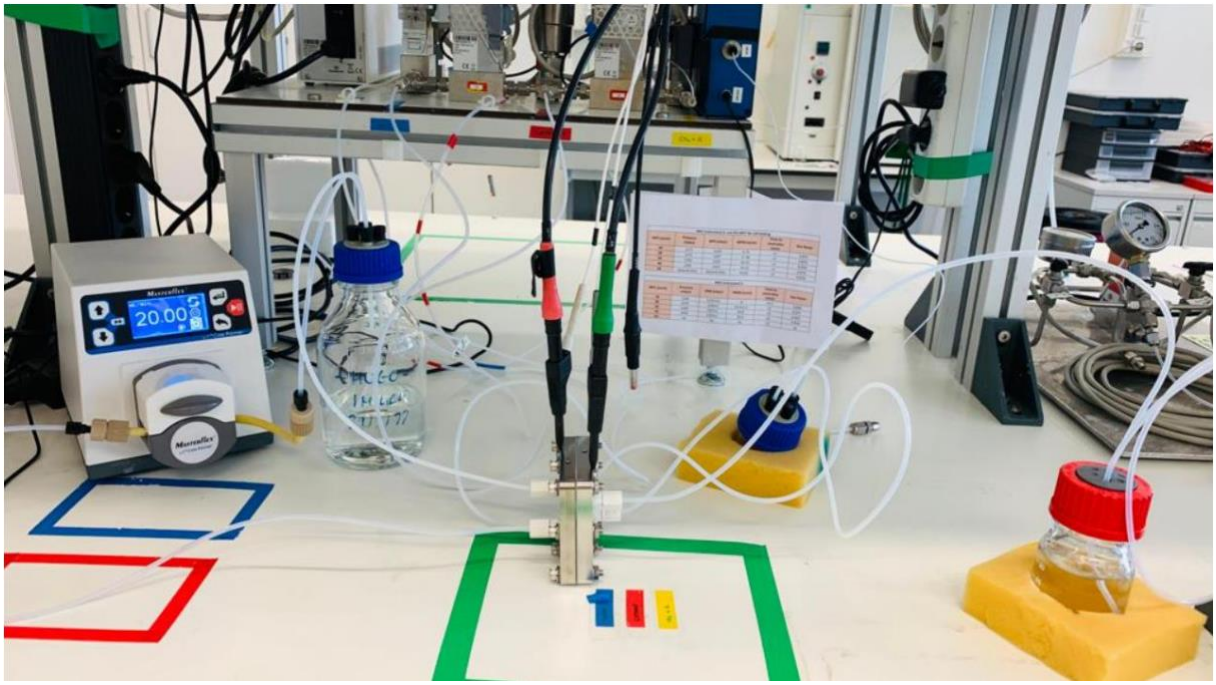

Figure S5.2. System configuration with on the left the anolyte and recirculation pump, in the center the electrochemical cell with above the mass flow meter, (potentiostat and gas chromatograph also above, out of shot) and on the right the CO_2 mass flow controller, humidification bottle and liquid trap.

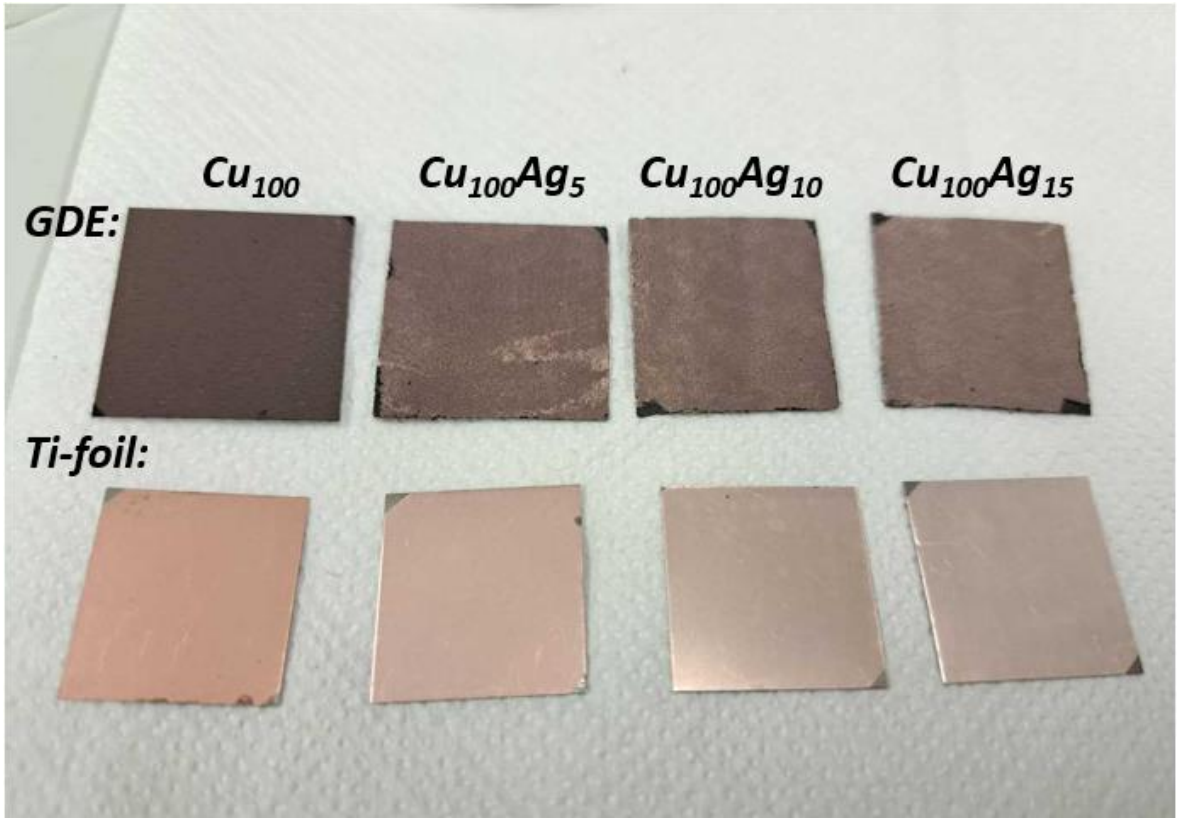

Figure S5.3. Fresh samples of Cu_{100}, $Cu_{100}Ag_5$, $Cu_{100}Ag_{10}$ and $Cu_{100}Ag_{15}$ on GDE (top) and titanium foil (bottom). The discoloration shows the increased surface coverage of Ag. The $Cu_{100}Ag_{15}$ on GDE sample shown in this image is used later on for SEM and XPS.

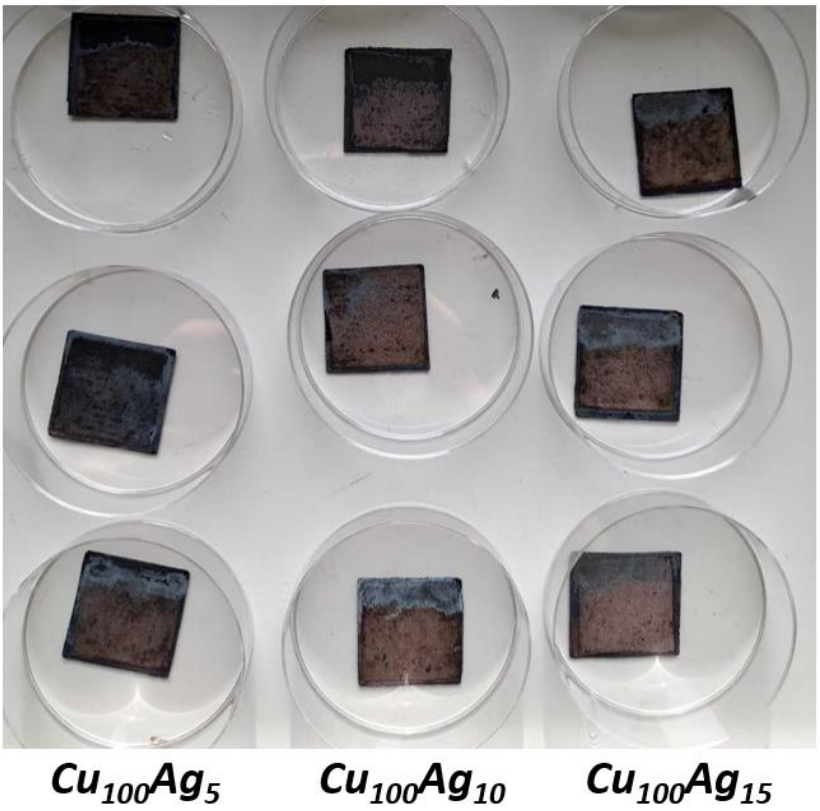

Figure S5.4. Triplo CuAg samples from after the experiments show a visual reformation of the surface near the top of the sample, where the inlet of CO_2 is placed and likely the highest activities are achieved. The increased activity causes a higher local pH and subsequently a greater Cu reformation, K^+ and CO_3^{2-} accumulation and ultimately, salt formation.

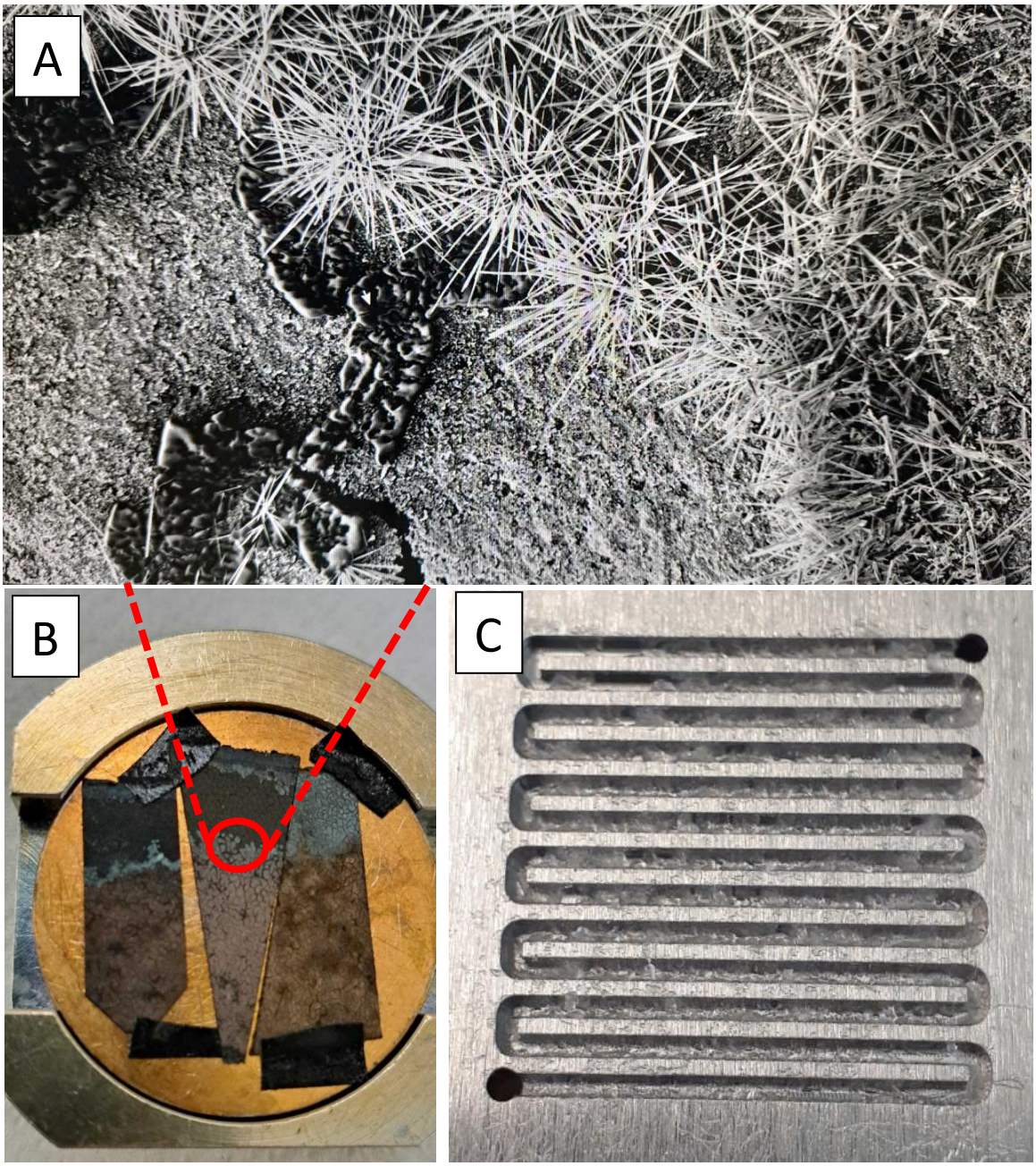

Figure S5.5. A. SEM image of the interface visible in B., where three separate samples show the same phenomenon. The most active parts of the catalyst show catalyst restructuring due to needle growth. The bottom part of the image shows little catalyst reformation, however salt deposition, shown in black, covers large parts of the surface and indicates some form of activity. C. After each 1 hour experiment the gas channel is found to contain large amounts of salt crystals.

Chapter 6.

Future Outlook

The progression of my academic career has been marked by changes. In particular, the past decade brought many technological changes that affected on-going CO_2 reduction research as well as societal changes that altered the way emissions policies are being carried out. While personally being involved and made aware of the changing environment, I would like to use this attained knowledge to project upon the future and elaborate on the pathway to the development and potential adoption of CO_2 reduction technologies. *Disclaimer: Seeing the highly turbulent state of the world, the foresight presented in this chapter is a projection of what I think the technological roadmap and societal impact of CO_2 electrolysis will be.*

6.1 Technological limitations

This thesis focuses on electrochemical intensification and is a testament to the developments made in the field of CO_2 electrochemistry and the strides towards industrial applicability. Researching and seeing the components of CO_2 reduction systems evolve through several stages from H-cells to flow cells and MEAs has shown the feasibility of it becoming a gamechanger in closing the carbon cycle. Still, the technology is in its infancy and the following limitations need to be addressed in order for systems to concretely contribute to combatting climate change and foster a fossil fuel free future.

- First and foremost, the issue of ***CO_2 utilization*** needs to be resolved. The dissolution of CO_2 in alkaline environments results in the formation of carbonate ions, wasting up to half of the purified CO_2 stream. Ideally the dissolution of CO_2 would be prevented by utilizing an acidic environment. The downside of this approach is that a lower pH would greatly promote the HER. In Chapter 3 of this thesis electrochemical intensification showed a shift in performance for almost all catalysts in alkaline media. For acidic systems the effects of electrochemical intensification will likely be similar, if not more extreme, due to the overproduction of OH^- in a H^+ rich environment that may basify the local catalyst environment. It is therefore important to study acidic CO_2 reduction systems not only under lab scale conditions to study mechanisms (e.g., RDEs

and in situ spectroscopy), but also under elevated current densities to focus more on the mass transport of a full-fledged device.

- Secondly, the ***formation of carbonate salts*** that further limits the long-term stability of electrolysis needs to be resolved. While it is complicated to reduce carbonate formation due to CO_2 dissolution in aqueous electrolytes, several strategies to mitigate detrimental formation of salts were presented in Chapter 4. Some examples that were described here are adjusting the electrolyte, using flushing or regenerative cycles and making the MEA less prone to cationic transport and nucleation. Other ongoing research that is going into the direct reduction of carbonates as a 'proxy-reactant' for performing the CO_2 reduction will have to show whether this alternative is feasible for upscaled applications.

- A third limitation that presents itself is the lack of ***energy efficiency*** of the process. Chapter 3 showed that high single product conversion can be achieved by choosing the right catalyst, but what is not considered is the low conversion of the CO_2 feed, also known as the single pass conversion efficiency. Flowing excess amounts of CO_2 is undesired in an industrial setting since it affects the energy intensive post-process separation and requires recycling of unreacted CO_2, lowering the overall energy efficiency. However, this mode of operation is a deliberately chosen by researchers, since it is helpful for deconvoluting the complex nature of the CO_2RR by minimizing the change in reactant composition as it travels through the reactor. A profitable system would need to tackle the issue of a feed that is gradually depleted of CO_2 to reduce post processing costs by for instance changing the catalyst composition as the mixture is transported across the electrochemical system. Alternatively, the desired product stream can be changed to adapt to the downstream processing, for instance by aiming for a specific CO-to-H_2 syngas ratio that can directly be used in Fisher-Tropsch synthesis without purification. A marginal fraction of all CO_2 reduction literature has investigated transient reactant compositions, giving room for in-depth studies to the optimal extent of single pass conversion. Future research should therefore not only study the selectivity of the catalyst towards a product, but also address the affinity of the catalyst towards reactants (this includes products that could act as secondary reactants).

6.2 Components for CO2 electrolysis

In addition to CO_2 utilization, salt formation, energy and conversion efficiency there is an array of technical concerns that are of importance not only to CO_2 electrochemistry, but to any electrocatalytic reaction. These concerns are related to long-term stability, the perm-selectivity of membranes, minimizing resistances and the overall balance of systems. While these issues are still detrimental to the cost-efficiency of the system, I believe solutions to these shortcomings are more graspable by looking into the following improvements:

- The stability of **substrate materials** is to be improved through comparative studies of commercially available materials to obtain higher understanding of parameters such as conductivity, morphological stability, fouling, phase separation and the adhesion of catalyst materials, ionomers and binders. Eventually customized substrates with high conductivity, stable embedding of the catalyst and proper gas-liquid balancing will be designed specifically for CO_2 reduction achieving lower resistance and improved stability.

- Similarly, **membranes** available today have limited perm-selectivity and high resistance. The use of bipolar membranes can be considered as one of the recent advances made in CO_2 reduction electrolysis, limiting product, carbonate and co-ion crossover at the cost of additional overpotential due to increased thickness. The ideal membrane of the future should have the functionality of a BPM while retaining the resistance of an AEM or CEM.

- The overall **resistance of the system** needs to be minimized in order to achieve an economically attractive and industrially scalable system. In addition to the substrate and membrane mentioned above, I project that future CO_2 reduction electrolysis will be conducted in gas-gas systems similar to PEM electrolysis. Solely providing dynamic humidified gas streams then give better control over salt formation, can stabilize product selectivity and lower resistance which in turn reduces cell voltage and improves overall energy efficiency.

- *The **balance of systems** is mainly dependent on the reactions at hand. In this thesis the focus was placed on the cathodic CO_2 reduction reaction, while accepting*

that the complementary oxygen evolution reaction is on one hand easily accessible and scalable, but on the other hand energy demanding and economically uninteresting. If CO_2 reduction makes it as an industrially relevant reaction, it will likely involve an alternative oxidation reaction producing e.g., hydrogen peroxide or oxidized saccharides. When looking at a futuristic gas-gas system, a profitable gas-based oxidation reaction should be considered.

6.3 Unfair climate change

One of the major issues of combatting climate change is its cause and effect across borders. Inequality and inequity of actions and consequences are an important topic in the ongoing international climate debates, caused by a discrepancy of resources and responsibilities between the greatest emitting countries and the hardest impacted countries. We are to expect millions of climate refugees and billions of Euros in infrastructural damages (e.g., flooding of lands, expansion of the Sahara Desert, wildfires in Australia).

The future of emissions is likely dictated not by developed nations, but by developing nations that currently use a lower energy profile but are rapidly electrifying as it improves quality of life. Developed nations are able to invest in a greener energy mix on the backs of their strong economies and established energy infrastructures. It is important here to recognize that these nations took centuries to reach this luxurious position without having to worry about accountability for their emissions. With this knowledge developing nations are now put in a precarious position. While energy demand and use are rapidly increasing, the less flexible economies and lack of existing infrastructure are making the direct implementation of green technologies troublesome, due to their high investment costs and increased system complexity. In other words, for developing nations individual daily survival outweighs structural improvements which will slow down climate restorative efforts. What developed countries can do to assist here is take a leading role and invest in implementation and continued development of green technologies to make them cheaper and more reliable so that they become the preferred choice for all. Even today, this approach has already led to the implementation of PV systems in many parts of Africa, as it is an obvious choice for a continent with such an abundance of sunlight to buy the (now) affordable systems that profit from it.

In short, the ongoing rise in emissions will lead to further climate change and make the favorable continuation of 'business as usual' unacceptable. Gradually fossil fuels will have to be phased out, though the path to that goal is murky and covered in obstacles. While some countries opt out of involvement or reject its relevance in the eyes of economic competitiveness, others put in additional efforts to get their nation towards emission neutrality. Emphasis on the importance of the energy transition is increasing amongst the people and its leaders, but intensified efforts on a global regulatory level are required in order to retain a habitable world for all.

6.4 The future of a turbulent world

While this thesis primarily focused on the technological aspects of CO_2 electrolysis, the overarching societal need for green energies will be the determining factor to push the rates of research and implementation. In this day and age, the world is in a turbulent state; The consequences of climate change are increasing in severity and will continue to do so unless defossilization is realized in the coming decades. International goals and policies, such as CO_2 neutrality by 2050, are gaining more traction and cause debate of the best course of action to achieve a global energy transition.

At the center of this transition is the generation of renewable electricity and the green electrification of industrial processes. The first step, implementing sufficient renewable energy generation, is well on its way and will likely continue to be the desirable alternative to grey electricity. However, a pivotal bottleneck in the electrification of chemical industries is to work in harmony with the dynamic availability of renewable electricity. Contextually, the era of fossil fuels was marked by abundantly available grey electricity that allowed the optimization of reactors operating at a continuous rate for a prolonged period of time (months or even years of uninterrupted operation). In contrast, the fluctuant nature of renewable energies poses an issue that affects the technical and economic feasibility of said technologies. On one hand there is a question of priority; Maybe the production of chemicals only comes after direct electrification uses, and if so, is there room for electrically intensive processes like electrolysis? On the other hand, a question of technical feasibility; For CO_2 reduction technologies in particular, fluctuations in voltage or current density could induce catalyst and system instability as well as variance in product distribution as was shown in Chapter 3. Research efforts into the fluctuant operation of electrolyzers will tell industry whether this is a reasonable solution, if expensive

buffering and storage can still be used to obtain a cost-effective system or if renewable production of carbon-based chemicals should be achieved through other means, e.g., biobased fermentation processes or a renewable variant of the reverse water-gas shift reaction combined with Fischer Tropsch synthesis.

Interconnecting future technologies with the current energy infrastructure has many unknowns and only time will tell whether CO_2 electrolysis will come to fruition as an industrial process in the whole circular economy puzzle.

Summary

Nature has been in balance for tens of thousands of years, but since the Industrial Revolution mankind has been disturbing this balance by utilizing fossil fuels for technological advancement and for societal prosperity (Chapter 1). Fossil fuels like coal, oil and gas were able to power newly found inventions like the steam and combustion engines. Through oxidation their stored energy could be released and as waste greenhouse gasses, predominantly carbon dioxide (CO_2), were produced and ejected into the atmosphere. While initially the impact of our activities was unnoticeable, the continuously increasing world population and its energy demand has led to such a severe amount of emissions that the accumulation of CO_2 in the atmosphere started to impact natures balance. International agreements, such as CO_2 neutrality by 2050, have been made to phase out fossil fuels and implementing renewable energy technologies as substitutes. However, the phasing out of fossil fuels takes a long time to be realized due to both technological and economic reason. Furthermore, some essential chemical industries rely on carbon-based reagents to produce commodity products and need to find an attractive, non-fossil based process to continue in a sustainable manner. In order to still achieve the climate goals that have been set, alternative technologies to mitigate emissions are being researched, and this is where this doctoral thesis enters the stage.

One of the technologies that can assist in the mitigation of emissions is the electrochemical reduction of CO_2. While burning fossil fuels causes the release of energy and CO_2, the inverse reaction of combining CO_2 gas with electricity and water can lead to the production of 'synthetic fuels' and other commodity chemicals (Chapter 2). By using CO_2 as a reacting molecule instead of only seeing it as a waste product, this technology could be part of a 'closed carbon cycle' where only as much CO_2 is emitted during its use as is consumed during production. While this technology has been studied for many decades, the industrial implementation of CO_2 electrolysis is still not achieved due to the complexity of obtaining stable operation at industrially relevant rates. In the last 10 years, new configurations of the reactor have been developed to circumvent limitations and improve the rates of reaction. In this chapter the theory of the CO_2 reduction reaction (CO_2RR) and its competing side reactions are covered and

continues to describe the evolution of reactor configurations and the principles of its essential components.

One of the major bottlenecks in the development of CO_2 electrolysers is the variety in reactions that can occur. The goal of electrochemistry research is often to obtain the best catalyst for producing a desired product. With CO_2 electrochemistry in particular, whichever product is obtained is highly dependent on a wide range of conditions, such as the rate of reaction, configuration of the system, catalyst material, reaction medium, concentration of reagents and the presence of contaminants. This broad parameter space has caused discordance among researchers in how to interpret their own results and compare it fairly to the results of others. The scientist dr. Hori recognized this problem and meticulously described the conditions of a set of H-cell experiments so that he and his colleagues could produce a benchmark which could be used to fairly compare catalyst materials under identical conditions. This work inspired a similar empirical study for the more modern flow cell configuration, in which much higher reaction rates can be achieved (Chapter 3). Here we find that not only the type of material, but also the rate of the reaction can have a major effect on the performance metrics activity, selectivity and stability. While some catalysts like silver (Ag) are minimally affected in their performance by such fluctuations, other catalysts like gold (Au) and palladium (Pd) lose the majority of their selectivity under the same conditions. An interesting trend we find here is that among all tested catalysts, the influence of the solution in which the reaction takes place plays a lesser role as the rate of reaction increases.

Another limitation to the operation of electrolysers is the precipitation of salts during electrolysis. When CO_2 electrolysis is conducted at an industrial rate, essential cations from the solution tend to accumulate and crystallize at the cathode, forming a carbonate salt that covers the surface. This phenomenon is often observed, yet rarely addressed as a limiting condition for upscaling and long-term operation. Chapter 4 explains the mechanism of how salt formation in CO_2 electrolysers comes to being and covers the literature that explore operational solutions. By sorting these solutions into four categories, we hope to provide CO_2 reduction researchers with a new perspective of how to circumvent detrimental salt formation in CO_2 electrolysers.

While the previous chapters are providing guidelines on the functionality and limitations of future CO_2 electrolysers, Chapter 5 provides a more classical catalyst

screening study, albeit in a membrane electrode assembly (MEA). The elevated reaction rates used in the MEA (200 mA/cm^2) cause much greater fluctuation in the mass transport of reactants and products, leading to uneven distribution of reactant and product concentrations throughout the system. The study presented in Chapter 5 is used to see if silver (Ag), and copper (Cu) can be combined in a tandem configuration to obtain a synergistic effect. The idea here is that Ag is a catalyst that effectively converts CO_2 to CO at a low overpotential, after which the Cu catalyst can sequentially dimerize the locally elevated CO concentration into C_{2+} products more effectively than a pure Cu catalyst can do with a CO_2 feed. Although a higher selectivity for C_{2+} products was not obtained, the conclusion was drawn that the presence of the Ag catalyst made Cu perform more as if it was in a CO environment while being in a CO_2 fed system. This provides an interesting pathway for further research into non-uniform catalyst distributions and creative catalyst solutions for transient reactant streams.

Finally, Chapter 6 provides an outlook on the state, bottlenecks and ongoing development of CO_2 electrolysis systems as we move into a future where renewable technologies will dictate the habitability and relation we hold with our environment. The culmination of read literature, experimental developments and scientific discussions enable my transparent view on what needs to be done in order to achieve the next chapter of CO_2 electrolysis and the renewable production of commodity chemicals.

Samenvatting

De natuur is voor tienduizenden jaren in balans geweest, maar na de Industriële Revolutie heeft de mensheid deze balans verstoord door het utiliseren van fossiele brandstoffen voor technologische vooruitgang en sociale welvaart (Hoofdstuk 1). Fossiele brandstoffen zoals kolen, aardolie en aardgas waren in staat om nieuwe uitvindingen zoals de stoom en verbrandingsmotoren te bekrachtigen. Door middel van oxidatie kan de energie die opgeslagen is in deze brandstoffen worden vrijgemaakt, waarbij de broeikasgassen, voornamelijk koolstofdioxide (CO_2), die als bijproduct ontstaan worden uitgestoot in de atmosfeer. Toen fossiele brandstoffen voor het eerst in gebruik werden genomen waren de gevolgen hiervan niet op te merken. De toename van zowel de wereldbevolking als de vraag naar energie zorgde in de 20ste eeuw voor een drastische toename van CO_2 in de atmosfeer met als gevolg een verstoring van de natuurlijke balans met de gevolgen van dien. Internationale overeenkomsten, zoals CO_2 neutraal voor 2050, zijn in de laatste drie decennia tot stand gekomen om fossiele brandstoffen te vervangen door duurzame energiebronnen. Deze transitie duurt echter een lange tijd om te realiseren wegens technologische en economische redenen. Daarbij opgeteld zijn sommige essentiële chemische industrieën afhankelijk van grondstoffen die koolstof bevatten, en dus niet kunnen worden vervangen door elektrische alternatieven. Voor deze industrieën is het noodzakelijk een aantrekkelijk, fossiel-vrij alternatief te vinden om deze productie te verduurzamen. Om de gezette klimaatdoelen te bereiken moeten er alternatieve technologieën worden uitgevonden en geoptimaliseerd. Dit is waar deze doctorale thesis om de hoek komt kijken.

Een van de technologieën die kan bijstaan in het minderen van emissies is de elektrochemische conversie van CO_2. Bij het verbranden van fossiele brandstoffen komen energie en CO_2 vrij. Bij CO_2 wordt de inverse reactie gefaciliteerd, waarbij CO_2 gas, elektrische energie en water worden samengevoegd om 'synthetische brandstoffen' en andere basischemicaliën te produceren (Hoofdstuk 2). Door gebruik te maken van CO_2 als een reactant en het niet alleen te zien als een afvalstof is het voor deze technologie mogelijk om de koolstofcyclus te sluiten, waarbij er alleen zoveel CO_2 wordt uitgestoot als dat er is opgevangen voor de productie. Alhoewel deze technologie al tientallen jaren wordt onderzocht is er nog geen sprake van industriële applicatie

wegens de complexiteit van de reactie en het verkrijgen van stabiele operatie onder industrieel relevantie condities. In de laatste 10 jaar zijn er echter nieuwe reactorconfiguraties ontwikkeld die een aantal limitaties omzeilen, waardoor de snelheid van de reactie kon worden opgeschroefd. In Hoofdstuk 2 wordt de theorie van de CO_2 reductie reactie (CO_2RR) en de competitieve nevenreacties behandeld, waarna de evolutie van reactor configuraties en de essentiële onderdelen worden beschreven.

Een van de grote knelpunten in de ontwikkeling van CO_2 elektrolyse is de variatie van reacties die kunnen plaatsvinden. Het doel van elektrochemisch onderzoek is vaak om de beste katalysator te vinden, waarbij er veel wordt gelet op materiaalkeuze en morfologie. Specifiek in het kader van CO_2 reductie is het produceren van het gewilde product lastig, gezien deze ontwikkeling afhankelijk is van een brede set aan operationele condities, zoals de snelheid van de reactie, de configuratie van het systeem, de eigenschappen van de gekozen materialen, het reactor medium, concentraties van reactanten en de aanwezigheid van contaminaties. Deze grote set aan parameters heeft in het verleden gezorgd voor onenigheid tussen wetenschappers in hoe eigen resultaten moeten worden geïnterpreteerd en hoe deze resultaten kunnen worden vergeleken met die van anderen gezien de set aan verschillende parameters. De wetenschapper dr. Hori herkende dit probleem en maakte een gedetailleerde omschrijving van zijn experimenten zodat hij, samen met zijn collega's, een maatstaf had om de prestaties van materialen objectief te kunnen interpreteren onder identieke condities en de resultaten van andere onderzoeksgroepen eerlijk te kunnen vergelijken. Dit werk inspireerde een empirische studie waarin 5 verschillende katalysatormaterialen worden getest in een *flow cell*, een modernere reactor configuratie waarin hogere reactiesnelheden kunnen worden gefaciliteerd (Hoofdstuk 3). Bij deze experimenten werd het duidelijk dat niet alleen de keuze van materiaal, maar ook de snelheid van de reactie een grote rol speelt voor de activiteit, selectiviteit en stabiliteit van het systeem. Waar sommige katalysatoren zoals zilver (Ag) weinig effect ervaren van hogere reactiesnelheden, verliezen andere katalysatoren zoals goud (Au) en palladium (Pd) een groot deel van hun selectiviteit onder dezelfde condities. Een andere interessante trend die was gevonden voor alle geteste katalysatoren is dat de invloed van het reactiemedium een kleinere rol speelt wanneer de reactiesnelheid wordt opgevoerd.

Nog een limitatie voor industriële toepassing is de precipitatie van zouten tijdens elektrolyse. Wanneer CO_2 elektrolyse wordt uitgevoerd bij industriële snelheden accumuleren en kristalliseren essentiële kationen zich aan de kathode, waardoor er carbonaatzouten worden gevormd aan het oppervlak van de katalysator. Dit fenomeen is in recent onderzoek vaak geobserveerd, maar niet altijd benoemd als een limiterende conditie voor opschaling en langdurige operatie. Hoofdstuk 4 legt uit wat het mechanisme is achter de vorming van zouten in CO_2 elektrolyse apparaten, en behandeld de literatuur die dit probleem wel benoemen en operationele oplossingsmethoden testen. Door deze oplossingen op te delen in vier categorieën hopen wij CO_2 reductie onderzoekers een nieuw perspectief te bieden over hoe de nadelige gevolgen van zoutvorming kunnen worden aangepakt.

Waar de vorige hoofdstukken voornamelijk richtlijnen geven over de functionaliteit en de limitaties van toekomstige CO_2 elektrolyse apparaten, wordt er in Hoofdstuk 5 een meer klassieke katalysator screening uitgevoerd in een membraan electrode assemblage (MEA). De verhoogde reactiesnelheid van de MEA (200 mA/cm^2) zorgt ervoor dat het massatransport tussen de voedingsstroom en het reactieoppervlak vele malen groter is, waardoor ongelijke distributies van reactant- en productconcentraties ontstaan. In Hoofdstuk 5 wordt er bestudeerd of zilver en koper als gelaagde tandemkatalysator kunnen worden gebruikt om een synergistisch effect van de twee elementen te verkrijgen. Het idee hier is dat zilver (Ag) een goede katalysator is voor de conversie van CO_2 naar CO bij een lager voltage en koper (Cu) een goede katalysator is voor de dimerisatie van CO naar langere koolstofketens (C_{2+}). De hoofdvraag hier is dan ook of de tandem AgCu katalysator een hogere C_{2+} product conversie kan behalen dan een pure Cu katalysator onder dezelfde omstandigheden. Uit de experimenten bleek dat alhoewel er geen hogere concentratie aan C_{2+} producten werd gevonden wegens excessieve productie van CO op het zilveroppervlak, er wel geconcludeerd kon worden dat de tandem configuratie zorgde voor een lokaal hogere CO concentratie in de buurt van de koper katalysator, waardoor deze een andere ratio aan producten produceerde dan zonder de additie van zilver. Dit laat zien dat het mogelijk is de productselectiviteit van katalysatoren kan worden geoptimaliseerd door het gebruik van niet-uniforme katalysator distributies en dat vervolgonderzoek naar creatieve katalysatoroplossingen voor veranderende productstromen essentieel is voor optimalisatie van grotere systemen.

Ten slotte wordt er in Hoofdstuk 6 een vooruitzicht gegeven over de staat, de limitaties en de benodigde ontwikkelingen van CO_2 elektrolyse systemen terwijl we in rap tempo verplaatsen naar een toekomst waar duurzame technologieën zullen dicteren hoe de leefbaarheid en onze relatie tot het klimaat zich zal ontwikkelen. De culminatie van gelezen literatuur, experimentele ervaringen en wetenschappelijke discussies hebben ervoor gezorgd dat ik hier een transparant beeld kan laten zien van wat er nodig is om het volgende hoofdstuk van CO_2 elektrolyse en de duurzame productie van basischemicaliën te bewerkstelligen.

Acknowledgements

A well-supported road of change

In the journey that has been my PhD a recurring topic has been change, and change came in many forms. Surely, the technical aspects of change have been covered aplenty in this thesis, but let me highlight how conditional changes can incur a world of difference in the overall performance of a system. In catalysis changes of **operational system**, of **support structure**, of **catalyst morphology**, of **local environment**, of **salt coverage** and of **electron affinity** have major implications on performance also. In my metamorphosis from a rookie scientist to a slightly-less-rookie, slightly-more-knowledgeable scientist I have been met by parallel social changes that resulted in a positive boost of my overall performance. So, if you would indulge me, allow me to fill in these off-beat metaphors:

The **operational system**, TU Delft, changed temporarily into CU Boulder and NREL during my second year. It was both an opportunity and a challenge to be so far away from everything that I know and gave me a chance to experience a new living and working environment, prove my independence and test my ability to adapt to any situation. While some pillars were constant, the shifts in proximity and time led to a great change in my **support structure** and the shape in which support was available to me. With the colleagues and friends I made starting my PhD, during my exchange in the US and while reintegrating after my return to Delft it is safe to say my **local environment** went through significant change. While catalysts normally degrade under such conditions, I feel like I got sturdier and more resistant. During my PhD I experienced loss of love, temporary isolation of the COVID pandemic and experienced climate change first-hand in the form of a 40 °C SurfCat conference in Denmark and the forest fires in Colorado. While these are reason enough to remain salty, the combination of science, experience and Chapter 4 taught me that your performance does not benefit from being forever **covered in salt**, but from happiness and a positive attitude. As for **electron affinity**, if I describe myself as a highly reactive molecule, bouncing through the halls of university for all these years, my affinity

towards the people around me has been more of a motivator than anything. Making people laugh and finding who resonate well to my natural frequency has kept me enthusiastic to come to work every day and I will miss it dearly.

Before I go into the personal 'thank-you's', I'd like to put a little disclaimer and an invitation. Throughout my PhD I have met a hundred people I want to thank, but since I do wish to finish my thesis before the end of this year, I have decided to keep it concise. I would like to apologize for not giving everyone their own personalized section or a complementary piece of art. If you ever decide you want one, or my two cents about our relationship, feel free to reach out to me and we can see what is possible!

First and foremost, I'd like to thank **Wilson** for being so much more than just my promotor. From the moment we met, almost 10 years ago when I drew a schematic battery, you inspired me to not only be a creative scientist, but more importantly to be a kind-hearted and unique person. You taught me valuable lessons on obtaining and maintaining connections, of picking low-hanging fruits, of inclusion and of teamwork. I will always remember the meetings we had in your office when I was going through a rough patch and the guidance you gave if projects were not moving. You made me keep my head up through Rocky and Star Wars quotes, appreciated my nerdy habits and cheeky 90's references like no other and quite literally opened the doors to a whole new world when I needed it the most. Winging it in flip-flops at my first conference, bolting down A-Basin or meeting in the Mountain Sun, there are a hundred memories of us that I will carry with me forever. Until this day you embody many characteristics of what I aspire to be and I am ecstatic to have you as a mentor and a friend.

Tom, you came into our group with so many bright ideas and such a drive to make the technology we work on a reality. While initially you were just a bright and humble postdoc in my eyes, I soon found you to be a reliable, proficient and incredibly friendly teammate that was invaluable in the completion of my publications and the scheduling of my PhD. Coming back from the US became my co-promotor, overseeing my reintegration and providing a safe haven for my insecurities. Your passion for the job helped me reflect on my writing, research and methods and the similarities in our understanding released me of my worries. Thank you for 'deploying' me in your courses, letting me represent the group in Japan, and being my equal on a daily basis. Whether it was through our *walkie-talkie* discussions regarding our advancements in Miyazaki's nightmares or bouncing thoughts off each other regarding science, you were

truly a safe haven focused on my development and wellbeing until the very end. I hope to see you around for lunch at *X* and meet professionally to make the world a brighter place.

Bernard, during my bachelor I attended your Thermodynamics course, but I never thought I'd grow so much because of you beyond the scope of that course *(and I'm not talking about just TA'ing those courses)*. I remembered after I just defended my bachelor thesis on bipolar membranes and solar water splitting you mentioned that I should do a PhD after my master. Somehow that really stuck to me and got me to where I am now, so thanks for that. The true learning moments I had with you were from our discussions on ethics, politics and history over coffee. To me you are the embodiment of a true scientist. Objective yet opinionated, critical yet kind. I consider myself lucky for having you nearby. Thank you for your watchful eye and helping me across the finish line.

Diana, traveling with the bus, venting and screeching about our setbacks, dropping fat beats, enjoying coffee and gossiping away. We started out mildly, but along the way you have set an insanely high bar for being the best office buddy. Thank you for checking on my sanity and giving me advice. Somehow we ended up still being semi-colleagues, and I will see you around. I hope you read this and think to yourself: '*Ditto*'.

If I mention, Diana, I surely have to mention sporty, impulsive **Giorgio**, who made our vacation a lot spicier being my *right*++ navigator in the hills of France and always showing up with a smile. Maybe next time be a bit less of an agent of chaos, but thank you for being the right type of crazy. Relaxed, yet coffee-based **Dylan**, our small competitions of making the working place a bit more colorful with 3D models were an absolute joy. And precise, provoking **Peter**, you will always be my first DM and one of the few that caught my jokes when they went under the radar. Thank you all for being a wonderful crew and making my fantasy of becoming a world-sailing pirate a bit more of a reality.

Joost and **Herman**, you truly are the core of MECS, in spirit and in presence. Without your technical contribution my experiments would have never worked, as goes for so many others. Thank you for the trainings, reparations, lab assistance, and oversight. It was a pleasure serving you coffee and laughing together every day.

Nate, always smiling, you made my time at both MECS and CU Boulder so much more enjoyable by being outgoing and wondering about the wildest things. Thank you for physically bringing me to the highest height I've ever experienced. You wove seamlessly in and out of my PhD journey and if I meet you in a day, or 10 years from now, our interaction will always remain the same. Thanks!

To the 'old guard' members of MECS to who I owe gratitude; Always working beauty **Kailun,** wise witch **Sanjana,** hokage **Kai,** curious **Recep,** climber **Nienke,** Belgian pride and membrane master **Marijn,** LO2 laser disaster **Martin,** fashionable **Davide,** clever coder **Divya,** laughing CTO **Anirudh**, always publishing **Maryam**, critical **Erdem**, smiling **Aaron**, mademoiselle **Audrey,** resin **Robin,** and master student **Reinier** who did a phenomenal job in conducting what seemed like endless experiments. There are too many memories I look back on fondly, Christmas dinners, blasting music in the lab, group meetings, you name it. Thank you for our talks in the building and our adventures during the conferences, the group outings, the parties, the lab hours together, and so much more.

And to the 'new kids on the block' **Sid, Hugo, Jesse, Mark** and **Jasper**. The group is in your hands now and I believe you will do just fine. Thank you for the discussions, the salt-production, the sharp criticism, the cool thermal images, the office confusions over our name and taking over the HPLC. I wish you all the best for the battles to come.

In the halls of ChemE and during conferences I have interacted with so many professors (**Ferdinand**, **Tom**, **Atsushi**, **Johan** …), staff members (**Bart, Marcel, Joyce,** …) and other colleagues (**Elmira, Elena, Ali, Yanyan, Jence, Joe, Bernhard, Aaron, Lorenz, Jorrit, Kosta, Isabell, Boaz, Zimu, Katie** …) that have helped me feel like I worked where I belonged for all these years. Thank you for your kindness and all the moments we shared. Through my eccentric behavior, my colorful appearance racing through the hallways, my skills being the coffee master, a custodian of the HPLC, a candyman, or an experienced colleague, one way or another, I am sure I left my mark on all of ChemE, and now it is finally time for your Mark to leave ChemE.

My year in Colorado was scary at first, but luckily I was accompanied by the old guard Nate and Recep as well as the newfound *Electrobuffs:* **Hunter**, **Allison**, **Yuval**, **Paige**, **Hussain** and **Maria.** Discussing science, traveling to Golden, exploring

Colorado, going for diners, drinks, hikes and driving to snowboard resorts. Without your support my stay in the US with all its wild events would have been a lot less tolerable. In NREL I had an educative and memorable time (although somewhat tumultuous due to the lockdown) thanks to the teachings from **Ellis, Yingying, Ashlee, Fry, Huyen, Guido** and **Christian**. Thank you for your professionalism, hospitality, patience and kindness along the way.

Speaking of hospitality, during my stay I found **Dillon** and **Tony,** two great software developers, who allowed me to squat at their house for a large part of the pandemic. You truly saved me from isolation and taught me some of the American habits. The cuisine, shopping trips, regular boarding, going for wild hikes, watching Samurai Jack, hitting diamond, exploring the city, moving to your new places and always making fun while everything else was doom and gloom. Just the two of you would have made the trip been worthwhile.

I'd like to thank my close friends, **Joop, Vincent, Lody** and **Wim**, for letting me unwind after a long week of work. Playing games, collecting cards, painting figurines, watching movies, or just relaxing, our Friday night adventures have been legendary and always allowed me to recharge. In doomsday terms 'a minute to midnight' is used to describe the final moments before something bad happens. For you guys, we're only getting started at that time! Thank you for having my back and know that you can always rely on mine if you need me.

En ten slotte voor mijn familie. **Mam** en **Pap,** jullie hebben mij door en door gesteund om altijd te gaan voor wat ik wil behalen. Ik heb deze lange tocht altijd naar huis kunnen komen waar jullie mij met warm eten en goede zorg hebben verwelkomd. Zonder jullie waren mijn prestaties nooit mogelijk geweest en daarvoor wil ik jullie bedanken. **Richard**, communicatie is niet ons sterkste punt, maar je hebt toch voor een belangrijk deel van mijn ontwikkeling gezorgd. Ik heb altijd op jullie kunnen rekenen en daarvoor wil ik jullie bedanken. En daarnaast natuurlijk ook mijn grote familie, alle oma's, opa's. tantes, ooms, nichtjes en neven, waarmee het bijna altijd wel een gezellige boel is. Nu kunnen we het eindelijk gaan vieren!

And thank you, dear reader, for sticking with me until the end.

Mark Sassenburg =) Barendrecht, May 2023